



**HAL**  
open science

# Co-Optimisation du Dimensionnement et du Contrôle des Groupe Motopropulseurs Innovants

Jianning Zhao

► **To cite this version:**

Jianning Zhao. Co-Optimisation du Dimensionnement et du Contrôle des Groupe Motopropulseurs Innovants. Autre. Université Paris Saclay (COmUE), 2017. Français. NNT : 2017SACL057 . tel-01694273

**HAL Id: tel-01694273**

**<https://theses.hal.science/tel-01694273>**

Submitted on 27 Jan 2018

**HAL** is a multi-disciplinary open access archive for the deposit and dissemination of scientific research documents, whether they are published or not. The documents may come from teaching and research institutions in France or abroad, or from public or private research centers.

L'archive ouverte pluridisciplinaire **HAL**, est destinée au dépôt et à la diffusion de documents scientifiques de niveau recherche, publiés ou non, émanant des établissements d'enseignement et de recherche français ou étrangers, des laboratoires publics ou privés.

# Co-Optimisation du dimensionnement et du contrôle des groupes motopropulseurs innovants

Thèse de doctorat de l'Université Paris-Saclay  
préparée à IFP Energies nouvelles

École doctorale n°580 Sciences et technologies de l'information et de  
la communication (STIC), CentraleSupélec

Spécialité de doctorat: Automatique

Thèse présentée et soutenue à IFPEN, Rueil-Malmaison, le 26 octobre 2017, par

**M. Jianning ZHAO**

## Composition du Jury :

Hugues MOUNIER Professeur, CentraleSupélec	Président
Yann CHAMAILLARD Professeur, Université d'Orléans	Rapporteur
Sébastien DELPRAT Professeur, Université de Valenciennes et du Hainaut-Cambrésis	Rapporteur
Lars ERIKSSON Professeur, Linköping University	Examineur
Federico MILLO Professeur, Politecnico di Torino	Examineur
Antonio SCIARRETTA IFP Energies Nouvelles	Directeur de thèse



UNIVERSITÉ PARIS-SCALAY  
IFP ENERGIES NOUVELLES

Doctoral School ED STIC N°580  
Laboratory IFP Energies nouvelles

Thesis defended by Jianning ZHAO

Defended on 26<sup>th</sup> October, 2017

In order to become Doctor from Université Paris-Scalay  
Academic Field **Digital Technology and Science**  
Speciality **Automation**

Thesis Title

# Design and Control Co-Optimization for Advanced Vehicle Propulsion Systems

Thesis supervised by Antonio SCIARRETTA

## Committee members

<i>Referees</i>	Prof. Yann CHAMAILLARD	Université d'Orléans	
	Prof. Sébastien DELPRAT	Université de Valenciennes et du Hainaut-Cambrésis	
<i>Examiners</i>	Prof. Hugues MOUNIER	CentraleSupélec	Committee President
	Prof. Lars ERIKSSON	Linköping University	
	Prof. Federico MILLO	Politecnico di Torino	
<i>Supervisor</i>	Antonio SCIARRETTA	IFP Energies nouvelles	



The Université Paris-Scalay neither endorse nor censure authors' opinions expressed in the theses: these opinions must be considered to be those of their authors.



**Keywords:** design optimization, control optimization, vehicle propulsion system, hybrid electric vehicle, electric vehicle, conventional vehicle

**Mots clés:** optimisation du dimensionnement, optimisation du contrôle, groupes moto-propulseurs, véhicule électrique hybride, véhicule électrique, véhicule conventionnel



This thesis has been prepared at

**IFP Energies nouvelles**

1 & 4, avenue de Bois-Préau  
92852 Rueil-Malmaison Cedex - France

☎ (33) (0)1 47 52 60 00

📠 (33) (0)1 47 52 70 00

Web Site <http://www.ifpenergiesnouvelles.fr>





*To my parents and Xiang*



**DESIGN AND CONTROL CO-OPTIMIZATION FOR ADVANCED VEHICLE PROPULSION SYSTEMS****Abstract**

Advanced technologies are highly demanded in automotive industry to meet the more and more stringent regulations of fuel consumption. Co-optimization of design and control for vehicle propulsion systems with an enhanced computational efficiency is investigated in this thesis. Powertrain components, such as internal combustion engines, batteries, and electric motor/generators, are analytically modeled at descriptive and predictive level correspondingly for the development of fast-running control optimization and for the scalability of design optimization. The minimal fuel consumption of a hybrid-electric vehicle is evaluated through novel optimization methods. These methods – including the Selective Hamiltonian Minimization, and the GRaphical-Analysis-Based energy Consumption Optimization – are able to evaluate the minimal energy consumption with the enhanced computational efficiency. In addition, the Fully-Analytic energy Consumption Evaluation method approximates the minimal energy consumption in closed form as a function of the mission characteristics and the design parameters of powertrain components. A few case studies are presented in details via the bi-level and uni-level co-optimization approaches, showing an effective improvement in the computational efficiency for the overall co-optimization process.

**Keywords:** design optimization, control optimization, vehicle propulsion system, hybrid electric vehicle, electric vehicle, conventional vehicle

---

**CO-OPTIMISATION DU DIMENSIONNEMENT ET DU CONTRÔLE DES GROUPES MOTOPROPULSEURS INNOVANTS****Résumé**

Des technologies avancées sont très demandées dans l'industrie automobile pour respecter les réglementations de consommation de carburant de plus en plus rigoureuses. La co-optimisation du dimensionnement et du contrôle des groupes motopropulseurs avec une efficacité de calcul améliorée est étudiée dans cette thèse. Les composants des groupes motopropulseurs, tels que le moteur, la batterie et le moteur électrique, sont modélisés analytiquement au niveau descriptif et prédictif afin de permettre une optimisation du contrôle rapide et une optimisation du dimensionnement scalable. La consommation d'énergie minimale des véhicules hybrides-électriques est évaluée par des nouvelles méthodes optimales. Ces méthodes – y compris Selective Hamiltonian Minimization et GRaphical-Analysis-Based energy Consumption Optimization – permettent d'évaluer une consommation minimale d'énergie avec une efficacité de calcul améliorée. De plus, la méthode de Fully-Analytic energy Consumption Evaluation (FACE) approxime la consommation d'énergie minimale sous forme analytique en fonction des caractéristiques de la mission et des paramètres de conception des composants du groupe motopropulseur. Plusieurs cas d'études sont présentées en détail par rapport aux approches de co-optimisation à bi-niveaux et à uni-niveau, ce qui montre une réduction efficace du temps de calcul requis par le processus global de co-optimisation.

**Mots clés :** optimisation du dimensionnement, optimisation du contrôle, groupes motopropulseurs, véhicule électrique hybride, véhicule électrique, véhicule conventionnel

---

**IFP Energies nouvelles**

1 & 4, avenue de Bois-Préau – 92852 Rueil-Malmaison Cedex - France



# Acknowledgements

This thesis would not have been possible without the full support of IFP Energies nouvelles. I am especially indebted to my supervisor Antonio Sciarretta who has been a tremendous adviser for me. I would like to thank him for encouraging and strengthening my research in both academia and industry and for allowing me to grow as a research engineer of innovativeness.

I would like to express my sincere gratitude to the members of my Thesis Committee for their professional remarks and suggestions. In particular, the detailed comments remarked by Prof. Sébastien Delprat have been of great help to improve this thesis.

I am grateful to Prof. Lars Eriksson for offering me a great opportunity to collaborate with Scania during my exchange at Linköping University and for the warm and inspiring discussions with him and his group members, such as Olov Holmer, Viktor Leek, and Kristoffer Ekkberg.

None has been more important to me in the pursuit of this doctoral study than my family members. I would like to thank my parents and my sister for their forever love and eternal support. Most importantly, I wish to convey my thanks to Xiang Zheng for his supportive inspirations.



# Acronyms

**A | B | C | D | E | F | G | H | I | L | M | N | O | P | Q | S | T | V**

## **A**

**AIM** Asynchronous Induction Machine. 51–56, 164, 177, 183

**APU** Auxiliary Power Unit. 13, 75–77, 80, 81, 107–109

**AT** Automatic Transmission. 40, 43, 44

## **B**

**BAT** Battery. 27, 49, 65, 87, 90

## **C**

**CI** Compression Ignition. 29, 33, 35

**CVX** Convex Optimization. 16, 18, 19, 25

## **D**

**DCT** Dual Clutch Transmission. 40, 42–44

**DIRECT** Dividing Rectangles Optimization. 22, 24

**DP** Dynamic Programming. 15, 18, 19, 22, 23

## **E**

**EDU** Electric Drive Unit. 77

**EMG** Electric Motor/Generator. 27, 51–53, 65

**EMS** Energy Management Strategy. 65, 66

**ENG** Internal Combustion Engine. 27–29, 31, 35, 36, 64, 87

## **F**

**FACE** Fully-Analytic energy Consumption Estimation. 5, 97–105, 107, 109, 111, 112, 114–116, 126, 127, 129, 131, 132, 136, 137, 140–142, 144, 146, 151, 152, 162–165, 207

**FTP-72** Federal Test Procedure – 72. 63, 68, 89, 90, 92, 103, 111, 133, 138, 148, 191

**G**

**GA** Genetic Algorithms. 22, 24

**GHG** Green-House Gas. 9, 10

**GRAB-ECO** GRaphical-Analysis-Based Energy Consumption Optimization. 5, 71, 80, 81, 86, 88–94, 107, 109, 140, 141, 144, 161, 162, 164, 165

**H**

**HDV** Heavy-Duty Vehicle. 9

**HE** High Energy. 46–49

**HEV** Hybrid Electric Vehicle. 12–19, 23, 39, 40, 66, 71, 72, 74, 75, 80, 81, 83–92, 109, 114, 115, 119, 144

**HOT** Hybrid Optimization Tool. 73, 74, 79, 86–88, 93, 94

**HP** High Power. 46–49

**HYWFET** Highway Fuel Economy Test cycle. 44, 45, 63, 68, 89, 90, 92, 104, 111, 115, 133, 138, 148, 151, 163, 191

**I**

**ICDC** Inner City Driving Cycle. 63, 141, 142, 144, 191

**L**

**LB** Lean-Burn. 29, 35

**LDV** Light-Duty Vehicle. 9

**LIB** Lithium-Ion Battery. 46

**M**

**MT** Manual Transmission. 40, 43, 44

**N**

**NA** Naturally Aspirated. 29, 35

**NEDC** New European Driving Cycle. 1, 44, 45, 63, 68, 81, 89, 91, 111, 115, 131, 138, 139, 147, 148, 163, 191

**O**

**OOL** Optimal Operating Line. 75

**P**

**PMP** Pontryagin's Minimum Principle. 16, 19, 73, 162, 164

**PMSM** Permanent Magnet Synchronous Machine. 51–56, 69, 87, 90, 164, 177, 183

**PSO** Particle Swarm Optimization. 22, 24, 25

**Q**

**QSS** Quasi-Static Simulation. 67, 86, 97, 103–105, 114, 115, 131, 137

**S**

**SB** Stoichiometric-Burn. 29, 35

**SHM** Selective Hamiltonian Minimization. 5, 71, 74, 79, 86–94, 109–111, 144, 146–148, 155, 156, 161, 162, 164, 165

**SI** Spark Ignition. 29, 33, 35

**SUDC** Suburban Driving Cycle. 63, 141, 144, 191

**T**

**TC** Turbo-Charged. 29, 35

**TRA** Transmission. 27

**V**

**VHOT** Vectorized Hybrid Optimization Tool. 73, 74, 79, 86–89, 92–94, 114–116, 140, 141, 144, 146–148, 155, 164

**VPS** Vehicle Propulsion System. 12–14, 27, 29, 119



# List of Symbols

## Greek Symbols

Symbol	Description	Units
$\alpha$	slope	
$\beta$	battery-related number	
$\Delta$	quantity step	
$\epsilon$	engine-related number	
$\kappa$	generic parameters derived from FACE	
$\mu$	specific weight of powertrain components	[kg/unit]
$\nu$	transmission-related number	
$\omega$	rotational speed	[rad/s]
$\Phi$	generic function of burned fuel power evaluation in an HEV	
$\Psi$	generic function of electrochemical power evaluation in an HEV	
$\rho$	air density	[kg/m <sup>3</sup> ]
$\sigma$	set of time steps	[s]
$\tau$	transformed time	[s]
$\epsilon$	relative error	[%]

## Roman Symbols

Symbol	Description	Units
$\mathcal{C}$	cycle-related parameters	
$\mathcal{D}$	dimension-related parameters	

---

$\mathcal{E}$	total energy of battery	[kWh]
$\mathcal{I}$	technological variable	
$\mathcal{K}$	number	
$\mathcal{N}$	rotational speed	[rpm]
$\mathcal{P}$	rated power	[kW]
$\mathcal{Q}$	nominal capacity	[Ah]
$\mathcal{R}$	gear ratio	
$\mathcal{S}$	set of dimensioning parameters	
$\mathcal{T}$	rated torque	[Nm]
$\mathcal{V}$	engine displacement	[m <sup>3</sup> ]
$A$	frontal area	[m <sup>2</sup> ]
$a$	acceleration	[m/s <sup>2</sup> ]
$C$	coefficients	
$c$	coefficients in predictive analytic models	
$D$	all-electric range	[km]
$d$	generic design parameter	
$F$	force	[N]
$g$	acceleration due to gravity	[m/s <sup>2</sup> ]
$I$	best-efficiency indicator	
$k$	parameters in descriptive analytic models	
$m$	mass	[kg]
$n$	number	
$P$	power	[W]
$R$	radius	[m]
$s$	adjoint state variable	
$T$	torque	[Nm]
$t$	time	[s]

$U$	control space	
$u$	control variable	
$v$	velocity	[m/s]
$x$	state variable	

### Superscripts

Symbol	Description	Units
*	optimum	
$b$	battery-related	
$d$	descriptive	
$e$	engine-related	
$eqv$	equivalent	
$opt$	optimal	
$p$	predictive	
$ref$	reference	

### Subscripts

Symbol	Description	Units
100	100 km/h	
$adm$	admissible	
$apu$	auxiliary power unit	
$ar$	aerodynamic resistance	
$b$	battery	
$be$	electrochemical quantity of battery	
$c$	powertrain component	
$d$	drivetrain	
$e$	engine	
$ec$	engine corner	
$ef$	engine fuel	

---

$ek$	engine speed at 1000 rpm
$eP$	rated power of engine
$eT$	rated torque of engine
$ev0$	fixed electric vehicle mode
$ev1$	flexible electric vehicle mode
$f$	final
$fd$	final drive
$g$	electric generator
$gr$	gravitation resistance
$h$	Hamiltonian
$hs$	high speed
$hv0$	fixed hybrid vehicle mode
$hv1$	flexible hybrid vehicle mode
$ir$	inertia resistance
$l$	load
$ls$	low speed
$m$	electric motor
$me$	electrical quantity of electric motor
$ref$	reference
$rr$	rolling resistance
$s$	identification set
$t$	transmission
$tk$	$\mathcal{K}^{th}$ gear
$to$	output shaft of transmission
$top$	maximum
$u$	unit of assembled powertrain components
$v$	vehicle

$vb$  baseline quantity of vehicle

$w$  wheel



# Table of Contents

<b>Abstract</b>	<b>xv</b>
<b>Acknowledgements</b>	<b>xvii</b>
<b>Acronyms</b>	<b>xix</b>
<b>List of Symbols</b>	<b>xxiii</b>
<b>Table of Contents</b>	<b>xxix</b>
<b>List of Tables</b>	<b>xxxv</b>
<b>List of Figures</b>	<b>xxxix</b>
<b>Introduction</b>	<b>1</b>
Background . . . . .	1
Motivation . . . . .	2
Objective . . . . .	3
Contribution . . . . .	4
<b>I Modeling of Advanced Vehicle Propulsion Systems</b>	<b>7</b>
<b>1 State-of-the-Art Review</b>	<b>9</b>
1.1 Need for Better Energy Efficiency . . . . .	9
1.2 Single-Source Vehicle . . . . .	10
1.2.1 Conventional Vehicle . . . . .	10
1.2.2 Battery-Electric Vehicle . . . . .	11
1.2.3 Vehicle Propulsion System Design . . . . .	12
1.3 Hybrid-Electric Vehicle: Architecture and Control . . . . .	12
1.3.1 Powertrain Architecture . . . . .	12
1.3.2 Powertrain Control . . . . .	15
1.4 Hybrid-Electric Vehicle: Powertrain Design . . . . .	20
1.4.1 Heuristic Design Approach . . . . .	20

1.4.2	Optimal Design Approach . . . . .	21
<b>2</b>	<b>Modeling for Energy Consumption Evaluation</b>	<b>27</b>
2.1	Modeling of Vehicle Propulsion System . . . . .	27
2.2	Internal Combustion Engine . . . . .	29
2.2.1	Dimensioning Parameter . . . . .	29
2.2.2	Analytic Model . . . . .	30
2.2.3	Model Validation . . . . .	34
2.3	Drivetrain . . . . .	38
2.3.1	Dimensioning Parameter . . . . .	40
2.3.2	Analytic Model of Transmissions . . . . .	40
2.3.3	Model Validation . . . . .	42
2.4	Battery . . . . .	45
2.4.1	Dimensioning Parameter . . . . .	45
2.4.2	Analytic Model . . . . .	46
2.4.3	Model Validation . . . . .	47
2.5	Electric Motor/Generator . . . . .	50
2.5.1	Dimensioning Parameter . . . . .	50
2.5.2	Analytic Model . . . . .	51
2.5.3	Model Validation . . . . .	52
2.6	Vehicle Load Estimation . . . . .	57
<b>II</b>	<b>Numeric Evaluation of Energy Consumption for Advanced Vehicle Propulsion Systems</b>	<b>59</b>
<b>3</b>	<b>Energy Consumption Evaluation for Single-Source Vehicles</b>	<b>61</b>
3.1	Simulation Method . . . . .	61
3.1.1	Quasi-static Simulation . . . . .	61
3.1.2	Dynamic Simulation . . . . .	62
3.2	Simulation Set-Up . . . . .	63
3.2.1	Mission Profile . . . . .	63
3.2.2	Signal Flow . . . . .	64
3.3	Numeric Evaluation of Energy Consumption . . . . .	67
3.3.1	Conventional Vehicle . . . . .	67
3.3.2	Battery-Electric Vehicle . . . . .	69
<b>4</b>	<b>Minimal Energy Consumption of Hybrid-Electric Vehicles</b>	<b>71</b>
4.1	Optimal Control Problem Formulation . . . . .	71
4.2	Fully Numeric Solution . . . . .	73
4.3	Semi-Analytic Solution . . . . .	74
4.3.1	Series Hybrid-Electric Vehicle . . . . .	75
4.3.2	Parallel Hybrid-Electric Vehicle . . . . .	77
4.3.3	Summary . . . . .	79

4.4	Approximate Solution . . . . .	79
4.4.1	Fundamentals of GRAB-ECO . . . . .	80
4.4.2	Essential Steps of GRAB-ECO . . . . .	81
4.4.3	Summary . . . . .	86
4.5	Evaluation of Minimal Energy Consumption . . . . .	86
4.5.1	Series Hybrid-Electric Vehicle . . . . .	87
4.5.2	Parallel Hybrid-Electric Vehicle . . . . .	90
<b>III Fully-Analytic Energy Consumption Estimation for Advanced Vehicle Propulsion Systems</b>		<b>95</b>
<b>5</b>	<b>Analytic Energy Consumption of Single-Source Vehicles</b>	<b>97</b>
5.1	Conventional Vehicle . . . . .	97
5.1.1	Fully Analytic Energy Consumption Estimation . . . . .	98
5.1.2	Sensitivity of Dimensioning Parameters . . . . .	99
5.2	Battery-Electric Vehicle . . . . .	100
5.2.1	Fully Analytic Energy Consumption Estimation . . . . .	101
5.2.2	Sensitivity of Dimensioning Parameters . . . . .	102
5.3	Analytic Evaluation of Energy Consumption . . . . .	103
5.3.1	Conventional Vehicle . . . . .	103
5.3.2	Battery-Electric Vehicle . . . . .	104
<b>6</b>	<b>Analytic Minimal Energy Consumption of Hybrid-Electric Vehicles</b>	<b>107</b>
6.1	Series Hybrid-Electric Vehicle . . . . .	107
6.1.1	Auxiliary Power Unit . . . . .	107
6.1.2	Fully Analytic Energy Consumption Estimation . . . . .	109
6.2	Parallel Hybrid-Electric Vehicle . . . . .	109
6.2.1	Analytic Model of Assembled Battery and Motor . . . . .	110
6.2.2	Equivalent Energy Consumption Model . . . . .	111
6.2.3	Fully Analytic Energy Consumption Estimation . . . . .	112
6.3	Analytic Evaluation of Minimal Energy Consumption . . . . .	114
6.3.1	Series Hybrid-Electric Vehicle . . . . .	114
6.3.2	Parallel Hybrid-Electric Vehicle . . . . .	115
<b>IV Design and Control Co-Optimization for Advanced Vehicle Propulsion Systems</b>		<b>117</b>
<b>7</b>	<b>Optimal Design Problem Formulation</b>	<b>119</b>
7.1	Design Objective . . . . .	119
7.2	Design Constraint . . . . .	120
7.2.1	Vehicle Attribute . . . . .	120
7.2.2	Design Space . . . . .	123

7.3	Design Method . . . . .	126
7.3.1	Bi-Level Co-Optimization Approach . . . . .	126
7.3.2	Uni-Level Co-Optimization Approach . . . . .	127
<b>8</b>	<b>Optimal Design of Vehicle Propulsion Systems</b>	<b>129</b>
8.1	Design Optimization of a Conventional Vehicle . . . . .	129
8.1.1	Reference Vehicle . . . . .	129
8.1.2	Optimal Design Problem . . . . .	130
8.1.3	Result and Discussion . . . . .	131
8.2	Design Optimization of a Battery-Electric Vehicle . . . . .	134
8.2.1	Reference Vehicle . . . . .	134
8.2.2	Optimal Design Problem . . . . .	135
8.2.3	Result and Discussion . . . . .	136
8.3	Co-Optimization of a Series Hybrid-Electric Truck . . . . .	139
8.3.1	Reference Vehicle . . . . .	139
8.3.2	Co-Optimization Problem . . . . .	140
8.3.3	Result and Discussion . . . . .	141
8.4	Co-Optimization of a Parallel Hybrid-Electric Vehicle . . . . .	144
8.4.1	Reference Vehicle . . . . .	144
8.4.2	Co-Optimization Problem . . . . .	144
8.4.3	Result and Discussion . . . . .	146
8.5	Co-Optimization of a Parallel Hybrid-Electric Truck . . . . .	153
8.5.1	Reference Vehicle . . . . .	153
8.5.2	Co-Optimization Problem . . . . .	154
8.5.3	Result and Discussion . . . . .	155
	<b>Conclusion</b>	<b>161</b>
	Summary . . . . .	161
	Contribution and Limitation . . . . .	163
	Contribution . . . . .	163
	Limitation . . . . .	164
	Future Work . . . . .	165
	State Constraint . . . . .	165
	Power-Split Hybrid-Electric Vehicle . . . . .	165
	Vehicle Design Criteria . . . . .	165
	Dedicated Solver for FACE . . . . .	165
	<b>Bibliography</b>	<b>167</b>
	<b>A Résumé</b>	<b>175</b>
	<b>B Contour Maps of Chapter 2</b>	<b>177</b>
	B.1 Internal Combustion Engine . . . . .	177
	B.2 Electric Motor/Generator . . . . .	183

---

<b>C Implemented Missions</b>	<b>191</b>
C.1 Main Characteristics . . . . .	191
C.2 Graphical Illustration . . . . .	191
<b>D Detailed Dimension-Related Parameters of Chapter 5</b>	<b>193</b>
D.1 Conventional Vehicle . . . . .	193
D.2 Battery-Electric Vehicle . . . . .	197
<b>E Detailed Dimension-Related Parameters of Chapter 6</b>	<b>205</b>
E.1 Series Hybrid Electric Vehicle . . . . .	205
E.2 Parallel Hybrid Electric Vehicle . . . . .	207
<b>Contents</b>	<b>219</b>



# List of Tables

- 1.1 Energy efficiency targets of three major automotive markets in the near future. . . . . 10
- 1.2 Summary of powertrain design optimization for hybrid- and battery-electric vehicles. . . . . 23
- 2.1 Values of coefficients  $c_{ei}(i = 1, \dots, 6)$  for light-duty engines. . . . . 33
- 2.2 Values of coefficients  $c_{ei}(i = 7, \dots, 14)$  for light-duty engines. . . . . 33
- 2.3 Values of coefficients  $c_{ei}(i = 15, \dots, 21)$  for heavy-duty engines. . . . . 34
- 2.4 Identification set of light-duty engines. . . . . 34
- 2.5 Identification set of heavy-duty engines. . . . . 35
- 2.6 Values of coefficients  $c_{ti}(i = 1, \dots, 5)$  for stepped-ratio transmissions. . . . . 41
- 2.7 Identification set of stepped-ratio transmissions. . . . . 43
- 2.8 Values of coefficients  $c_{bi}(i = 1, \dots, 6)$  for lithium-ion battery. . . . . 47
- 2.9 Values of coefficients  $c_{bi}(i = 7, \dots, 9)$  for lithium-ion battery. . . . . 47
- 2.10 Values of coefficients  $c_{bi}(i = 10, \dots, 17)$  for lithium-ion battery. . . . . 48
- 2.11 Identification set of Li-ion battery cells. . . . . 48
- 2.12 Values of coefficients  $c_{mi}(i = 1, \dots, 18)$  for electric motor/generator. . . . . 52
- 2.13 Values of coefficients  $c_{mi}(i = 20, \dots, 25)$  for electric motor/generator. . . . . 52
- 2.14 Identification set of electric motor/generators in terms of PMSM. . . . . 53
- 2.15 Identification set of electric motor/generators in terms of AIM. . . . . 53
- 3.1 Features of investigated conventional vehicle. . . . . 68
- 3.2 Descriptive and predictive errors of energy consumption with respect to grid-point data. . . . . 69
- 3.3 Features of investigated battery-electric vehicle. . . . . 69
- 3.4 Relative errors of energy consumption based on descriptive and predictive analytic models. . . . . 70
- 4.1 Main features of investigated series hybrid-electric vehicle. . . . . 87
- 4.2 Relative errors of minimal fuel consumption over NEDC. . . . . 88
- 4.3 Comparison of average computation time over NEDC. . . . . 89
- 4.4 Relative errors of minimal fuel consumption over FTP-72. . . . . 90
- 4.5 Relative errors of minimal fuel consumption over HYWFET. . . . . 90
- 4.6 Comparison of average computation time over FTP-72. . . . . 90

4.7	Comparison of average computation time over HYWFET. . . . .	90
4.8	Main features of investigated parallel hybrid-electric vehicle. . . . .	91
4.9	Relative errors of minimal fuel consumption over NEDC. . . . .	92
4.10	Comparison of average computation time over NEDC. . . . .	92
4.11	Relative error of fuel consumption over FTP-72. . . . .	93
4.12	Relative errors of minimal fuel consumption over HYWFET. . . . .	93
4.13	Comparison of average computation time over FTP-72. . . . .	93
4.14	Comparison of average computation time over HYWFET. . . . .	93
5.1	Main features of investigated conventional vehicles. . . . .	104
5.2	Main features of investigated battery-electric vehicles. . . . .	105
6.1	Main features of investigated series hybrid-electric vehicles. . . . .	114
6.2	Main features of investigated parallel hybrid-electric vehicles. . . . .	116
8.1	Features of reference conventional vehicle. . . . .	130
8.2	Dimensioning parameters of optimized conventional vehicles via bi- and uni-level optimization approach based on NEDC. . . . .	132
8.3	Vehicle performance of optimized conventional vehicle compared with reference one. . . . .	132
8.4	Dimensioning parameters of optimized conventional vehicles based on various missions. . . . .	134
8.5	Features of reference battery-electric vehicle. . . . .	134
8.6	Dimensioning parameters of optimized battery-electric vehicles via bi- and uni-level optimization approach based on NEDC. . . . .	137
8.7	Vehicle performance of optimized battery-electric vehicle compared with reference one. . . . .	138
8.8	Dimensioning parameters of optimized battery-electric vehicles based on various missions. . . . .	139
8.9	Vehicle performance of optimized battery-electric vehicles based on various missions. . . . .	139
8.10	Main features of investigated series hybrid-electric vehicle. . . . .	140
8.11	Average computation time of each function evaluation. . . . .	143
8.12	Main features of investigated parallel hybrid-electric vehicle. . . . .	144
8.13	Computational characteristics of bi-level co-optimization via SHM and VHOT. . . . .	147
8.14	Dimensioning parameters of optimized parallel hybrid-electric vehicles based on SHM and VHOT. . . . .	148
8.15	Computational characteristics of bi-level co-optimization approach based on various missions. . . . .	150
8.16	Dimensioning parameters of optimized parallel hybrid-electric vehicles based on various missions. . . . .	151
8.17	Gear ratios of optimized parallel hybrid-electric vehicles based on various missions. . . . .	151

---

8.18 Performance of optimized parallel hybrid-electric vehicles based on various missions. . . . .	151
8.19 Main features of investigated parallel hybrid-electric truck. . . . .	154
8.20 Dimensioning parameters of optimized hybrid-electric truck. . . . .	159
C.1 Features of various missions applied in this thesis. . . . .	191



# List of Figures

- 1 Average CO<sub>2</sub> emissions of new cars in EU in the 2014–2030 time frame, assuming a 3.9% per year and 6.8% per year CO<sub>2</sub> reduction scenario. . . . . 2
- 1.1 Propulsion system of a four-wheel drive conventional vehicle. . . . . 10
- 1.2 Propulsion system of a battery-electric vehicle. . . . . 11
- 1.3 Propulsion system of a series hybrid-electric vehicle. . . . . 13
- 1.4 Propulsion system of a parallel hybrid-electric vehicle. . . . . 14
- 1.5 Propulsion system of a power-split hybrid-electric vehicle. . . . . 15
- 1.6 DP-based nested optimal control techniques. . . . . 19
- 1.7 CVX-based nested optimal control technique. . . . . 20
- 1.8 Optimal design methods for vehicle propulsion systems. . . . . 22
- 2.1 Main powertrain components of a parallel hybrid-electric vehicle. . . . . 28
- 2.2 Corner torque  $T_{cc}$  of an internal combustion engine. . . . . 31
- 2.3 Speed variables of turbocharged internal combustion engines. . . . . 32
- 2.4 Map of burned fuel power of light-duty engine ID1. . . . . 35
- 2.5 Efficiency map of heavy-duty engine ID2. . . . . 36
- 2.6 Mean relative error of each engine and the whole identification set. . . . . 37
- 2.7 Maps of relative errors of light-duty engine ID1. . . . . 37
- 2.8 Comparison of burned fuel power for light-duty engine ID1. . . . . 37
- 2.9 Maps of relative errors of heavy-duty engine ID2. . . . . 38
- 2.10 Comparison of burned fuel power for heavy-duty engine ID2. . . . . 38
- 2.11 Universal configuration of vehicle propulsion systems. . . . . 39
- 2.12 Gear ratio comparison of transmission identification set. . . . . 44
- 2.13 Fuel consumption evaluated with grid-point data, description, and prediction of stepped-ratio transmissions. . . . . 44
- 2.14 Output power comparison of stepped-ratio transmission. . . . . 45
- 2.15 Electrochemical power of battery cell ID2. . . . . 49
- 2.16 Mean relative errors of battery identification set. . . . . 50
- 2.17 Comparison of electrochemical power of battery for battery cell ID2. . . . . 50
- 2.18 Efficiency map of PMSM ID14. . . . . 54
- 2.19 Efficiency map of AIM ID14. . . . . 54
- 2.20 Mean relative error of each electric motor/generator and the whole identification set. . . . . 55

2.21	Maps of relative errors of PMSM ID14. . . . .	55
2.22	Maps of relative errors of AIM ID14. . . . .	56
2.23	Comparison of electric power of PMSM ID14. . . . .	56
2.24	Comparison of electric power of AIM ID14. . . . .	56
2.25	Longitudinal forces acting on a vehicle moving on an inclined road. . . . .	57
3.1	Quasi-static simulation for energy consumption evaluation. . . . .	62
3.2	Dynamic simulation for energy consumption evaluation. . . . .	63
3.3	Speed trajectory of NEDC. . . . .	64
3.4	Gear shift schedule over NEDC. . . . .	64
3.5	Quasi-static simulation for conventional vehicles. . . . .	65
3.6	Quasi-static simulation for battery-electric vehicles. . . . .	65
3.7	Quasi-static simulation for series hybrid-electric vehicles. . . . .	66
3.8	Quasi-static simulation for parallel hybrid-electric vehicles. . . . .	67
3.9	Fuel consumption of reference conventional vehicle based on different types of powertrain component models. . . . .	68
3.10	Energy consumption of reference battery-electric vehicle based on different types of powertrain component models. . . . .	70
4.1	Flow chart of PMP-based standard approaches. . . . .	74
4.2	Flow chart of SHM. . . . .	75
4.3	Flow chart of GRAB-ECO. . . . .	80
4.4	Example of best-efficient indicator and power of drivetrain over NEDC. . . . .	82
4.5	Example of mapping between actual and sorted time index over NEDC. . . . .	82
4.6	Example of sorted variables over NEDC. . . . .	83
4.7	Operating mode determination of GRAB-ECO for parallel HEVs. . . . .	84
4.8	Resulting electrochemical energy of battery in accordance with the operating modes. . . . .	85
4.9	Minimal energy consumption of reference series HEV over NEDC. . . . .	88
4.10	Minimal energy consumption of reference series HEV over FTP-72 and HYWFET. . . . .	89
4.11	Minimal energy consumption of reference parallel HEV over NEDC. . . . .	92
4.12	Minimal energy consumption of reference parallel HEV over FTP-72 and HYWFET. . . . .	93
5.1	Fuel consumption of conventional vehicles evaluated through QSS and FACE. . . . .	105
5.2	Energy consumption of battery-electric vehicles evaluated with QSS and FACE . . . . .	106
6.1	Best-efficiency point of APU in terms of gear ratio. . . . .	108
6.2	Best-efficiency point of APU in terms of engine displacement. . . . .	108
6.3	Minimal fuel consumption of different battery models. . . . .	111
6.4	Equivalent minimal fuel consumption of hybrid-electric vehicles. . . . .	112

6.5	Minimal energy consumption of reference and investigated series hybrid-electric vehicles. . . . .	115
6.6	Minimal energy consumption of reference and investigated parallel hybrid electric vehicles. . . . .	116
7.1	Comparison of estimated and published acceleration time for conventional vehicles. . . . .	122
7.2	Comparison of estimated and published acceleration time for battery-electric vehicles. . . . .	123
7.3	Comparison of rated torque and torque of rated power for SI/TC engines.	125
7.4	Comparison of rated torque and torque of rated power for SI/NA engines.	125
7.5	Comparison of rated torque and torque of rated power for CI/TC engines.	125
7.6	Scheme of bi-level co-optimization approach. . . . .	126
7.7	Scheme of uni-level co-optimization approach. . . . .	127
8.1	Energy consumption of optimized and reference conventional vehicles over NEDC. . . . .	132
8.2	Acceleration performance of optimized and reference conventional vehicles.	133
8.3	Energy consumption of optimized conventional vehicles over different missions. . . . .	133
8.4	Energy consumption of reference and optimized battery-electric vehicles over NEDC. . . . .	137
8.5	Acceleration performance of optimized and reference battery-electric vehicle. . . . .	138
8.6	Energy consumption of optimized battery-electric vehicles over different missions. . . . .	139
8.7	Speed trajectory of ICDC. . . . .	141
8.8	Speed trajectory of SUDC. . . . .	141
8.9	Energy consumption in function of gear ratio between engine and generator.	142
8.10	Energy consumption in function of battery cell number. . . . .	142
8.11	Energy consumption in function of rated torque of traction motor. . . . .	143
8.12	Energy consumption in function of rated power of traction motor. . . . .	143
8.13	Trajectory of bi-level co-optimization through SHM. . . . .	147
8.14	Trajectory comparison of bi-level co-optimization through SHM and VHOT.	147
8.15	Trajectory of relevant signals over NEDC. . . . .	149
8.16	Energy consumption of reference and optimized parallel hybrid-electric vehicles over different missions. . . . .	150
8.17	Operating mode percentage in terms of time and demanded energy. . . . .	150
8.18	Acceleration performance of optimized and reference parallel hybrid-electric vehicles. . . . .	151
8.19	Influence of engine displacement on fuel consumption. . . . .	152
8.20	Influence of battery cell capacity on fuel consumption. . . . .	153
8.21	Investigated mission for reference hybrid-electric truck. . . . .	153
8.22	Minimal fuel consumption of the reference hybrid-electric truck. . . . .	156

8.23	Minimized fuel consumption of different powertrain control optimizations.	156
8.24	Trajectory of varied electrochemical energy of battery over investigated mission. . . . .	157
8.25	Optimized gear shift schedule over the mission. . . . .	157
8.26	Operating points of internal combustion engine on its fuel consumption map. . . . .	158
8.27	Minimized fuel consumption of powertrain control and design optimizations. . . . .	158
B.1	Map of burned fuel power of light-duty engine ID2. . . . .	177
B.2	Map of burned fuel power of light-duty engine ID3. . . . .	178
B.3	Map of burned fuel power of light-duty engine ID4. . . . .	178
B.4	Map of burned fuel power of light-duty engine ID5. . . . .	178
B.5	Map of burned fuel power of light-duty engine ID6. . . . .	178
B.6	Map of burned fuel power of light-duty engine ID7. . . . .	179
B.7	Map of burned fuel power of light-duty engine ID8. . . . .	179
B.8	Map of burned fuel power of light-duty engine ID9. . . . .	179
B.9	Map of burned fuel power of light-duty engine ID10. . . . .	179
B.10	Map of burned fuel power of light-duty engine ID11. . . . .	180
B.11	Map of burned fuel power of light-duty engine ID12. . . . .	180
B.12	Map of burned fuel power of light-duty engine ID13. . . . .	180
B.13	Map of burned fuel power of light-duty engine ID14. . . . .	180
B.14	Efficiency map of heavy-duty engine ID1. . . . .	181
B.15	Efficiency map of heavy-duty engine ID3. . . . .	181
B.16	Efficiency map of heavy-duty engine ID4. . . . .	181
B.17	Efficiency map of heavy-duty engine ID5. . . . .	181
B.18	Efficiency map of heavy-duty engine ID6. . . . .	182
B.19	Efficiency map of heavy-duty engine ID7. . . . .	182
B.20	Efficiency map of heavy-duty engine ID8. . . . .	182
B.21	Efficiency map of heavy-duty engine ID9. . . . .	182
B.22	Efficiency map of heavy-duty engine ID10. . . . .	183
B.23	Efficiency map of PMSM ID1. . . . .	183
B.24	Efficiency map of PMSM ID2. . . . .	183
B.25	Efficiency map of PMSM ID3. . . . .	184
B.26	Efficiency map of PMSM ID4. . . . .	184
B.27	Efficiency map of PMSM ID5. . . . .	184
B.28	Efficiency map of PMSM ID6. . . . .	184
B.29	Efficiency map of PMSM ID7. . . . .	185
B.30	Efficiency map of PMSM ID8. . . . .	185
B.31	Efficiency map of PMSM ID9. . . . .	185
B.32	Efficiency map of PMSM ID10. . . . .	185
B.33	Efficiency map of PMSM ID11. . . . .	186
B.34	Efficiency map of PMSM ID12. . . . .	186

---

B.35 Efficiency map of PMSM ID13. . . . .	186
B.36 Efficiency map of PMSM ID15. . . . .	186
B.37 Efficiency map of AIM ID1. . . . .	187
B.38 Efficiency map of AIM ID2. . . . .	187
B.39 Efficiency map of AIM ID3. . . . .	187
B.40 Efficiency map of AIM ID4. . . . .	187
B.41 Efficiency map of AIM ID5. . . . .	188
B.42 Efficiency map of AIM ID6. . . . .	188
B.43 Efficiency map of AIM ID7. . . . .	188
B.44 Efficiency map of AIM ID8. . . . .	188
B.45 Efficiency map of AIM ID9. . . . .	189
B.46 Efficiency map of AIM ID10. . . . .	189
B.47 Efficiency map of AIM ID11. . . . .	189
B.48 Efficiency map of AIM ID12. . . . .	189
B.49 Efficiency map of AIM ID13. . . . .	190
B.50 Efficiency map of AIM ID15. . . . .	190
B.51 Efficiency map of AIM ID16. . . . .	190
C.1 Speed trajectory of FTP-72. . . . .	192
C.2 Gear shift schedule of FTP-72. . . . .	192
C.3 Speed trajectory of HYWFET. . . . .	192
C.4 Gear shift schedule of HYWFET. . . . .	192



# Introduction

## Background

Transport sector consumes more than half of global oil production, which is more than a quarter of global final energy [1] and leads to the anthropogenic CO<sub>2</sub> emissions. The level of CO<sub>2</sub> emissions in the transport sector increased from 15% in year 1990 to 23.2% in year 2014<sup>1</sup>. In particular, road transportation, including light- and heavy-duty vehicles, took up almost three quarters of the total amount in year 2010 [2].

Large amounts of CO<sub>2</sub> emissions have brought a series of public concerns on climate change, energy security, environmental issues, etc. In reaction to public concerns, the European Union (EU) legislation sets mandatory targets of emission reduction for new vehicles. As illustrated in Fig. 1, new passenger cars and light-commercial vehicles (vans) are subject to mandatory and stringent CO<sub>2</sub> emission standards, which is to reduce the level of average CO<sub>2</sub> emissions to 95 and 147 g/km by year 2021 for new passenger cars and light-commercial vehicles, respectively. Moreover, the European Parliament recommended an "indicative range" in 2013 for a 2025 new-car CO<sub>2</sub> emission target of 68-78 g/km (in NEDC terms) and, if "duly justified," consideration of a lower target as well (Fig. 1) [3].

Concerning heavy-duty vehicles, their CO<sub>2</sub> emissions are reduced by the market-driven competition in European countries, although European market is the only major vehicle market without mandatory CO<sub>2</sub> emission standards around the world [3].

To meet the stringent CO<sub>2</sub> emission targets, advanced technologies of vehicle design, propulsion system design, and powertrain control are highly demanded. Concerning vehicle design, novel vehicle propulsion systems, light-weight design, new materials, etc. can help reduce CO<sub>2</sub> emissions. As for the design of vehicle propulsion systems, proper selection of powertrain configurations, well-sized dimensions of powertrain compo-

---

<sup>1</sup>Eurostat Statistics Explained – Greenhouse gas emission statistics (last update: December, 2016), [http://ec.europa.eu/eurostat/statistics-explained/index.php/Greenhouse\\_gas\\_emission\\_statistics](http://ec.europa.eu/eurostat/statistics-explained/index.php/Greenhouse_gas_emission_statistics)

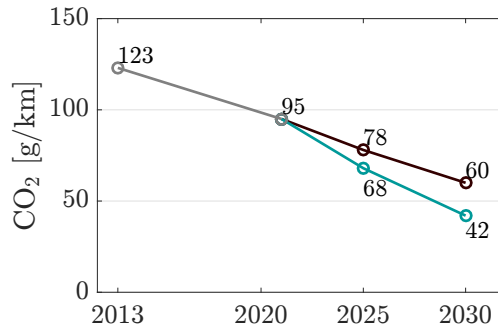


Figure 1 – Average CO<sub>2</sub> emissions of new cars in EU in the 2014–2030 time frame, assuming a 3.9% per year and 6.8% per year CO<sub>2</sub> reduction scenario.

nents, and efficiency-improved powertrain components are of great help to reduce CO<sub>2</sub> emissions. Regarding powertrain control, novel technologies, such as optimal energy management in hybrid-electric vehicles and intelligent transportation, are capable of further decreasing CO<sub>2</sub> emissions.

## Motivation

The energy consumption and corresponding CO<sub>2</sub> emissions of a vehicle are affected by powertrain dimensions (e.g. engine displacement), powertrain control (e.g. energy management strategy), vehicle parameters (e.g. aerodynamic properties), missions, etc. As an efficient approach, numeric simulation is often implemented to analyze and validate the design of new vehicle concepts, especially for the estimation of energy consumption. Furthermore, numeric simulation plays a vital role in the development of powertrain control, such as the energy management strategy for a hybrid-electric vehicle.

Numeric simulation greatly facilitates optimal designs of vehicle propulsion systems. In a single-source vehicle (conventional or battery-electric vehicle), dimensioning parameters of powertrain components are selected to reduce energy consumption through exhaustive or trial-and-error simulations. Compared with hybrid-electric vehicles, single-source vehicles have a less complex powertrain control. Therefore, optimal design of vehicle propulsion systems of single-source vehicles can be easily realized through numeric simulations for the least energy consumption. Because of lack of powertrain control in the numeric simulation of backward approach, the optimal design process takes reasonable computation time.

On the contrary, optimal design of hybrid-electric vehicles confronts high complexities. The complexities are caused by multiple powertrain architectures, various powertrain components, indispensable powertrain control, and the resulting higher number of degrees of freedom. To achieve the minimum energy consumption, the optimal control of powertrain must be considered rather than heuristic control during the optimal design process. Therefore, a co-optimization of design and control problem is raised and tailored for hybrid-electric vehicles.

To solve the co-optimization of design and control for hybrid-electric vehicles, bi-level co-optimization approach is frequently implemented to find the optimal design such that the energy consumption is minimized. The bi-level co-optimization approach selects the optimal dimensioning parameters of powertrain components by an optimizer at the outer level; whereas the energy consumption is minimized via optimal control techniques at the inner level. Because of massive evaluations in the outer level and the embedded optimal control of each evaluation in the co-optimization process, it takes too much computation time to complete the. For example, it took about one hundred hours to entirely optimize four types of parameters for the optimal design of a parallel hybrid-electric vehicle with heuristic control laws [4]. In a co-optimization process, it took more than eight hours to optimize the design and control parameters in the application of series and parallel hybrid-electric vehicles [5]. Concerning the computation time of optimal control technique, a combined dynamic programming and Pontryagin's minimum principle needs nine seconds to evaluate the minimum fuel consumption [6]; whereas an enhanced dynamic programming by the implementation of analytic formulation still requires five seconds [7].

## Objective

In the subject of co-optimization of control and design for advanced vehicle propulsion systems, the ultimate goal is to optimize the dimensioning parameters of powertrain components for various vehicle propulsion systems within shortened computation time compared with current technologies.

Regarding the bi-level co-optimization approach, it consists of two levels that are dedicated to design optimization and control optimization. To achieve the reduction of computation time in the co-optimization process, novel techniques of powertrain control are investigated for hybrid-electric vehicles. The requirement of novel optimal control techniques must be fast-running and accurate.

In addition to the improvement on the computational efficiency for the bi-level

co-optimization approach, an inaugural uni-level co-optimization approach is proposed to optimize the design of vehicle propulsion systems with the instantaneous estimation of the minimum fuel consumption. In the uni-level co-optimization approach, the instantaneous estimation of the minimum fuel consumption is done by a fully analytic energy consumption estimation method (FACE) that is valid for various types of vehicle propulsion systems, such as conventional, battery-electric, and hybrid-electric ones. The FACE shows the explicit relation between energy consumption and dimensioning parameters of powertrain components as well.

To achieve the aforementioned objectives, the thesis is organized with four parts. Part I summarizes the state-of-the-art review of optimal design for current vehicle propulsion systems in Chapter 1 and the analytic models of vehicle propulsion systems for the development of the novel powertrain control techniques and the uni-level co-optimization approach in Chapter 2.

Numeric evaluations of energy consumption for single-source and hybrid-electric are introduced in Part II, where Chapter 3 describes quasi-static simulation approaches for conventional, battery-electric, and hybrid-electric vehicles. The novel techniques of optimal control for hybrid-electric vehicles, including Selective Hamiltonian Minimization and Graphical-Analysis-Based Energy Consumption Optimization, are detailed in Chapter 4. On the contrary, the fully analytic energy consumption estimation method is presented in Part III, where the one for single-source and for hybrid-electric vehicles are in Chapter 5 and 6, respectively.

General design issues and case studies are found in Part IV to demonstrate the capabilities of the proposed optimal control methods and the uni-level co-optimization approach. Chapter 7 formulates the generic optimal design problem, whereas Chapter 8 summarized several case studies including conventional, battery-electric, and hybrid-electric vehicles. The conclusion, including contributions, limitations, and future work, is summarized at the end of this thesis.

## **Contribution**

The main contributions of this thesis are summarized into three aspects, which are the descriptive and predictive analytic models of powertrain components, fast-running methods for control optimization of hybrid-electric vehicles, and the uni-level co-optimization of design and control for hybrid-electric vehicles.

As a fundamental to achieve the objective of this thesis, powertrain components are modeled analytically at two different levels, which are the descriptive and predictive

level. The analytic models of the descriptive level aim at describing energy losses of an individual powertrain component, whereas analytic models of the predictive level are capable of scaling a powertrain component to different dimensioning parameters in its corresponding identified set. Thanks to the analytic models, the computation time of the energy evaluation can be further reduced compared with the numeric simulation of grid-point data.

Based on the analytic models of powertrain components, two types of control optimization are developed that significantly reduce the computation time of the evaluation of the minimal energy consumption for a given hybrid-electric vehicle. These two novel control optimization techniques are Selective Hamiltonian Minimization (SHM) and GRaphical-Analysis-Based Energy Consumption Optimization (GRAB-ECO), which are developed based on Pontryagin's Minimum Principle and the maximization of the average operating efficiency of the primary energy source, respectively.

Moreover, Fully-Analytic energy Consumption Estimation (FACE) is developed to estimate the (minimal) energy consumption for various types of vehicle propulsion systems. The uni-level co-optimization method optimizes the dimensioning parameters of powertrain components such that the energy consumption evaluated by FACE is minimized. The instantaneous estimation of energy consumption contributes to reducing the total computation time of uni-level co-optimization process.

Part work of this thesis has been the subject of the following publications:

- Jianning Zhao, and Antonio Sciarretta. "Design and Control Co-Optimization for Hybrid Powertrains: Development of Dedicated Optimal Energy Management Strategy." *IFAC-PapersOnLine* 49.11 (2016): 277-284.
- Jianning Zhao, and Antonio Sciarretta. "A Fully-Analytical Fuel Consumption Estimation for the Optimal Design of Light-and Heavy-Duty Series Hybrid Electric Powertrains." No. 2017-01-0522. SAE Technical Paper, 2017.
- Jianning Zhao, Antonio Sciarretta, and Lars Eriksson. "GRAB-ECO for Minimal Fuel Consumption Estimation of Parallel Hybrid-Electric Vehicles." *Oil & Gas Science and Technology Rev. IFP Energies nouvelles*, 72.6 (2017): 39.



**Part I**

**Modeling of Advanced Vehicle  
Propulsion Systems**



# State-of-the-Art Review

State-of-the-art review of the co-optimization of design and control for advanced vehicle propulsion systems is concisely synthesized from the latest literatures on powertrain components and vehicle propulsion systems.

## 1.1 Need for Better Energy Efficiency

In response to the global climate change caused by Green-House Gas (GHG)s, CO<sub>2</sub> emissions are stringently regulated on the new vehicle models in the worldwide automotive industry. Considering CO<sub>2</sub> emissions of a Light-Duty Vehicle (LDV), regulations on passenger cars and light-duty commercial vehicles have been adopted globally. Details of three major automotive markets around the world are exemplified in Table 1.1. In the near future, CO<sub>2</sub> emissions of 95 g/km and 143 g/mi are obliged to achieve in EU and US, receptively; whereas, fuel consumption of 5 L/hkm (hkm: hundred kilometers) is mandatory in China. Nevertheless, more stringent energy efficiency targets in terms of CO<sub>2</sub> emissions or fuel consumption are under development. The continuously improved energy efficiency targets advance powertrain technologies and innovations, for example, market penetration of battery-electric and hybrid-electric vehicles.

Compared with the obliged energy efficiency targets of LDVs, the one of a Heavy-Duty Vehicle (HDV) is less widely controlled by regulations around the world. The main reason is due to the European countries, where a market-driven policy of the energy efficiency is adopted rather than mandatory CO<sub>2</sub> emission targets. However, targets of the energy efficiency of HDVs have been regulated in China and US by Phase 2 and Phase 1 (2014-2018), respectively. In the future, HDVs in all three major markets

Region	Target Year	Standard Type	Fleet Target
European Union	2021	CO <sub>2</sub>	95 gCO <sub>2</sub> /km
China	2020	fuel consumption	5 L/100km
United States	2025	fuel economy/ CO <sub>2</sub> +other GHGs	56.2 mpg or 143 gCO <sub>2</sub> /mi

Table 1.1 – Energy efficiency targets of three major automotive markets in the near future.

must meet more stringent energy efficiency targets because of the development of CO<sub>2</sub> emission certification, monitoring, reporting, and standards in EU.

## 1.2 Single-Source Vehicle

### 1.2.1 Conventional Vehicle

As a leading player in the automotive market, conventional vehicle must meet the stringent regulations on fuel consumption and pollutant emissions. Technologies to improve fuel efficiency concentrate on the continuous improvement of powertrain components, which are essentially composed of an internal combustion engine, a transmission, and a final drive (see Fig. 1.1).

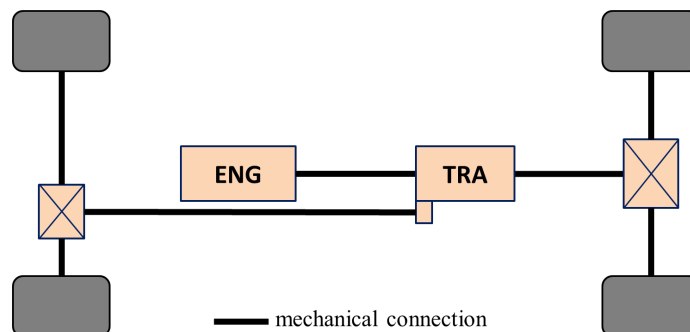


Figure 1.1 – Propulsion system of a four-wheel drive conventional vehicle.

Considering internal combustion engines, their efficiencies are always under improvement by advanced technologies, which consist of engine downsizing technology [8], turbocharger technology [9], friction reduction technology [10], variable compression ratio technology [11], alternative fuels [12], and the advanced combustion technology [13]. However, details of these technologies are out of the scope of this thesis work. Nonetheless, some of them are used as dimensioning parameters to develop the pre-

dictive analytic models for internal combustions. For instance, the implementation of turbocharger affects the descriptive analytic models.

As for transmissions, current technologies include advanced gear ratio design [14], implementation of higher gear number [15], sophisticated shift strategy [16], highly efficient transmission [15], and advanced automatic transmissions [17, 18], which directly influence the fuel consumption of a conventional vehicle. Therefore, the optimization of transmission dimensioning parameters is capable of further improving the energy efficiency.

In addition to technologies of engines and transmissions, stop-start systems are implemented to conventional vehicles so that the idling fuel consumption is eliminated [19]. Throughout this thesis, the idling fuel consumption is not considered in conventional and hybrid-electric vehicles, due to the wide application of stop-start systems.

### 1.2.2 Battery-Electric Vehicle

Battery electric vehicle, as a technological endpoint to achieve tank-to-wheel zero emission, is continuously penetrating the automotive market around the world. As shown in Fig. 1.2, key powertrain components of a battery-electric vehicle consist of an electric motor/generator, a battery, a power electronics, and a transmission.

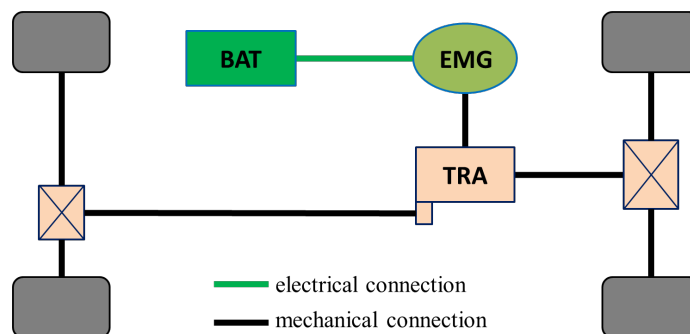


Figure 1.2 – Propulsion system of a battery-electric vehicle.

The main technological concerns on battery-electric vehicles are over the electric vehicle range, battery cost and lifespan, performance in cold weather, maintenance, available charging infrastructures. Nonetheless, the energy consumption of a battery-electric vehicle can be further reduced by improvements on powertrain efficiency, power electronics, aerodynamics, and light-weighting technologies, which enlarges electric vehicle range in turn [20].

Recent studies show that the optimized design of power electronics [21], suitable topology of transmission [22], and intelligent control technologies – such as gear shift schedule design [23] and eco-driving technique [24] – are capable of enhancing the powertrain efficiency of a battery-electric vehicle.

### **1.2.3 Vehicle Propulsion System Design**

To meet the desired vehicle performance, single-source vehicle propulsion systems for conventional and battery-electric vehicles are often designed through heuristic methods, such as an iterative process to find suitable powertrain components that meet the requirement. Despite lack of systematic design optimization approach, the design of a battery-electric vehicle can be optimized by finding the best dimensioning parameters of powertrain components such that the energy consumption is minimized. A battery-electric vehicle is optimally designed through multi-objective optimization method by optimizing dimensioning parameters of electric motor and battery size to meet the design targets defined by drivability parameters [25]. Alternatively, genetic algorithm method is also used to optimize the design of an battery-electric vehicle with two-speed dual-clutch transmission at system level [26].

## **1.3 Hybrid-Electric Vehicle: Architecture and Control**

The propulsion system of a Hybrid Electric Vehicle (HEV) is characterized by multiple energy sources, which are internal combustion engine and battery. A Vehicle Propulsion System (VPS) of a hybrid-electric vehicle consists of powertrain components of conventional and battery-electric vehicles. Moreover, several aspects of hybrid-electric vehicles are of essence, including powertrain architecture, powertrain control, and VPS design, of which the first two aspects are introduced in this section.

### **1.3.1 Powertrain Architecture**

Hybridization of conventional vehicles can be realized in three different basic architectures, including series, parallel, and power-split architecture. Sub-configurations of each basic architecture may exist, such as pre-transmission and through-the-road configuration in the parallel architecture.

### Series HEV

A series hybrid-electric vehicle consists of a propulsion system in which two electrical power sources feed a single electric traction motor that propels the vehicle. A simplified configuration with the major powertrain components is sketched in Fig. 1.3. The unidirectional energy converter, which is an internal combustion engine, is mechanically coupled to an electric generator through a simple gear train or rigid connection, which are usually referred to as Auxiliary Power Unit (APU). The bidirectional energy source is a battery pack that provides and stores electrical energy during different operating phase of a hybrid-electric VPS. Power electronics manages all of the electrical power flows in the propulsion system.

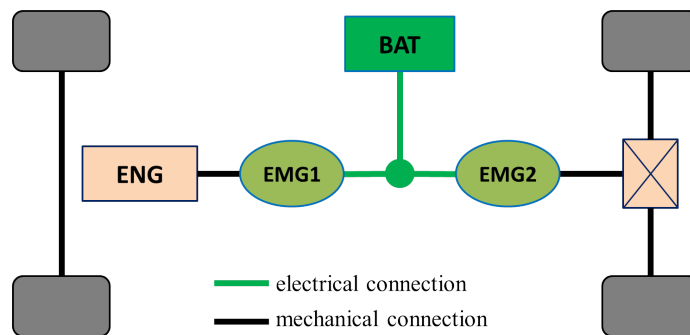


Figure 1.3 – Propulsion system of a series hybrid-electric vehicle.

In a series HEV, the full electrical connection between power sources and driven wheels is through an electric traction motor, instead of a mechanical transmission. This substitution allows the internal combustion engine to potentially operate at the desired region, such as maximum efficiency zone, according to the control objectives. Therefore, the performance of the internal combustion engine, such as efficiency and emissions, may be further improved by design and calibration. On the other hand, the absence of transmission results in a simple powertrain structure. Furthermore, the energy management of this hybrid architecture is simple, since internal combustion engine is often controlled to be more efficient.

However, disadvantages of series HEV are obvious. One is the poor efficiency of whole propulsion system resulting from multiple conversions of energy between electrical and mechanical form. Another one is the additional cost and weight by adding the electric motor/generator in APU. Additionally, traction motors are not so competitive as internal combustion engines in the heavy-duty application.

### Parallel HEV

A parallel hybrid-electric vehicle consists of a propulsion system in which one mechanical power and one electrical power source propel the vehicle through a transmission or directly. Simplified configurations of parallel HEVs with the major powertrain components are sketched in Fig. 1.4. The unidirectional energy converter (internal combustion engine), is mechanically coupled to the driven wheels through a transmission; whereas the bidirectional energy source (battery pack) provides and stores electrical energy in the propelling and braking phase, respectively. Power electronics manages the electrical power flows in the propulsion system.

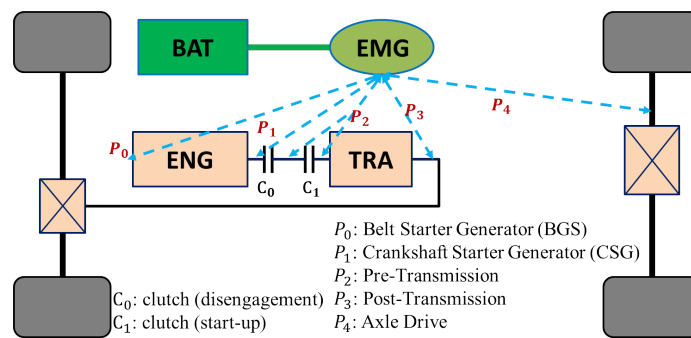


Figure 1.4 – Propulsion system of a parallel hybrid-electric vehicle.

In a parallel HEV, the mechanical connection between internal combustion engine and driven wheels remains the same as that in a conventional VPS. However, electric motor/generator propels the driven wheels either through the transmission or directly according to the coupling position between the mechanical drivetrain and electric motor/generator. Furthermore, different coupling positions result in several configurations, which are composed of  $P_0$  (belt-driven stator generator),  $P_1$  (crankshaft-mounted stator generator),  $P_2$  (pre-transmission),  $P_3$  (post-transmission), and  $P_4$  (axle drive) as depicted in Fig. 1.4.

As many attributes of a conventional VPS are preserved, parallel HEV allows direct torque supply from both engine and electric motor/generator to the driven wheels, which makes the energy losses possibly less. The vehicle propulsion system of a parallel hybrid is compact since it is unnecessary for an additional electric generator and smaller dimensions of the electric traction motor than that in series HEV.

However, the mechanical coupling between the engine and driven wheels with an additional electric motor/generator causes the complex problems, such as energy management, and drivability issues.

### Power-Split HEV

A power-split hybrid-electric vehicle consists of one mechanical and one electrical power source propelling the vehicle through a planetary gear set. Simplified power-split HEV with the major powertrain components is sketched in Fig. 1.5. The unidirectional energy converter (internal combustion engine) is mechanically coupled to the driven wheels and an electric motor/generator (denoted by EMG1) through a planetary gear set; whereas the bidirectional energy source (battery pack) provides and stores electrical energy via both electric motor/generators depending on vehicle's operating modes. Power electronics manages all of the electrical power flows in the propulsion system.

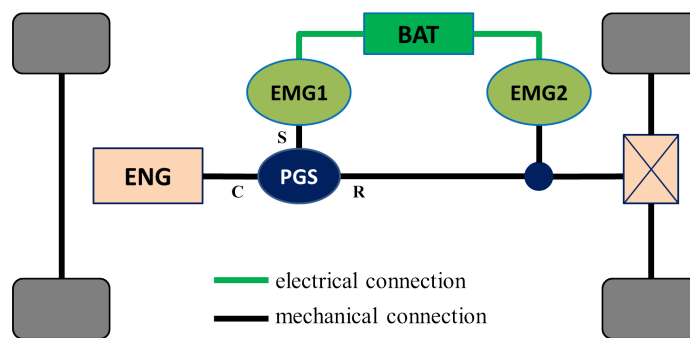


Figure 1.5 – Propulsion system of a power-split hybrid-electric vehicle.

In a power-split HEV, the mechanical connection between internal combustion engine and driven wheels is realized through a planetary gear set. Thanks to an additional mechanical connection of the planetary gear set and another mechanical coupler, two electric motor/generators are implemented in this architecture. Both internal combustion engine and electric motor/generator EMG2 can propel the driven wheels; and both EMG1 and EMG2 are capable of recharging the battery.

Compared with parallel HEVs, power-split HEVs benefit better fuel economy, drivability, and electric drive efficiency; however, the maximum vehicle speed and grade capability are not as good as parallel HEVs [27].

#### 1.3.2 Powertrain Control

In an HEV, powertrain control manages power flows to meet the desired operation. Particularly, optimal control has been investigated for almost forty years to achieve the minimum fuel consumption since dynamic programming was firstly introduced in [28]. To homogeneously benchmark the optimal design of a hybrid-electric vehicle propulsion system, optimal control techniques are implemented that consist of Dynamic

Programming (DP), Pontryagin's Minimum Principle (PMP), Convex Optimization (CVX), and their variants.

The optimal control problem of a hybrid-electric vehicle consists of finding the optimal signal of control variables, for instance battery power in a series HEV and motor power in a parallel HEV, such that the fuel consumption is minimized and the final state of charge of the battery meets the desired value, such as maintaining the same as its initial one. Assuming that battery electrochemical power is independent from the state of charge, the optimal control problem is summarized as

$$\min_{u \in U} \int_{t_0}^{t_f} P_{ef}(u(t), t) dt, \quad (1.1)$$

$$s.t. \dot{x}(t) = P_{be}(u(t), t), \quad (1.2)$$

$$x(t_0) = E_{be0}, x(t_f) = E_{be0}, \quad (1.3)$$

$$h(u(t), t) = 0, \quad (1.4)$$

$$g_i(u(t), t) \leq 0, \quad \text{for each } i \in \{1, \dots, m\}, \quad (1.5)$$

where the optimal control problem is over time horizon  $[t_0, t_f]$ ; the control variable  $u$  in its admissible set  $U$  is defined depending on the hybrid powertrain architecture; the burned fuel power  $P_{ef}$  estimates the fuel consumption over an investigated mission; the system dynamics  $\dot{x}$  is defined by the electrochemical power of battery; the initial and final state  $x$  are equal to the battery energy  $E_{be0}$ ; the equality constraint  $h(u(t), t)$  refers to the power balance; and the in-equality constraints  $g_i(u(t), t)$  represent the operating constraints due to physical limits of powertrain components. For example, the operating power of an electric motor must be always constrained within its limits ( $P_m \in [\underline{P}_m, \bar{P}_m]$ ). The constraint of system dynamics is not considered throughout this thesis.

### Pontryagin's Minimum Principle

Embodied by variational methods, Pontryagin's Minimum Principle (PMP) states a necessary condition that must hold on an optimal trajectory. For the optimal control problem in Eq. 1.1, the Hamiltonian function is defined as

$$H(u(t), s(t), t) = P_{ef}(u(t), t) + s(t)P_{be}(u(t), t), \quad (1.6)$$

where  $s$  is a scalar adjoint variable.

PMP states that if  $u^*(t)$  is the optimal control law for problem in Eq. 1.1, the following conditions are satisfied: (1) the state and adjoint state must satisfy the following

conditions:

$$\dot{x}^*(t) = \left. \frac{\partial H}{\partial s} \right|_{u^*(t)} = P_{be}(u^*(t), t), \quad (1.7)$$

$$\dot{s}^*(t) = \left. \frac{\partial H}{\partial x} \right|_{u^*(t)} = 0, \quad (1.8)$$

$$x^*(t_0) = E_{be0}, \quad (1.9)$$

$$x^*(t_f) = E_{be0}, \quad (1.10)$$

(2) for all  $t \in [t_0, t_f]$ ,  $u^*(t)$  globally minimizes the Hamiltonian:

$$H(u(t), s^*(t), t) \geq H(u^*(t), s^*(t), t), \quad \forall u \in U, \forall t \in [t_0, t_f],$$

i.e., the optimal solution  $u^*(t)$  is such that

$$u^*(t) = \underset{\substack{h(u,t)=0 \\ g(u,t) \leq 0}}{\operatorname{arg\,min}} H(u, s^*, t), \quad (1.11)$$

where  $s$  is a constant adjoint state, the minimization of Hamiltonian function can be solved either through numeric computation or by analytic solution.

### Dynamic Programming

Dynamic programming, as an alternative optimal control technique to solve the optimal control problem of HEVs, is based on the Bellman's Principle of Optimality [29]:

An optimal policy has the property that whatever the initial state and the initial decisions are, the remaining decisions must constitute an optimal policy with regard to the state resulting from the first decisions. Alternatively, from any point on an optimal state space trajectory, the remaining trajectory is optimal for the corresponding problem initiated at that point.

As the Principle of Optimality implies, a complex optimal control problem is solved by breaking the problem down into a collection of simpler subproblems, and then computed "backwards". Accordingly, the formulation is discretized by sampling period  $\Delta t$  to  $x(k)$  and  $u(k)$ ,  $k = 0, \dots, N - 1$ . The system dynamics is expressed by a difference equation,

$$x(k+1) = f(x(k), u(k), k). \quad (1.12)$$

The objective function in Eq. 1.1 is replaced by

$$J(u(k)) = \sum_0^{N-1} P_{ef}(x(k), u(k)). \quad (1.13)$$

In practice, implementation of DP requires the state variable to be quantified. Hence, the curse of dimensionality is induced. As a result, computational load of DP is not negligible, especially in the massive evaluations.

### Convex Optimization

Convex Optimization (CVX) is also implemented to solve optimal control problems of HEVs. As indicated, CVX minimizes objective function which is convex over convex sets. Detailed theory of CVX is introduced in [30].

To implement CVX in the energy management problem of an HEV, the core is the convexification of the optimal control problem. The objective functional and constraints must be adapted to be convex. Therefore, the objective function in Eq. 1.1 and inequality constraints in Eq. 1.5 must be convex functions, and the equality constraints Eq. 1.4 are affine. With the convex formulation, the optimal control problem can be solved through convex optimization. However, convexification is always challenging due to inevitable non-convex models and signals during the formulation of the optimal control problem.

### Nested Optimal Control Techniques

Recent studies present a novel method to solve the optimal control problem, which is the nested optimal control technique. The nested technique targets to solve the drawbacks of single optimal control techniques, such as restrictions of system dimensions in DP, non-convex models and signals in CVX. Two representatives are summarized as follows, which are dynamic-programming-based and convex-optimization-based nested optimal control technique.

DP-based nested optimal control technique, as the name implies, solves the optimal control problem directly by dynamic programming that determines the whole set of control variables. A second optimal control technique is implemented to find the optimal value of a few limited number of control variables. DP-based nested optimal control technique helps to cope with the dimensionality curse of DP, which is the exponential increment of computation time as state variables augment.

DP-based nested optimal control technique solves the optimal control of a parallel HEV by taking three control variables and three state variables into account [6, 31]. Through the nested optimal control technique of DP-PMP, the multi-variable mixed-integer non-linear problem is solved with significantly reduced computation time.

A scheme of this complex optimal control technique is illustrated in Fig. 1.6a. The battery power  $u_3^*$  optimized by PMP is transferred to DP for further optimization. When determining control variable  $u_3^*$ , the adjoint state variable in PMP is mildly tuned by a proportional controller. The whole control variables, including gear shift command  $u_1$  and engine on/off command  $u_2$ , are concurrently optimized by DP. Compared with single DP approach, DP-PMP nested optimal control technique presents 0.4% difference of the fuel consumption but an average 420 times reduction of the computation time [6].

To solve a similar problem, another nested methodology based on DP is proposed to optimally determine the adjoint state variable in PMP. In [32], the objective function is rewritten as a function of Hamiltonian function for easy implementation of DP. The scheme of this approach is depicted in Fig. 1.6b. The objective function is minimized by DP, in which the optimal adjoint state  $u_3^*$  is solved by convex optimization. Results of fuel consumption obtained by DP(PMP)-CVX nested optimal control approach are almost the same as that of DP. In addition, the computation time is reduced significantly.

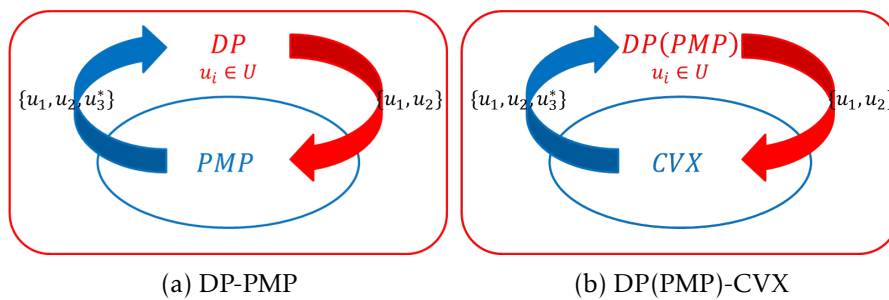


Figure 1.6 – DP-based nested optimal control techniques.

CVX-based nested optimal control technique, solves the optimal control problem of HEVs directly through convex optimization. To cope with the non-convex signals and models in the optimal control problem, extra optimal control techniques can be of great help to solve the mixed-integer problem first (such as engine on/off decision or gear selection). Albeit CVX-DP nested optimal control technique for series HEV application is proposed in [33], in fact, it is a DP-based nested optimal control technique because the philosophy is the same as DP(PMP)-CVX one. The CVX-based nested optimal control technique is implemented as reported in [34, 35].

As illustrated in Fig. 1.7, the mechanism of CVX-PMP nested optimal control technique solves the optimal engine on/off strategy  $B_e^*$  by PMP, and the optimal adjoint state  $s^*$  is numerically determined.

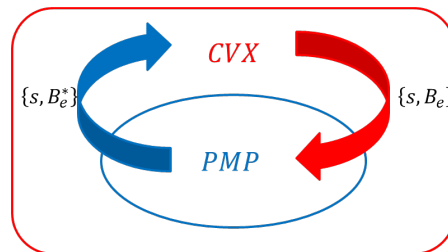


Figure 1.7 – CVX-based nested optimal control technique.

## 1.4 Hybrid-Electric Vehicle: Powertrain Design

The optimization of a vehicle propulsion system consists of the design and control optimizations. Depending on different optimization methods, optimal control techniques are applied in terms of various combinations, or only one optimization method. Commonly applied powertrain design methods are summarized as heuristic and optimal design approach.

### 1.4.1 Heuristic Design Approach

Fundamentals of vehicle design are embedded in the basic mechanics, particularly in Newton's second law of motion relating force and acceleration [36]. The power and energy requirements to internal combustion engine and electric motor/generator are estimated by analyzing the vehicle longitudinal dynamics [37]. The power and energy characteristics of powertrain components strongly depend on the experience of design engineers due to the development of energy management strategy.

Heuristic design approach determines dimensioning parameters of powertrain components to meet the technical targets. Iterative simulation is often used in the heuristic design approach [38, 39]. The dimensions of main powertrain components are firstly estimated according to the technical targets. If the first estimation fails, a second one is performed in the next iteration. The dimensions of mechanical and electrical powertrain components are required to account for powertrain architectures [40, 41].

Evidently, the heuristic design approach is only a primary solution that needs to optimize. Further improvement of the hybrid powertrain design can be achieved by

considering more factors, such as fuel consumption.

### 1.4.2 Optimal Design Approach

Three-layer optimization problems exist in the design problem of vehicle propulsion systems, which consists of the structural optimization, parametric optimization, and control system optimization [42]. Moreover, the structural optimization can be aggregated into the parametric optimization when the structure is parameterized in the design problem.

Optimal design of hybrid propulsion systems faces grave inherent complexity because of the necessity of control optimization to benchmark the minimal energy consumption. Basically, two types of optimizations reside in the optimal design of vehicle propulsion systems, which are design and control optimization. The design optimization finds the best dimensioning parameters of powertrain components such that the energy consumption is minimized, whereas the control optimization minimizes the energy consumption of an investigated vehicle propulsion system by identifying optimal control laws. However, optimal control laws are developed based on optimal control techniques and affected by dimensioning parameters of powertrain components.

Recent investigations on the optimal design of vehicle propulsion systems are classified into three categories as shown in Fig. 1.8, where  $\mathcal{D}$  indicates the dimension-related parameters. Three categories of optimization methods are composed of bi-level design optimization (see Fig.1.8a), bi-level co-optimization (see Fig.1.8b), and simultaneous co-optimization (see Fig.1.8c). Bi-level indicates that powertrain design and powertrain control are performed at separate levels with different optimization techniques; whereas co-optimization means that both powertrain design and powertrain control are optimized to achieve the minimum energy consumption. For example, the powertrain dimensioning parameters are optimized in the outer level through an optimization technique in the bi-level co-optimization method. Meanwhile, the powertrain control is optimized with another technique in the inner level so that the minimum fuel consumption is achieved. Both optimizations find the optimal dimensioning parameters such that the fuel consumption is minimized over an investigated mission.

Furthermore, details of recent investigations are summarized and listed in Table 1.2, including reference paper, published year, design optimizer and parameter, control optimizer, and powertrain architecture. Design parameters are summarized into the overall set of design parameters  $\mathcal{S}$ , which consists of internal combustion engine  $\mathcal{S}_e$ , drivetrain (including transmission and differential)  $\mathcal{S}_d$ , battery  $\mathcal{S}_b$ , electric motor  $\mathcal{S}_m$ , and

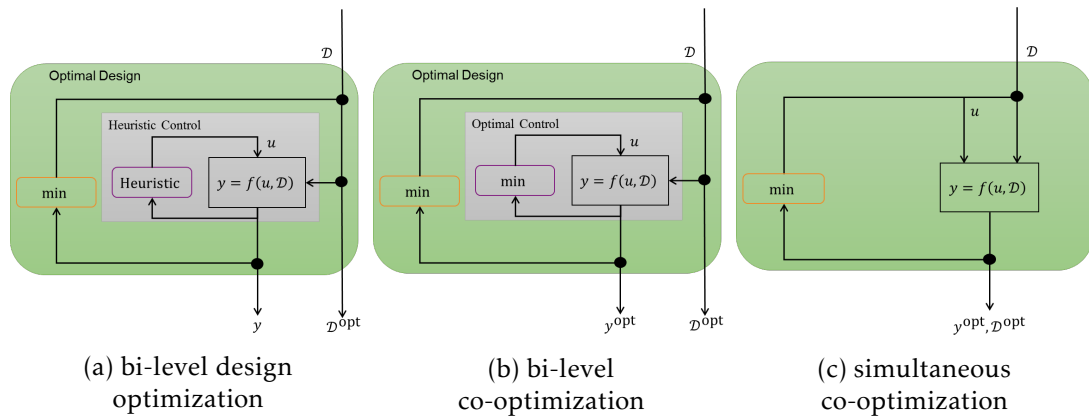


Figure 1.8 – Optimal design methods for vehicle propulsion systems.

electric generator  $S_g$ . In addition, design parameters  $S_h$  and  $S_u$  refer to hybridization ratio and control variables, respectively.

Various design optimizers are applied to optimize the dimensioning parameters. The design optimizer consists of sequential quadratic programming (SQP), bundle method, Dividing Rectangles Optimization (DIRECT), Simulated Annealing (SA), Genetic Algorithms (GA), Particle Swarm Optimization (PSO), Non-dominated Sorting Genetic Algorithm (NSGA-II), Feature-Based Generic Algorithm (FBGA), Non-Linear Programming by Quadratic Lagrangian (NLPQL), General Purpose Solver (GPS), Constraint Programming (CP), Spearman Rank Correlation Coefficient Method (SRCCM), and Requirements engineering, Functional analysis, Logical design and Physical design (RFLP). Particularly, the short line indicates that no specific nonlinear solver is applied.

Considering the control optimizer, it includes heuristic one, Hamilton–Jacobi–Bellman method (HJB), dynamic programming (DP), combined convex optimization and Pontryagin’s Minimum Principle (CVX-PMP), rule-based one (RB), combine convex optimization and dynamic programming (CVX-DP), equivalent fuel consumption minimization strategy (ECMS), vectorized hybrid optimization tool (VHOT), selective Hamiltonian minimization (SHM), graphical-analysis-based energy consumption optimization (GRAB-ECO), and fully-analytic energy consumption estimation (FACE).

### Bi-Level Design Optimization

Compared with bi-level co-optimization, the bi-level design optimization refers to only one optimization technique that is implemented to solve the optimal design problem. However, only one problem of powertrain design and control is optimized. Therefore,

Ref.	Year	Design Optimizer	Parameter	Control Optimizer	Architecture
[43]	1999	SQP	$\mathcal{S}_i(i = e, b, m)$	Heuristic	parallel
[44]	2004	Bundle Method	$\mathcal{S}_d$	HJB	parallel
[4]	2005	DIRECT/SA/GA	$\mathcal{S}_i(i = e, b, m, d)$	Heuristic	power-split
[45]	2007	–	$\mathcal{S}_i(i = b, m, g)$	DP	power-split
[46]	2015	–	$\mathcal{S}_f$	DP	power-split
[47]	2009	–	$\mathcal{S}_h$	DP	parallel
[48]	2012	PSO	$\mathcal{S}_i(i = e, b, m)$	DP	parallel
[34]	2014	CVX-PMP	$\mathcal{S}_b$	CVX-PMP	series
[49]	2010	–	$\mathcal{S}_i(i = e, b, m)$	PMP	parallel
[50]	2011	–	$\mathcal{S}_i(i = b, m)$	DP	parallel
[51]	2011	NSGA-II/DIRECT /SA/GA/PSO	$\mathcal{S}_i(i = e, b, m, u)$ $\mathcal{S}_i(i = e, b, m, d)$	Heuristic	series/ parallel
[52]	2011	GA/FBGA	$\mathcal{S}_i(i = e, b, m, u)$	GA/FBGA	series
[53]	2012	NLPQL	$\mathcal{S}_i(i = e, b, m, d)$	DP	parallel
[54]	2011	CVX	$\mathcal{S}_b$	CVX+RB	series/parallel
[55]	2013	CVX	$\mathcal{S}_b$	CVX+RB	series
[56]	2013	CVX	$\mathcal{S}_i(i = e, b, m)$	CVX+RB	parallel
[33]	2015	CVX-DP	$\mathcal{S}_i(i = b, e, g)$	CVX+DP	series
[5]	2015	GA	$\mathcal{S}_i(i = a, e, b, m, u)$	ECMS	series/parallel
[6]	2014	GPS (SQP)	$\mathcal{S}_i(i = a, m)$	DP	parallel
[57]	2015	CP/SQP/PSO/ GA/DIRECT	$\mathcal{S}_i(i = e, b, m)$	DP	parallel
[25]	2015	SRCCM	$\mathcal{S}_i(i = b, m, d)$	–	electric vehicle
[58]	2015	RFLP (NSGA-II)	$\mathcal{S}_i(i = b)$	–	electric vehicle
[59]	2016	DIRECT	$\mathcal{S}_i(i = e)$	SHM	parallel
[60]	2017	–	$\mathcal{S}_i(i = e, b, m, g, d)$	VHOT, FACE SHM, GRAB-ECO	series

Table 1.2 – Summary of powertrain design optimization for hybrid- and battery-electric vehicles.

the bi-level design optimization is regarded as a partial optimization method. The partial optimality could be achieved either at the outer loop that determines the optimal dimensioning parameters or at the inner loop that minimizes the fuel consumption. In [4, 43, 51], the design parameter set of hybrid-electric vehicles are optimized only at the outer loop, yet the control laws are heuristic.

On the contrary, the bi-level design optimization solely occurs at the inner loop in [47, 49, 50], where optimal control laws are realized by DP mainly due to the global optimality without considering the heavy computational load. The outer loops are performed iteratively or manually. As for power-split HEVs [45, 46], only the possible topologies of the planetary gear sets are screened in the exhaustive research method since the presence and absence of clutches significantly impact the operating modes of

power-split HEV.

### **Bi-Level Co-Optimization**

As listed in Table 1.2, the bi-level co-optimization method for the optimal design of vehicle propulsion systems has been widely used by optimizing various objectives, for example, the cost of hybridization and operation, the fuel economy, and the pollutant emissions.

The bi-level co-optimization refers to the design optimization in the outer loop and the control optimization in the inner loop. Design optimization selects the best dimensioning parameters, whereas control optimization derives the optimal control laws discussed in previous section. The optimal design problem that globally optimizes the dimensioning parameters are solved by various optimization techniques, such as DIRECT, GA, and PSO.

#### ***DIRECT***

Dividing RECTangles (DIRECT) optimization algorithm is motivated by a modification to Lipschitzian optimization that eliminates the need to specify the Lipschitz constant [61]. It is created in order to solve difficult global optimization problems with bound constraints and a real-valued objective function. Unfortunately, this global optimal convergence may come at the expense of a large and exhaustive search over the domain. In [4], a parallel hybrid-electric vehicle is optimally designed with the implementation of heuristic control laws. Heavy computational load eventually leads to hundred hours for the complete optimization process. Possible improvements is proposed as well in order to overcome the slow convergence.

#### ***Genetic Algorithms***

Genetic Algorithms (GA) are adaptive heuristic search methods that mimic the natural biological evolutionary idea of natural selection and genetics. They present an intelligent exploitation of a random search to solve optimization problems. Despite randomized, GA use historical knowledge to direct the search into the region of better performance within the search space. Being a global search method, GA are capable to optimize the hybrid powertrain design once the control system optimization is achieved. In [5], the hybrid powertrain design is optimally designed through the combination of GA and equivalent fuel consumption minimization strategy. The fuel consumption is minimized in the condition that the final state of charge of battery is maintained the same as the initial one. The investigated dimensioning parameters associate with powertrain architecture, internal combustion engine, electric motor/generator, battery, and control

variable. Results proved the effectiveness of bi-level co-optimization approach in the optimal design of a hybrid powertrain.

#### ***Particle Swarm Optimization***

Particle Swarm Optimization (PSO) is a stochastic search method that optimizes a problem by iteratively trying to improve a candidate solution with regard to a given measure of quality. The change in direction and velocity of each individual particle is the effect of cognitive, social and stochastic influences. The common goal of all group members is to find the favourable location within a specified search space. In [48], the primary optimization problem is to find the design parameter set  $\mathcal{S} = \{\mathcal{V}_e, \mathcal{P}_m, \mathcal{Q}_b\}$  that minimizes the objective function subject to inequality constraints. Both objective function and constraints are non-convex functions with respect to  $\mathcal{S}$ . An efficient tuning methodology of the intrinsic parameters are established by exploiting the results of exhaustive search as a look-up table for PSO algorithm.

#### **Simultaneous Co-Optimization**

Simultaneous co-optimization means that both powertrain design and control are optimized through the only one optimization technique. Due to the application of one optimization technique, powertrain design and optimal control are merged into the same level. Thus, powertrain design and control are simultaneously optimized. The simultaneous co-optimization is currently realized by convex optimization (CVX), which is elaborated in [33, 55, 62]. The essence of convex optimization is to construct convex objective function and constraints.



# Modeling for Energy Consumption Evaluation

Mission profiles, powertrain characteristics, and vehicle specifications, are fundamental to the evaluation of the energy consumption of a vehicle propulsion system. In this chapter, powertrain components of various vehicle propulsion systems are analytically modeled at descriptive and predictive level. Specifically, descriptive analytic models estimate the intrinsic features; whereas predictive analytic models predict those features for components of different dimensioning parameters. In addition, vehicle load is analytically estimated for the evaluation of energy consumption over a mission.

## 2.1 Modeling of Vehicle Propulsion System

Vehicle propulsion systems of conventional, battery-electric, and hybrid-electric vehicles are significantly different from each other due to the composition of powertrain components and control system. The main powertrain components are composed of Internal Combustion Engine (ENG), Transmission (TRA), Battery (BAT), and Electric Motor/Generator (EMG), as depicted in Fig. 2.1.

The main powertrain components are analytically modeled to estimate the energy consumption of a vehicle over a specified mission in an accurate and rapid way. The analytic models are control-oriented to develop optimal control techniques for hybrid-electric vehicles. Moreover, these analytic models are design-oriented as well for the optimization of dimensioning parameters. In other words, they are scalable. As a consequence, the analytic models of powertrain components are established at two

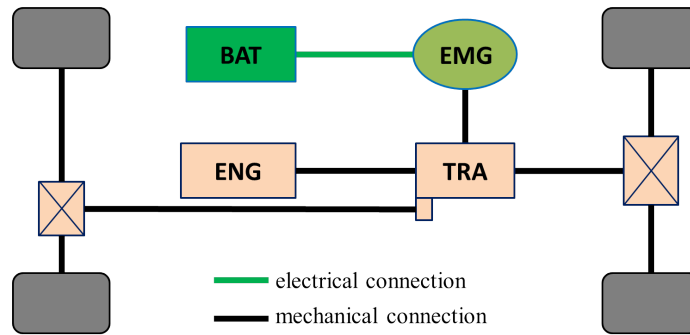


Figure 2.1 – Main powertrain components of a parallel hybrid-electric vehicle.

distinct levels: the descriptive and predictive level.

At descriptive level, *descriptive analytic models* describe the main features of a specific powertrain component, such as the energy losses of an ENG. The descriptive analytic model is directly applied for the energy consumption evaluation of any given vehicles, and for the optimal control laws identification for hybrid-electric vehicles. Parameters of descriptive analytic models are identified from each powertrain component.

At predictive level, *predictive analytic models*, on the other hand, allow the prediction of the main features for powertrain components of different dimensioning parameters. For instance, the power losses of an ENG of the varied engine displacements can be approximated by predictive analytic models. Coefficients in predictive analytic models are identified from the identification set of powertrain components in the same family of technology.

To validate descriptive and predictive analytic models, estimations are compared with grid-point data. For the sake of clarity, the results estimated by descriptive analytic models alone are designated as **description** in the following sections; whereas, results approximated by predictive analytic models are designated as **prediction**.

To present the accuracy of descriptive and predictive analytic models, the mean relative error between description and grid point data is denoted by  $\varepsilon^d$ ; whereas, the relative mean error between description and grid-point data is indicated by  $\varepsilon^p$ . Regardless of descriptive or predictive error, the mean relative error, denoted by subscript  $c$ , is evaluated for each powertrain component in its identification set. In contrast, the average relative error is evaluated based on the whole identification set, and indicated by the subscript  $s$ . Statistic characteristics between estimations (description and prediction) and grid-point data are illustrated to supplement the mean relative error of each component.

Apart from the validation at powertrain component and identification set level,

the accuracy of descriptive and predictive analytic models is investigated at vehicle propulsion system level. At the propulsion system level, the energy consumption is estimated based on different types of powertrain data for various types of vehicle propulsion systems. The powertrain data consists of grid-point data, description, and prediction; whereas vehicle propulsion systems include conventional, battery-electric, and hybrid-electric vehicles. The accuracy of analytic models is most important at vehicle propulsion system level since it determines their validity. The difference of energy consumption of different vehicle propulsion systems will be demonstrated in Chapter 3.3 and 4.5.

Considering the perspective of system identification, the proposed analytic models are needed to validate with components different from the identification set, particularly the predictive analytic models. However, analytic models of powertrain components are validated from the corresponding identification sets due to the availability of data.

## 2.2 Internal Combustion Engine

As the primary power source in a conventional or hybrid-electric vehicle, an internal combustion engine (ENG) provides mechanical power to propel the vehicle by burning hydrocarbon-containing fuels, such as gasoline, diesel, natural gas, and bio-fuels. The ENGs can be classified with respect to various criteria. Concerning the ignition method, there are Spark Ignition (SI) and Compression Ignition (CI) engines. Regarding the charging technology, it is composed of Naturally Aspirated (NA) and Turbo-Charged (TC) method. In regard to NA engines, engineers develop various combustion modes, such as Stoichiometric-Burn (SB) and Lean-Burn (LB) methods.

### 2.2.1 Dimensioning Parameter

The technological dimensioning parameter of ENGs, denoted by  $\mathcal{I}_e$ , contains four types of engines for light-duty vehicles, which are combinations of different engine technologies. Four types of engines are listed in  $\mathcal{I}_e = \{\text{SI/NA/SB}, \text{SI/NA/LB}, \text{SI/TC}, \text{CI/TC}\}$ , and represented by integers in the design optimization of vehicle propulsion systems.

Apart from the technological parameter  $\mathcal{I}_e$ , dimensioning parameters of an engine are essential to develop predictive analytic models. The overall dimensioning parameter set is defined as

$$\mathcal{S}_e = \{\mathcal{I}_e, \mathcal{V}_e, \mathcal{T}_e, \mathcal{P}_e, \mathcal{N}_{eT}, \mathcal{N}_{eP}\}, \quad (2.1)$$

where  $\mathcal{V}_e$  is engine displacement in [m<sup>3</sup>],  $\mathcal{T}_e$  is the rated engine torque in [Nm],  $\mathcal{P}_e$  is the rated engine power in [kW],  $\mathcal{N}_{eT}$  and  $\mathcal{N}_{eP}$  are engine speeds in [rpm] corresponding to the rated torque and the rated power.

Although engine displacement, rated torque, and rated power are listed separately, they are not independent from each other. The rated torque and rated power depend on engine displacement because of the similar maximum brake mean effective pressure.

### 2.2.2 Analytic Model

Parameterization of the engine fuel consumption map is performed for both light- and heavy-duty engines. Accordingly, analytic models at both descriptive and predictive level are developed and validated separately.

#### At Descriptive Level

Inspired by the Willans line models [63], the descriptive analytic models of internal combustion engines evaluate the burned fuel power as a function of engine speed and engine brake power. The burned fuel power is converted directly from fuel consumption maps by taking the lower heating value of fuel into account. The chosen descriptive analytic model for light-duty engines is expressed by

$$P_{ef}(\omega_e, P_e) = \begin{cases} k_{e0}(\omega_e) + k_{e1}(\omega_e)P_e, & P_e \leq P_{ec}(\omega_e) \\ k_{e0}(\omega_e) + (k_{e1}(\omega_e) - k_{e2})P_{ec}(\omega_e) + k_{e2}P_e, & P_e > P_{ec}(\omega_e) \end{cases}, \quad (2.2)$$

where  $\omega_e$  is the engine speed in [rad/s];  $P_e$  is the engine brake power of engine in [W];  $P_{ec}$  is the engine corner power of maximal efficiency [W], whose corresponding torque is depicted in Fig. 2.2; and  $P_{ef}$  is the power of burned fuel in [W], which is converted from the mass flow rate of an engine map. Parameters  $k_{ei}$  ( $i = 0, 1, 2$ ) are identified for each individual engine from the engine identification set of Table 2.4.

Concerning turbo-charged diesel engines for heavy-duty applications, the descriptive analytic model is

$$P_{ef}(\omega_e, P_e) = k_{e3}(\omega_e) + k_{e4}(\omega_e)P_e + k_{e5}(\omega_e)P_e^2, \quad (2.3)$$

where parameters  $k_{ei}$  ( $i = 3, 4, 5$ ) are identified for each individual engine in its identification set of Table 2.5.

In addition to analytic models of burned fuel power, the full-load torque of an ENG is modeled analytically as well. Concerning *SI/NA* ENGs for light-duty applications,

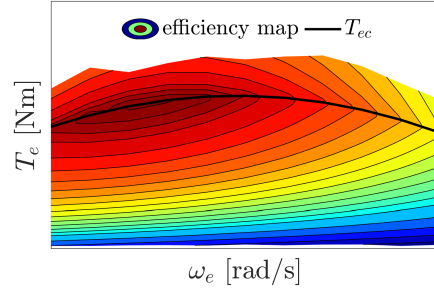


Figure 2.2 – Corner torque  $T_{ec}$  of an internal combustion engine.

the analytic model of full-load torque is

$$\bar{T}_e(\omega_e) = k_{e6} + k_{e7}\omega_e + k_{e8}\omega_e^2, \quad (2.4)$$

where  $\bar{T}_e$  is the full-load torque. As a convention, variables with over-line (e.g.  $\bar{T}$ ) indicates the maximum admissible value; whereas, the under-line (e.g.  $\underline{T}$ ) represents the minimum admissible value.

Parameters  $k_{ei}$  ( $i = 6, 7, 8$ ) are identified by solving the following linear system that contains the engine dimensioning parameters  $T_e$ ,  $\mathcal{P}_e$ ,  $\mathcal{N}_{eT}$ , and  $\mathcal{N}_{eP}$ .

$$\begin{bmatrix} 1 & \frac{1000\pi}{30} & \left(\frac{1000\pi}{30}\right)^2 \\ 1 & \frac{\mathcal{N}_{eT}\pi}{30} & \left(\frac{\mathcal{N}_{eT}\pi}{30}\right)^2 \\ 1 & \frac{\mathcal{N}_{eP}\pi}{30} & \left(\frac{\mathcal{N}_{eT}\pi}{30}\right)^2 \end{bmatrix} \begin{bmatrix} k_{e6} \\ k_{e7} \\ k_{e8} \end{bmatrix} = \begin{bmatrix} T_{ek} \\ T_e \\ \frac{30\mathcal{P}_e}{\pi\mathcal{N}_{eP}} \end{bmatrix}, \quad (2.5)$$

where  $T_{ek}$  is the engine torque at 1000 rpm for light-duty engines.

Regardless of light-duty or heavy-duty engines, turbocharged engines have a piecewise analytic model to approximate the full-load torque,

$$\bar{T}_e(\omega_e) = \begin{cases} k_{e9} + k_{e10}\omega_e, & \omega_e \leq \frac{\pi\mathcal{N}_{eT1}}{30} \\ T_e, & \frac{\pi\mathcal{N}_{eT1}}{30} \leq \omega_e \leq \frac{\pi\mathcal{N}_{eT2}}{30} \\ k_{e11} + k_{e12}\omega_e, & \omega_e \geq \frac{\pi\mathcal{N}_{eT2}}{30} \end{cases}, \quad (2.6)$$

where  $\mathcal{N}_{eT1}$  and  $\mathcal{N}_{eT2}$  are the minimal and maximal speed of the rated torque, respectively.

Parameters  $k_{e9}$  and  $k_{e10}$ ,  $k_{e11}$  and  $k_{e12}$  are identified by solving the following two linear equation systems,

$$\begin{bmatrix} 1 & \frac{1000\pi}{30} \\ 1 & \frac{\pi\mathcal{N}_{eT1}}{30} \end{bmatrix} \begin{bmatrix} k_{e9} \\ k_{e10} \end{bmatrix} = \begin{bmatrix} \mathcal{T}_{ek} \\ \mathcal{T}_e \end{bmatrix}, \quad (2.7)$$

and

$$\begin{bmatrix} 1 & \frac{\pi\mathcal{N}_{eT2}}{30} \\ 1 & \frac{\pi\mathcal{N}_{eP}}{30} \end{bmatrix} \begin{bmatrix} k_{e11} \\ k_{e12} \end{bmatrix} = \begin{bmatrix} \mathcal{T}_e \\ \frac{30\mathcal{P}_e}{\pi\mathcal{N}_{eP}} \end{bmatrix}, \quad (2.8)$$

where engine speed  $\mathcal{N}_{eT1}$ ,  $\mathcal{N}_{eT2}$ , and  $\mathcal{N}_{eP}$  are indicated in Fig. 2.3.

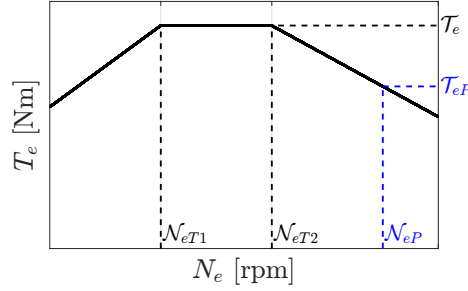


Figure 2.3 – Speed variables of turbocharged internal combustion engines.

### At Predictive Level

Parameters  $k_{ei}$  ( $i = 0, \dots, 12$ ) in descriptive analytic models in Eq. 2.2 and 2.3 are further expressed as function of engine dimensioning parameters. As for light-duty engines, their predictive analytic models are expressed by

$$k_{e0} = \frac{\mathcal{V}_e \omega_e}{4\pi} \left( c_{e1} + \frac{30c_{e2}\omega_e}{\pi} \right), \quad (2.9)$$

$$k_{e1} = c_{e3} + \frac{30c_{e4}\omega_e}{\pi} + \frac{900c_{e5}\omega_e^2}{\pi^2}, \quad (2.10)$$

$$k_{e2} = c_{e6}, \quad (2.11)$$

where coefficients  $c_{ei}$  ( $i = 1, \dots, 6$ ), depending on engine-technological parameter  $\mathcal{I}_e$ , are listed in Table 2.1.

$\mathcal{I}_e$	$c_{e1}$	$c_{e2}$	$c_{e3}$	$c_{e4}$	$c_{e5}$	$c_{e6}$
SI/LB	$3.24 \times 10^5$	54.0	2.541	$-1.892 \times 10^{-4}$	$3.863 \times 10^{-8}$	4.546
SI/SB			2.456	$-4.349 \times 10^{-5}$	$1.032 \times 10^{-8}$	
CI	$1.84 \times 10^5$	112.5	2.363	0	0	3.061

Table 2.1 – Values of coefficients  $c_{ei}(i = 1, \dots, 6)$  for light-duty engines.

The engine corner power in the piece-wise linear model of burned fuel power in Eq. 2.2 is calculated by

$$P_{ec}(\omega_e) = \begin{cases} 0.8\omega_e \bar{T}_e(\omega_e), & NA, \\ \frac{1000\mathcal{V}_e\omega_e}{4\pi} \sum_{i=7}^{14} c_{ei} \left(\frac{\omega_e}{2\pi}\right)^{i-7}, & TC, \end{cases} \quad (2.12)$$

where coefficients  $c_{ei}(i = 7, \dots, 14)$  are taken from the PERE Report [64]. Their values are presented in Table 2.2 correspondingly for spark ignition (SI) and compression ignition (CI) engines.

$\mathcal{I}_e$	$c_{e7}$	$c_{e8}$	$c_{e9}$	$c_{e10}$
SI	-1200.5	298.93	-17.586	0.56342
CI	-19950.8	3479.90	-231.809	8.25775

$\mathcal{I}_e$	$c_{e11}$	$c_{e12}$	$c_{e13}$	$c_{e14}$
SI	-0.010463	$1.132 \times 10^{-4}$	$-6.645 \times 10^{-7}$	$1.631 \times 10^{-9}$
CI	-0.169919	$2.023 \times 10^{-3}$	$-1.292 \times 10^{-5}$	$3.422 \times 10^{-8}$

Table 2.2 – Values of coefficients  $c_{ei}(i = 7, \dots, 14)$  for light-duty engines.

At the predictive level, the torque at 1000 rpm for light-duty engines is estimated by

$$T_{ek} = \begin{cases} \frac{1000\mathcal{V}_e}{4\pi} \sum_{i=7}^{14} c_{ei} \left(\frac{\omega_e}{2\pi}\right)^{i-7}, & NA, \\ \frac{11 \times 10^8 \mathcal{V}_e}{4\pi}, & TC. \end{cases} \quad (2.13)$$

Concerning heavy-duty engines, their predictive analytic models are written as follows:

$$k_{e3} = \frac{10^5 \mathcal{V}_e \omega_e}{4\pi} (c_{e15} + c_{e16} \omega_e + c_{e17} \omega_e^2), \quad (2.14)$$

$$k_{e4} = 10^5 c_{e18}, \quad (2.15)$$

$$k_{e5} = \frac{4 \times 10^5 \pi}{\mathcal{V}_e \omega_e} (c_{e19} + c_{e20} \omega_e + c_{e21} \omega_e^2), \quad (2.16)$$

where coefficients  $c_{ei}(i = 15, \dots, 21)$  are listed in Table 2.3.

$c_{e15}$	$c_{e16}$	$c_{e17}$	$c_{e18}$	$c_{e19}$	$c_{e20}$	$c_{e21}$
2.000	$2.190 \times 10^{-3}$	$7.008 \times 10^{-5}$	1.884	$8.549 \times 10^{-2}$	$1.024 \times 10^{-3}$	$3.435 \times 10^{-6}$

Table 2.3 – Values of coefficients  $c_{ei}(i = 15, \dots, 21)$  for heavy-duty engines.

### 2.2.3 Model Validation

The identification sets of engines are introduced in terms of light- and heavy-duty applications, respectively. The whole identification set is implemented to develop descriptive and predictive analytic models, and to validate these models. After the demonstration of engine grid-point data in terms of maps, the mean relative error and statistic characteristics are illustrated and discussed hereafter.

#### Identification Set

Due to different vehicle applications, two types of engine identification sets are used to develop and validate the descriptive and predictive analytic models. The identification set of light-duty engines is listed in Table 2.4, including specifications of the dimensioning parameters; whereas the set of heavy-duty engines is summarized in Table 2.5, containing corresponding specifications of the dimensioning parameters.

ID	$\mathcal{I}_e$	$\mathcal{V}_e$ [L]	$\mathcal{T}_e$ [Nm]	$\mathcal{N}_{eT}$ [rpm]	$\mathcal{P}_e$ [kW]	$\mathcal{N}_{eP}$ [rpm]
1	CI/TC	2.2	292	2000	90	4000
2	CI/TC	1.6	242	1750	80	4000
3	CI/TC	2.0	324	2000	98	4000
4	CI/TC	2.2	327	1750	88	3000
5	CI/TC	1.5	202	2000	78	4000
6	CI/TC	2.0	368	1750	121	4000
7	CI/TC	1.2	145	2000	43	4000
8	SI/TC	0.9	145	3000	58	5000
9	SI/NA/LB	1.5	120	4500	60	5500
10	SI/NA/LB	1.9	166	4000	82	5000
11	SI/TC	2.0	302	2500	150	5000
12	SI/TC	1.8	312	2000	148	5500
13	SI/NA/SB	1.0	95	4000	54	6000
14	SI/NA/LB	1.4	128	4500	70	5500

Table 2.4 – Identification set of light-duty engines.

ID	$\mathcal{I}_e$	$\mathcal{V}_e$ [L]	$\mathcal{T}_e$ [Nm]	$\mathcal{N}_{eT}$ [rpm]	$\mathcal{P}_e$ [kW]	$\mathcal{N}_{eP}$ [rpm]
1	CI/TC	9.3	1600	1050	235	1900
2	CI/TC	9.3	1400	1000	210	1700
3	CI/TC	12.7	2375	1000	335	1700
4	CI/TC	12.7	2375	1000	340	1700
5	CI/TC	12.7	2350	1000	358	1600
6	CI/TC	12.7	2275	1000	325	1700
7	CI/TC	12.7	2600	1000	376	1700
8	CI/TC	16.4	3000	1000	444	1700
9	CI/TC	16.4	3000	1000	490	1700
10	CI/TC	16.4	3500	1000	544	1900

Table 2.5 – Identification set of heavy-duty engines.

## Result

Description and prediction of each engine are comparatively illustrated with respect to the grid-point data. For simplicity reason, one light- and one heavy-duty engine are exemplified individually. The comparisons among grid-point data, description, and prediction of other engines are found in Appendix B.1.

Fig. 2.4 demonstrates the grid-point data, description, and prediction in terms of burned fuel power for ENG ID1. As shown in Fig. 2.4c, the contour lines of prediction are smoothest compared with the grid-point data and the description. Nonetheless, both description and prediction present a similar trend compared with the grid-point data.

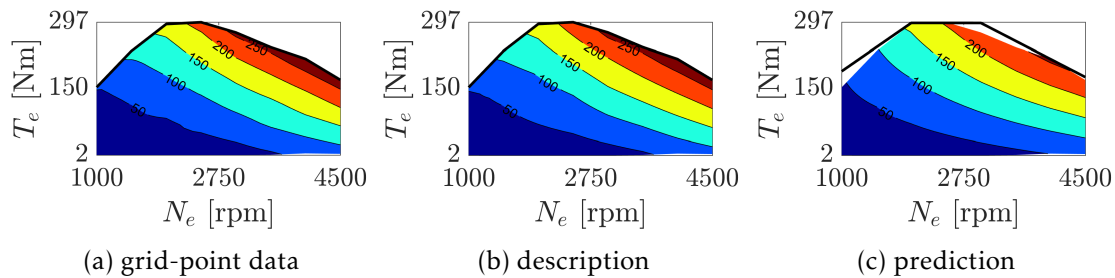


Figure 2.4 – Map of burned fuel power of light-duty engine ID1.

Concerning the exemplified heavy-duty engine, the grid-point data, description, and prediction of ENG ID2 are comparatively depicted in terms of efficiency in Fig. 2.5. Due to confidential issues, the horizontal and vertical axis are scaled compared to original data. The best efficiency area of prediction are enlarged significantly, as illustrated in

Fig. 2.5c. Nevertheless, the description and prediction are still comparable with respect to the grid-point data.

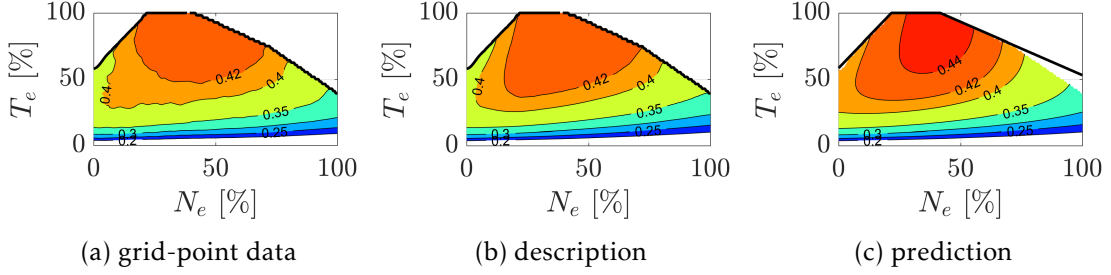


Figure 2.5 – Efficiency map of heavy-duty engine ID2.

### Analysis

The analysis of mean relative error and linear regression is performed to evaluate the accuracy of descriptive and predictive analytic models for both light- and heavy-duty engines. In particular, analysis of mean relative error is completed both for each engine and the whole engine identifications set. Then, the exemplified light- and heavy-duty engine are used to depict their contour maps of mean relative error and the linear regression analysis.

Mean relative errors – including the mean description error of each component  $\varepsilon_c^d$ , the mean prediction error of each component  $\varepsilon_c^p$ , the average description error of whole identification set  $\varepsilon_s^d$ , and the average prediction error of whole identification set  $\varepsilon_s^p$  – are illustrated in Fig. 2.6 for both light- and heavy-duty engines. In summary, the maximum of mean relative error was 7.7% for light-duty engine ID10. The mean relative error of heavy-duty engine identification set is lower than that of light-duty engine identification set.

Considering light-duty engine ID1, its descriptive and predictive relative errors are illustrated in Fig. 2.7a and Fig. 2.7b, respectively. Clearly, large errors occur at the high engine speed and high load zone particularly for predictive analytic models.

Linear regression analysis is separately carried out between the description and the grid-point data, and between the prediction and the grid-point data. The power of burned fuel is normalized to a constant value. Fig. 2.8 presents the corresponding characteristics. To summarize, the descriptive analytic models can well represent grid-point data. Albeit the predictive analytic models have a smaller value of  $r^2$ , it can still predict the grid-point data for the intended study of vehicle energy consumption.

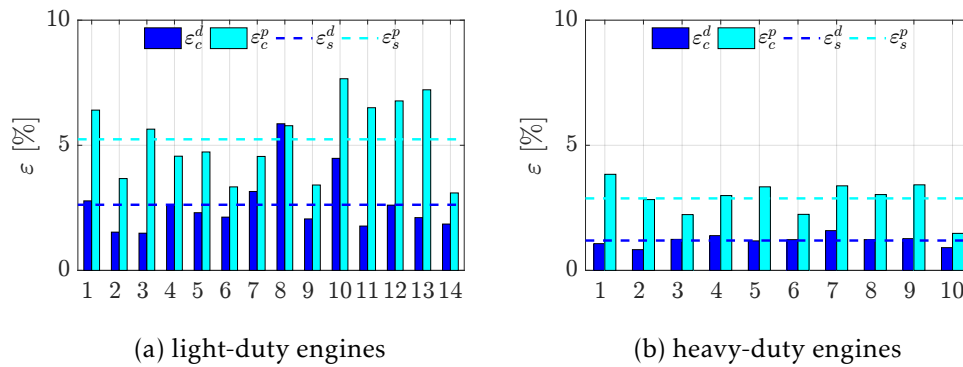


Figure 2.6 – Mean relative error of each engine and the whole identification set.

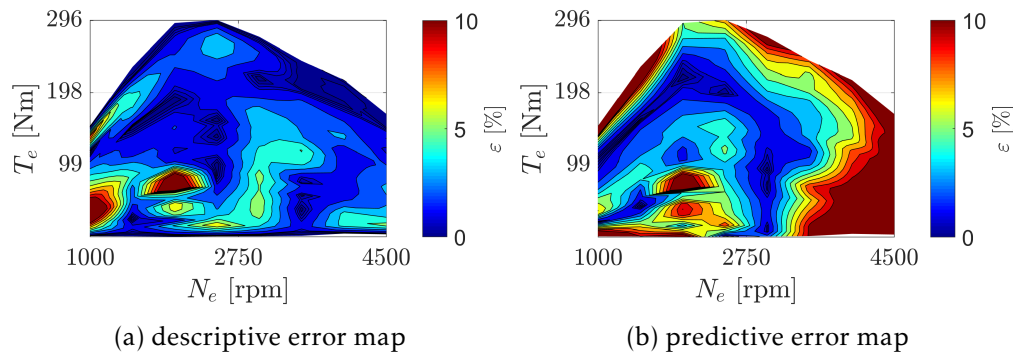


Figure 2.7 – Maps of relative errors of light-duty engine ID1.

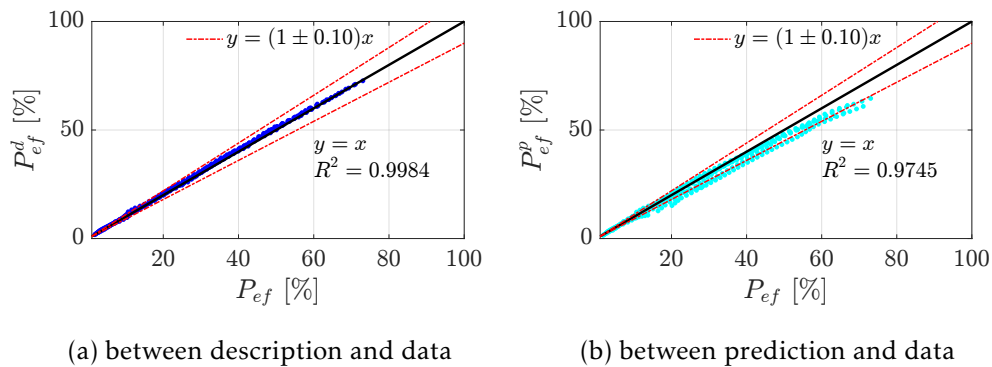


Figure 2.8 – Comparison of burned fuel power for light-duty engine ID1.

As for the heavy-duty engine ID2, the descriptive and predictive maps of mean relative errors are depicted in Fig. 2.9. The mean relative errors of both level analytic models are at low level. In details, high errors only occur in extremely low load condition

for the descriptive analytic models; whereas high errors are shifted to slightly higher-load and lower-speed zone for the predictive analytic models.

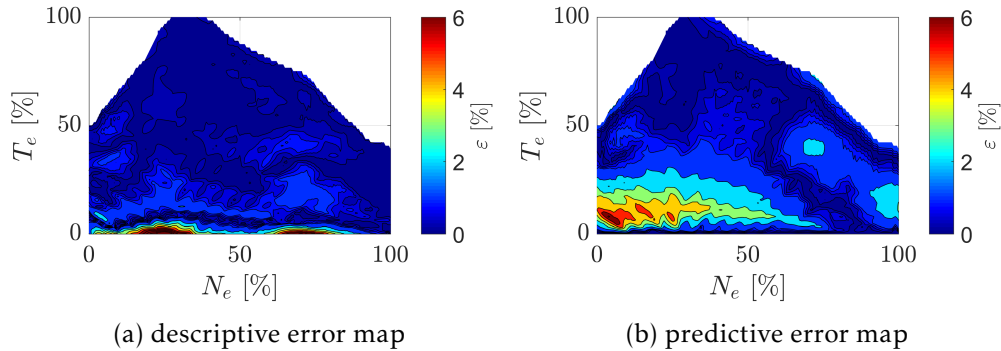


Figure 2.9 – Maps of relative errors of heavy-duty engine ID2.

Linear regression analysis is carried out for the heavy-duty engine ID2 in a similar way as for light-duty engine ID1. Results are correspondingly summarized in Fig. 2.10, where values of  $r^2$  are presented. The high  $r^2$  values indicate the goodness of developed analytic models.

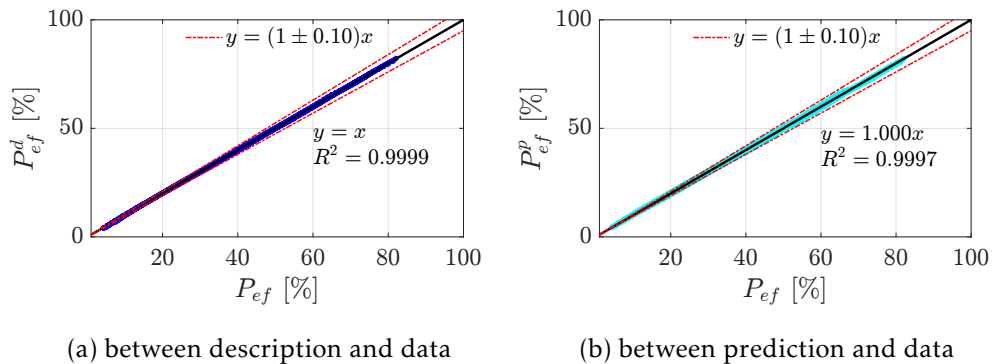


Figure 2.10 – Comparison of burned fuel power for heavy-duty engine ID2.

## 2.3 Drivetrain

Drivetrain delivers power from engine or electric motor to drive wheels. The main components of a drivetrain consist of a transmission, a final drive, and other simple gear-trains, depending on their technologies. Compared with the universal configuration in [65], Fig. 2.11 depicts an updated version for various vehicle propulsion systems,

including conventional, battery-electric, and hybrid-electric vehicle. Ratios of transmission and final drive are denoted by  $\mathcal{R}_t$  and  $\mathcal{R}_{fd}$ , respectively; whereas parameter  $\mathcal{R}_e$  and  $\mathcal{R}_g$  denote the ratio between engine shaft and node  $N_1$ , and the ratio gear between electric generator shaft and node  $N_1$ , respectively. In addition, parameter  $\mathcal{R}_m$  means the ratio between electric motor shaft and node  $N_2$ .

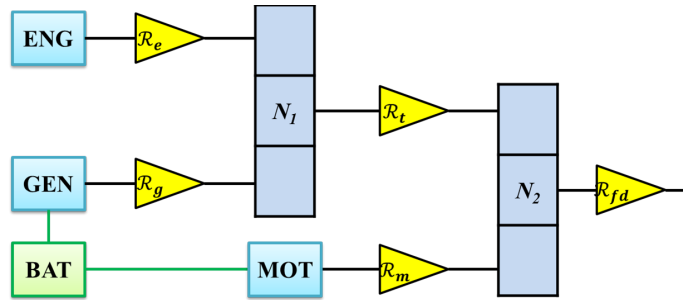


Figure 2.11 – Universal configuration of vehicle propulsion systems.

In a conventional vehicle, the drivetrain consists of transmission  $\mathcal{R}_t$  and final drive  $\mathcal{R}_{fd}$ ; in a battery-electric vehicle, the drivetrain is composed of simple gear-train  $\mathcal{R}_m$  and final drive  $\mathcal{R}_{fd}$ ; in a hybrid-electric vehicle, components of drivetrain depend on the powertrain architecture. For example, the drivetrain of a series HEV may consist of gear-train  $\mathcal{R}_g$  and  $\mathcal{R}_m$ ; whereas, it may include transmission  $\mathcal{R}_t$ , final drive  $\mathcal{R}_{fd}$ , and gear-train  $\mathcal{R}_m$  in a parallel HEV. Although power-split HEVs are not investigated in this thesis, its configuration can also be represented by the universal configuration in Fig. 2.11. Assuming the ratio of a planetary gear set is the ratio between radius of ring gear and the one of sun gear, which is  $\mathcal{R} = \frac{R_{ring}}{R_{sun}}$ , the Toyota Prius Hybrid can be represented by setting corresponding ratios as follows:

$$\mathcal{R}_g = 1 + \mathcal{R}, \quad (2.17)$$

$$\mathcal{R}_t = \frac{\mathcal{R}}{1 + \mathcal{R}}, \quad (2.18)$$

$$\mathcal{R}_e = 1, \quad (2.19)$$

$$\mathcal{R}_m = 1. \quad (2.20)$$

The ratio  $\mathcal{R}_{fd}$  is the final drive of the investigated vehicle.

Considering conventional and parallel hybrid-electric vehicles, transmissions specifically refer to multi-gear gearboxes alone in this thesis. In contrast, all the other gear-trains in Fig. 2.11 are considered as simple gear-trains with only one ratio.

Although transmissions can be classified into different types of technologies, the investigated transmissions only include Manual Transmission (MT), Automatic Transmission (AT), and Dual Clutch Transmission (DCT). Thus, the technological parameter of stepped-ratio transmission is

$$\mathcal{I}_t = \{\text{MT, AT, DCT}\}, \quad (2.21)$$

which are represented by integers.

### 2.3.1 Dimensioning Parameter

Except for transmission, the dimensioning parameter set of a drivetrain in generic form is expressed as

$$\mathcal{S}_d = \{\mathcal{R}_{fd}, \mathcal{R}_t, \mathcal{R}_m, \mathcal{R}_e, \mathcal{R}_g\}. \quad (2.22)$$

As for transmission, the typical dimensioning parameters consist of the ratios of first gear and last gear, and total gear number, which yields

$$\mathcal{S}_t = \{\mathcal{I}_t, \mathcal{R}_{t1}, \mathcal{R}_{tk}, \mathcal{K}_t\}, \quad (2.23)$$

where  $\mathcal{R}_{t1}$  and  $\mathcal{R}_{tk}$  are gear ratios of the first and last gear, respectively;  $\mathcal{K}_t$  is the total gear number.

### 2.3.2 Analytic Model of Transmissions

Regarding stepped-ratio transmissions, both gear ratios and transmission efficiency are parameterized at descriptive and predictive level below.

#### At Descriptive Level

The chosen descriptive analytic model of gear ratios for a  $\mathcal{K}$ -speed transmission ( $\mathcal{K} \geq 4$ ) is

$$\mathcal{R}_t(n_t) = k_{t0} + k_{t1}n_t + k_{t2}n_t^2 + k_{t3}n_t^3 + k_{t4}n_t^4, \quad (2.24)$$

where  $\mathcal{R}_t$  represents the gear ratio and  $n_t$  is the gear number.

Under the investigation of four-speed transmissions, parameter  $k_{t4}$  in Eq. 2.24 is equal to zero; whereas other parameters  $k_{ti}(i = 0, 1, \dots, 3)$  are identified through the

least squares fitting method. This method is implemented as well to identify descriptive parameters for the stepped-ratio transmissions in the identification set of Table 2.7.

In regard to gear efficiency, the chosen descriptive analytic model of the transmission power at the output shaft is modeled by

$$P_{t0} = \begin{cases} k_{t5} + k_{t6}P_t, & P_t \geq 0, \\ -k_{t5} + \frac{P_t}{k_{t6}}, & P_t < 0, \end{cases} \quad (2.25)$$

where  $P_t$  is the transmission power at the input shaft, and  $P_{t0}$  is the transmission power at output shaft.

### At Predictive Level

The specific dimensioning parameters of a stepped-ratio transmission consist of first gear ratio, last gear ratio, and gear number, which are summarized as  $\{\mathcal{R}_{t1}, \mathcal{R}_{tk}, \mathcal{K}_t\}$ .

Predictive analytic models of stepped-ratio transmission are developed based on the parameters in the previous descriptive analytic models in Eq. 2.24 and 2.25. Considering predictive analytic models of transmission gear ratio, they are written in the matrix equation form as

$$\begin{bmatrix} k_{t0} \\ k_{t1} \\ \vdots \\ k_{t4} \end{bmatrix} = (\mathcal{R}_{t1} - \mathcal{R}_{tk}) \begin{bmatrix} c_{t1} \\ c_{t2} \\ \vdots \\ c_{t5} \end{bmatrix} + \begin{bmatrix} 1 \\ 0 \\ \vdots \\ 0 \end{bmatrix}, \quad (2.26)$$

where the coefficients  $c_{ti}$  ( $i = 1, \dots, 5$ ) depend on gear number  $\mathcal{K}_t$  and technological parameter  $\mathcal{I}_t$ . The values are listed in Table 2.6.

$\mathcal{I}_t$	$\mathcal{K}_t$	$c_{t1}$	$c_{t2}$	$c_{t3}$	$c_{t4}$	$c_{t5}$
MT	5	2.259	-1.766	0.6009	-0.1	$6.485 \times 10^{-3}$
	6	2.041	-1.391	0.4023	-0.05578	$2.985 \times 10^{-3}$
DCT	6	1.786	-1.003	0.2473	-0.03035	$1.455 \times 10^{-3}$

Table 2.6 – Values of coefficients  $c_{ti}$  ( $i = 1, \dots, 5$ ) for stepped-ratio transmissions.

Note that, the analytic models in Eq. 2.24 and 2.26 are valid solely at the transmission level when the final drive is single-speed. However, in some drivetrain, particularly a dual clutch transmission (DCT), the final drive are typically of two speeds, which are

engaged to specific gears of transmissions. In this case, ratios  $\mathcal{R}_{t1}$  and  $\mathcal{R}_{tk}$  are considered in terms of the overall gear ratio of transmission and final drive.

In regard to gear efficiency, the predictive analytic models are simplified as in Eq. 2.27 and 2.28 because of limited available transmission efficiency data.

$$k_{t5} = c_{t6}, \quad (2.27)$$

$$k_{t6} = c_{t7}, \quad (2.28)$$

where the coefficient  $c_{t6}$  is zero for light-duty transmissions, and -660.6 for heavy-duty transmissions; the coefficient  $c_{t7}$  is 0.95 for light-duty transmissions, and 0.977 for heavy-duty transmissions.

### 2.3.3 Model Validation

The identification set of stepped-ratio transmissions for the light-duty vehicles is presented and used to identify the coefficients in predictive analytic models. After demonstration of results of gear ratios, the relative errors between description of gear ratio and grid-point data and between prediction and grid-point data are comparatively illustrated and discussed in terms of energy consumption of a reference conventional vehicle over different missions.

The verification of efficiency model is carried out only for one transmission in heavy-duty applications. Due to limited available data and the low energy loss, however, the efficiency of stepped-ratio transmissions is assumed to be constant in light-duty applications.

#### Identification Set

The identification set of stepped-ratio transmissions is composed of five- and six-speed MTs, six-speed ATs, and six-speed DCTs. Main characteristics of these transmissions, including technological parameter  $\mathcal{I}_t$ , gear number  $\mathcal{K}_t$ , speed count of final drive  $\mathcal{K}_{fd}$ , and relating vehicle models, are summarized in Table 2.7. The whole identification set of stepped-ratio transmissions is only for light-duty vehicles.

#### Result

Description and prediction of each stepped-ratio transmission are comparatively illustrated with respect to the grid-point data. The complete identification set is classified into four groups for the presentation of results, which are five-speed MT (denoted by

ID	$\mathcal{I}_t$	$\mathcal{K}_t$	$\mathcal{K}_{fd}$	Vehicle Model
01	MT	5	1	Suzuki Celerio
02	MT	5	1	Audi A1
03	MT	5	1	BMW 318i
04	MT	5	1	VW Der Polo
05	MT	5	1	Renault CLIO II
06	MT	6	1	Volvo V40
07	MT	6	1	Volvo V40
08	MT	6	1	Audi A3
09	MT	6	1	Audi A5
10	MT	6	1	BMW 116i
11	AT	6	1	Ford Kuga
12	AT	6	1	KIA Sportage
13	DCT	6	2	Ford Kuga
14	DCT	6	2	VW Jetta

Table 2.7 – Identification set of stepped-ratio transmissions.

MT-5), six-speed MT (denoted by MT-6), six-speed AT (denoted by AT-6), and six-speed DCT (denoted by DCT-6).

Results of each group, including grid-point data, description, and prediction, are summarized in Fig. 2.12 with different markers. Markers of dot ( $\bullet$ ), circle ( $\circ$ ), and star ( $*$ ) represent the grid-point data, description, and prediction, respectively. Note that, overall gear ratio is considered in the group of DCTs because that DCTs require dual-speed final drive to constitute the stepped ratios.

### Analysis

Analytic models of stepped ratios do not cause any energy losses in Eq. 2.24. However, they affect the operating points of internal combustion engines by shifting engine speed and torque. Therefore, a further analysis was completed to investigate the influences of descriptive and prediction analytic models on the energy consumption of a reference vehicle over two distinct missions. The investigated mission consists of New European Driving Cycle (NEDC) and Highway Fuel Economy Test cycle (HYWFET).

Fig. 2.13 illustrates the results of energy consumption of the reference vehicle with different transmissions from the identification set in Table 2.7. Thanks to descriptive and predictive analytic models in Eq. 2.24 and 2.26, predictions of the energy consumption are close to that evaluated with transmissions of grid-point data over mission profiles of NEDC and HYWFET. The largest error of energy consumption among the investigations

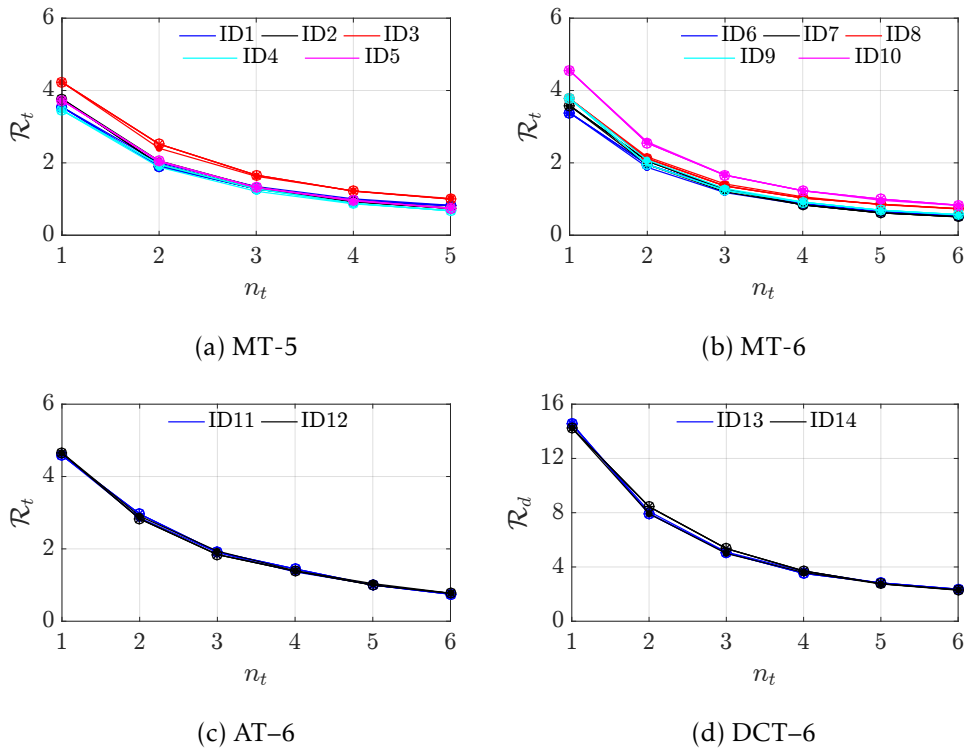


Figure 2.12 – Gear ratio comparison of transmission identification set.

is about 2.7%.

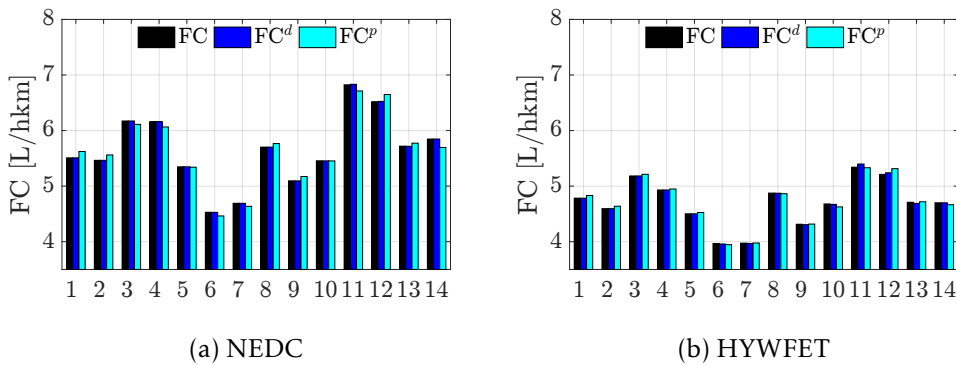


Figure 2.13 – Fuel consumption evaluated with grid-point data, description, and prediction of stepped-ratio transmissions.

Apart from the analysis for analytic models of gear ratios, the analysis for transmission efficiency models is performed in terms of linear regression. The investigated case

is a stepped-ratio transmission for heavy-duty applications.

As shown in Fig. 2.14, results between output power of grid-point data and the one of prediction obtained by Eq. 2.25, 2.27, and 2.28 are presented along the normalized axes. The 5% error lines are depicted with two dashed red lines.

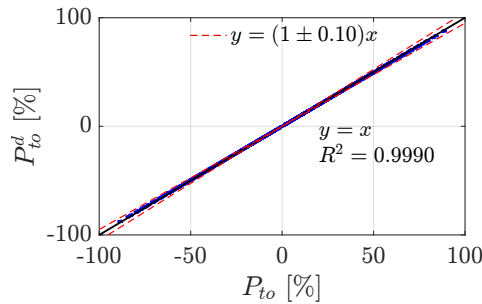


Figure 2.14 – Output power comparison of stepped-ratio transmission.

The the output power of prediction is almost the same as the output power of grid-point data. Yet, the error reduces as the absolute magnitude of the power increase. In other words, the smaller absolute magnitude the power is, the larger the error will be.

## 2.4 Battery

As an essential electric component in hybrid- and battery-electric vehicles, battery is the energy storage component that releases electric power to propel a vehicle in traction phase, and stores electric energy in the regenerative braking phase. As one of the major technologies in the automotive application, the pouch shape Lithium-Ion Battery (LIB) is classified into two types: High Energy (HE) and High Power (HP) type. These two technological dimensioning parameters of LIB are denoted by  $\mathcal{I}_b = \{HE, HP\}$ .

### 2.4.1 Dimensioning Parameter

In an electrified vehicle propulsion system, battery is installed as a battery pack, which contains numerous battery cells in series and/or parallel connection. Battery pack is quantified by battery cell number (denoted by  $\mathcal{K}_b$ ) and nominal parameters of battery cells. Battery cell technology, battery cell number, and battery cell nominal capacity  $\mathcal{Q}_b$ , are considered as the dimensioning parameters of batteries, which yields

$$\mathcal{S}_b = \{\mathcal{I}_b, \mathcal{K}_b, \mathcal{Q}_b\}. \quad (2.29)$$

### 2.4.2 Analytic Model

Parameterization of the battery electrochemical and terminal power (denoted by  $P_{be}$  and  $P_b$ , respectively) is performed for both HE and HP battery cells. The electrochemical and terminal power are calculated based on instantaneous battery state of charge and terminal current. Accordingly, analytic models at both descriptive and predictive level are developed to evaluate the electrochemical power as a function of battery terminal power.

#### At Descriptive Level

Two different descriptive analytic models are established for specific applications. A piece-wise linear predictive analytic model of battery is tailored for the development of fully analytic energy consumption method for hybrid-electric vehicles, whereas a quadratic predictive analytic model of battery is developed for better accuracy and applied to the rest cases.

The chosen quadratic descriptive analytic model of a battery is written by

$$P_{be}(P_b) = k_{b0} + k_{b1}P_b + k_{b2}P_b^2, \quad (2.30)$$

where parameters  $k_{bi}$  ( $i = 0, 1, 2$ ) are identified for each individual battery in the identification set of battery cells in Table 2.11.

On the other hand, the piece-wise linear descriptive model estimates the electrochemical power with a further limited operating range compared with the one in the battery quadratic mode. The piece-wise linear model is expressed by

$$P_{be}(P_b) = \begin{cases} k_{b3} + k_{b4}P_b, & P_b \geq 0, \\ k_{b5} + k_{b6}P_b, & P_b < 0, \end{cases} \quad (2.31)$$

where parameters  $k_{bi}$  ( $i = 3, \dots, 6$ ) are identified for each individual battery in the identification set of battery cells in Table 2.11.

#### At Predictive Level

Corresponding to the descriptive analytic models, two series of predictive models are herein developed. The parameters  $k_{bi}$  ( $i = 0, \dots, 6$ ) in descriptive analytic models of Eq.

2.30 and 2.31 are further expressed as functions of battery dimensioning parameters. The predictive analytic models for the quadratic descriptive analytic model in Eq. 2.30 are expressed in matrix form as

$$\begin{bmatrix} k_{b0} \\ k_{b1} \\ k_{b2} \end{bmatrix} = \begin{bmatrix} c_{b1} & c_{b2} & c_{b3} \\ c_{b4} & c_{b5} & c_{b6} \\ c_{b7} & c_{b8} & c_{b9} \end{bmatrix} \begin{bmatrix} \mathcal{K}_b \\ Q_b \\ \frac{Q_b^2}{\mathcal{K}_b} \end{bmatrix}, \quad (2.32)$$

where coefficients  $c_{bi}$  ( $i = 1, \dots, 9$ ), depending on the battery technological parameter  $\mathcal{I}_b$  and battery cell capacity  $Q_b$ , are listed in Table 2.8 and 2.9.

$\mathcal{I}_b$	$c_{b1}$	$c_{b2}$	$c_{b3}$	$c_{b4}$	$c_{b5}$	$c_{b6}$
HP	-9.542	0.5901	$-5.868 \times 10^{-3}$	1.016	$-2.219 \times 10^{-3}$	$2.305 \times 10^{-5}$
HE	0.1	0	0	0.983	$-7.617 \times 10^{-4}$	$1.224 \times 10^{-5}$

Table 2.8 – Values of coefficients  $c_{bi}$  ( $i = 1, \dots, 6$ ) for lithium-ion battery.

$\mathcal{I}_b$	$Q_b$	$c_{b7}$	$c_{b8}$	$c_{b9}$
HP	–	$1.904 \times 10^{-4}$	$-2.068 \times 10^{-6}$	$4.812 \times 10^{-9}$
HE	$\leq 53$ Ah	$4.489 \times 10^{-4}$	$-6.017 \times 10^{-6}$	0
	$> 53$ Ah	$1.383 \times 10^{-4}$	0	0

Table 2.9 – Values of coefficients  $c_{bi}$  ( $i = 7, \dots, 9$ ) for lithium-ion battery.

The predictive analytic models for the piece-wise linear descriptive analytic model in Eq. 2.31 are expressed as

$$\begin{bmatrix} k_{b3} \\ k_{b4} \\ k_{b5} \\ k_{b6} \end{bmatrix} = \begin{bmatrix} c_{b10} & 0 & 0 & 0 \\ 0 & c_{b11} & c_{b12} & c_{b13} \\ c_{b14} & 0 & 0 & 0 \\ 0 & c_{b15} & c_{b16} & c_{b17} \end{bmatrix} \begin{bmatrix} \mathcal{K}_b \\ Q_b \\ Q_b^2 \\ Q_b^3 \end{bmatrix}, \quad (2.33)$$

where coefficients  $c_{bi}$  ( $i = 10, \dots, 17$ ), depending only on the battery technological parameter  $\mathcal{I}_b$ , are listed in Table 2.10.

### 2.4.3 Model Validation

The identification set of batteries is introduced and used to identify coefficients in predictive analytic models. After the comparative illustration of battery electrochemical

$\mathcal{I}_b$	$c_{b10}$	$c_{b11}$	$c_{b12}$	$c_{b13}$
HP	-0.1138	$7.741 \times 10^{-2}$	$-1.745 \times 10^{-3}$	$1.211 \times 10^{-5}$
HE	-0.0628	$6.561 \times 10^{-2}$	$-1.315 \times 10^{-3}$	$8.368 \times 10^{-6}$
$\mathcal{I}_b$	$c_{b14}$	$c_{b15}$	$c_{b16}$	$c_{b17}$
HP	-0.1767	$6.279 \times 10^{-2}$	$-1.39 \times 10^{-3}$	$9.548 \times 10^{-6}$
HE	-0.1328	$6.036 \times 10^{-2}$	$-1.274 \times 10^{-3}$	$8.496 \times 10^{-6}$

Table 2.10 – Values of coefficients  $c_{bi}(i = 10, \dots, 17)$  for lithium-ion battery.

and terminal power of an example, the mean relative error and statistic characteristics are presented and discussed.

### Identification Set

The identification set of lithium-ion battery cells, including high energy (HE) and high power (HP) type, is presented in Table 2.11 with technological parameter, nominal voltage, and energy density.

ID	$\mathcal{I}_b$	$Q_b$ [Ah]	Nominal Voltage [V]	Energy Density [Wh/kg]
1	HE	25	3.7	162
2	HE	31	3.7	166
3	HE	40	3.7	166
4	HE	53	3.7	171
5	HE	75	3.7	178
6	HP	31	3.7	147
7	HP	40	3.7	153
8	HP	63	3.7	156
9	HP	75	3.7	159

Table 2.11 – Identification set of Li-ion battery cells.

### Result

For simplicity reason, description and prediction of one exemplified battery cell are comparatively illustrated with respect to the grid-point data. The description and prediction are separately evaluated with the quadratic and piece-wise linear analytic models.

Fig. 2.15 demonstrates the grid-point data, description, and prediction in terms of electrochemical power for BAT ID2. The grid-point data, description, and prediction are

aligned well with each other for both quadratic and piece-wise linear analytic models. However, the maximal charging and discharging current are limited more for the piece-wise linear analytic models. Therefore, the magnitude in Fig. 2.15b is smaller than that in Fig. 2.15a.

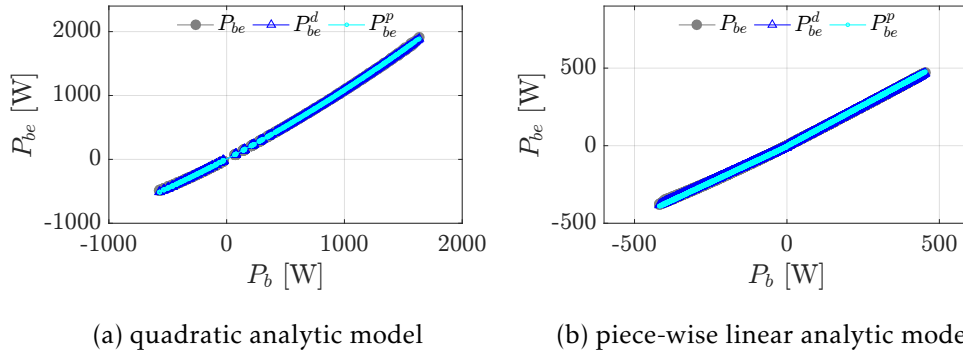


Figure 2.15 – Electrochemical power of battery cell ID2.

### Analysis

The analysis of mean relative error and linear regression is performed to evaluate the accuracy of descriptive and predictive analytic models for lithium-ion battery cells. In particular, analysis of mean relative error is completed for both battery cells and their whole identifications set. Then, the previous exemplified battery cell is further analysed through linear regression method.

Results of mean relative errors – including the mean description error of each battery cell  $\varepsilon_c^d$ , the mean prediction error of each battery cell  $\varepsilon_c^p$ , the average description error of battery cell identification set  $\varepsilon_s^d$ , and the average prediction error  $\varepsilon_s^p$  – are illustrated in Fig. 2.16. To summarize, the quadratic analytic model produces less mean relative errors than the piece-wise linear analytic model did at both descriptive and predictive level. Nonetheless, the maximum mean relative error is less than 10% (battery cell ID4) which is evaluated via the piece-wise linear analytic model.

Considering the linear regression analysis for battery cell ID2, results are summarized in Fig. 2.17. Both description and prediction of different types of analytic models are separately compared with respect to the grid-point data. Obviously, high relative errors occurs at the low absolute power region.

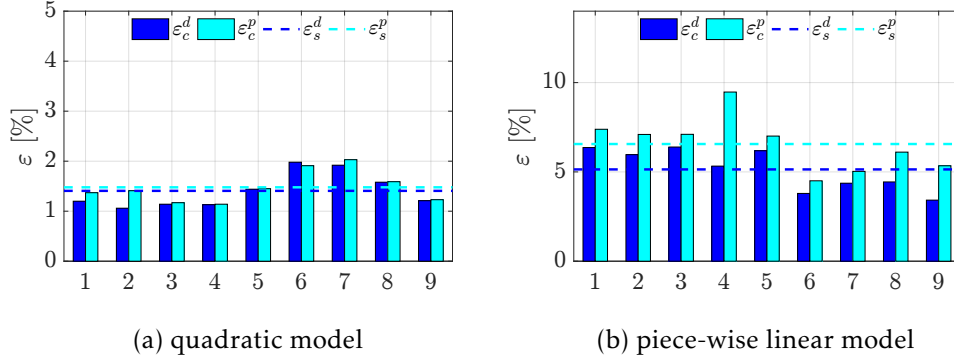


Figure 2.16 – Mean relative errors of battery identification set.

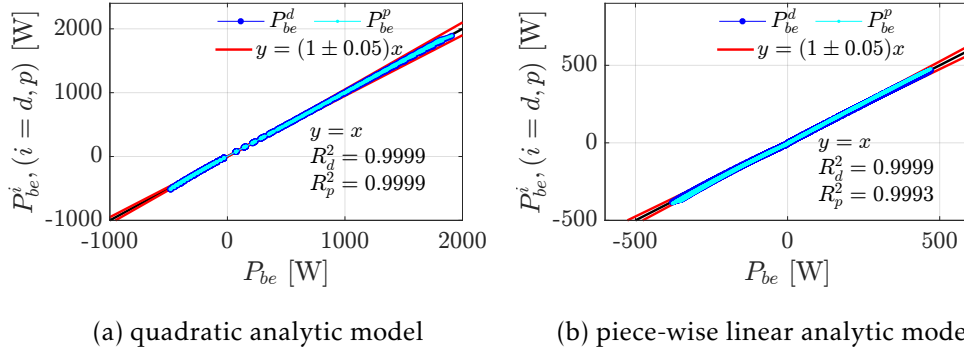


Figure 2.17 – Comparison of electrochemical power of battery for battery cell ID2.

## 2.5 Electric Motor/Generator

Electric Motor/Generator (EMG) is another essential component in an electrified vehicle propulsion system to convert the energy form, such as from electric power to mechanical one, or vice versa. Two types of EMGs are frequently applied in the automotive applications, which are the Permanent Magnet Synchronous Machine (PMSM) and the Asynchronous Induction Machine (AIM). Therefore, the technological parameter of EMG consists of  $\mathcal{I}_m = \{\text{PMSM}, \text{AIM}\}$ .

### 2.5.1 Dimensioning Parameter

An EMG is dimensioned by its nominal torque and power, maximal torque and power, maximum rotational speed in vehicle propulsion systems. In order to evaluate energy consumptions of hybrid- and battery-electric vehicles, the dimensioning parameters are

simplified as nominal torque and nominal power. Meanwhile, peak torque and peak power are assumed to be identical to the nominal torque and power, respectively.

Because the nominal power is the product of the motor base speed and the nominal torque, the dimensioning parameter of nominal power is substituted by the base speed. Thus, the dimensioning parameter set of electric motor/generators is expressed as

$$\mathcal{S}_m = \{\mathcal{T}_m, \mathcal{N}_m\}, \quad (2.34)$$

where  $\mathcal{T}_m$  is the nominal torque, and  $\mathcal{N}_m$  is the base speed. Note that, subscript  $m$  refers to electric motor; whereas subscript  $g$  represents electric generator.

### 2.5.2 Analytic Model

Parameterization of the energy maps is performed to both types of EMGs. Accordingly, analytic models at both descriptive and predictive level are separately developed and validated. Both the losses of an electric machine and the one of power electronics are lumped into the energy map to identify.

#### At Descriptive Level

Regardless of technologies of electric motor/generators, the chosen descriptive analytic model is always expressed by

$$P_{me}(\omega_m, P_m) = k_{m0} + k_{m1}\omega_m + k_{m2}\omega_m^2 + k_{m3}P_m + \frac{k_{m4}}{\omega_m^2}P_m^2, \quad (2.35)$$

where  $\omega_m$  is the rotational speed in [rad/s],  $P_m$  is the mechanical power in [W], and  $P_{me}$  is the electric power in [W]. Parameters  $k_{mi}$  ( $i = 0, \dots, 4$ ) are identified for each individual electric motor/generator in Table 2.14 and 2.15.

#### At Predictive Level

The parameters  $k_{mi}$  ( $i = 0, \dots, 4$ ) in the descriptive analytic model of Eq. 2.35 are further expressed as functions of the dimensioning parameters of electric motor/generators.

These predictive analytic models are expressed in matrix form, such as

$$\begin{bmatrix} k_{m0} \\ k_{m1} \\ k_{m2} \\ k_{m3} \\ k_{m4} \end{bmatrix} = \begin{bmatrix} c_{m1} & c_{m2} & c_{m3} & c_{m4} & c_{m5} & c_{m6} \\ c_{m7} & c_{m8} & c_{m9} & c_{m10} & c_{m11} & c_{m12} \\ c_{m13} & c_{m14} & c_{m15} & c_{m16} & c_{m17} & c_{m18} \\ c_{m19} & 0 & 0 & 0 & 0 & 0 \\ c_{m20} & c_{m21} & c_{m22} & c_{m23} & c_{m24} & c_{m25} \end{bmatrix} \begin{bmatrix} 1 \\ \mathcal{I}_m \\ \mathcal{I}_m^2 \\ \frac{\pi \mathcal{N}_m}{30} \\ \frac{\pi^2 \mathcal{N}_m^2}{30^2} \\ \frac{30^2}{\pi \mathcal{N}_m \mathcal{I}_m} \\ 30 \times 10^3 \end{bmatrix}, \quad (2.36)$$

where coefficients  $c_{mi}$  ( $i = 1, \dots, 25$ ), depending on the technological parameter  $\mathcal{I}_m$ , are listed in Table 2.12 and 2.13; whereas coefficient  $c_{m19}$  is 1 for both PMSM and AIM.

$\mathcal{I}_m$	$c_{m1}$	$c_{m2}$	$c_{m3}$	$c_{m4}$	$c_{m5}$	$c_{m6}$
PMSM	270.7	-13.738	0.0714	0.228	$-3.681 \times 10^{-4}$	8.782
IM	5665.7	-30.811	0.0332	-3.759	$-2.618 \times 10^{-3}$	25.331
$\mathcal{I}_m$	$c_{m7}$	$c_{m8}$	$c_{m9}$	$c_{m10}$	$c_{m11}$	$c_{m12}$
PMSM	-1.215	0.0608	$-2.778 \times 10^{-4}$	$-4.775 \times 10^{-4}$	$1.331 \times 10^{-6}$	-0.0374
IM	-0.326	0.0222	$-2.621 \times 10^{-5}$	$-7.089 \times 10^{-3}$	$8.615 \times 10^{-6}$	$1.859 \times 10^{-5}$
$\mathcal{I}_m$	$c_{m13}$	$c_{m14}$	$c_{m15}$	$c_{m16}$	$c_{m17}$	$c_{m18}$
PMSM	$2.333 \times 10^{-3}$	$-7.110 \times 10^{-6}$	$7.062 \times 10^{-8}$	$-3.476 \times 10^{-6}$	$1.480 \times 10^{-9}$	$2.650 \times 10^{-5}$
IM	$-1.224 \times 10^{-3}$	$7.484 \times 10^{-6}$	$-1.114 \times 10^{-10}$	$5.998 \times 10^{-6}$	$-4.239 \times 10^{-9}$	$-1.118 \times 10^{-5}$

Table 2.12 – Values of coefficients  $c_{mi}$  ( $i = 1, \dots, 18$ ) for electric motor/generator.

$\mathcal{I}_m$	$c_{m20}$	$c_{m21}$	$c_{m22}$	$c_{m23}$	$c_{m24}$	$c_{m25}$
PMSM	0.4441	-0.01356	$7.245 \times 10^{-5}$	0.001948	$2.9231 \times 10^{-7}$	$-6.7541 \times 10^{-3}$
IM	$1.044 \times 10^{-3}$	$5.846 \times 10^{-5}$	$-3.703 \times 10^{-7}$	$4.650 \times 10^{-4}$	$-2.359 \times 10^{-7}$	$-8.128 \times 10^{-5}$

Table 2.13 – Values of coefficients  $c_{mi}$  ( $i = 20, \dots, 25$ ) for electric motor/generator.

### 2.5.3 Model Validation

The identification sets of EMGs, generated by EMTool [66], are presented at the beginning in terms of PMSMs and AIMs, respectively. After the demonstration of electric motor grid-point data in terms of contour maps, the mean relative error and statistic characteristics are summarized and discussed.

### Identification Set

Due to different vehicle applications, two types of identification sets are used to develop and validate the descriptive and predictive analytic models. The identification set of permanent magnet synchronous machine is listed in Table 2.14, including specifications of dimensioning parameters; whereas the identification set of induction machines is summarized in Table 2.15.

Note that, the maximum speed of PMSM and AIM identification set is 20 and 14 krpm, respectively. These values are close to the FLEX HEV developed by IFPEN and early generation of Tesla's electric motor.

ID		1	2	3	4	5	6	7	8
$\mathcal{T}_m$	[Nm]	36	36	36	36	36	72	72	72
$\mathcal{P}_m$	[kW]	15	21	26	32	38	30	41	53
ID		9	10	11	12	13	14	15	
$\mathcal{T}_m$	[Nm]	72	72	108	108	108	108	108	
$\mathcal{P}_m$	[kW]	64	75	45	62	79	96	113	

Table 2.14 – Identification set of electric motor/generators in terms of PMSM.

ID		1	2	3	4	5	6	7	8
$\mathcal{T}_m$	[Nm]	270	270	270	270	330	330	330	330
$\mathcal{P}_m$	[kW]	85	113	141	170	104	138	173	207
ID		9	10	11	12	13	14	15	16
$\mathcal{T}_m$	[Nm]	390	390	390	390	450	450	450	450
$\mathcal{P}_m$	[kW]	123	163	204	245	141	188	136	238

Table 2.15 – Identification set of electric motor/generators in terms of AIM.

### Result

Description and prediction of each electric motor/generator are comparatively illustrated with respect to the grid-point data. For the sake of simplicity, one PMSM and one AIM are depicted and discussed separately. The comparison among grid-point data, description, and prediction of other electric motor/generators are found in Appendix B.2.

Fig. 2.18 demonstrates the grid-point data, description, and prediction in terms of terminal electric power of PMSM ID14, whereas Fig. 2.19 illustrates the grid-point data,

description, and prediction of AIM ID14. The high efficiency zones are enlarged with the description and the prediction compared with the grid-point data for both electric machines. Nonetheless, both description and prediction are still close to the grid-point data. In addition, AIMS work better with the developed analytic models than PMSMs do.

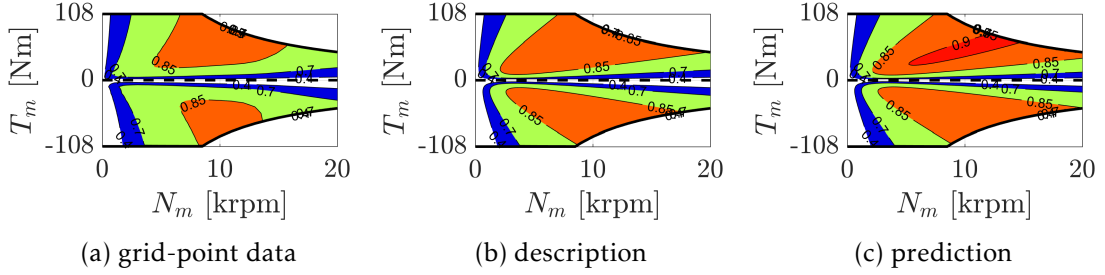


Figure 2.18 – Efficiency map of PMSM ID14.

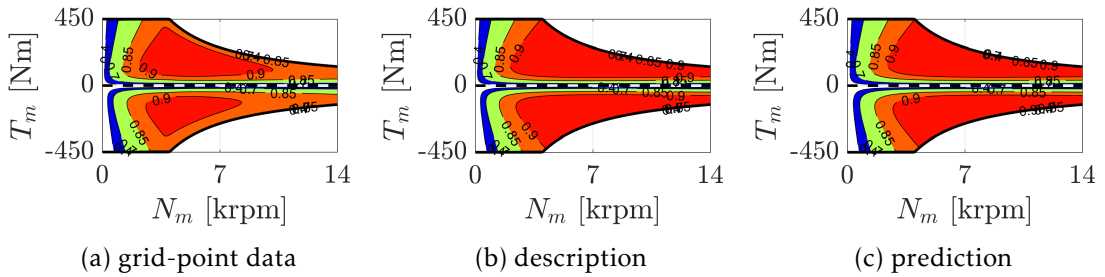


Figure 2.19 – Efficiency map of AIM ID14.

## Analysis

The analysis of mean relative error and linear regression are performed to evaluate the accuracy of descriptive and predictive analytic models for both PMSMs and AIMS. In particular, analysis of mean relative error is completed both for each electric machine and the whole identifications set. Then, the exemplary electric machines depict their contour maps of mean relative error and perform the linear regression analysis.

Mean relative errors – including the mean description error of each component  $\varepsilon_c^d$ , the mean prediction error of each component  $\varepsilon_c^p$ , the average description error of whole identification set  $\varepsilon_s^d$ , and the average prediction error of whole identification set  $\varepsilon_s^p$  – are illustrated in Fig. 2.20 for both PMSMs and AIMS. In summary, the maximum of mean relative error is slightly higher than 10% for AIM ID6. The mean relative error of the identification set of PMSM is lower than that of AIMS.

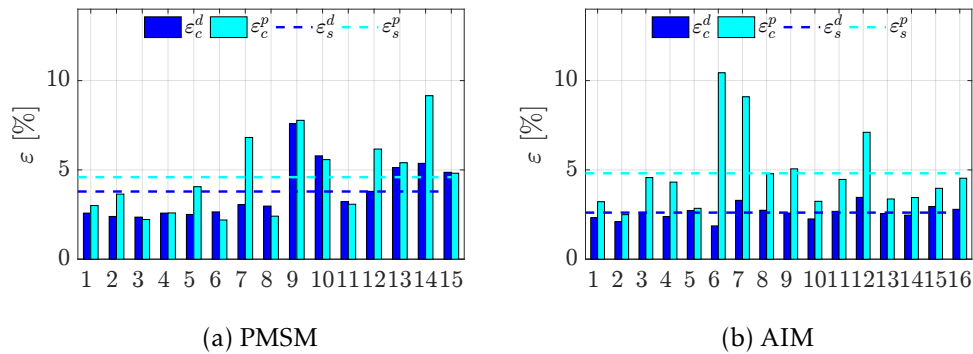


Figure 2.20 – Mean relative error of each electric motor/generator and the whole identification set.

Considering PMSM ID14, its descriptive and predictive relative errors are illustrated in Fig. 2.21a and 2.21b, respectively. The high errors occur at the low torque area. The error in the low-speed high-torque in the generator mode is the intrinsic error from the estimation of EMTool.

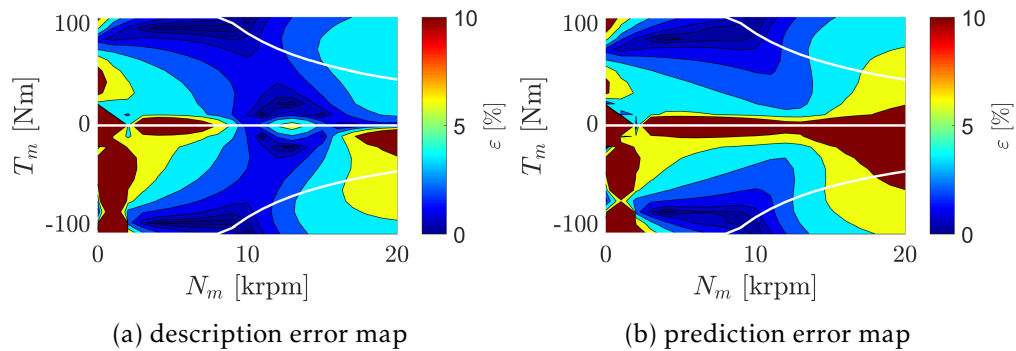


Figure 2.21 – Maps of relative errors of PMSM ID14.

As for AIM ID14, its descriptive and predictive relative errors are illustrated in Fig. 2.22a and 2.22b, separately. Compared with previous case, AIM ID14 shows larger low efficiency area in description and prediction error map, respectively. Yet, the intrinsic error of EMTool is still presented in the low-speed high-torque zone in the generator mode.

Regarding the linear regression analysis, Fig. 2.23 and 2.24 compare the results of electrical power of PMSM ID14 and AIM ID14, respectively. The relative error of the description is limited within 10%, whereas most of relative error of the prediction is limited within 10%.

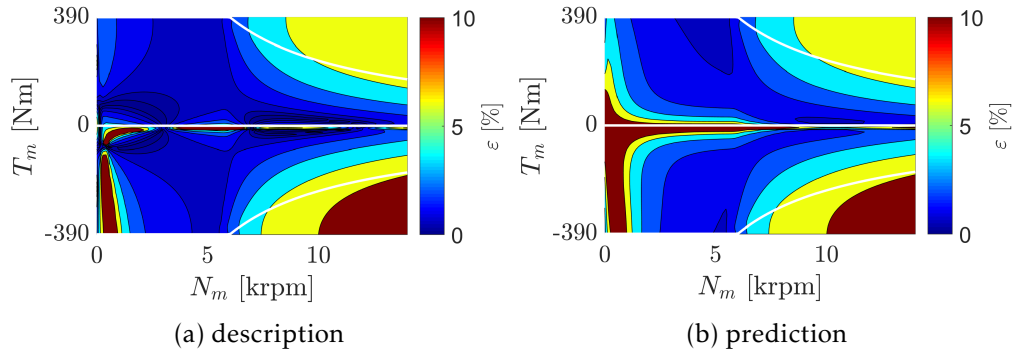


Figure 2.22 – Maps of relative errors of AIM ID14.

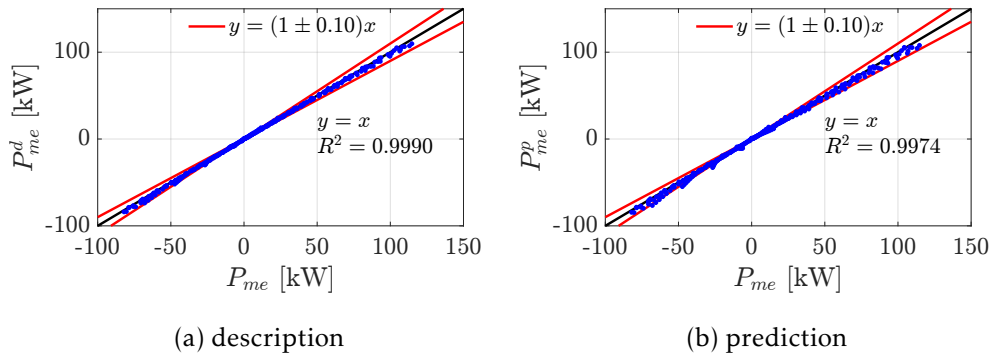


Figure 2.23 – Comparison of electric power of PMSM ID14.

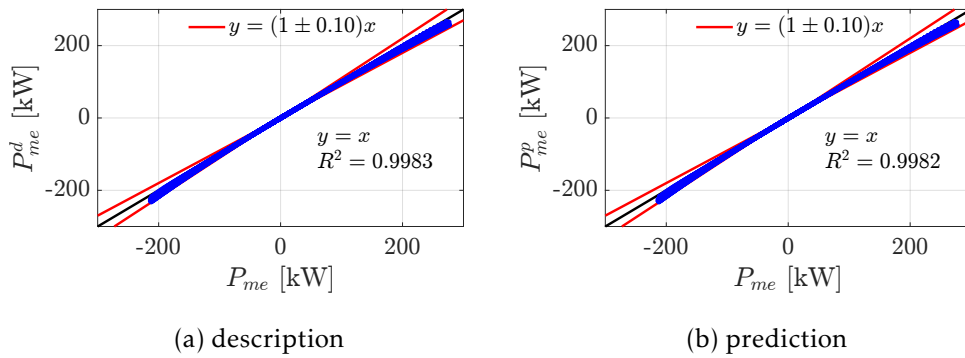


Figure 2.24 – Comparison of electric power of AIM ID14.

## 2.6 Vehicle Load Estimation

Apart from the dimensioning parameters of main powertrain components, vehicle parameters affect the energy consumption as well because of the impacts on vehicle load. In analogue to powertrain dimensioning parameter set, the vehicle parameter set is defined as

$$\mathcal{S}_v = \{m_v, R_w, C_{v0}, C_{v1}, C_{v2}\}, \quad (2.37)$$

where  $m_v$  is the weight of vehicle in [kg],  $R_w$  is the wheel radius in [m],  $C_{vi}$  ( $i = 0, 1, 2$ ) are load parameters identified through coast-down tests.

The vehicle longitudinal dynamics is the essence in vehicle load estimation for the energy consumption evaluation. Considering a vehicle moving on an inclined road as depicted in Fig. 2.25, the vehicle load is evaluated by

$$F_l = C_{v0} \cos \alpha + C_{v1} v \cos \alpha + C_{v2} v^2 + F_{gr} + F_{ir}, \quad (2.38)$$

where  $F_{gr}$  is the gravitational force calculated by  $F_{gr} = m_v g \sin \alpha$ , and  $F_{ir}$  is the inertia force due to acceleration and deceleration.

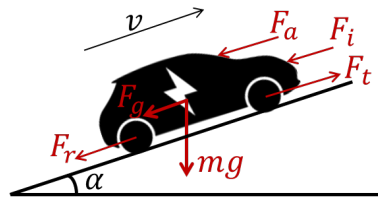


Figure 2.25 – Longitudinal forces acting on a vehicle moving on an inclined road.

Considering the road load parameters  $C_{vi}$  ( $i = 0, 1, 2$ ), they can be approximated with physical ones by

$$C_{v0} \approx m_v g C_{rr}, \quad (2.39)$$

$$C_{v1} \approx 0, \quad (2.40)$$

$$C_{v2} \approx \frac{\rho_{ar} C_{ar} A_{ar}}{2}, \quad (2.41)$$

where  $C_{rr}$  is rolling resistance coefficient,  $C_{ar}$  is drag coefficient,  $A_{ar}$  is frontal area, and  $\rho_{ar}$  is air density.

As for the vehicle mass  $m_v$ , it depends on the dimensioning parameters of powertrain components, which yields

$$m_v = m_{v0} + \mu_e \mathcal{V}_e + \mu_b \mathcal{E}_b + \mu_m \mathcal{P}_m + \mu_g \mathcal{P}_g, \quad (2.42)$$

where  $\mu_i (i = e, b, m, g)$  is a generic weight factor in kilogram per unit, and  $m_{v0}$  is the baseline weight of vehicle.

## **Part II**

# **Numeric Evaluation of Energy Consumption for Advanced Vehicle Propulsion Systems**



# Energy Consumption Evaluation for Single-Source Vehicles

Apart from experimental tests, numeric simulation is a useful approach to estimate the energy consumption of single-source and hybrid-electric vehicles. After a brief introduction of simulation method for energy consumption evaluation, signal flows of quasi-static simulation are summarized for various types of vehicles. The analytic models developed in Chapter 2 are further validated at vehicle propulsion system level in terms of energy consumption.

## 3.1 Simulation Method

Numeric simulation is an efficient and effective method for the energy consumption evaluation. In general, two approaches are frequently applied to the energy consumption simulation: one is the quasi-static approach; and the other one is the dynamic approach.

### 3.1.1 Quasi-static Simulation

In quasi-static simulation, the energy consumption of a vehicle is estimated based on a given mission profile, efficiencies of the vehicle propulsion system depending on operating conditions, and parameters of vehicle features [42, 67]. The quasi-static simulation is performed in backward approach as sketched in Fig. 3.1.

Mission profile, including speed, road slope, etc., is discretized into many intervals by time step  $\Delta t$ . At each interval, variables of a mission profile are assumed to be constant.

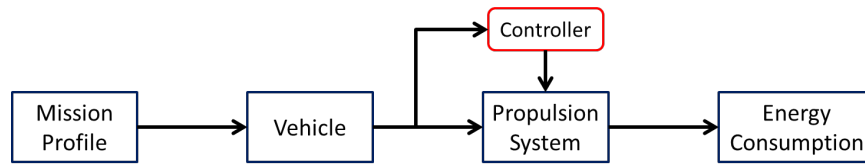


Figure 3.1 – Quasi-static simulation for energy consumption evaluation.

Then, vehicle load is estimated with vehicle parameters and mission variables through the load model in Chapter 2.6. Apart from the estimation of vehicle loads, kinetics of powertrain components are also evaluated with vehicle parameters (such as dynamic radius of tyre), mission variables, and powertrain parameters (for instance, final drive, transmission).

Next, vehicle load and kinetic variables are transmitted to the power source by the drivetrain. For example, vehicle load and speed of a conventional vehicle are transferred to the internal combustion engine in terms of torque and rotational speed, thus leading to the estimation of instantaneous fuel consumption. In contrast, vehicle load and speed in a battery-electric vehicle determine the torque and rotational speed of electric motor/generator, then these signals are used to evaluate voltage and current of battery. As a result, the instantaneous electrochemical power of battery is evaluated with previous proposed analytic models.

Finally, the instantaneous fuel consumption of the internal combustion engine or the electrochemical power of the battery are accumulated to the corresponding energy consumption. Energy consumption of conventional and hybrid-electric vehicles is measured by [L/hkm] (which is identical to [L/100km]); whereas, the metric for battery-electric vehicles is [kWh/km].

The quasi-static simulation is capable of the evaluation of energy consumption of advanced vehicle propulsion systems, particularly the minimum energy consumption of hybrid-electric vehicles. However, the physical causality cannot be respected due to the backward formulation.

### 3.1.2 Dynamic Simulation

Dynamic simulation is based on a mathematical description that represents the physical causality. The model is often formulated in forward approach using sets of ordinary differential equations in its state-space form to describe dynamic effects in a vehicle propulsion system.

Compared with quasi-static simulation, extra powertrain control systems and a

particular driver model are always required, as shown in Fig. 3.2. Powertrain control systems, such as engine control unit and transmission control unit, are lumped into the block of Controller. Because dynamic simulation is not implemented throughout this dissertation, this simulation method is not introduced in details. For example, a typical forward simulation tool ALPHA [68, 69] is available to the public.

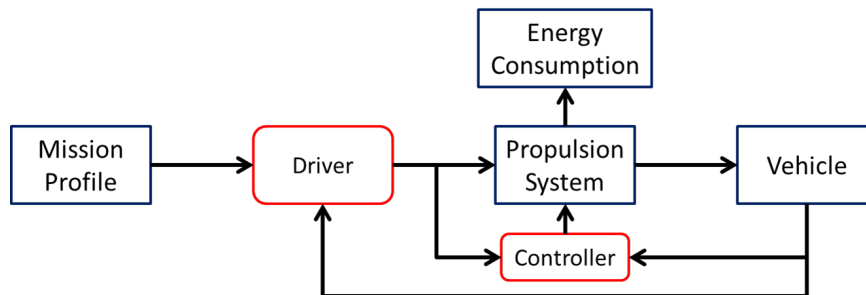


Figure 3.2 – Dynamic simulation for energy consumption evaluation.

## 3.2 Simulation Set-Up

Contributions of this thesis are based on quasi-static simulation method. Therefore, simulation set-ups are solely introduced for the quasi-static simulation in this section.

### 3.2.1 Mission Profile

Mission profile, also known as driving cycle, consists of historical trajectories of typical variables, and is an essential input to energy consumption evaluation for all categories of vehicles. Typical variables consist of speed and road slope (or, alternatively, altitude).

In general, mission profile includes two categories: the standardized driving cycles and the real-world driving cycles. Standardized driving cycles are used for regulation purpose. Energy consumption of a light-duty vehicle is certified by carrying out tests over a standardized driving cycle, such as the New European Driving Cycle (NEDC) in Fig. 3.3. As for real world driving cycles, they are recorded for specific purposes during experimental tests, for instance, a typical mission for urban delivery vans or trucks. More missions applied in this thesis are presented in Appendix C.2, which consists of Federal Test Procedure – 72 (FTP-72), Highway Fuel Economy Test Cycle (HYWFET), Inner City Driving Cycle (ICDC) and Suburban Driving Cycle (SUDC). The main characteristics, including mean speed, distance, and maximal speed, are summarized in Appendix C.1.

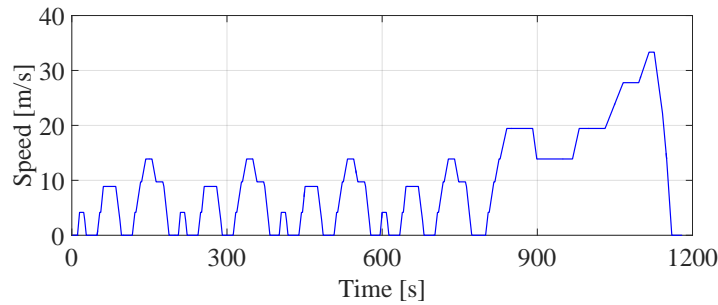


Figure 3.3 – Speed trajectory of NEDC.

Additionally, the trajectory of gear shift is required for vehicles equipped with manual transmissions. Gear shift schedules are usually provided in accordance with the standardized driving cycles. For example, the gear shift schedules, based on [70], for vehicles with five- or six-speed manual transmissions are depicted in Fig. 3.4.

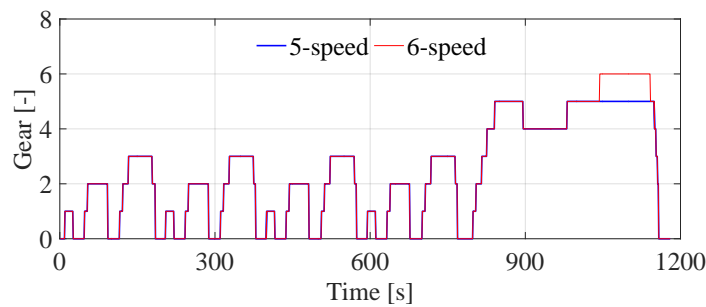


Figure 3.4 – Gear shift schedule over NEDC.

### 3.2.2 Signal Flow

Data in regard with mission profile, vehicle parameters, and vehicle propulsion system features is vital in quasi-static simulations. Variable flows and exchanges for conventional, battery-electric, and hybrid-electric vehicles, are summarized and sketched in terms of quasi-static simulations hereafter.

The evaluation of energy consumption for a conventional vehicle is completed through the quasi-static simulation illustrated in Fig. 3.5. A mission profile abbreviates to MP, whereas vehicle is shorten as VEH. The main powertrain components consist of internal combustion engine (ENG) and drivetrain (short for DRT), latter of which mainly contains a stepped-ratio transmission and final drive.

As shown in Fig. 3.5, vehicle speed  $v$ , acceleration  $a$ , and gear number  $n_t$  are provided by mission profiles. Then, the rotational speed of wheels (denoted by  $\omega_w$ ) and vehicle load in terms of torque (denoted by  $T_l$ ) are evaluated with mission variables and vehicle parameters. Then, the wheel speed and vehicle load are transmitted by the drivetrain to the internal combustion engine. Thus, the output of drivetrain in terms of speed  $\omega_d$  and torque  $T_d$  is identical to the input speed and torque (indicated by  $\omega_e$  and  $T_e$ , respectively) to the internal combustion engine. Losses due to clutches or other coupling devices are not considered. Thanks to the determined engine speed and torque, the instantaneous power of burned fuel is converted from the fuel mass flow rate based on fuel consumption maps. Finally, the fuel consumption in [L/hkm] is computed over the test mission.



Figure 3.5 – Quasi-static simulation for conventional vehicles.

As the other type of single-source vehicles, battery-electric vehicles only consume electric energy stored in battery. The scheme of quasi-static simulation is depicted in Fig. 3.6 for the energy consumption evaluation of a battery-electric vehicle. Apart from mission profiles and vehicle parameters, the main powertrain components of a battery-electric vehicle consist of drivetrain (DRT), electric motor/generator (EMG), and battery (BAT). Currently, a simple drivetrain, including final drive and a single-speed transmission, is widely implemented to battery-electric vehicles.

Due to the implementation of simple gear-trains, variables of a mission profile only account for speed  $v$  and acceleration  $a$ . Then, vehicle load in terms of torque ( $T_l$ ) and wheel speed ( $\omega_w$ ) are calculated using vehicle parameters. The output torque and speed of the drivetrain (indicated by  $T_d$  and  $\omega_d$ ) are directly transmitted to the electric motor/generator. Thus, the speed and torque of EMG ( $\omega_m$  and  $T_m$ ) are equal to the ones of drivetrain. After the electric power of EMG is determined by its speed and torque, the electric power  $P_{me}$  is provided by the battery. Thus, the terminal power of battery  $P_b$  is assumed to be the electric power of EMG. Finally, electrochemical power of battery  $P_{be}$  is estimated at each time step, and then used to evaluate the energy consumption over the test mission.

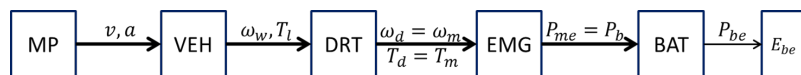


Figure 3.6 – Quasi-static simulation for battery-electric vehicles.

As for hybrid-electric vehicles, the energy consumption is evaluated through quasi-static simulations depending on powertrain architecture. In addition, an energy management strategy (Energy Management Strategy (EMS)) is requested to split the power between different energy sources.

Considering a series HEV, mission variables and vehicle parameters are similar to those of battery-electric vehicles. Compared with powertrain of a battery-electric vehicle, more powertrain components are installed in a series HEV, as illustrated in Fig. 3.7. The additional components consist of an electric generator (short for GEN) and an internal combustion engine (ENG).

Exchanges of variables and parameters are the same as in a battery-electric vehicle except for the involvement of EMS. The electric power of electric motor (MOT)  $P_{me}$  is satisfied by the terminal power of battery  $P_b$  and the electric power of generator  $P_{ge}$ . To minimize the energy consumption of internal combustion engine ( $E_{ef}$ ), optimal control is required to determine control variable  $u$ . Throughout this thesis, control variable is always defined as  $u(t) := P_b(t)$  for series HEVs, and the battery final state of energy is maintained the same as the initial one.

After the determination of control variable  $u$ , the power demand to battery (denoted by  $P_b$ ) and to electric generator (indicated by  $P_{ge}$ ) are used to evaluate the electrochemical power  $P_{be}$  and the power of burned fuel  $P_{ef}$ , respectively. Note that, the mechanical power of electric generator  $P_g$  is identical to the mechanical power of engine  $P_e$ .

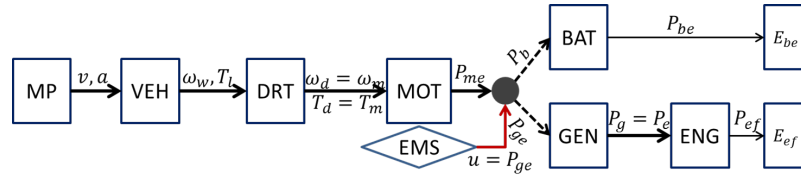


Figure 3.7 – Quasi-static simulation for series hybrid-electric vehicles.

The quasi-static simulation for parallel hybrid-electric vehicles is illustrated in Fig. 3.8, where the parallel HEV is of pre-transmission configuration. Variables and parameters are transmitted in the same way as those are transferred in a conventional vehicle except for the involvement of EMS. The control variable is  $u(t) := P_m(t)$  for parallel HEVs.

Thanks to the pre-transmission configuration, the speed from drivetrain ( $\omega_d$ ) is equal to the speed of engine ( $\omega_e$ ) and the one of electric motor ( $\omega_m$ ). Optimal control techniques are applied to determine the control variable in order to minimize the energy consumption of the internal combustion engine. With determined control variable, the

mechanical power of engine and motor (denoted by  $P_e$  and  $P_m$ , respectively) are used to compute the burned-fuel power  $P_{ef}$  and electrochemical power of battery  $P_{be}$ . Therefore, the energy consumption is evaluated based on the minimized fuel energy  $E_{ef}$ .

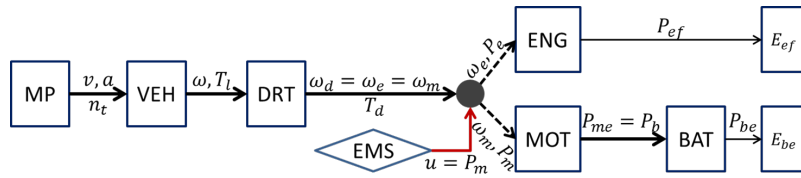


Figure 3.8 – Quasi-static simulation for parallel hybrid-electric vehicles.

To summarize, the quasi-static simulation in backward approach evaluates the instantaneous power based on the discretized variables of the investigated mission profile at each time step. In particular, the traditional optimal control is also realized based on the discretized control variable. Because of the quasi-static simulation, the approach for the energy consumption evaluation is designated as Quasi-Static Simulation (QSS).

### 3.3 Numeric Evaluation of Energy Consumption

In this section, energy consumption of single-source vehicles is evaluated through quasi-static simulation (QSS) based on different types of powertrain data. The categories of component data consist of grid-point data, description (estimated with the descriptive analytic models), and prediction (approximated with the descriptive analytic models). Energy consumption based on different types of powertrain data is compared, analysed, and discussed.

#### 3.3.1 Conventional Vehicle

##### Reference Vehicle

Main features of the investigated conventional vehicle are summarized in Table 3.1, where the internal combustion engine and transmission are the engine ID1 and the dual clutch transmission ID14 in Table 2.5 and Table 2.7, respectively.

##### Results and Analysis

Results of energy consumption in terms of fuel consumption (FC) are depicted in Fig. 3.9 based on three standardized missions, which are NEDC, FTP-72, and HYWFET. The black bars represent the energy consumption evaluated with powertrain models

Vehicle	$m_v$ [kg]	1595
	$R_w$ [m]	0.308
	$C_{v0}$ [N]	134.094
	$C_{v1}$ [N/(m/s)]	3.746
	$C_{v2}$ [N/(m/s) <sup>2</sup> ]	0.3486
Engine	$\mathcal{I}_e$	CI/TC
	$\mathcal{V}_e$ [L]	2.0
	$\mathcal{T}_e$ [Nm]	324
	$\mathcal{P}_e$ [kW]	98
Drivetrain	$\mathcal{I}_t$	DCT-6
	$\mathcal{R}_{fd}$	4.12 & 3.04

Table 3.1 – Features of investigated conventional vehicle.

of grid-point data; the blue bars indicate the evaluations based on descriptive analytic models of powertrain components; and the cyan bars show the evaluations based on predictive analytic models of powertrain components.

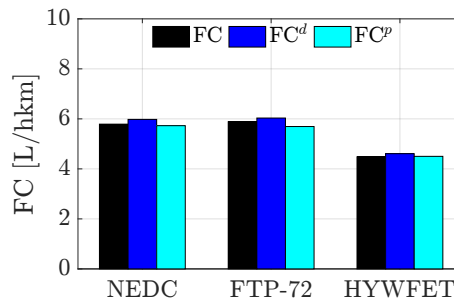


Figure 3.9 – Fuel consumption of reference conventional vehicle based on different types of powertrain component models.

In general, both descriptive and predictive analytic models of powertrain components can estimate energy consumption with high accuracy. The descriptive analytic models slightly overestimate the energy consumption over all mission profiles; whereas the predictive analytic models illustrate less errors than the descriptive analytic models over NEDC and HYWFET. The relative errors are quantified and summarized in Table 3.2 in terms of descriptive and predictive relative error (denoted correspondingly by  $\varepsilon^d$  and  $\varepsilon^p$ ).

Mission Profile	$\varepsilon^d$ [%]	$\varepsilon^p$ [%]
NEDC	3.28	-1.05
FTP-72	2.53	-3.24
HYWFET	2.79	0.42

Table 3.2 – Descriptive and predictive errors of energy consumption with respect to grid-point data.

### 3.3.2 Battery-Electric Vehicle

#### Reference Vehicle

The investigated battery-electric vehicle is specified in Table 3.3, in which battery cells are of high energy ID4 and the electric motor/generator is PMSM ID7 in Table 2.11 and Table 2.14, respectively. The gear ratio of drivetrain is the combination of final drive and the motor gear ratio, which is computed by  $\mathcal{R}_d = \mathcal{R}_m \mathcal{R}_{fd}$ .

Vehicle	$m_v$ [kg]	1318
	$R_w$ [m]	0.287
	$C_{v0}$ [N]	94.731
	$C_{v1}$ [N/(m/s)]	5.931
	$C_{v2}$ [N/(m/s) <sup>2</sup> ]	0.2865
Battery	$\mathcal{I}_b$	HE
	$\mathcal{Q}_b$ [Ah]	53
	$\mathcal{K}_b$	88
Electric Motor	$\mathcal{I}_m$	PMSM
	$\mathcal{T}_m$ [Nm]	108
	$\mathcal{P}_m$ [kW]	45
Drivetrain	$\mathcal{R}_d$	21

Table 3.3 – Features of investigated battery-electric vehicle.

### Results and Analysis

Similar to the investigated conventional vehicle, energy consumption of the battery-electric vehicle are evaluated based on grid-point data, descriptive analytic models, and predictive analytic models of powertrain components. As two types of descriptive analytic models are developed for battery, results of energy consumption are presented into two groups, which are illustrated in Fig. 3.10a and 3.10b, respectively.

The quadratic analytic model of battery presents less errors in energy consumption

evaluation than the piece-wise linear analytic model does. Therefore, quadratic analytic model of battery is widely implemented in all types of electrified vehicle propulsion systems. In contrast, the piece-wise linear battery model is only applied in the fully-analytic energy consumption evaluation method for hybrid-electric vehicles, which aims to involve more powertrain dimensioning parameters as well as to reduce the complexity of combined analytic model of battery and electric motor/generator.

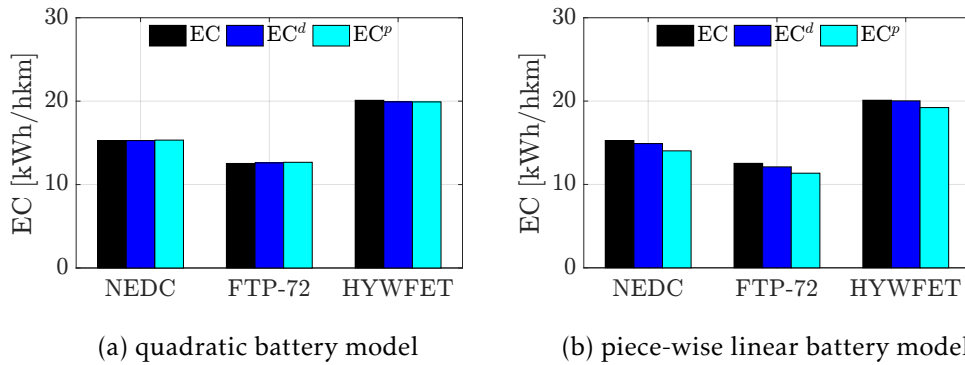


Figure 3.10 – Energy consumption of reference battery-electric vehicle based on different types of powertrain component models.

Furthermore, relative errors of energy consumption of descriptive and predictive analytic models compared with those of grid-point data are listed in Table 3.4b and 3.4a correspondingly for the quadratic and piece-wise linear battery model. The quadratic battery model shows higher accuracy than the piece-wise linear model. As a result, the piece-wise linear battery model is used only in limited conditions where the quadratic battery model is no longer feasible.

Mission Profile	$\varepsilon^d$ [%]	$\varepsilon^p$ [%]
NEDC	0	0.39
FTP-72	0.56	1.12
HYWFET	-0.90	-0.95

(a) quadratic battery model

Mission Profile	$\varepsilon^d$ [%]	$\varepsilon^p$ [%]
NEDC	-2.42	-8.12
FTP-72	-3.35	-9.42
HYWFET	0.35	-4.38

(b) piece-wise linear battery model

Table 3.4 – Relative errors of energy consumption based on descriptive and predictive analytic models.

# Minimal Energy Consumption of Hybrid-Electric Vehicles

In this chapter, novel fast-running methods are proposed to estimate the minimal energy consumption of hybrid-electric vehicles, particularly series and parallel HEVs. Benchmarked by standard approaches of Pontryagin's Minimum Principle, the novel methods, Selective Hamiltonian Minimization (SHM) and GRaphical-Analysis-Based Energy Consumption Optimization (GRAB-ECO), significantly decrease the computation time of the evaluation of the minimum energy consumption for hybrid-electric vehicles.

## 4.1 Optimal Control Problem Formulation

Energy consumption is influenced by the powertrain control technique in a hybrid-electric vehicle. To benchmark the energy consumption in the early design stage, optimal control technique is applied to evaluate the minimum energy consumption. The optimal control problem of an HEV is formulated to minimize the objective function, which is

$$J(u(t)) = \int_{t_0}^{t_f} P_{ef}(u(t), t) dt, \quad (4.1)$$

where control variable  $u(t)$  depends on powertrain architectures, which yields

$$u(t) = \begin{cases} P_b(t), & \text{series HEV,} \\ P_m(t), & \text{parallel HEV.} \end{cases} \quad (4.2)$$

Considering the system dynamics  $\dot{x}$ , it is independent from the system state and defined by

$$\dot{x}(t) = P_{be}(t). \quad (4.3)$$

The minimal energy consumption of an HEV is tailored for the charge-sustaining mode throughout this thesis. In other words, the final battery state of charge is  $x(t_f) = x(t_0)$ , thus leading to the varied electrochemical energy  $\Delta E_{be}(t_f) = 0$ .

According to Pontryagin's Minimum Principle and the independence of system state, the Hamiltonian function is expressed by

$$H(u(t), t) = P_{ef}(u(t), t) + s \cdot P_{be}(u(t), t), \quad (4.4)$$

where  $s$  is the adjoint state variable.

Within the full control space  $U$  in-between the bottom and top boundaries of the control variable, optimal control laws  $u^*(t)$  are determined by finding

$$u^*(t) = \underset{u \in U}{\operatorname{argmin}} H(u(t), s^*, t), \quad (4.5)$$

where the proper adjoint state variable  $s^*$  is evaluated based on the final state of charge requirement, which yields

$$\Delta E_{be}(t_f, s^*) = 0. \quad (4.6)$$

The constraints in the optimal control problem consist of singularity, equality and in-equality conditions due to powertrain limitations and models. Depending on the hybrid architecture, the equality constraint refers to the "power balance" yielding

$$\begin{cases} P_{ge}(t) + P_b(t) = P_{me}(t), & \text{series HEV,} \\ P_m(t) + P_e(t) = P_d(t), & \text{parallel HEV,} \end{cases} \quad (4.7)$$

where  $P_{me}$  is the electric power of traction motor satisfied by battery terminal power  $P_b$  and electric power of generator  $P_{ge}$ ;  $P_d$  is the power demand of drivetrain satisfied by engine brake power  $P_e$  and mechanical power of electric motor  $P_m$ .

Concerning the inequality constraints, they originate from the physical limits of the powertrain components and the operating limits, such as the boundaries of battery

terminal power. However, the constraint of instantaneous battery state of charge is not considered throughout this thesis.

## 4.2 Fully Numeric Solution

Based on PMP, Hybrid Optimization Tool (HOT) [71] and Vectorized Hybrid Optimization Tool (VHOT) [72] are simulation tools of iterative and vectorized approach, respectively. As standard approaches, both HOT and VHOT benchmark the performance of novel fast-running methods in Section 4.3 and 4.4.

Because HOT and VHOT are not the main outcomes of this thesis, the basic ideas and characteristics are briefly summarized for introduction. In both HOT and VHOT, the control variable  $u(t)$  at each time step is quantified as

$$u_k(t) = u_0(t) + k\Delta u, \quad (k = 0, 1, \dots, n_u), \quad (4.8)$$

where  $u_0$  is the minimal admissible value of control variable  $u(t)$ ,  $\Delta u$  is the control variable step, and  $n_u$  is the resolution of discretization. According to the power balance in Eq. 4.7, the Hamiltonian function in Eq. 4.4 is evaluated for each discretized control variable  $u_k(t)$  at each time step.

The main difference between HOT and VHOT is the minimization process. The minimal energy consumption is evaluated through iterative processes in HOT as shown in Fig. 4.1a, whereas the minimization of energy consumption is performed through the array operation in VHOT as depicted in Fig. 4.1b. HOT needs three loops to evaluate the minimum energy consumption, which complete a specific mission, find optimal control laws, and determine proper adjoint state variable. The discrepancy of the final state of the control system is taken into account by the equivalent fuel consumption model in Chapter 6.2.2. In contrast, VHOT minimizes the energy consumption based on array operation. The final battery state of charge is maintained to be the same as the desired value, thereby leading to the estimation of the proper adjoint state variable by numeric interpolation. Thanks to the substitution of iteration with array operation, VHOT takes much less computation time than HOT does. Relevant results are found in Section 4.5.

In the flow charts of HOT and VHOT in Fig 4.1, variable  $\mathcal{C}$  denotes the cycle-related variables (such as speed, acceleration); whereas  $\mathcal{D}$  indicates the dimension-related parameters (including dimensioning parameters of powertrain components and vehicle parameters). Variable  $V(t, u, s)$  represents generic variables along dimensions of time  $t$ , control  $u$ , and adjoint variable  $s$ .

As a solution of LMS Imagine.Lab Amesim, HOTA is introduced with details in [65, 71, 73]. The improved version VHOTA is specifically reported in [72].

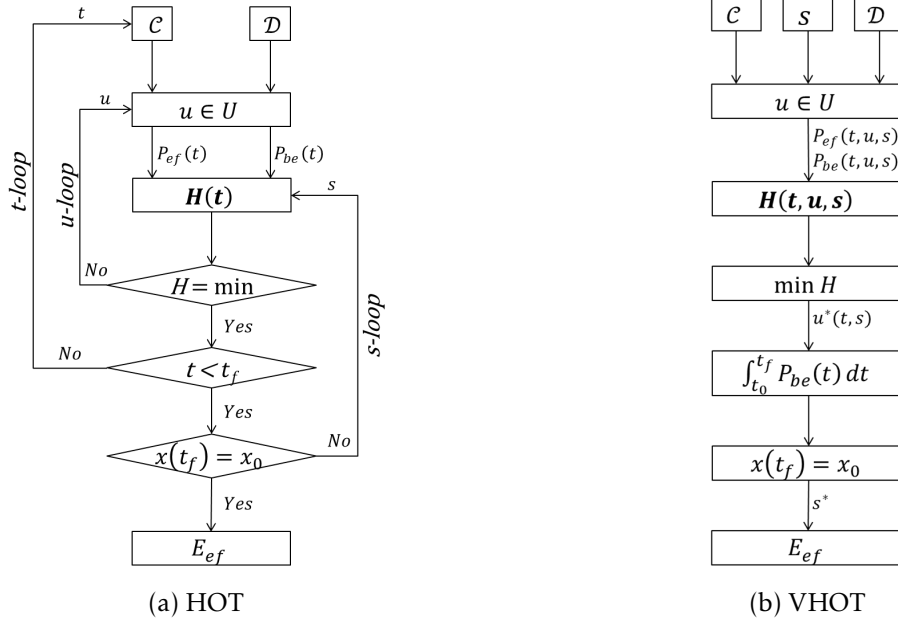


Figure 4.1 – Flow chart of PMP-based standard approaches.

### 4.3 Semi-Analytic Solution

A novel semi-analytic method is proposed to estimate the minimal energy consumption for series or parallel hybrid-electric vehicles, which takes less computation time than both HOTA and VHOTA. Thanks to analytic models of powertrain components, the Hamiltonian function is formulated in closed form in the novel method. Therefore, solution to the minimization of Hamiltonian is derived analytically. Due to further limited possible optimal control cases (denoted by  $U_i (i = 1, 2, \dots)$ ) in the full control space, this method is designated as Selective Hamiltonian Minimization (SHM).

The flow chart of SHM is illustrate in Fig. 4.2. Compared with the full quantification of control variable in HOTA and VHOTA, SHM reduces its full control space into limited number of cases. In details, five ( $i = 5$ ) cases are considered for series HEVs; whereas six ( $i = 6$ ) cases exist for parallel HEVs. Except for the dimension reduction of the full control space, the procedure and operation of SHM is the same as that of VHOTA. Therefore, SHM can be concluded as an analytic version of VHOTA.

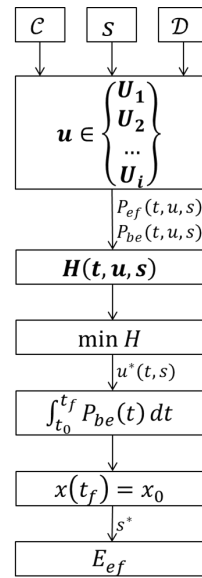


Figure 4.2 – Flow chart of SHM.

### 4.3.1 Series Hybrid-Electric Vehicle

Analytically solvable Hamiltonian is formulated based on analytic models of powertrain components and vehicle load given in Chapter 2. However, the Hamiltonian function cannot be formulated in closed form due to the operation of the internal combustion engine and electric generator.

#### Auxiliary Power Unit

In series HEVs, the auxiliary power unit is a combination of internal combustion engine and electric generator. Due to the engine speed is independent from the wheel speed, the operating condition of an Auxiliary Power Unit (APU) is totally independent from the vehicle operating condition. To simplify the operation of an APU, it is managed to follow the Optimal Operating Line (OOL), which represents the best operating efficiency. Therefore, the analytic model required to formulate the closed form Hamiltonian is given by

$$P_{ef}(P_{ge}) = k_{u0} + k_{u1}P_{ge} + k_{u2}P_{ge}^2, \quad (4.9)$$

where coefficients  $k_{ui}$  ( $i = 0, 1, 2$ ) are numerically identified from either the descriptive or the predictive analytic models of internal combustion engines and electric generators.

### Hamiltonian Function

According to the power balance in Eq. 4.7, the electric power of an APU is calculated by

$$P_{ge}(t) = P_{me}(t) - P_b(t). \quad (4.10)$$

Combining Eq. 4.9 and 4.10, Hamiltonian in Eq. 4.4 is rewritten as

$$H(t, u, s) = k_{h0} + k_{h1}(s)P_b(t) + k_{h2}(s)P_b^2(t), \quad (4.11)$$

where the control variable is  $u := P_b(t)$ , and parameters  $k_{hi}$  ( $i = 0, 1, 2$ ) are expressed as

$$k_{h0}(t, s) = k_{u0} + k_{u1}P_{me}(t) + k_{u2}P_{ge}^2(t) + sk_{b0}, \quad (4.12)$$

$$k_{h1}(t, s) = sk_{b1} - k_{u1} - 2k_{u2}P_{me}(t), \quad (4.13)$$

$$k_{h2}(s) = sk_{b2} + k_{u2}. \quad (4.14)$$

Due to physical limits, the operating constraints of battery are summarized as

$$P_b(t) \in [\underline{P}_b, \overline{P}_b]. \quad (4.15)$$

Taking the physical limits of APU ( $P_{ge}(t) \in [0, \overline{P}_{ge}]$ ) and the power balance in Eq. 4.10 into account, another operating constraint of battery is derived as

$$P_b(t) \in [P_{me}(t) - \overline{P}_{ge}, P_{me}(t)]. \quad (4.16)$$

### Minimization of Hamiltonian

The unconstrained solution to the minimization of Hamiltonian is derived from  $\frac{\partial H}{\partial u} = 0$  ( $u = P_b(t)$ ), which yields

$$P_{b,unc}(t, s) = \frac{k_{u1} + 2k_{u2}P_{me}(t) - sk_{b1}}{2(sk_{b2} + k_{u2})}. \quad (4.17)$$

Considering the possible constrained solutions resulting from the physical and operating limits of powertrain components, the constrained possible solutions to the minimization of Hamiltonian are expressed by

$$P_{b,c1}(t) = P_{me}(t), \quad (4.18)$$

$$P_{b,c2}(t) = P_{me}(t) - \bar{P}_{ge}, \quad (4.19)$$

$$P_{b,c3}(t) = \bar{P}_b, \quad (4.20)$$

$$P_{b,c4}(t) = \underline{P}_b. \quad (4.21)$$

Considering  $U_1 := P_{b,unc}(t, s)$ ,  $U_2 := P_{b,c1}(t)$ ,  $U_3 := P_{b,c2}(t)$ ,  $U_4 := P_{b,c3}(t)$ ,  $U_5 := P_{b,c4}(t)$ , the full control space  $U$  for series hybrid-electric vehicles is defined by

$$u \in \{U_1, U_2, \dots, U_5\}. \quad (4.22)$$

### 4.3.2 Parallel Hybrid-Electric Vehicle

Being comparable to APU, the Electric Drive Unit (EDU) is applied in parallel hybrid-electric vehicles to formulate the closed-form Hamiltonian function so that it can be solved analytically. The EDU is a combination of the battery and electric motor, which both have quadratic analytic models. To formulate the closed-form Hamiltonian function, an analytic model of EDU must be derived.

#### Electric Drive Unit

Considering the analytic model of battery in Eq. 2.30 and the one of electric motor/-generator in Eq. 2.35, the electrochemical power of an EDU is analytically modeled by

$$P_{be}(P_m, \omega_m) = k_{u0}(\omega_m) + k_{u1}(\omega_m)P_m(\omega_m) + k_{u2}(\omega_m)P_m^2(\omega_m), \quad (4.23)$$

where the coefficients  $k_{ui}$  ( $i = 0, 1, 2$ ) are numerically identified from either the grid-point data, description, or prediction of batteries and electric motor/generators. Note that, the quadratic analytic model of battery is applied for better accuracy.

#### Hamiltonian Function

According to the power balance in Eq. 4.7, the engine power is calculated by

$$P_e(t) = P_d(t) - P_m(t). \quad (4.24)$$

Combining Eq. 4.23 and 4.24, the Hamiltonian function in Eq. 4.4 is re-written by

$$H(t, u, s) = k_{h0}(t, s) + k_{h1}(t, s)P_m(t) + k_{h2}(t, s)P_m^2(t), \quad (4.25)$$

where the control variable is  $u := P_m(t)$ . The parameters  $k_{hi}$  ( $i = 0, 1, 2$ ) are

$$k_{h0}(t, s) = k_{e0}(t) + k_{e1}(t)P_d(t) + k_{e2}(t)P_d^2(t) + sk_{u0}(t), \quad (4.26)$$

$$k_{h1}(t, s) = sk_{u1}(t) - k_{e1}(t) - 2k_{e2}(t)P_d(t), \quad (4.27)$$

$$k_{h2}(t, s) = sk_{u2}(t) + k_{e2}(t), \quad (4.28)$$

where parameter  $k_{e2}$  is null when light-duty engines are applied.

As given by Eq.4.25, the closed-form Hamiltonian is formulated as a quadratic function of control variable  $P_m$ , despite the piece-wise linear model for light-duty engines in Eq.2.2. In fact, only the first case of the piece-wise linear model is considered, because the complete range of engine efficiency has been fully considered in this case. To remind that engine corner power  $P_{ec}$  represents the best efficiency of an engine.

Considering the physical limits, the constraints of electric motor/generator are given by

$$P_m(t) \in [\underline{P}_m(t), \bar{P}_m(t)]. \quad (4.29)$$

In addition, the physical limits of internal combustion engine ( $P_e(t) \in [0, \bar{P}_e(t)]$ ) and the power balance in Eq. 4.24 result a second constraint, which is

$$P_m(t) \in [P_d(t) - \bar{P}_e(t), P_d(t)]. \quad (4.30)$$

Apart from operating constraints, an extra discontinuity in Eq. 2.2 is considered that leads to the mechanical power of electric motor

$$P_m(t) = P_d(t) - P_{ec}(t). \quad (4.31)$$

### Minimization of Hamiltonian

The unconstrained solution to the Hamiltonian minimization is derived by  $\frac{\partial H}{\partial u} = 0$  ( $u = P_m(t)$ ), which yields

$$P_{m,unc}(t, s) = \frac{k_{e1}(t) + 2k_{e2}(t)P_d(t) - sk_{u1}(t)}{2(sk_{u2}(t) + k_{e2}(t))}. \quad (4.32)$$

The possible constrained solutions resulting from the operating constraints of pow-

ertain components are expressed as

$$P_{m,c1} = P_d(t), \quad (4.33)$$

$$P_{m,c2} = P_d(t) - \bar{P}_e(t), \quad (4.34)$$

$$P_{m,c3} = \bar{P}_m(t), \quad (4.35)$$

$$P_{m,c4} = \underline{P}_m(t). \quad (4.36)$$

As for the discontinuous solution, it is written by

$$P_{m,s1} = P_d(t) - P_{ec}(t). \quad (4.37)$$

Considering  $U_1 := P_{m,unc}(t, s)$ ,  $U_2 := P_{m,c1}(t)$ ,  $U_3 := P_{m,s1}(t)$ ,  $U_4 := P_{m,c3}(t)$ ,  $U_5 := P_{m,c4}(t)$ ,  $U_6 := P_{m,c2}(t)$ , the full control space  $U$  for parallel hybrid-electric vehicles is defined by

$$u \in \{U_1, U_2, \dots, U_6\}. \quad (4.38)$$

### 4.3.3 Summary

One unconstrained solution and a limited number of constrained and discontinuous solutions owing to operating limits and discontinuity of analytic models constitute the full control space  $U$  of the Selective Hamiltonian Minimization (SHM). The computation time of SHM benefits from the decreased dimensions of the full control space  $U$ .

Compared with HOT and VHOT, SHM is characterized by an analytic solution of the Hamiltonian function. Although the engine on/off signal is not handled explicitly in the minimization of Hamiltonian, the corresponding case of engine off exists in the full control space. However, analytic method cannot find a suitable adjoint state variable  $s^*$  such that the varied electrochemical energy of battery meets the requirement.

Furthermore, it is impossible to evaluate the energy consumption through a closed-form solution along the time dimension. In other words, SHM evaluates the minimal energy consumption step by step along the time dimension. The procedure and operation of energy consumption minimization of SHM is the same as VHOT.

## 4.4 Approximate Solution

It is always not enough to reduce the computation time of minimal energy consumption estimation for hybrid-electric vehicles as the optimal design of vehicle propulsion

systems is always time-consuming. An extreme fast-running sub-optimal method, GRAB-ECO, is proposed to approximate the minimal energy consumption for series and parallel HEVs.

#### 4.4.1 Fundamentals of GRAB-ECO

GRAB-ECO, standing for GRaphical-Analysis-Based Energy Consumption Optimization, approximates the minimal energy consumption by maximizing the average operating efficiency of the primary energy source, which has the worst efficiency. The primary energy source is the auxiliary power unit in a series HEV, and the internal combustion engine in a parallel HEV.

The working flow of GRAB-ECO is summarized and sketched in Fig. 4.3. The GRAB-ECO is characterized by a best-efficiency indicator  $I_e(t)$ , permutation of variables  $I_e(\tau)$ , and limited operating modes.

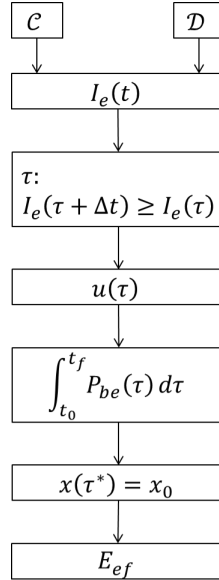


Figure 4.3 – Flow chart of GRAB-ECO.

The best-efficiency indicator evaluates the ratio between the demanded power to the power of the best efficiency of the primary energy source (e.g. APU in series hybrid-electric vehicles, and engine in parallel hybrid-electric vehicles) as well as determines the operating mode at each time step.

In regard with operating modes over a given mission, they consist of the **electric vehicle operation** and **hybrid vehicle operation**. In each operating mode, two sub-modes are categorized in terms of the **fixed mode** and **flexible mode**. Therefore, the

four operating modes are the *fixed electric vehicle mode (ev0)*, the *flexible electric vehicle mode (ev1)*, the *fixed hybrid vehicle mode*, and the *flexible hybrid vehicle mode (hv1)*. A mathematical definition of these four operating modes will be found in Step 2 in the following section.

#### 4.4.2 Essential Steps of GRAB-ECO

GRAB-ECO consists of four essential steps: the evaluation of best-efficiency indicator, the determination of instantaneous operating mode, the approximation of battery state of charge, and the estimation of minimal energy consumption.

##### Step 1: Indicator Evaluation

An indicator evaluates the distance between the power demand and the best-efficiency operating condition of the primary power source. Thus, this indicator is designated as the best-efficiency indicator. The higher the best-efficiency indicator, the greater the opportunity to shift the operation of the primary energy source to the best-efficiency point. On the other hand, the lower the best-efficiency indicator, the higher the opportunity to eliminate the operation of the primary energy source. In the unconstrained condition, the best-efficiency indicator  $I_e$  is evaluated by

$$I_e(t) = \begin{cases} \frac{P_{me}(t)}{P_{apu}}, & \text{series HEV,} \\ \frac{P_d(t)}{P_{ec}(t)}, & \text{parallel HEV,} \end{cases} \quad (4.39)$$

where  $P_{apu}$  is the absolute electrical power of the best-efficiency operating point of APU,  $P_{me}$  the power demand of the electric motor in a series HEV,  $P_d$  is the power demand of the drivetrain in a parallel HEV, and  $P_{ec}$  is the corner power of an internal combustion engine.

When the indicator  $I_e(t) = 0$ , the primary energy source does not provide any power. In other words, an HEV could be in standstill condition or in pure battery electric vehicle operating condition. When the indicator  $I_e(t) = 1$ , the primary energy source is working at its best efficiency regardless of the battery operating conditions. An example of the unconstrained best-efficiency indicator  $I_e$  is illustrated in Fig. 4.4 for a parallel HEV. The power of drivetrain estimated over NEDC is presented as well.

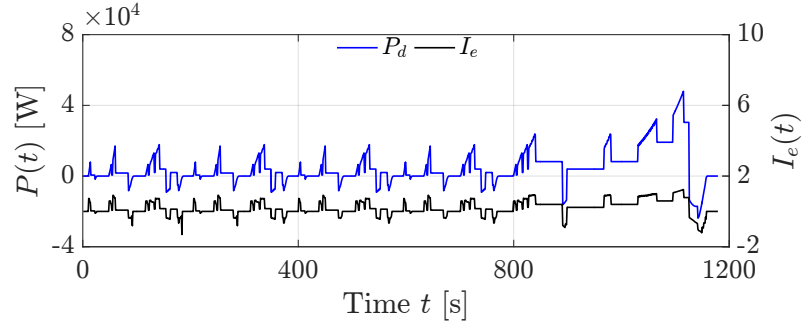


Figure 4.4 – Example of best-efficient indicator and power of drivetrain over NEDC.

### Step 2: Mode Determination

To explicitly determine the vehicle operating mode, a sorted best-efficiency indicator  $I_e(\tau)$  is obtained according to a new time series  $\tau$ . The new time series  $\tau$  is the permutation of time  $t$ , such that

$$I_e(\tau + \Delta t) \geq I_e(\tau), \forall \tau \in [t_0, t_f], \quad (4.40)$$

where  $\Delta t$  is the time step,  $t_0$  and  $t_f$  correspond to the first and last time step of the investigated mission. For example, a mapping between the actual discrete time index (denoted by  $t$ ) and the sorted index (denoted by  $\tau$ ) is illustrated in Fig. 4.5.

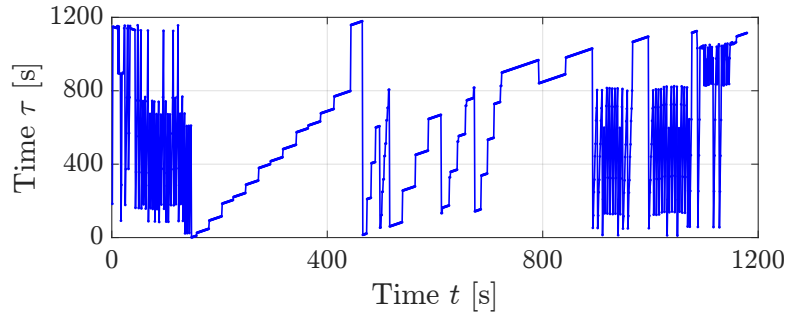


Figure 4.5 – Example of mapping between actual and sorted time index over NEDC.

Based on the sorted best-efficiency indicator  $I_e(\tau)$  over time series  $\tau$  (see Fig. 4.6), operating constraints of powertrain components are sorted and then considered to determine vehicle operating modes. The basic idea to cope with the operating constraints is to maximize the instantaneous operating efficiency of the primary energy source at

each time interval either by eliminating the engine operation or by implementing the maximal efficiency of the primary energy source. An example of the implementation of constraints is reported in [60].

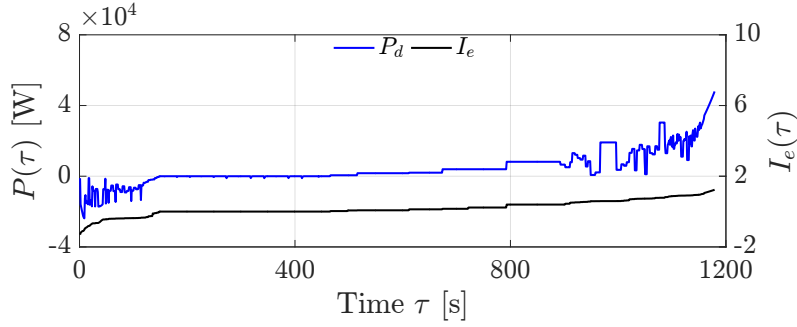


Figure 4.6 – Example of sorted variables over NEDC.

The operating modes of a series HEV and of a parallel HEV are correspondingly determined by

$$u(\tau) := P_b(\tau) = \begin{cases} P_{me}(\tau), & \tau \in [\tau_0, \tau_1], \\ P_{me}(\tau), & \tau \in (\tau_1, \tau^*], \\ P_{me}(\tau) - P_{apu}(\tau), & \tau \in (\tau^*, \tau_2), \\ P_{me}(\tau) - P_{apu}(\tau), & \tau \in [\tau_2, \tau_f], \end{cases} \quad (4.41)$$

and

$$u(\tau) := P_m(\tau) = \begin{cases} P_d(\tau), & \tau \in [\tau_0, \tau_1], \\ P_d(\tau), & \tau \in (\tau_1, \tau^*], \\ P_d(\tau) - P_{ec}(\tau), & \tau \in (\tau^*, \tau_2), \\ P_d(\tau) - P_{ec}(\tau), & \tau \in [\tau_2, \tau_f]. \end{cases} \quad (4.42)$$

As shown in Fig. 4.7, the determination of the operating mode of a parallel HEV is exemplified. The green area refers to the operating mode  $ev0$ , when time  $\tau \in [\tau_0, \tau_1]$ ; the cyan area represents the operating mode  $ev1$ , when time  $\tau \in (\tau_1, \tau^*]$ ; the magenta area indicates the operating mode  $hv1$ , while time  $\tau \in (\tau^*, \tau_2)$ ; and, the red area is the operating mode  $hv0$ , while time  $\tau \in [\tau_2, \tau_f]$ .

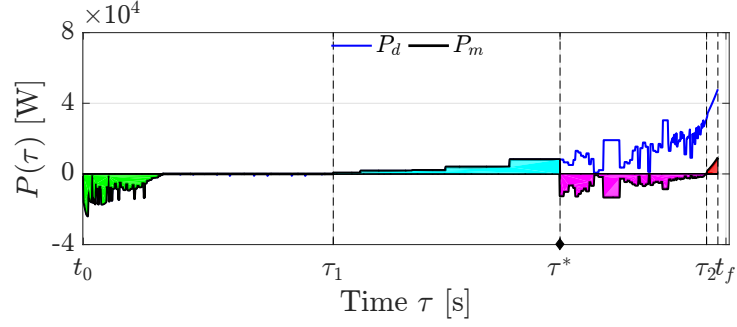


Figure 4.7 – Operating mode determination of GRAB-ECO for parallel HEVs.

The time instant  $\tau_1$  and  $\tau_2$  are correspondingly defined by

$$\{\tau_1 : I_e(\tau_1) \leq 0 \cap I_e(\tau_1 + \Delta t) > 0\}, \quad (4.43)$$

$$\{\tau_2 : I_e(\tau_2) < 1 \cap I_e(\tau_2 + \Delta t) \geq 1\}. \quad (4.44)$$

As for the time instant  $\tau^*$ , it is an essential time instant that is introduced in the following step.

### Step 3: State Approximation

According to the operating modes determined in the previous step, the resulting electrochemical energy of the battery in each operating mode is calculated by

$$E_{be,ev0} = \sum_{\tau=t_0}^{\tau_1} \Psi(u_{ev0}(\tau)) \Delta t, \quad (4.45)$$

$$E_{be,hv0} = \sum_{\tau=\tau_2}^{\tau_f} \Psi(u_{hv0}(\tau)) \Delta t, \quad (4.46)$$

$$E_{be,ev1}(\tau^*) = \sum_{\tau=\tau_1}^{\tau^*} \Psi(u_{ev1}(\tau)) \Delta t, \quad (4.47)$$

$$E_{be,hv1}(\tau^*) = \sum_{\tau=\tau^*}^{\tau_2} \Psi(u_{hv1}(\tau)) \Delta t, \quad (4.48)$$

where  $\Psi$  represents the generic function that evaluates the electrochemical power of battery of a given HEV.

The essential time instant  $\tau^*$ , affected by the requirement of the final state of charge of

the battery, is found in-between the instant  $\tau_1$  and  $\tau_2$ . As a result, the flexible operating modes *ev1* and *hv1* are segmented by the time instant  $\tau^*$  that is evaluated using the algorithm of root-finding in terms of interpolation. In other words, the turning point  $\tau^*$  is a time instant such that

$$\Delta E_{be}(\tau^*) = 0, \quad (4.49)$$

where the varied electrochemical energy of battery is calculated by

$$\Delta E_{be}(\tau^*) = E_{be,ev0} + E_{be,hv0} + E_{be,ev1}(\tau^*) + E_{be,hv1}(\tau^*). \quad (4.50)$$

Fig. 4.8 presents the resulting electrochemical energy of battery in each operating mode. The varied electrochemical energy  $\Delta E_{be}$  is depicted as a function of time  $\tau$ . Numeric interpolation is used to evaluate the essential time instant  $\tau^*$  marked with a black bullet.

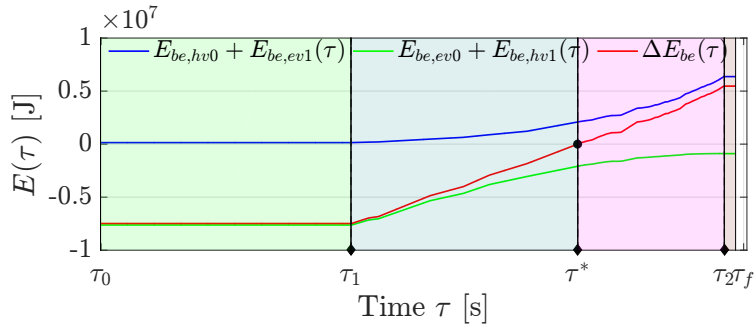


Figure 4.8 – Resulting electrochemical energy of battery in accordance with the operating modes.

#### Step 4: Energy Estimation

As a consequence of the essential time instant determination, the control variable of a series HEV is simplified as

$$u(\tau) = \begin{cases} P_{me}(\tau), & \tau \leq \tau^*, \\ P_{me}(\tau) - P_{apu}(\tau), & \tau > \tau^*, \end{cases} \quad (4.51)$$

whereas the control variable of a parallel HEV is

$$u(\tau) = \begin{cases} P_d(\tau), & \tau \leq \tau^*, \\ P_d(\tau) - P_{ec}(\tau), & \tau > \tau^*. \end{cases} \quad (4.52)$$

Consequently, the minimal energy consumption of an HEV in terms of series or parallel architecture is approximated by

$$E_{ef} = \sum_{\tau=\tau^*}^{\tau_f} \Phi(u^*(\tau))\Delta t, \quad (4.53)$$

where  $\Phi$  represents the generic function to evaluate the burned fuel power for an HEV.

### 4.4.3 Summary

GRAB-ECO approximates the minimal energy consumption of HEVs based on the maximization of average operating efficiency of the primary energy source. Compared with SHM, GRAB-ECO further decreases the control space  $U$  to only two operating conditions (electric and hybrid condition). Consequently, GRAB-ECO has the potential to further reduce the computation time compared with SHM. The results will be found in the following section.

## 4.5 Evaluation of Minimal Energy Consumption

In this section, minimal energy consumption of hybrid-electric vehicles is evaluated through QSS based on different types of powertrain component models, which consist of grid-point data, description (estimated with the descriptive analytic models), and prediction (approximated with the descriptive analytic models).

For each kind of powertrain component models, various methods are applied to evaluate the minimal energy consumption, including SHM, GRAB-ECO, HOT and VHOT. The performance of SHM and GRAB-ECO is benchmarked by HOT and VHOT in terms of fuel consumption and computation time. The corresponding computation time is the average value of twenty repetitions in terms of CPU time. Evaluations of minimum energy consumption are performed in MATLAB R2015b on a i7-4810QM CPU @ 2.80 GHz machine with 16 GB RAM.

Results of the minimum energy consumption as well as the average computation time of the investigated hybrid-electric vehicles are comparatively illustrated over various

investigated missions. Considering the evaluation based on HOT, the error of the final state of charge is compensated by the equivalent fuel consumption model introduced in Chapter 6.2.2; whereas the proper adjoint state variable  $s$  is found by the root-finding algorithm of Newton's method. The discretization step the adjoint variable  $s$  in VHOT is maintained the same as in SHM. As for the discretization step of time is always one second for all investigated methods.

#### 4.5.1 Series Hybrid-Electric Vehicle

##### Reference Vehicle

Main features of the investigated series HEV are summarized in Table 4.1, where the internal combustion engine, electric generator, battery, and electric motor correspond to ENG ID7 in Table 2.5, PMSM ID6 in Table 2.14, BAT ID4 in Table 2.11, and PMSM ID11 in Table 2.14.

Vehicle	$m_v$ [kg]	1648
	$R_w$ [m]	0.308
	$C_{v0}$ [N]	152.383
	$C_{v1}$ [N/(m/s)]	1.346
	$C_{v2}$ [N/(m/s) <sup>2</sup> ]	0.3751
Engine	$\mathcal{I}_e$	CI/TC
	$\mathcal{V}_e$ [L]	1.2
	$\mathcal{T}_e$ [Nm]	145
	$\mathcal{P}_e$ [kW]	43
Electric Generator	$\mathcal{I}_g$	PMSM
	$\mathcal{T}_g$ [Nm]	72
	$\mathcal{P}_g$ [kW]	30
Battery	$\mathcal{I}_b$	HE
	$Q_b$ [Ah]	53
	$\mathcal{K}_b$	96
Electric Motor	$\mathcal{I}_m$	PMSM
	$\mathcal{T}_m$ [Nm]	108
	$\mathcal{P}_m$ [kW]	45
Drivetrain	$\mathcal{R}_d$	9.7

Table 4.1 – Main features of investigated series hybrid-electric vehicle.

## Results and Analysis

Fig. 4.9 shows minimal energy consumption in terms of fuel consumption evaluated through various minimization methods over NEDC. Moreover, the minimal fuel consumption is estimated based on different types of powertrain component models. The black, blue, and cyan bars correspondingly indicate the evaluation based on grid-point data, descriptive analytic models, and predictive ones.

The main errors were caused by the powertrain component models (in terms of grid-point data, descriptive analytic models, and predictive models). This was always true to all of the minimization methods including HOT, VHOT, SHM, and GRAB-ECO. However, the discrepancies among the energy consumption evaluated based on the same type of powertrain component model but different minimization methods are not so significant as the typology of powertrain component models.

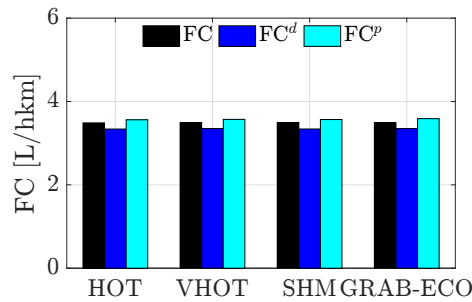


Figure 4.9 – Minimal energy consumption of reference series HEV over NEDC.

In addition, the exact errors of minimal energy consumption between grid-point data and descriptive analytic models and between grid-point data and predictive analytic models are listed in Table 4.2. In summary, the predictive analytic models of powertrain components are able to evaluate the minimal energy consumption of series HEVs through the proposed minimization methods in this chapter.

	HOT	VHOT	SHM	GRAB-ECO
$\varepsilon^d$ [%]	-4.26	-4.07	-4.43	-4.19
$\varepsilon^p$ [%]	2.13	2.26	2.06	2.69

Table 4.2 – Relative errors of minimal fuel consumption over NEDC.

The average computation time is summarized in Table 4.3 in terms of CPU time in [s]. The CPU time is the mean value of the computation time of twenty repetitions. Computation time is denoted by  $t_c^g$ ,  $t_c^d$ , and  $t_c^p$  corresponding to the average time asso-

ciated with grid-point data, descriptive, and predictive analytic models. Specifically, SHM minimized energy consumption within tens of milliseconds, which was about ten times less than that of VHOT. Moreover, GRAB-ECO took seven to twelve milliseconds, which was about six times less than that of SHM.

The analytic models either at descriptive level or at predictive level shortened the computation time compared with the grid-point data. Significant computation time abatement was achieved by GRAB-ECO that shrunk the dimension of full control space. Therefore, the smaller dimension of the full control space results in the less computation time of minimal energy consumption evaluation.

	HOT	VHOT	SHM	GRAB-ECO
$t_c^g$ [s]	963.93	0.4607	0.0916	0.0124
$t_c^d$ [s]	838.11	0.5302	0.0412	0.0070
$t_c^p$ [s]	675.69	0.4379	0.0410	0.0069

Table 4.3 – Comparison of average computation time over NEDC.

Apart from NEDC, the reference series HEV is also investigated over FTP-72 and HYWFET. Results of energy consumption over FTP-72 and HYWFET are correspondingly illustrated in Fig. 4.10a and 4.10b. Observations of the minimal energy consumption over NEDC were also true to those over FTP-72 and HYWFET.

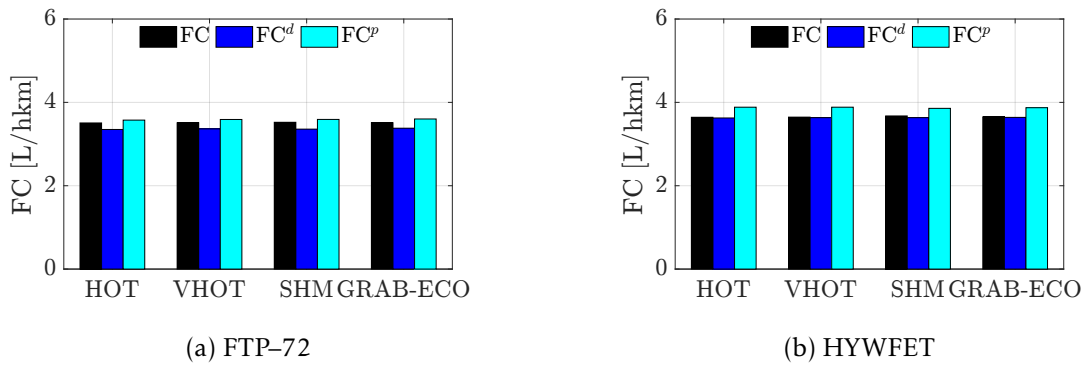


Figure 4.10 – Minimal energy consumption of reference series HEV over FTP-72 and HYWFET.

The relative errors of minimal energy consumption are summarized in Table 4.4 and 4.5 for FTP-72 and HYWFET, respectively. The discrepancies of minimal energy consumption between grid-point data and of predictive analytic models were higher over HYWFET. In addition, the minimal energy consumption was significantly overestimated

with powertrain models of predictive analytic models over HYWFET, compared with other missions.

	HOT	VHOT	SHM	GRAB-ECO
$\varepsilon^d$ [%]	-4.46	-4.14	-4.66	-3.75
$\varepsilon^p$ [%]	1.94	2.29	1.96	2.55

Table 4.4 – Relative errors of minimal fuel consumption over FTP-72.

	HOT	VHOT	SHM	GRAB-ECO
$\varepsilon^d$ [%]	-0.45	-0.34	-1.12	-0.32
$\varepsilon^p$ [%]	6.65	6.55	4.96	6.03

Table 4.5 – Relative errors of minimal fuel consumption over HYWFET.

As for average computation time of each evaluation, they are listed in Table 4.6 and 4.7 for FTP-72 and HYWFET, respectively. Apart from the significant abatement of computation time by SHM and GRAB-ECO, the average computation time also associated with the duration of missions. However, the average computation time of GRAB-ECO seemed not to be affected by the duration of missions.

	HOT	VHOT	SHM	GRAB-ECO
$t_c^g$ [s]	1246.95	0.48280	0.10300	0.0128
$t_c^d$ [s]	915.02	0.74540	0.04740	0.0073
$t_c^p$ [s]	988.95	0.67450	0.04740	0.0071

Table 4.6 – Comparison of average computation time over FTP-72.

	HOT	VHOT	SHM	GRAB-ECO
$t_c^g$ [s]	700.89	0.2943	0.0536	0.0121
$t_c^d$ [s]	538.21	0.6169	0.0333	0.0076
$t_c^p$ [s]	538.98	0.3308	0.0270	0.0068

Table 4.7 – Comparison of average computation time over HYWFET.

## 4.5.2 Parallel Hybrid-Electric Vehicle

### Reference Vehicle

Main features of the investigated parallel HEV are summarized in Table 4.8, where battery is BAT ID1 in Table 2.11, and electric motor is PMSM ID5 in Table 2.14.

Vehicle	$m_v$ [kg]	1814
	$R_w$ [m]	0.317
	$C_{v0}$ [N]	93.5
	$C_{v1}$ [N/(m/s)]	5.29
	$C_{v2}$ [N/(m/s) <sup>2</sup> ]	0.536
Engine	$\mathcal{I}_e$	SI/NA
	$\mathcal{V}_e$ [L]	1.4
	$\mathcal{T}_e$ [Nm]	130
	$\mathcal{P}_e$ [kW]	60
Battery	$\mathcal{I}_b$	HP
	$\mathcal{Q}_b$ [Ah]	31
	$\mathcal{K}_b$	60
Electric Motor	$\mathcal{I}_m$	PMSM
	$\mathcal{T}_m$ [Nm]	36
	$\mathcal{P}_m$ [kW]	38
Drivetrain	$\mathcal{I}_t$	MT-5
	$\mathcal{R}_{fd}$	3.7

Table 4.8 – Main features of investigated parallel hybrid-electric vehicle.

## Results and Analysis

Fig. 4.11 illustrates the minimal energy consumption evaluated via various minimization methods over NEDC based on different powertrain component models. The black, blue, and cyan bars correspondingly represent the evaluations based on grid-point data, descriptive analytic models, and predictive ones.

The main errors were from SHM and GRAB-ECO with powertrain components models in terms of grid-point data. In fact, the minimal energy consumption via SHM is not strictly based on powertrain model of grid-point data due to the analytic nature of Hamiltonian function. As for GRAB-ECO with powertrain model of grid-point data, the error may be caused by the discretization level of driving cycle, and the non-strict fulfillment of final state of charge of the battery.

Detailed figures of the relative errors of minimal energy consumption are summarized in Table 4.9. In summary, both SHM and GRAB-ECO can evaluate the minimal energy consumption for parallel HEVs. Predictive analytic models of powertrain components were able to provide very similar minimal energy consumption for parallel HEVs compared with powertrain model of grid-point data.

The computation time of each evaluation is listed in Table 4.10 in terms of CPU time

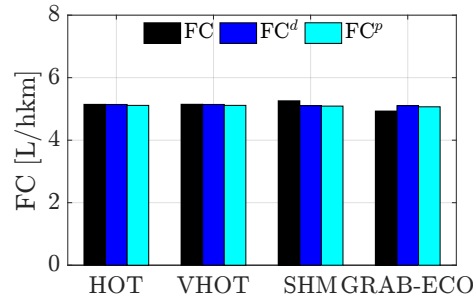


Figure 4.11 – Minimal energy consumption of reference parallel HEV over NEDC.

	HOT	VHOT	SHM	GRAB-ECO
$\varepsilon^d$ [%]	-0.06	-0.10	-3.01	3.49
$\varepsilon^p$ [%]	-0.63	-0.67	-3.22	2.78

Table 4.9 – Relative errors of minimal fuel consumption over NEDC.

in [s]. Significant computation time abatement was achieved by GRAB-ECO through shrinking the dimensions of control space.

Specifically, SHM minimized energy consumption within hundred of milliseconds, which was about threes times less than that of VHOT. Moreover, GRAB-ECO approximated the minimal energy consumption with eight to thirteen milliseconds, which was about ten times less than that of SHM.

	HOT	VHOT	SHM	GRAB-ECO
$t_c^g$ [s]	204.78	0.2759	0.0928	0.0135
$t_c^d$ [s]	224.82	0.3263	0.0912	0.0083
$t_c^p$ [s]	224.46	0.2722	0.0918	0.0081

Table 4.10 – Comparison of average computation time over NEDC.

In addition to NEDC, the reference parallel HEV is investigated over FTP-72 and HYWFET. The minimal energy consumption are depicted in Fig. 4.10. Regardless of missions, the minimal energy consumption obtained through different optimal control techniques but with the same powertrain model typology was close to each other.

Exact errors of the minimal energy consumption are summarized in Table 4.11 and 4.12 for FTP-72 and HYWFET, respectively. The largest one was less than 4%.

The average computation time of evaluations is separately listed in Table 4.13 and 4.14 for FTP-72 and HYWFET. Apart from the significant abatement of computation

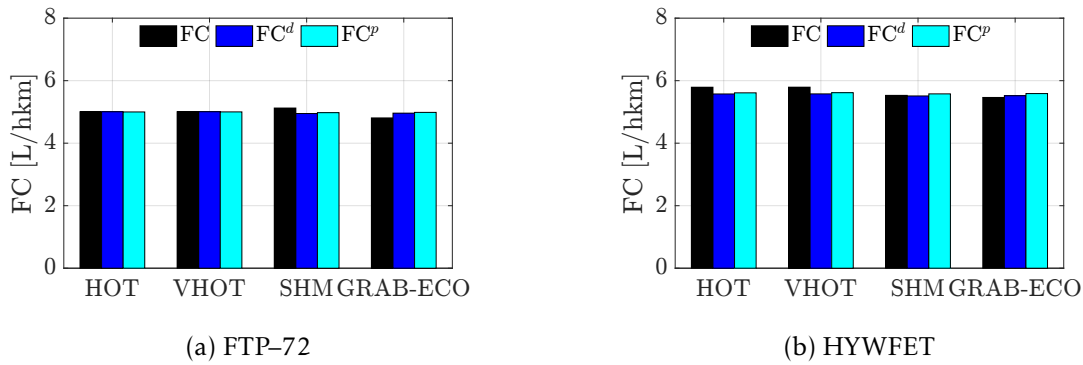


Figure 4.12 – Minimal energy consumption of reference parallel HEV over FTP-72 and HYWFET.

	HOT	VHOT	SHM	GRAB-ECO
$\varepsilon^d$ [%]	0.01	0.01	-3.42	3.17
$\varepsilon^p$ [%]	-0.12	-0.10	-2.88	3.69

Table 4.11 – Relative error of fuel consumption over FTP-72.

	HOT	VHOT	SHM	GRAB-ECO
$\varepsilon^d$ [%]	-3.71	-3.69	-0.33	1.02
$\varepsilon^p$ [%]	-3.10	-3.04	0.87	2.27

Table 4.12 – Relative errors of minimal fuel consumption over HYWFET.

time of SHM and GRAB-ECO, the average computation time was mission-dependent as well. This dependency was significant to HOT, VHOT, and SHM, except for GRAB-ECO.

	HOT	VHOT	SHM	GRAB-ECO
$t_c^g$ [s]	221.84	0.3143	0.1056	0.0138
$t_c^d$ [s]	262.14	0.3071	0.1041	0.0085
$t_c^p$ [s]	285.07	0.3254	0.1056	0.0082

Table 4.13 – Comparison of average computation time over FTP-72.

	HOT	VHOT	SHM	GRAB-ECO
$t_c^g$ [s]	243.23	0.1896	0.0656	0.0132
$t_c^d$ [s]	187.30	0.1887	0.0638	0.0091
$t_c^p$ [s]	186.82	0.1915	0.0648	0.0080

Table 4.14 – Comparison of average computation time over HYWFET.

To summarize, the average computation time of energy consumption minimization was gradually diminished from hundreds of seconds via HOT, to a few hundreds of milliseconds via VHOT, to about hundred of milliseconds through SHM, finally to about ten of milliseconds through GRAB-ECO. Meanwhile, the accuracy of minimal energy consumption was maintained at the same level.

## **Part III**

# **Fully-Analytic Energy Consumption Estimation for Advanced Vehicle Propulsion Systems**



# Analytic Energy Consumption of Single-Source Vehicles

In comparison with Quasi-Static Simulation (QSS), FACE is developed to fast approximate energy consumption and to optimize dimensioning parameters of a vehicle propulsion system. Based on reference vehicles and specific missions, FACE analytically approximates the energy consumption of single-source vehicles, including conventional and battery-electric vehicles. Sensitivity of powertrain dimensioning parameters is presented in simplified expressions for the intuition purpose. The FACE is further compared with QSS in terms of the energy consumption.

## 5.1 Conventional Vehicle

FACE, standing for Fully-Analytic energy Consumption Estimation, analytically approximates the energy consumption of a conventional vehicle with dimension-related parameters and cycle-related parameters. Dimension-related parameters consist of dimensioning parameters of powertrain components and vehicles. The dimension-related parameters are vehicle-dependent, such as engine displacement and vehicle mass. Cycle-related parameters are in function of mission variables, such as velocity and acceleration. For conventional vehicles, gear sequence is also a mission variable. For example, a cycle-related parameter can be  $v^2 a n_t$ . Details of the dimension- and cycle-related parameters are found in the following section.

Considering the evaluation of energy consumption, the dimension-related parameters are originated from the investigated conventional vehicle; whereas cycle-related

parameters are determined a priori based on a reference vehicle. Moreover, cycle-related parameters are influenced by the status of the internal combustion engine. Specifically, an engine converts burned fuel to mechanical power in propulsion phase; whereas the engine does not consume any fuel during the braking condition. Moreover, the idling fuel consumption is assumed to omit due to the adoption of stop-start systems.

### 5.1.1 Fully Analytic Energy Consumption Estimation

Due to high performance of an internal combustion engine, the operating points over a standardized mission are often concentrated at low speed and low- and mid-load area in its efficiency map. Thus, only the first case of the light-duty engine piece-wise model is implemented in FACE. Combining analytic models of internal combustion engine in Eq. 2.2 (only first case), transmission in Eq. 2.24 and 2.25, and vehicle load model in Eq. 2.38, the power of burned fuel at time  $t$  is written by

$$P_{ef} = k_{e0} + \frac{k_{e1}C_{v0}v}{k_{t5}} + \frac{k_{e1}C_{v1}v^2 + k_{e1}C_{v2}v^3 + k_{e1}va}{k_{t5}}, \quad (5.1)$$

where  $P_{ef}$  is valid only when vehicle load  $F_l > 0$ .

Descriptive parameters in Eq. 5.1, such as  $k_{e0}$ ,  $k_{e1}$ , and  $k_{t5}$ , are substituted with their corresponding predictive models introduced in Chapter 2. Thus, dimensioning parameters constitute the dimension-related parameters, which depend on the investigated vehicle. Then, cycle-related parameters are separated in each term of the full expansion of Eq. 5.1. Because of the implementation of a reference vehicle, cycle-related parameters are constant in FACE.

Consisting of dimension-related variables and cycle-related parameters, FACE for conventional vehicles is expressed as

$$E_{ef} = \sum_{i=1, j=0, k=0}^{i=5, j=1, k=8} \mathcal{D}_{ijk} \mathcal{C}_{ijk}, \quad (5.2)$$

where  $\mathcal{D}_{ijk}$  are dimension-related variables of the investigated vehicle, and  $\mathcal{C}_{ijk}$  are cycle-related parameters of a reference vehicle, subscripts  $i, j, k$  correspond to the exponents of velocity, acceleration, and gear number.

The dimension of the full expansion of Eq. 5.2 is so large that both dimension-and cycle-related parameters are simplified. Details of each dimension-related parameter are found in Appendix D.1. As for the cycle-related parameters based on a reference

vehicle, they are summarized by

$$C_{ijk} = \sum_{t \in \sigma} v^i(t) a^j(t) n_t^k(t) \Delta t, \quad (5.3)$$

where the mission variables – including, velocity  $v$ , acceleration  $a$ , and gear shift schedule  $n_t$  – the set of effective time steps  $\sigma$ , and the time interval  $\Delta t$  are involved.

The set of effective time steps  $\sigma$  is defined by

$$\sigma = \{t : F_l(t) > 0, t \in [t_0, t_f]\}, \quad (5.4)$$

where  $F_l$  is vehicle load estimated in Eq. 2.38,  $\sigma$  is the set of valid time steps based on the reference vehicle.

Since not all of the combinations of  $i$ ,  $j$ , and  $k$  exist in FACE, the valid combinations for conventional vehicles are summarized as

$$\begin{aligned} i = 1, jk &= \{00, 01, 02, 03, 04, 10\}, \\ i = 2, jk &= \{00, 01, 02, 03, 04, 05, 06, 07, 08, 10, 11, 12, 13, 14\}, \\ i = 3, jk &= \{00, 01, 02, 03, 04, 05, 06, 07, 08, 10, 11, 12, 13, 14, 15, 16, 17, 18\}, \\ i = 4, jk &= \{00, 01, 02, 03, 04, 05, 06, 07, 08\}, \\ i = 5, jk &= \{00, 01, 02, 03, 04, 05, 06, 07, 08\}. \end{aligned} \quad (5.5)$$

### 5.1.2 Sensitivity of Dimensioning Parameters

Although FACE is developed, relations between energy consumption and powertrain dimensioning parameters are implicit in Eq. 5.2. To make FACE more intuitive, sensitivity of powertrain dimensioning parameters proffers explicit relations below.

Concerning dimensioning parameters of internal combustion engines, the energy consumption is a linear function of engine displacement, which yields

$$E_{ef}(\mathcal{V}_e) = \kappa_{e0} + \kappa_{e1} \mathcal{V}_e, \quad (5.6)$$

where parameters  $\kappa_{(\dots)}$  are generic and derived from Eq. 5.2. Expressions of parameters  $\kappa$  will not be fully expanded for simplicity reason.

Regarding the dimensioning parameters of drivetrain, quadratic models are feasible to the gear ratios of first and last gear ( $\mathcal{R}_{t1}$  and  $\mathcal{R}_{tk}$ ) and the ratio of final drive ( $\mathcal{R}_{fd}$ ),

which are given by

$$E_{ef}(\mathcal{R}_{t1}) = \kappa_{t0} + \kappa_{t1}\mathcal{R}_{t1} + \kappa_{t2}\mathcal{R}_{t1}^2, \quad (5.7)$$

$$E_{ef}(\mathcal{R}_{tk}) = \kappa_{t3} + \kappa_{t4}\mathcal{R}_{tk} + \kappa_{t2}\mathcal{R}_{tk}^2, \quad (5.8)$$

$$E_{ef}(\mathcal{R}_{fd}) = \kappa_{d0} + \kappa_{d1}\mathcal{R}_{fd} + \kappa_{d2}\mathcal{R}_{fd}^2. \quad (5.9)$$

Note that, the overall gear ratios are considered for  $\mathcal{R}_{t1}$  and  $\mathcal{R}_{tk}$  if the final drive is of multiple speeds. Meanwhile, the ratio  $\mathcal{R}_{fd}$  is assumed to be one in this condition.

In addition, energy consumption is also expressed as functions of vehicle parameters. Since parameter  $C_{v0}$  is approximated by  $C_{v0} \approx m_v g C_{rr}$ , the relations between the energy consumption and vehicle parameters are separately presented as

$$E_{ef}(C_{v2}) = \kappa_{v0} + \kappa_{v1}C_{v2}, \quad (5.10)$$

$$E_{ef}(C_{v1}) = \kappa_{v2} + \kappa_{v3}C_{v1}, \quad (5.11)$$

$$E_{ef}(C_{v0}) = \kappa_{v4} + \kappa_{v5}C_{v0}, \quad (5.12)$$

$$E_{ef}(m_v) = \kappa_{v6} + \kappa_{v7}m_v. \quad (5.13)$$

## 5.2 Battery-Electric Vehicle

To optimize the dimensioning parameters of powertrain components, FACE is also developed for battery-electric vehicles with single-speed transmissions. Similar to conventional vehicles, FACE estimates the energy consumption of a battery-electric vehicle with dimension- and cycle-related parameters. Dimension-related parameters associate with a battery-electric vehicle to investigate, including battery, electric motor/generator, and single-speed transmission; whereas cycle-related parameters are mission-dependent and reference-vehicle-dependent constants.

In a battery-electric vehicle, battery is discharged as an energy source to propel the vehicle. Yet, it can also be charged to recuperate energy during braking. These operations segment the analytic model of battery electrochemical power into to conditions because of the efficiency of the drivetrain. The standstill operation is included in the propelling operation.

### 5.2.1 Fully Analytic Energy Consumption Estimation

The consumed electrochemical power of battery is calculated in a piecewise function by combining analytic models of battery in Eq. 2.30 (the quadratic model), electric motor/generator in Eq. 2.35, and single-speed transmission in Eq. 2.22 and 2.25, and vehicle load model in Eq. 2.38.

In the fully expanded electrochemical power of battery, the same items of mission variables are merged that account for the cycle-related parameters. The rest terms, consisting of powertrain dimensioning parameters and constants, make up the dimension-related parameters.

Because of its too large dimension, the expression of FACE for battery-electric vehicles is simplified as

$$E_{be} = \sum_{\beta=1}^2 \sum_{i=0, j=0}^{i=8, j=4} \mathcal{D}_{ij}^{b\beta} \mathcal{C}_{ij}^{\beta}, \quad (\beta = 1, 2), \quad (5.14)$$

where  $\beta$  refers traction ( $\beta = 1$ ) and braking operation ( $\beta = 2$ );  $\mathcal{D}_{ij}^{b\beta}$  are dimension-related parameters in accordance with vehicle operating conditions; and  $\mathcal{C}_{ij}^{\beta}$  are cycle-related parameters based on a reference vehicle.

The detailed dimension-related parameters are listed in Appendix D.2; whereas the cycle-related parameters of a reference battery-electric vehicle are summarized as

$$\mathcal{C}_{ij}^{\beta} = \sum_{t \in \sigma_{b\beta}} v^i(t) a^j(t) \Delta t, \quad (\beta = 1, 2), \quad (5.15)$$

where  $\sigma_{b\beta}$  are sets of time steps corresponding to vehicle operating conditions.

The time sets  $\sigma_{b\beta}$  ( $\beta = 1, 2$ ) in accordance with the operating conditions of a reference vehicle are summarized in an overall time set  $\sigma_{b\beta}$ , which yields

$$\sigma_{b\beta} = \left\{ \begin{array}{l} \sigma_{b1} = \{t : F_l(t) \geq 0\} \\ \sigma_{b2} = \{t : F_l(t) < 0\} \end{array} \right\}. \quad (5.16)$$

The existing combinations of  $i$  and  $j$  in Eq. 5.14 and 5.15 are summarized as

$$\begin{aligned} i &= \{0, 1, 2, 3, 4, 5, 6, 7, 8\}, j = 0, \\ i &= \{0, 1, 2, 3, 4, 5, 6\}, j = 1, \\ i &= \{0, 1, 2, 3, 4\}, j = 2, \end{aligned} \quad (5.17)$$

$$i = \{0, 1, 2\}, j = 3,$$

$$i = \{0\}, j = 4.$$

Because of the implemented transmissions, the FACE in this section is dedicated to battery-electric vehicles of single-speed transmissions.

### 5.2.2 Sensitivity of Dimensioning Parameters

Explicit relations between energy consumption and powertrain dimensioning parameters (including vehicle parameters) are formulated to make FACE intuitive and obvious.

Concerning dimensioning parameters of battery, FACE is nonlinear as a function of battery cell number  $\mathcal{K}_b$  and battery cell capacity  $\mathcal{Q}_b$  as expressed by

$$E_{be}(\mathcal{K}_b) = \kappa_{b0} + \kappa_{b1}\mathcal{K}_b + \frac{\kappa_{b2}}{\mathcal{K}_b}, \quad (5.18)$$

$$E_{be}(\mathcal{Q}_b) = \kappa_{b3} + \kappa_{b4}\mathcal{Q}_b + \kappa_{b5}\mathcal{Q}_b^2. \quad (5.19)$$

Regarding to dimensioning parameters of electric motor/generators, FACE is a fourth degree polynomial as a function of rated torque  $\mathcal{T}_m$  and of base speed  $\mathcal{N}_m$ . The quartic polynomials are re-written by

$$E_{be}(\mathcal{T}_m) = \kappa_{m0} + \kappa_{m1}\mathcal{T}_m + \kappa_{m2}\mathcal{T}_m^2 + \kappa_{m3}\mathcal{T}_m^3 + \kappa_{m4}\mathcal{T}_m^4, \quad (5.20)$$

$$E_{be}(\mathcal{N}_m) = \kappa_{m5} + \kappa_{m6}\mathcal{N}_m + \kappa_{m7}\mathcal{N}_m^2 + \kappa_{m8}\mathcal{N}_m^3 + \kappa_{m9}\mathcal{N}_m^4. \quad (5.21)$$

With regard to dimensioning parameters of a drivetrain, high nonlinearity of FACE exists, such as

$$E_{be}(\mathcal{R}_t) = \sum_{i=0}^4 \kappa_{di}\mathcal{R}_t^i + \frac{\kappa_{d5}}{\mathcal{R}_t} + \frac{\kappa_{d6}}{\mathcal{R}_t^2} + \frac{\kappa_{d7}}{\mathcal{R}_t^4}, \quad (5.22)$$

$$E_{be}(\mathcal{R}_{fd}) = \sum_{i=0}^4 \kappa_{di}\mathcal{R}_{fd}^i + \frac{\kappa_{d5}}{\mathcal{R}_{fd}} + \frac{\kappa_{d6}}{\mathcal{R}_{fd}^2} + \frac{\kappa_{d7}}{\mathcal{R}_{fd}^4}. \quad (5.23)$$

Relations between energy consumption and vehicle parameters are given by

$$E_{be}(C_{v2}) = \kappa_{v0} + \kappa_{v1}C_{v2} + \kappa_{v2}C_{v2}^2 + \kappa_{v3}C_{v2}^3 + \kappa_{v4}C_{v2}^4, \quad (5.24)$$

$$E_{be}(C_{v1}) = \kappa_{v5} + \kappa_{v6}C_{v1} + \kappa_{v7}C_{v1}^2 + \kappa_{v8}C_{v1}^3 + \kappa_{v9}C_{v1}^4, \quad (5.25)$$

$$E_{be}(C_{v0}) = \kappa_{v10} + \kappa_{v11}C_{v0} + \kappa_{v12}C_{v0}^2 + \kappa_{v13}C_{v0}^3 + \kappa_{v14}C_{v0}^4, \quad (5.26)$$

$$E_{be}(m_v) = \kappa_{v15} + \kappa_{v16}m_v + \kappa_{v17}m_v^2 + \kappa_{v18}m_v^3 + \kappa_{v19}m_v^4. \quad (5.27)$$

### 5.3 Analytic Evaluation of Energy Consumption

FACE is applied to approximate the energy consumption of several single-source vehicles. The energy consumption is compared based on the evaluation with different methods, such as of FACE and Quasi-Static Simulations (QSS). The predictive analytic models of powertrain components are applied to the evaluation of energy consumption through FACE. Instead, the grid-point data is used in the evaluation via QSS. As a result, errors of different types of powertrain data is introduced.

#### 5.3.1 Conventional Vehicle

Conventional vehicles of different engine technologies but same drivetrain and vehicle are investigated through both FACE and QSS. Note that, the type of powertrain models in FACE is different from that in QSS.

#### Reference Vehicles

Main characteristics of the investigated conventional vehicles are summarized in Table 5.1. The reference vehicle (Vehicle I) and the investigated vehicles (Vehicle II, III, and IV) have the same vehicle parameters and drivetrain. The varied dimension-related variables are composed of engine displacement and the engine rated torque and power. In addition, Vehicle I is used to estimate the cycle-related parameters for the evaluation of fuel consumption of Vehicle II, III, and IV over various missions.

#### Results and Analysis

Comparisons of fuel consumption are illustrated in Fig. 5.1. The highest error between FACE and QSS is presented by Vehicle I over FTP-72, which is 3.85%. As for the least one, it is about 0.83% of Vehicle II over HYWFET. However, there are several sources of errors that could impact the comparisons. Firstly, models of powertrain components are different, which are grid-point data and predictive analytic model. Secondly, FACE is developed based on the first case of light-duty engine model in Eq. 2.2, which means engine power that is larger than the corner power ( $P_e > P_{ec}$ ) requires

Vehicle		I	II	III	IV
	$m_v$ [kg]	1595			
	$R_w$ [m]	0.3017			
	$C_{v0}$ [N]	134.094			
	$C_{v1}$ [N/(m/s)]	3.747			
	$C_{v2}$ [N/(m/s) <sup>2</sup> ]	0.3486			
Engine	$\mathcal{I}_e$	CI/TC	SI/TC	SI/NA/LB	SI/NA/SB
	$\mathcal{V}_e$ [L]	2.1	2.1	1.9	1.9
	$\mathcal{T}_e$ [Nm]	292	302	166	166
	$\mathcal{P}_e$ [kW]	90	150	80	80
Drivetrain	$\mathcal{I}_t$	DCT-6			
	$\mathcal{R}_{fd}$	4.12 & 3.04			

Table 5.1 – Main features of investigated conventional vehicles.

less fuel consumption. The reference cycle-related parameters may affect the energy consumption as well. In addition, accumulative effect is not negligible due to repeated or very similar operating points.

Taking the errors between models of powertrain components into account, good accuracy allows FACE to approximate fuel consumption and to optimize powertrain dimensioning parameters.

### 5.3.2 Battery-Electric Vehicle

Two battery-electric vehicles with different electric motor/generators are investigated to show the accuracy of FACE.

#### Reference Vehicles

Features of the investigated battery-electric vehicles are listed in 5.2, in which Vehicle I is the reference vehicle for the evaluation of cycle-related parameters. The dimension-related variables are composed of the rated torque and power of electric motors.

The battery-electric vehicles are investigated through QSS and FACE over three missions. The energy consumption is depicted in Fig. 5.2. Considering the powertrain model of the electric motor/generators, grid-point data is implemented in the evaluation of QSS; whereas predictive analytic models are applied in the approximation of FACE.

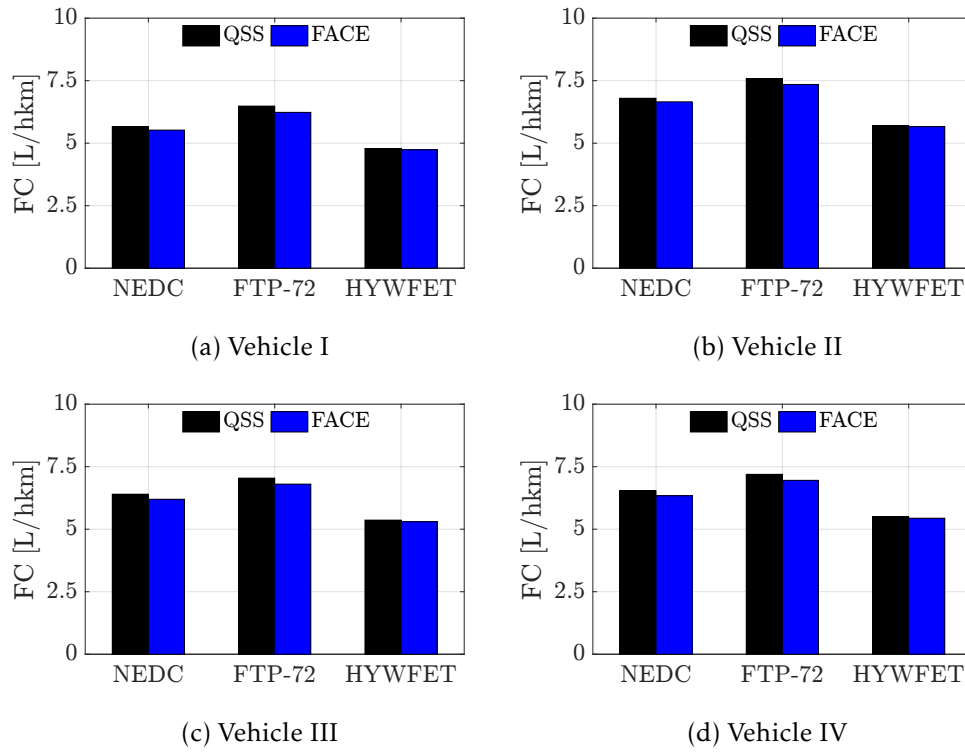


Figure 5.1 – Fuel consumption of conventional vehicles evaluated through QSS and FACE.

Vehicle		I	II
	$m_v$ [kg]	1648	
	$R_w$ [m]	0.3952	
	$C_{v0}$ [N]	141.947	
	$C_{v1}$ [N/(m/s)]	1.153	
	$C_{v2}$ [N/(m/s) <sup>2</sup> ]	0.3952	
Battery	$\mathcal{I}_b$	HE	
	$Q_b$ [Ah]	31	
	$\mathcal{K}_b$	192	
Electric Motor	$\mathcal{I}_m$	PMSM	
	$\mathcal{T}_m$ [Nm]	108	108
	$\mathcal{P}_m$ [kW]	79	45
Drivetrain	$\mathcal{R}_d$	14	

Table 5.2 – Main features of investigated battery-electric vehicles.

### Results and Analysis

Results of energy consumption of the reference and investigated vehicles are shown in Fig. 5.2, where Vehicle I is the reference. The energy consumption of Vehicle I is evaluated via the fully analytic approach, in which the cycle-related parameters do not cause any error. The greatest error of 7.69% is found, which is mainly caused by the model errors between grid-point data and the predictive analytic models of the electric motor/generator.

However, the differences of energy consumption of Vehicle II are smaller than Vehicle I over all investigated missions. FACE universally underestimates the energy consumption. The errors are caused by powertrain models, reference vehicle, and cumulation of similar operations of the electric motor/generator. Nonetheless, Vehicle II shows a good approximation (see Fig. 5.2b).

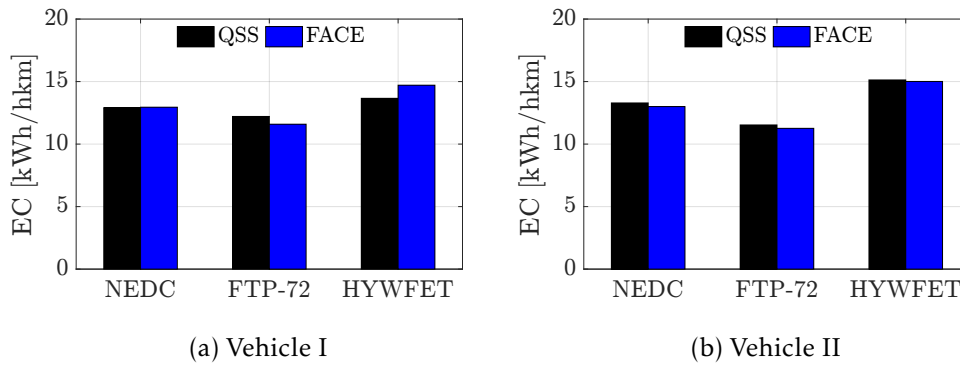


Figure 5.2 – Energy consumption of battery-electric vehicles evaluated with QSS and FACE

# Analytic Minimal Energy Consumption of Hybrid-Electric Vehicles

Compared with single-source vehicles, the mandatory control optimization for the evaluation of the minimal energy consumption significantly augments the complexity of the development of Fully-Analytic energy Consumption Estimation (FACE) for hybrid-electric vehicles. Nevertheless, FACE is developed based on distinct ideas for series and parallel hybrid-electric vehicles.

## 6.1 Series Hybrid-Electric Vehicle

For series hybrid-electric vehicles, FACE approximates the minimal energy consumption based on further simplified GRAB-ECO. The simplification requires an analytic model of an Auxiliary Power Unit (APU).

### 6.1.1 Auxiliary Power Unit

The operating point of an APU owning the best efficiency is analytically modeled by

$$\eta_{apu}^* = -\frac{128k_{g0}\pi^9}{\mathbf{p}_3\mathcal{V}_e\omega_{ei}} - \frac{128k_{g1}\pi^9\mathcal{R}_g}{\mathbf{p}_3\mathcal{V}_e} - \frac{128k_{g2}\pi^9\mathcal{R}_g^2\omega_{ei}}{\mathbf{p}_3\mathcal{V}_e} + \frac{125k_{g3}\mathbf{p}_2}{\mathbf{p}_3\omega_{ei}} - \frac{15625k_{g4}\mathbf{p}_1^2\mathcal{V}_e}{128\pi^9\mathcal{R}_g^2\mathbf{p}_3\omega_{ei}} + \frac{\mathbf{n}_1}{\mathbf{d}_1} + \frac{\mathbf{n}_2}{\mathbf{d}_2}, \quad (6.1)$$

where  $\mathbf{n}_i (i = 1, 2)$  and  $\mathbf{d}_i (i = 1, 2)$  are numerator and denominator terms, respectively; and  $\mathbf{p}_i (i = 1, \dots, 11)$  are polynomials, some of which are nested in  $\mathbf{n}_i (i = 1, 2)$  and  $\mathbf{d}_i (i = 1, 2)$ .

Fig. 6.1 depicts the efficiency of the best-efficiency point evaluated with analytic model (denoted by  $\eta_{apu}^*$ ), and the efficiency of the optimal operating line (indicated by  $\eta_{apu}$ ) as a function of engine speed for different gear ratios  $\mathcal{R}_g$  between the internal combustion engine and the electric generator.

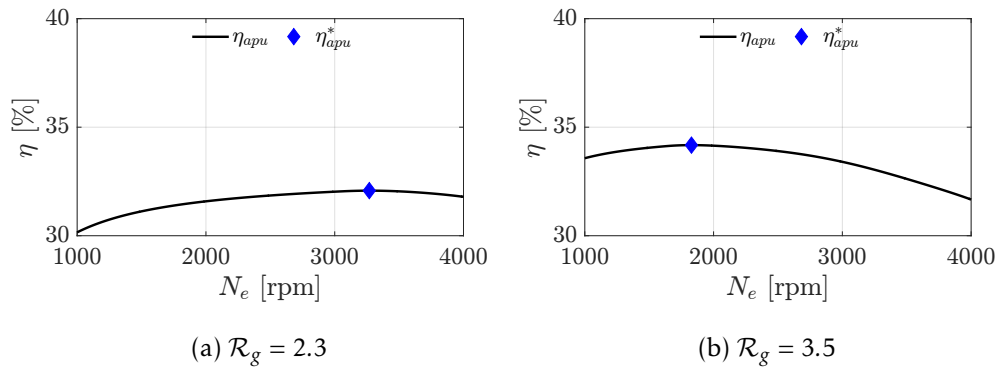


Figure 6.1 – Best-efficiency point of APU in terms of gear ratio.

As a supplementary, the impacts of engine displacement on the best-efficiency point of APU are illustrated in Fig. 6.2a. The developed analytic model of best-efficiency point can predict the best efficiency.

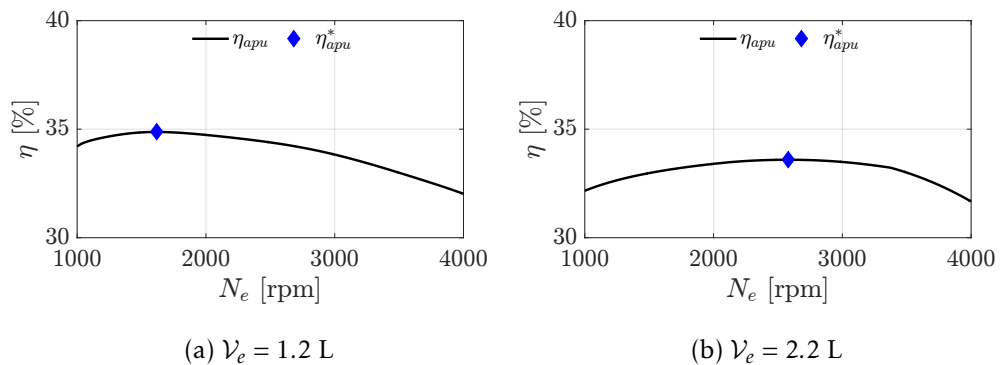


Figure 6.2 – Best-efficiency point of APU in terms of engine displacement.

### 6.1.2 Fully Analytic Energy Consumption Estimation

Considering the optimal control problem of series HEVs, it is simplified based on GRAB-ECO. The idea is to assume that a series HEV drives like a battery-electric vehicle over a given mission. At the end of the mission, battery is depleted due to various external resistances and powertrain efficiencies. The depleted energy is ultimately recuperated by recharging the battery with APU that works at its best-efficiency operating point.

Based on the developed analytic model of the best-efficiency point of an APU in Eq. 6.1, FACE fully involves dimensioning parameters of internal combustion engines, electric generators, and simple gear train  $\mathcal{R}_g$  for series hybrid-electric vehicles.

The FACE combines the consumed electrochemical energy of battery-electric vehicles in Eq. 5.14 and the analytic model of APU in Eq. 6.1. Therefore, FACE is expressed as

$$E_{ef} = \frac{\sum_{t \in \sigma_{b\beta}} P_{be}^\beta(t) \Delta t}{\eta_{apu}^*}, \quad (\beta = 1, 2), \quad (6.2)$$

where time sets  $\sigma_{b\beta}(\beta = 1, 2)$  are the same as those for battery-electric vehicles.

The analytic model of best-efficiency point is independent from the cycle-related parameters. As a result, the minimal energy consumption model in Eq. 6.2 can be further simplified by lumping the analytic model in Eq. 6.1 into dimension-related variables, which yields

$$E_{ef} = \sum_{\beta=1}^2 \sum_{i=0, j=0}^{i=8, j=4} \mathcal{D}_{ij}^{b\beta} \mathcal{C}_{ij}^\beta, \quad (\beta = 1, 2). \quad (6.3)$$

Despite the same form as battery-electric vehicles, FACE approximates the minimal fuel energy consumption for series HEVs. The analytic model relating to APU in Eq. 6.3 is involved in the dimension-related variables  $\mathcal{D}_{ij}^{b\beta}$ . Concerning the cycle-related parameters in Eq. 6.3, they are exactly the same as that for battery-electric vehicle in Eq. 5.15.

## 6.2 Parallel Hybrid-Electric Vehicle

FACE for parallel hybrid-electric vehicles is developed based on SHM with a few essential assumptions. Thus, the anticipated difficulties consist of combined analytic model of battery and electric motor/generator, estimation of the proper adjoint state variable, and an analytic model of the minimal energy approximation. Methods to resolve these

problems are individually introduced hereafter.

### 6.2.1 Analytic Model of Assembled Battery and Motor

In Section 4.3, Selective Hamiltonian Minimization (SHM) is developed based on the quadratic analytic model of battery in Eq. 2.30 for the sake of better accuracy, full operating range, and resulting shorter computational time. However, the analytic model of assembled battery and electric motor in Eq. 4.23 cannot directly account for dimensioning parameters of battery and electric motor/generator. Therefore, the bi-linear model of battery in Eq. 2.31, instead of the quadratic one, is implemented to encompass dimensioning parameters of battery and electric motor. Consequently, the analytic model of the combined battery and electric motor is given by

$$P_{be} = \begin{cases} k_{b3} + k_{b4}(k_{m0} + k_{m1}\omega_m + k_{m2}\omega_m^2) + k_{b4}k_{m3}P_m + \frac{k_{b4}k_{m4}}{\omega_m^2}P_m^2, & P_m \geq 0, \\ k_{b5} + k_{b6}(k_{m0} + k_{m1}\omega_m + k_{m2}\omega_m^2) + k_{b6}k_{m3}P_m + \frac{k_{b6}k_{m4}}{\omega_m^2}P_m^2, & P_m < 0. \end{cases} \quad (6.4)$$

As a result, the possible solutions to the optimal control problem in Eq. 4.38 is rewritten by

$$u(t, s) \in \left\{ \begin{array}{c} P_{m,unc1}(t, s) \\ P_{m,unc2}(t, s) \\ P_d(t) \\ P_d(t) - P_{ec}(t) \\ \bar{P}_m(t) \\ \underline{P}_m(t) \\ P_d(t) - \bar{P}_e(t) \end{array} \right\}, \quad (6.5)$$

where  $P_{m,unc1}(t, s)$  and  $P_{m,unc2}(t, s)$ , corresponding to two cases of the bi-linear model of battery, are expressed by

$$P_{m,unc1}(t, s) = \frac{(k_{e1}(t) - sk_{b4}k_{m3})\omega_m^2(t)}{2sk_{b4}k_{m4}}, \quad (6.6)$$

$$P_{m,unc2}(t, s) = \frac{(k_{e1}(t) - sk_{b6}k_{m3})\omega_m^2(t)}{2sk_{b6}k_{m4}}. \quad (6.7)$$

Additionally, the adapted control space is further simplified by  $u \in \{u_i : i = 1, \dots, 7\}$ , where subscript  $i$  indicates the  $i^{\text{th}}$  functional in the control space in Eq. 6.5.

A comparison has been made between the energy consumption based on the piece-

wise linear and the quadratic battery model. Selective Hamiltonian Minimization (SHM) is applied to evaluate the energy consumption of a reference vehicle. As illustrated in Fig. 6.3, the bilinear model of battery has different level of errors depending on missions. The discrepancy of minimal fuel consumption is negligible over NEDC; where the differences over FTP-72 and HYWFET are slightly increased (the error is about 2.34%).

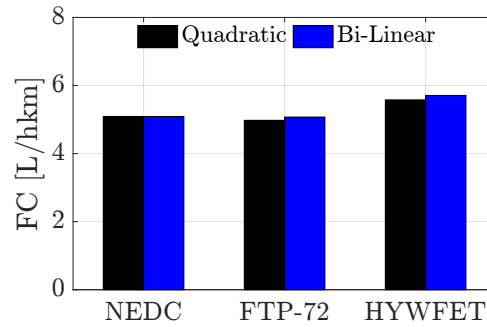


Figure 6.3 – Minimal fuel consumption of different battery models.

### 6.2.2 Equivalent Energy Consumption Model

To develop FACE based on SHM, an analytic model, known as the equivalent energy consumption model, is proposed to evaluate the minimal energy consumption. The equivalent energy consumption model is

$$E_{ef}^{eqv}(s) = \sum_{t=t_0}^{t_f} (P_{ef}^*(t) + sP_{be}^*(t)) \Delta t, \quad (6.8)$$

where  $E_{ef}^{eqv}$  is the equivalent fuel energy consumption,  $s$  is the adjoint state variable,  $P_{ef}^*$  is the burned fuel power resulting from optimal control laws, and  $P_{be}^*$  is the electrochemical power of battery based on optimal control laws.

The minimal energy consumption and the equivalent energy consumption are compared for an exemplified parallel hybrid-electric vehicle, as illustrated in Fig. 6.4. The energy of battery  $E_{be}$ , of burned fuel  $E_{ef}$ , and of equivalent energy consumption  $E_{ef}^{eqv}$  are presented as a function of adjoint state variable  $s$ . The minimal energy consumption is indicated by a red dot crossed by a horizontal red dashed line, which is determined by the proper adjoint state variable of the reference vehicle  $s^{ref}$ .

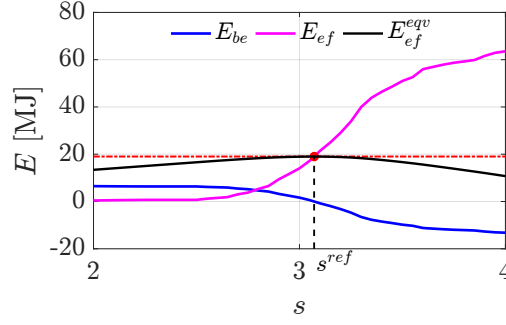


Figure 6.4 – Equivalent minimal fuel consumption of hybrid-electric vehicles.

As observed in Fig. 6.4, the minimal energy consumption is assumed to be approximated by the equivalent energy consumption for any given adjoint variable  $s$ , which yields

$$E_{ef} \approx E_{ef}^{eqv}(s), \forall s. \quad (6.9)$$

The equivalent energy consumption can approximate the minimal energy consumption for a hybrid-electric vehicle when the adjoint state variable  $s_{ref}$  is chosen. To further precise the approximation of equivalent fuel consumption, the adjoint state variable of a reference vehicle is used, thereby leading to

$$E_{ef} = E_{ef}^{eqv}(s^{ref}). \quad (6.10)$$

### 6.2.3 Fully Analytic Energy Consumption Estimation

Based on the equivalent energy consumption model and a reference hybrid-electric vehicle, the Fully Analytic fuel Energy Consumption Estimation (FACE) is expressed by

$$E_{ef} = \sum_{i,j,\epsilon,\nu} \mathcal{D}_{ij}^{e\epsilon\nu} \mathcal{C}_{ij}^{e\epsilon\nu} + s^{ref} \sum_{i,j,\epsilon,\nu} \mathcal{D}_{ij}^{b\beta\nu} \mathcal{C}_{ij}^{e\epsilon\nu}, \quad (6.11)$$

where  $\mathcal{D}_{ij}^{e\epsilon\nu}$  and  $\mathcal{D}_{ij}^{b\beta\nu}$  are dimension-related parameters relating to engine and battery, respectively;  $\mathcal{C}_{ij}^{e\epsilon\nu}$  denotes cycle-related parameters derived from a reference hybrid-electric vehicle, parameters  $i, j, \epsilon$ , and  $\nu$  are given by  $i = 0, \dots, 6$ ;  $j = 0, \dots, 2$ ;  $\epsilon = 1, \dots, 10$ ;  $\nu = 1, \dots, \mathcal{K}_t$ ; and  $s^{ref}$  is the adjoint state variable of the reference vehicle.

Considering the dimension-related parameters, they are further clustered into  $\mathcal{K}_t$  groups due to the stepped-ratio transmission. The dimension-related parameters are given in Appendix E.2 because of too many equations. The cycle-related parameters are summarized as

$$C_{ij}^{\epsilon v} = \sum_{t \in \sigma_{\epsilon v}} v^i(t) a^j(t) \Delta t, \quad (6.12)$$

where the time set  $\sigma_{\epsilon v}$  is defined by

$$\sigma_{\epsilon v} = \{t : u^*(t, s^{ref}) = u_{\epsilon}(t, s^{ref}), \mathcal{K}_t(t) = v\}. \quad (6.13)$$

The valid combinations of  $i$  and  $j$  for hybrid-electric vehicles are summarized as

$$\begin{aligned} i &= \{0, 1, 2, 3, 4, 5, 6\}, j = 0, \\ i &= \{0, 1, 2, 3\}, j = 1, \\ i &= \{0\}, j = 2. \end{aligned} \quad (6.14)$$

A possible optimal control solution is exemplified to show how dimension- and cycle-related parameters are derived. The burned fuel power in the first unconstrained condition ( $\epsilon = 1$ ) is expressed by

$$P_{ef}^{1v} = \mathcal{D}_{10}^{e1v} v + \mathcal{D}_{20}^{e1v} v^2 + \mathcal{D}_{30}^{e1v} v^3 + \mathcal{D}_{40}^{e1v} v^4 + \mathcal{D}_{50}^{e1v} v^5 + \mathcal{D}_{60}^{e1v} v^6 + \mathcal{D}_{11}^{e1v} va + \mathcal{D}_{21}^{e1v} v^2 a. \quad (6.15)$$

Consequently, the energy of burned fuel in the unconstrained condition is evaluated by

$$\begin{aligned} E_{ef}^{1v} &= \sum_{v=1}^{\mathcal{K}_t} \left( \mathcal{D}_{10}^{e1v} \sum_{t \in \sigma_{1v}} v + \mathcal{D}_{20}^{e1v} \sum_{t \in \sigma_{1v}} v^2 + \mathcal{D}_{30}^{e1v} \sum_{t \in \sigma_{1v}} v^3 + \mathcal{D}_{40}^{e1v} \sum_{t \in \sigma_{1v}} v^4 \right. \\ &\quad \left. + \mathcal{D}_{50}^{e1v} \sum_{t \in \sigma_{1v}} v^5 + \mathcal{D}_{60}^{e1v} \sum_{t \in \sigma_{1v}} v^6 + \mathcal{D}_{11}^{e1v} \sum_{t \in \sigma_{1v}} va + \mathcal{D}_{21}^{e1v} \sum_{t \in \sigma_{1v}} v^2 a \right) \\ &= \sum_{v=1}^{\mathcal{K}_t} \sum_{i=0, j=0}^{i=6, j=1} \mathcal{D}_{ij}^{\epsilon v} C_{ij}^{\epsilon v}. \end{aligned} \quad (6.16)$$

The sensitivity of dimensioning parameters are not presented owing to the high

nonlinearity of FACE for parallel HEVs.

### 6.3 Analytic Evaluation of Minimal Energy Consumption

Energy consumption of hybrid-electric vehicles of series and parallel architectures is evaluated through FACE and compared the one via QSS.

#### 6.3.1 Series Hybrid-Electric Vehicle

##### Reference Vehicles

A baseline series hybrid-electric vehicle and the one of partially varied dimensioning parameters are separately investigated with FACE and VHOT. Features of these two series HEVs are summarized in Table 6.1.

Vehicle		I	II
	$m_v$ [kg]	1400	
	$R_w$ [m]	0.36	
	$C_{v0}$ [N]	137.74	
	$C_{v1}$ [N/(m/s)]	0	
	$C_{v2}$ [N/(m/s) <sup>2</sup> ]	0.432	
Engine	$\mathcal{I}_e$	CI	
	$\mathcal{V}_e$ [L]	0.7	
	$\mathcal{T}_e$ [Nm]	66	
	$\mathcal{P}_e$ [kW]	44	
Electric Generator	$\mathcal{I}_g$	PMSM	
	$\mathcal{T}_g$ [Nm]	90	
	$\mathcal{P}_g$ [kW]	49	
Battery	$\mathcal{I}_b$	HE	
	$\mathcal{E}_b$ [kWh]	7	
Electric Motor	$\mathcal{I}_m$	PMSM	
	$\mathcal{T}_m$ [Nm]	250	
	$\mathcal{P}_m$ [kW]	98	120

Table 6.1 – Main features of investigated series hybrid-electric vehicles.

## Results and Analysis

The energy consumption in terms of fuel consumption are depicted for the reference and investigated vehicle in Fig. 6.5. The FACE approximates the minimal fuel consumption almost the same as the one by VHOT. The differences is mainly caused by the power losses of the electric components due to the simplified assumption for series hybrid-electric vehicles.

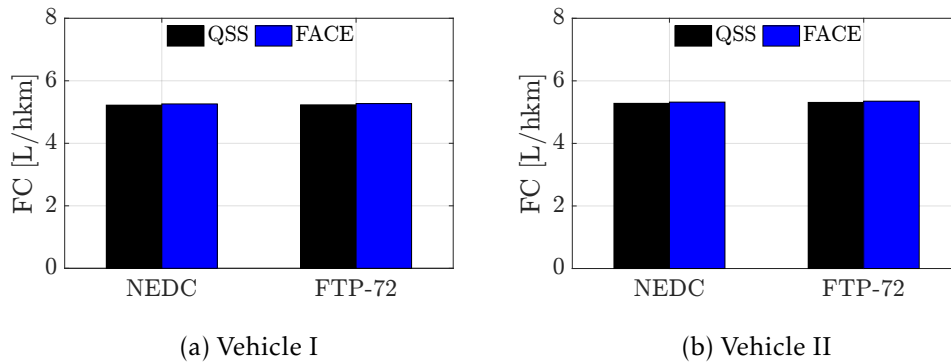


Figure 6.5 – Minimal energy consumption of reference and investigated series hybrid-electric vehicles.

### 6.3.2 Parallel Hybrid-Electric Vehicle

#### Reference Vehicles

Concerning parallel hybrid-electric vehicles, the characteristics of the reference parallel HEV Vehicle I and the investigated one Vehicle II are summarized in Table 6.2. The main difference is the installed internal combustion engine. When scaling the engine displacement for Vehicle II, the maximum brake effective pressure is maintained within 10% variation at most so that the scaled engine can be practical. The minimal energy consumption of Vehicle I and II is evaluated through both FACE and VHOT.

#### Results and Analysis

The minimum energy consumption of Vehicle I and II is illustrated and compared in Fig. 6.6 over NEDC and HYWFET. Concerning Vehicle I, the minimum energy consumption approximated by FACE is the same as the one evaluated through QSS in terms of VHOT. This is due to the application of the same type powertrain model. As for Vehicle II,

Vehicle		I	II
	$m_v$ [kg]	1814	
	$R_w$ [m]	0.3173	
	$C_{v0}$ [N]	93.5	
	$C_{v1}$ [N/(m/s)]	5.29	
	$C_{v2}$ [N/(m/s) <sup>2</sup> ]	0.536	
Engine	$\mathcal{I}_e$	SI/NA/SB	
	$\mathcal{V}_e$ [L]	1.40	1.26
	$\mathcal{T}_e$ [Nm]	130	
	$\mathcal{P}_e$ [kW]	60	
Battery	$\mathcal{I}_b$	HP	
	$Q_b$ [Ah]	31	
	$\mathcal{K}_b$	54	
Electric Motor	$\mathcal{I}_m$	PMSM	
	$\mathcal{T}_m$ [Nm]	28	
	$\mathcal{P}_m$ [kW]	37	
Drivetrain	$\mathcal{I}_t$	MT-5	

Table 6.2 – Main features of investigated parallel hybrid-electric vehicles.

the minimal energy consumption of FACE is slightly higher than the one of VHOT. However, the differences is neglected due to its small magnitude.

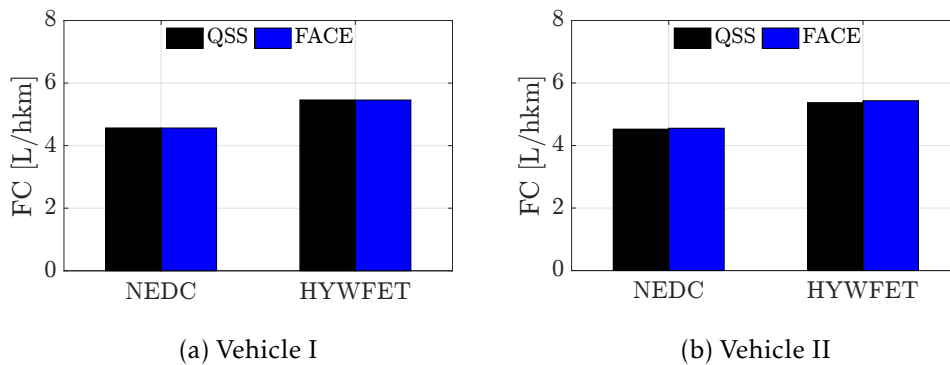


Figure 6.6 – Minimal energy consumption of reference and investigated parallel hybrid electric vehicles.

## **Part IV**

# **Design and Control Co-Optimization for Advanced Vehicle Propulsion Systems**



# Optimal Design Problem Formulation

In this chapter, generic issues relating to the optimal design of a vehicle propulsion system are briefly discussed, including the design objective and constraints. Furthermore, the problem of the optimal design for a vehicle propulsion system is formulated and solved through the bi-level and uni-level co-optimization approach.

## 7.1 Design Objective

Design of Vehicle Propulsion Systems (VPSs) is confronted with high complexities due to powertrain technology (conventional, battery-electric, or hybrid-electric vehicles), powertrain architecture (in particular, series, parallel, and power-split architecture for HEVs), powertrain component (mechanical and electrical ones, such as internal combustion engine, transmission, battery, electric motor/generator), powertrain control (powertrain control optimization for the minimal energy consumption in HEVs). Meanwhile new vehicle product offerings must concurrently response to meet customer wants and regulatory requirements. To cope with these complexities, the optimal design technique is highly requested to achieve the desired requirements, for instance, lower energy consumption.

Throughout this thesis, the objective of the optimal design problem for vehicle propulsion systems is solely to minimize the energy consumption by finding the best dimensioning parameters of powertrain components, which yields

$$\min_{d \in S_{adm}} \mathcal{L}(d), \quad (7.1)$$

$$s.t. \quad g_i(d) \leq 0, \text{ for each } i \in \{1, \dots, m\}, \quad (7.2)$$

$$h_j(d) = 0, \text{ for each } j \in \{1, \dots, n\}, \quad (7.3)$$

where  $d$  presents generic dimensioning parameters to optimize that is defined by  $d \in \{\mathcal{S} : \mathcal{S}_e \cup \mathcal{S}_d \cup \mathcal{S}_b \cup \mathcal{S}_m \cup \mathcal{S}_g\}$ ,  $\mathcal{S}_{adm}$  is the admissible design space that is constrained by desired requirements,  $\mathcal{L}(d)$  represents the energy consumption, and  $g_i(d)$  and  $h_j(d)$  indicate generic equality and in-equality constraints.

In particular, the objective function  $\mathcal{L}(d)$  depends on powertrain technologies. Considering a conventional vehicle, the design objective function is

$$\mathcal{L}(d) = \int_{t_0}^{t_f} P_{ef}(t, d) dt; \quad (7.4)$$

whereas, the objective function for battery-electric vehicles is

$$\mathcal{L}(d) = \int_{t_0}^{t_f} P_{be}(t, d) dt. \quad (7.5)$$

The objective function of hybrid-electric vehicles is more complex than that of single-source ones because of the inevitability of control optimization for the evaluation of the minimal energy consumption. Thus, the objective function of the optimal design is

$$\mathcal{L}(d) = \int_{t_0}^{t_f} P_{ef}(u(t), t, d) dt. \quad (7.6)$$

## 7.2 Design Constraint

Constraints of the optimal design for vehicle propulsion systems are introduced and partially determined by the parameters of vehicle attributes, such as top speed, acceleration, and gradeability. Simple analytic models are developed to evaluate the design constraints based on the required vehicle attributes.

### 7.2.1 Vehicle Attribute

The considered constraints in the design problem of vehicle propulsion systems mainly consist of vehicle performance parameters, which are known as vehicle attributes. Despite comprehensive vehicle attributes discussed in [27], the most interesting ones are composed of vehicle top speed  $v_{top}$ , gradeability of start-up  $\alpha_{ls}$  and of high speed  $\alpha_{hs}$ , and standstill acceleration time from 0 to 100 km/h  $t_{100}$ . Apart from the aforementioned

parameters, all-electric range  $D$  is of high interest, particularly for plug-in hybrid-electric and battery-electric vehicles.

### Top Speed

As a frequent mentioned vehicle attribute of light-duty vehicles, the top speed (denoted by  $v_{top}$ ) is defined as a constant cruising speed that is determined by the available power and the resistance on a flat road.

The tractive effort is further simplified, because the energy consumption of the rolling friction is typically one order of magnitude smaller than the aerodynamic friction consumed power at vehicle top speed. Thus, the approximation of the maximum traction power for passenger cars is written as

$$P_{i,v} \approx \frac{\rho_{ar} C_{ar} A_{ar} v_{top}^3}{2}, \quad (i = e, m), \quad (7.7)$$

where  $e$  indicates internal combustion engine in a conventional or hybrid-electric vehicle, whereas  $m$  refers to electric motor in a battery-electric or plug-in hybrid-electric vehicle.

### Gradeability

Gradeability is a relevant metric for both light- and heavy-duty vehicles. It is defined as the grade which a vehicle can overcome at a certain speed. The approximated tractive effort of a vehicle climbing an uphill road with a slope  $\alpha$  without accounting for powertrain efficiency is

$$T_{i,\alpha} = \frac{(m_v g C_{rr} \cos \alpha + m_v g \sin \alpha + 0.5 \rho_{ar} C_{ar} A_{ar} v_v^2) R_w}{\mathcal{R}_d}, \quad (i = e, m), \quad (7.8)$$

where  $\mathcal{R}_d$  is the dimensioning parameter of a drivetrain.

Correspondingly, the further simplified estimation of the maximum tractive power is

$$P_{i,\alpha} \approx m_v g v (\sin \alpha + C_{rr} \cos \alpha), \quad (i = e, m). \quad (7.9)$$

In addition to the gradeability, a similar performance parameter, i.e. startability, is considered as well for both light- and heavy-duty vehicles [74]. The startability is only considered when a vehicle starts movement from standstill. Note that, the full load of vehicle is applied in both gradeability and startability estimation.

### Acceleration Performance

The acceleration performance is usually described by the accelerating time from standstill to 100 km/h or to 60 mph and the distance covered from zero speed to a certain speed on level road. Using Newton's second law, the acceleration time  $t_{100}$  obtained from the maximum tractive effort is evaluated by

$$t_{100} = \int_0^{100/3.6} \frac{m_v}{T_i \mathcal{R}_d / R_w - m_v g C_{rr} - 0.5 \rho_{ar} C_{ar} A_{ar} v^2} dv. \quad (7.10)$$

The acceleration time from standstill to 100 km/h is not only valid for engine-based and hybrid-electric vehicles, but for some powerful battery-electric vehicles as well. Moreover, the acceleration time  $t_{100}$  is not able to compute directly due to the highly dynamic effects. A further simplified model between acceleration time and the maximal power of the main tractive powertrain component (such as internal combustion engine or electric motor/generator) is expressed as

$$t_{100} = c_{t100} \frac{m_v v_{100}^2}{P_{i,t}}, \quad (i = e, m), \quad (7.11)$$

where  $c_{t100} = 0.877$  for diesel engine vehicles,  $c_{t100} = 0.929$  for gasoline engine vehicles, and  $c_{t100} = 0.767$  for battery-electric vehicles.

A simple yet direct verification of the acceleration time model in Eq. 7.11 is demonstrated in Fig. 7.1 for conventional vehicles. The published acceleration time is denoted by  $t_{100}$ , whereas the estimated acceleration time is indicated by  $t_{100}^p$ . The estimated acceleration time agreed with the published one.

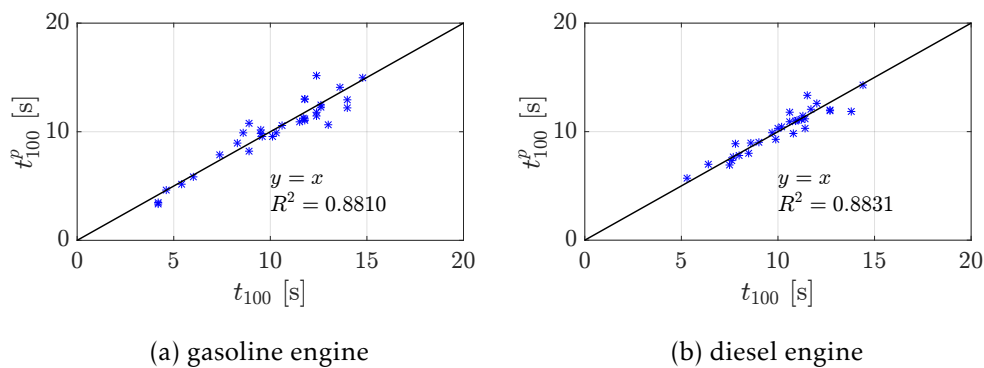


Figure 7.1 – Comparison of estimated and published acceleration time for conventional vehicles.

As for acceleration time of battery-electric vehicles, Fig. 7.2 shows the comparison between the estimated values and the published ones. Despite further simplified model in Eq. 7.11, the estimations of acceleration time agreed well with data.

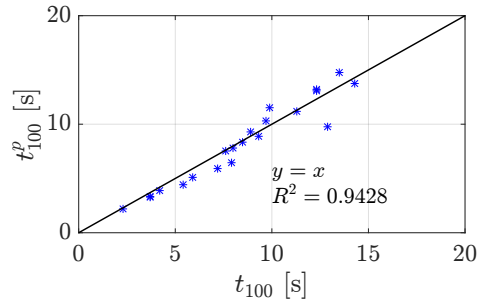


Figure 7.2 – Comparison of estimated and published acceleration time for battery-electric vehicles.

### All-Electric Range

All-electric range is an essential design constraint for plug-in hybrid-electric and battery-electric vehicles. The all-electric range is determined by the applicable energy of battery and the specific energy consumption of a battery-electric vehicle, which yields

$$E_b = D \frac{\int_{t_0}^{t_f} P_{be}(t, d) dt}{\int_{t_0}^{t_f} v(t) dt}, \quad (7.12)$$

where  $E_b$  is the applicable energy of battery,  $D$  is the desired all-electric range.

### 7.2.2 Design Space

Design space is the admissible range of dimensioning parameters resulting from the design constraints. Vehicle attribute significantly affects the rated power and rated torque of the power sources, such as internal combustion engine, electric motor/generator.

As a consequence, the rated power of internal combustion engine or electric motor/generator in different vehicle applications must satisfy

$$\mathcal{P}_i \geq \max\{P_{i,v}, P_{i,\alpha}, P_{i,t}\}, \quad (i = e, m). \quad (7.13)$$

As for the rated torque of an internal combustion engine or electric motor/generator,

it is expressed as

$$\mathcal{T}_i \geq T_{i,\alpha}, \quad (i = e, m). \quad (7.14)$$

In regard to the desired all-electric range, the minimal applicable energy of a battery is constrained as

$$\mathcal{E}_b \geq E_b, \quad (7.15)$$

where  $\mathcal{E}$  is the applicable energy of battery to size.

Additionally, implicit constraints on the dimensioning parameters of powertrain components are taken into account. For instance, battery must be capable of providing sufficient electrical power to electric motor/generator during vehicle operation. Considering an internal combustion engine, its rated torque is not independent from its displacement, which yields

$$\mathcal{T}_e = c_{et} \mathcal{V}_e, \quad (7.16)$$

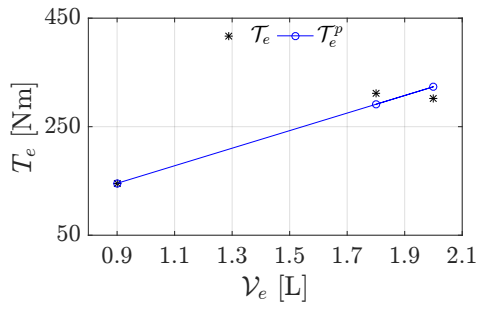
where the coefficient  $c_{et}$  is 148.63 Nm/L for CI/TC engines, 161.81 Nm/L for SI/TC engines, and 93.44 Nm/L for SI/NA engines.

Furthermore, its torque of the rated power is linearly modeled as a function of engine displacement, which is given by

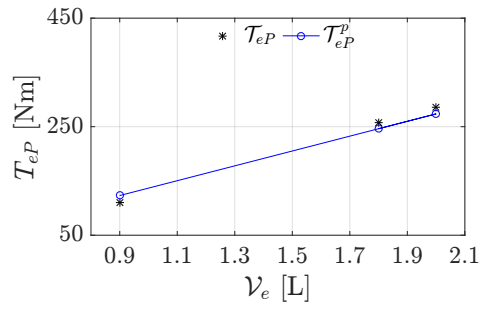
$$\mathcal{T}_{ep} = c_{ep} \mathcal{V}_e, \quad (7.17)$$

where the coefficient  $c_{ep}$  is 116.34 Nm/L for CI/TC engines, 136.80 Nm/L for SI/TC engines, and 85.63 Nm/L for SI/NA engines.

Coefficients in Eq. 7.16 and 7.17 are further validated with the light-duty engines in Table 2.4. Fig. 7.3a, 7.4a, and 7.5a illustrate the comparison of the rated torque and the estimated one for engines in terms of SI/TC, SI/NA, and CI/TC, respectively; whereas the comparison of the torque of rated power is correspondingly depicted in Fig. 7.3b to 7.5b.

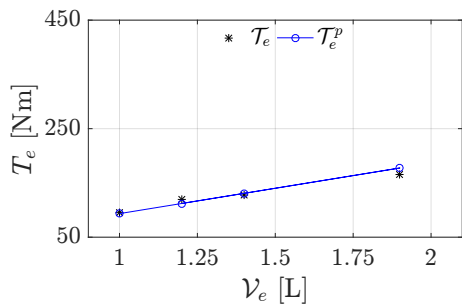


(a) rated torque

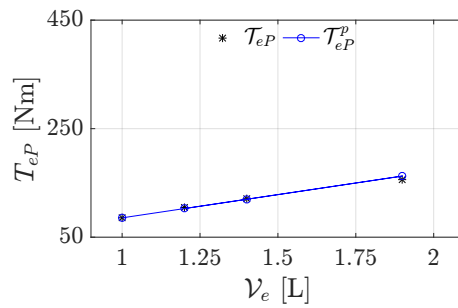


(b) torque of rated power

Figure 7.3 – Comparison of rated torque and torque of rated power for SI/TC engines.

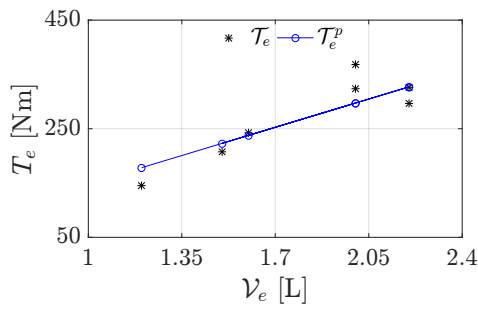


(a) rated torque

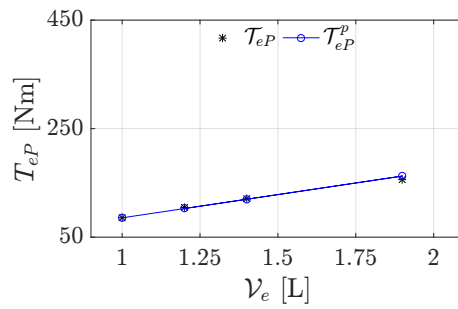


(b) torque of rated power

Figure 7.4 – Comparison of rated torque and torque of rated power for SI/NA engines.



(a) rated torque



(b) torque of rated power

Figure 7.5 – Comparison of rated torque and torque of rated power for CI/TC engines.

### 7.3 Design Method

The design optimization, particularly combining with control optimization for hybrid-electric vehicles, is commonly solved through a multidisciplinary system design optimization framework [75], for instance, through the bi-level co-optimization approach. As an alternative, the uni-level co-optimization approach is proposed as well, thanks to the development of FACE for hybrid-electric vehicles.

#### 7.3.1 Bi-Level Co-Optimization Approach

Bi-level co-optimization approach is characterized by two optimizers that minimize the energy consumption at two distinct levels, in which are specifically for powertrain design and powertrain control. At the level of powertrain design, dimensioning parameters are optimized to get the global minimal fuel consumption; optimal powertrain control is applied to evaluate the minimum fuel consumption at the level of powertrain control for an investigated vehicle.

A flow chart of bi-level co-optimization approach is illustrated in Fig. 7.6. Dimensioning parameters are initialized and transferred to control optimizer. Then the minimal fuel consumption of vehicle propulsion systems is minimized by the design optimizer so that the optimal dimensioning parameters are determined. Once exit criteria are satisfied, the bi-level co-optimization process is completed and terminated. Due to two types of optimizations, the bi-level co-optimization approach is tailored for hybrid-electric vehicles.

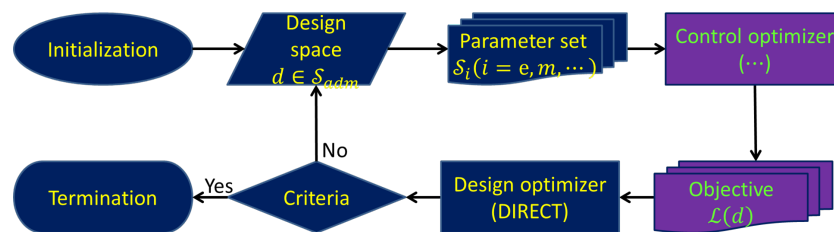


Figure 7.6 – Scheme of bi-level co-optimization approach.

The blue blocks in Fig. 7.6 represent operations relating to the powertrain design optimization in the outer loop; whereas the violet blocks are associated with the powertrain control optimization in the inner loop. Throughout this thesis, the design optimization is solely performed through DIRECT, whereas the control optimization is carried out by the methods presented in Chapter 4.

However, the bi-level co-optimization approach can be applied to single-source vehicles by replacing the powertrain control optimization with quasi-static simulation. Consequently, dimensioning parameters of single-source vehicles are optimized through the bi-level design optimization approach.

### 7.3.2 Uni-Level Co-Optimization Approach

As the development of FACE for single-source and hybrid-electric vehicles, the dimensioning parameter optimization can be regarded as a nonlinear programming problem, consisting of objective function (which is FACE) and general constraints (from the requirement of vehicle attributes).

By implementing FACE, the powertrain design optimization for hybrid-electric vehicles is performed in a uni-level co-optimization approach (see Fig.7.7) because powertrain control optimization is embedded in FACE. This uni-level co-optimization approach is much more complex compared with the bi-level co-optimization approach due to the high inherent nonlinearity of FACE, and the lack of suitable nonlinear solvers. However, the nonlinear solver is possibly replaced by simple method, such as the full space search method. Specific nonlinear solvers and optimization algorithms are introduced within corresponding case studies in Chapter 8.

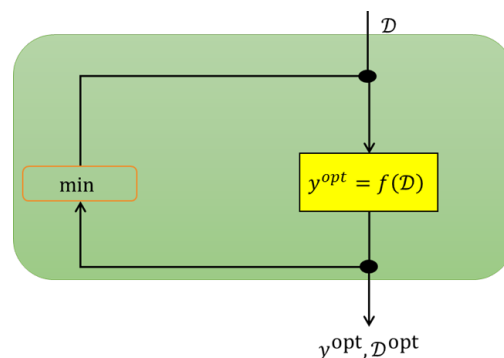


Figure 7.7 – Scheme of uni-level co-optimization approach.



# Optimal Design of Vehicle Propulsion Systems

Theories of analytic models of powertrain components, bi-level co-optimization, and uni-level co-optimization through FACE are applied to several case studies, including conventional, battery-electric and hybrid-electric vehicles. The energy consumption is always minimized by optimizing dimensioning parameters of powertrain components over specific missions through the bi-level co-optimization and the uni-level co-optimization approach.

## 8.1 Design Optimization of a Conventional Vehicle

The vehicle propulsion system of a reference conventional vehicle is optimized to further reduce energy consumption through the bi-level design optimization and uni-level design optimization approach. After the introduction of the main features of the powertrain and vehicle parameters, the optimal design problem describes the design constraints, resulting design space, and characteristics of design approaches. Results of optimized dimensioning parameters are comparatively presented and discussed.

### 8.1.1 Reference Vehicle

The main features of the reference conventional vehicle are listed in Table 8.1, including vehicle parameters [76], and dimensioning parameters of internal combustion engine and drivetrain in Table 2.4 and 2.7, respectively.

Vehicle	$m_v$ [kg]	1595
	$R_w$ [m]	0.308
	$C_{v0}$ [N]	134.094
	$C_{v1}$ [N/(m/s)]	3.7465
	$C_{v2}$ [N/(m/s) <sup>2</sup> ]	0.3486
Engine	$\mathcal{I}_e$	CI/TC
	$\mathcal{V}_e$ [L]	2.15
	$\mathcal{T}_e$ [Nm]	292
	$\mathcal{P}_e$ [kW]	90
Drivetrain	$\mathcal{I}_t$	DCT-6
	$\mathcal{R}_{fd}$	4.12 & 3.04

Table 8.1 – Features of reference conventional vehicle.

### 8.1.2 Optimal Design Problem

The optimal design problem specifies the design constraints based on the reference conventional vehicle and the resulting design space. Moreover, the applied nonlinear solver in the uni-level co-optimization approach is specified in this case study.

#### Constraints

Based on the reference vehicle, design constraints consist of vehicle top speed, acceleration time from 0 to 100 km/h, and gradeability, which lead to

$$\begin{aligned} \text{vehicle top speed in [km/h]} : & \geq 200 , \\ \text{acceleration time to 100 in [s]} : & \leq 13.5, \\ \text{gradeability in [\%]} : & \geq 30. \end{aligned}$$

The dimensioning parameters to optimize are summarized by  $\{\mathcal{I}_e, \mathcal{V}_e, \mathcal{I}_t\}$ , where  $\mathcal{I}_e$  contains SI/NA/SB, SI/NA/LB, and CI/TC;  $\mathcal{I}_t$  includes six-speed manual and automated transmission. Moreover, technological parameters  $\mathcal{I}_e$  and  $\mathcal{I}_t$  are represented by integers corresponding to different technologies.

Based on the desired top speed, the rated power of engine is initially constrained according to Eq. 7.1b. By combining Eq. 7.16 and 7.17, the minimum engine displacement of each engine technology is estimated, thus leading to the overall minimum of engine displacement  $\mathcal{V}_e \geq 1.82$  L.

As for the transmission technological parameter  $\mathcal{I}_t$ , the ratio of last gear  $\mathcal{R}_{tk}$  is determined by the required top speed; whereas the ratio of first gear  $\mathcal{R}_{t1}$  is determined by the engine displacement and the required gradeability.

### Approaches

Both approaches of bi-level and uni-level design optimization are implemented to optimize dimensioning parameters of powertrain components. DIRECT is applied in the bi-level design optimization approach.

Considering the uni-level design optimization, a nonlinear solver is applied to minimize the objective functional, which is FACE. As a nonlinear programming problem, the uni-level optimization is solved by the function "fmincon" in MATLAB. However, "fmincon" cannot handle the integer design parameters. Therefore, the uni-level design optimization repeats all the combinations of the integer parameters, which are the technological parameters of engine and transmission.

### 8.1.3 Result and Discussion

The optimized dimensioning parameters are reported in terms of bi-level and uni-level design optimization. In addition, the impact of missions on the optimal dimensioning parameters are investigated and discussed as well.

#### Impact of Optimization Approach

The reference vehicle is optimized separately through the bi-level design optimization (with quasi-static simulation in the inner loop) and the uni-level design optimization (with FACE) over NEDC. Because of implementation of QSS, results of the bi-level design optimization approach are denoted by QSS in this whole chapter. On the other hand, FACE is used to indicate the results of the uni-level design optimization approach.

As illustrated in Fig. 8.1, results of fuel consumption based on bi-level and uni-level design optimization are compared with the fuel consumption of the reference vehicle. About 8.27% of fuel consumption was saved by optimizing the design parameters of powertrain components over NEDC. Furthermore, both optimization approaches obtained the same improvement on fuel consumption.

In addition, the optimal dimensioning parameters are listed in Table 8.2, where VehR, VehNb, and VehNu stand for the reference conventional vehicle, optimized powertrain through the bi-level design optimization, and through the uni-level design optimization, respectively. Considering the results of the uni-level design optimization, the optimal design problem was solved by a nonlinear solver "fmincon" under the assumption that the initial solution referred to the reference vehicle. The initial solution did not affect the optimal solution of dimensioning parameters due to the convexity of FACE for conventional vehicles. Despite the restriction of integers, uni-level design optimization

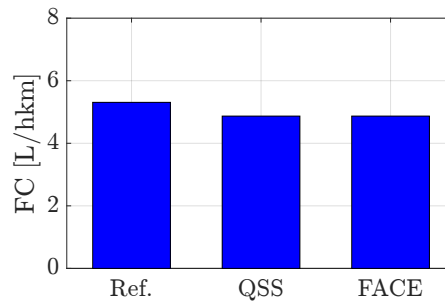


Figure 8.1 – Energy consumption of optimized and reference conventional vehicles over NEDC.

presented the same results of optimal dimensioning parameters as the bi-level design optimization.

	$\mathcal{I}_e$	$\mathcal{V}_e$ [L]	$\mathcal{T}_e$ [Nm]	$\mathcal{P}_e$ [kW]	$\mathcal{I}_t$	$\mathcal{R}_{t1}$	$\mathcal{R}_{t6}$
VehR	CI/TC	2.25	292	90	MT-6	14.25	2.31
VehNb	CI/TC	1.82	270	89	MT-6	11.39	2.26
VehNu	CI/TC	1.82	270	89	MT-6	11.39	2.26

Table 8.2 – Dimensioning parameters of optimized conventional vehicles via bi- and uni-level optimization approach based on NEDC.

Additionally, comparison of vehicle performance between the reference and the optimized one is presented in Table 8.3. With further reduced fuel consumption, the optimized vehicle propulsion system had a slightly higher top vehicle speed, poorer acceleration time, and lower gradeability. Nevertheless, both performance parameters satisfied the design constraints. The history of acceleration from 0 to 100 km/h is illustrated in Fig.8.2, where the initial acceleration capability of the optimized vehicle was worse than the reference one.

	$V_{top}$ km/h	$t_{100}$ [s]	$\alpha$ [%]
VehR	197	9.6	63.99
VehN	201	11.6	42.39

Table 8.3 – Vehicle performance of optimized conventional vehicle compared with reference one.

Concerning computation time, the bi-level design optimization needed about 44 min to complete the entire optimization process with 20 iterations and 447613 function evaluations; whereas, the uni-level design optimization only took about 0.56 s with 9

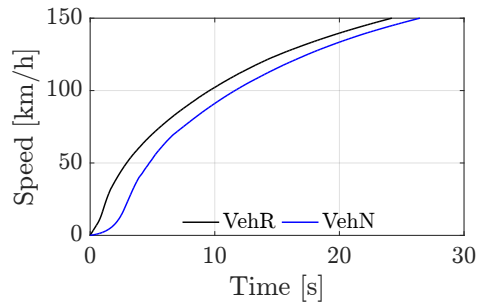


Figure 8.2 – Acceleration performance of optimized and reference conventional vehicles.

iterations and 22 function evaluations. Obviously, the uni-level design optimization significantly decreased the computation time compared with bi-level design optimization approach.

### Impact of Mission

Under the same design considerations, the reference vehicle is optimized via the uni-level design optimization approach over two other missions, which are FTP-72 and HYWFET.

Results of the energy consumption of each optimized vehicle propulsion system are illustrated in Fig. 8.3. The largest improvement of energy consumption (about 9%) was achieved by the optimized vehicle over FTP-72 (VehF); while the least (about 3%) was obtained by that over HYWFET (VehH). However, the optimized dimensioning parameters of different missions are identical to each other as summarized in Table 8.4. Thus, missions did not affect the optimal dimensioning parameters.

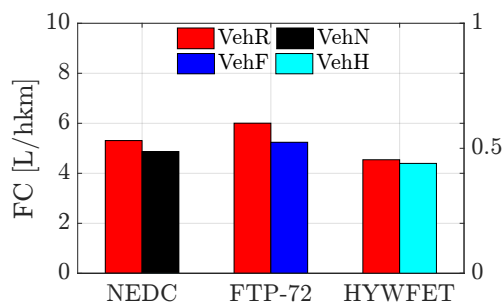


Figure 8.3 – Energy consumption of optimized conventional vehicles over different missions.

	$\mathcal{I}_e$	$\mathcal{V}_e$ [L]	$\mathcal{T}_e$ [Nm]	$\mathcal{P}_e$ [kW]	$\mathcal{I}_t$	$\mathcal{R}_{t1}$	$\mathcal{R}_{t6}$
VehN	CI/TC	1.82	270	89	MT-6	11.39	2.26
VehF	CI/TC	1.82	270	89	MT-6	11.39	2.26
VehH	CI/TC	1.82	270	89	MT-6	11.39	2.26

Table 8.4 – Dimensioning parameters of optimized conventional vehicles based on various missions.

## 8.2 Design Optimization of a Battery-Electric Vehicle

Both bi-level and uni-level design optimization are applied to minimize the electrical energy consumption of a reference battery-electric vehicle, therefore enlarging the all-electric range. The investigated dimensioning parameters are associated with battery and electric motor/generator. The structure of this case study is maintained the same as previous one, which consists of the introduction of a reference vehicle, further explanation of optimal design problem, and result discussion.

### 8.2.1 Reference Vehicle

Table 8.5 reports the main features of the reference battery-electric vehicle, consisting of vehicle parameters [77], dimensioning parameters of battery, electric motor/generator, and drivetrain. The battery and electric motor/generator are referred to the identification sets in Table 2.10 and 2.14, respectively. A single-speed transmission is installed in the drivetrain.

Vehicle	$m_v$ [kg]	1648
	$R_w$ [m]	0.3017
	$C_{v0}$ [N]	141.9465
	$C_{v1}$ [N/(m/s)]	1.1530
	$C_{v2}$ [N/(m/s) <sup>2</sup> ]	0.3952
Battery	$\mathcal{I}_b$	HE
	$Q_b$ [Ah]	31
	$\mathcal{K}_b$	192
Electric Motor	$\mathcal{I}_m$	PMSM
	$\mathcal{T}_m$ [Nm]	108
	$\mathcal{P}_m$ [kW]	78
Drivetrain	$\mathcal{R}_d$	14

Table 8.5 – Features of reference battery-electric vehicle.

### 8.2.2 Optimal Design Problem

Specific design constraints of the reference battery-electric vehicle are introduced with the resulting design space of the investigated dimensioning parameters. Further explanations regarding to the optimal design problem are given to clarify the powertrain design optimization, especially the uni-level design optimization.

#### Constraints

Based on the reference battery-electric vehicle, the technical targets, including top vehicle speed, acceleration time from 0 to 100 km/h, gradeability, and all-electric range are summarized as

$$\begin{aligned}
 \text{vehicle top speed in [km/h]} : & \geq 140, \\
 \text{acceleration time to 100 in [s]} : & \leq 13.5, \\
 \text{gradeability in [\%]} : & \geq 25, \\
 \text{all-electric range in [km]} : & \geq 130.
 \end{aligned}$$

The investigated dimensioning parameters are listed in  $\{Q_b, \mathcal{K}_b, \mathcal{T}_m, \mathcal{N}_m\}$ , where  $Q_b$  and  $\mathcal{N}_b$  are integer parameters. The battery cells of high-energy type are considered only because of better all-electric range, although another type of battery cell can also be investigated.

According to the constraint of top vehicle speed, the lower boundary of the rated power of electric motor is calculated by Eq. 7.11. Concerning the gradeability, the lower boundary of the rated torque of electric motor is evaluated through Eq. 7.8. The base speed of electric motor is within the base speeds of identification set of electric motor/generators in Table 2.14. As for their upper boundaries, random values are chosen without losing fidelity.

As for the battery, capacity of cells is referred to the identification set of battery of high-energy type in Table 2.11. Note that, the upper boundary is limited to 53 Ah for the sake of consistent predictive analytic models. The battery-cell number  $\mathcal{K}_b$  is randomly chosen but meet the requirement of all-electric range. In addition, battery must provide sufficient power to propel the electric motor/generator. Consequently, resulting design space are

$$Q_b \in [25, 53], \quad (8.1)$$

$$\mathcal{K}_b \in [90, 285], \quad (8.2)$$

$$\mathcal{T}_m \in [110, 277], \quad (8.3)$$

$$\mathcal{N}_m \in [4000, 8500], \quad (8.4)$$

$$\mathcal{P}_m \in [73, 150]. \quad (8.5)$$

Although no additional constraints are considered, battery terminal power has been cross-verified to meet the requirement of acceleration and the operating limits over investigated missions.

### Approaches

Both approaches of the bi-level and uni-level design optimization are implemented to optimize the mentioned dimensioning parameters of battery and electric motor/generator. The bi-level design optimization is done by DIRECT as the one in the previous case.

Regarding the uni-level design optimization, a new method of full-space search, instead of the "fmincon" function of MATLAB, is applied to optimize the dimensioning parameters. The reason is due to the higher nonlinearity of FACE for battery-electric vehicles than that for conventional vehicles.

Based on discretization of the design space, the full-space search method minimizes the energy consumption through multi-dimensional array operation that is effective for limited quantity of dimensioning parameters.

### 8.2.3 Result and Discussion

The optimized dimensioning parameters are summarized in terms of the bi-level and uni-level design optimization. In addition, the impact of missions on the optimized dimensioning parameters are investigated and discussed.

#### Impact of Optimization Approach

Fig. 8.4 compares the minimal energy consumption of the optimized vehicle through the bi-level (denoted by QSS) and the uni-level design optimization approach (indicated by FACE). Both the bi-level and uni-level design optimization reduced the minimal energy consumption to the same level, which was about 7.4% less than that of the reference vehicle.

As listed in Table 8.6, the optimal dimensioning parameters via the bi-level (marked by VehNb) and the uni-level design optimization (marked by VehNu) are compared with the ones of the reference vehicle (VehR). The optimized dimensioning parameters

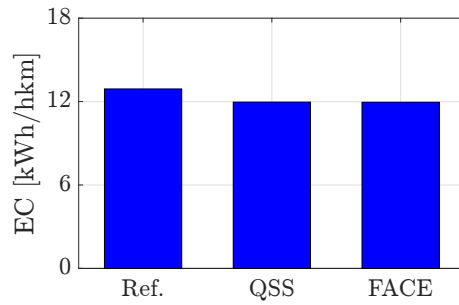


Figure 8.4 – Energy consumption of reference and optimized battery-electric vehicles over NEDC.

of VehNb and VehNu were almost the same to each other. The slight difference were probably caused by the discretization of the design space.

Compared with the reference vehicle, the battery capacity was increase to the upper boundary due to the lowest internal resistance of battery cells. Larger sizes of electric motor/generator were chosen because of the improved operating efficiency. For example, the electrical energy of electric motor in propulsion was reduced about 7% with respect to the reference vehicle.

	$Q_b$ [Ah]	$\mathcal{K}_b$	$\mathcal{T}_m$ [Nm]	$\mathcal{P}_m$ [kW]	$\mathcal{N}_m$ [rpm]
VehR	31	192	108	79	6985
VehNb	53	113	274	150	5232
VehNu	53	110	277	150	5163

Table 8.6 – Dimensioning parameters of optimized battery-electric vehicles via bi- and uni-level optimization approach based on NEDC.

A comparison of vehicle performance between the reference vehicle (VehR) and the optimized vehicle (VehN) is listed in Table 8.7. The optimized vehicle had similar top speed and all-electric range, but further enhanced gradeability and acceleration performance. The history of acceleration from 0 to 100 km/h is depicted in Fig.8.5 for both the reference and optimized vehicle, where a larger size of electric motor/generator improved the acceleration performance.

The computation time of the bi-level design optimization was about 12.7 s with 100 iterations and 2995 function evaluations. However, the computation time of the uni-level design optimization through multi-dimensional array operation only took 1.25 s, which was an improvement of one order of magnitude.

	$V_{top}$ [km/h]	$t_{100}$ [s]	$\alpha$ [%]	All-Electric Range [km]
VehR	143	12.4	21.2	134
VehN	143	5.6	64.0	133

Table 8.7 – Vehicle performance of optimized battery-electric vehicle compared with reference one.

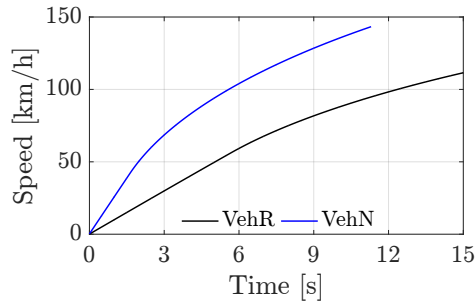


Figure 8.5 – Acceleration performance of optimized and reference battery-electric vehicle.

### Impact of Mission

The reference vehicle is optimized based on two other missions through the bi-level design optimization, in order to verify the impact of missions.

As illustrated in Fig. 8.6, the minimized energy consumption is compared between the optimized vehicles and the reference one. Apart from VehR and VehN, VehF and VehH represented the optimized vehicle based on FTP-72 and HYWFET, respectively. Among all of the optimized vehicles, the largest reduction of 7.4% was achieved by the one over NEDC; whereas the least energy consumption reduction of 3.5% was achieved over HYWFET.

The optimization of vehicle propulsion system design was affected by missions. The optimized vehicle VehN presented similar energy consumption to the other mission-dependent optimized vehicles. This is probably due to NEDC combines the urban and extra-urban driving conditions.

Table 8.8 summarizes the optimal dimensioning parameters over the investigated missions. The mission influenced the optimal dimensioning parameters of battery. However, the dimensioning parameters of electric motor/generator were almost maintained the same, since they were heavily affected by the design constraints.

Based on the optimized dimensioning parameters in Table 8.8, the performance of the optimized vehicles are summarized in Table 8.9. The significant difference was

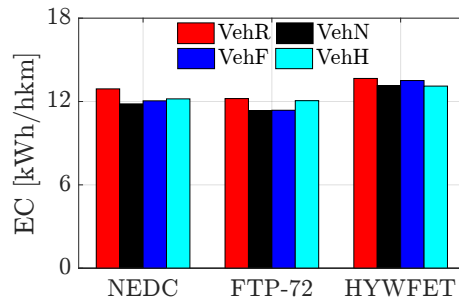


Figure 8.6 – Energy consumption of optimized battery-electric vehicles over different missions.

	$Q_b$ [Ah]	$\mathcal{K}_b$	$T_m$ [Nm]	$\mathcal{P}_m$ [kW]	$\mathcal{N}_m$ [rpm]
VehN	53	113	274	150	5232
VehF	53	121	261	150	5473
VehH	35	285	274	150	5232

Table 8.8 – Dimensioning parameters of optimized battery-electric vehicles based on various missions.

the all-electric-range due to the applicable energy of battery and the specific energy consumption.

	$V_{top}$ [km/h]	$t_{100}$ [s]	$\alpha$ [%]	All-Electric Range [km]
VehN	143	5.6	64.0	133
VehF	143	5.7	60.0	150
VehH	143	5.6	64.0	221

Table 8.9 – Vehicle performance of optimized battery-electric vehicles based on various missions.

## 8.3 Co-Optimization of a Series Hybrid-Electric Truck

VHOT, GRAB-ECO, and FACE are applied to optimize the dimensioning parameters of the propulsion system of a series hybrid-electric truck for better fuel savings.

### 8.3.1 Reference Vehicle

As reported in Table 8.10, the main features of the reference vehicle are summarized including vehicle parameters, internal combustion engine, electric generator, battery,

and electric motor.

Vehicle	$m_v$ [kg]	13500
	$R_w$ [m]	0.44
Engine	$\mathcal{I}_e$	CI
	$\mathcal{V}_e$ [L]	4.8
	$\mathcal{T}_e$ [Nm]	818
	$\mathcal{P}_e$ [kW]	167
Electric Generator	$\mathcal{I}_g$	PMSM
	$\mathcal{T}_g$ [Nm]	400
	$\mathcal{P}_g$ [kW]	70
Battery	$\mathcal{I}_b$	LiB
	$\mathcal{Q}_b$ [Ah]	138
	$\mathcal{K}_b$	48
Electric Motor	$\mathcal{I}_m$	AIM
	$\mathcal{T}_m$ [Nm]	450
	$\mathcal{P}_m$ [kW]	103

Table 8.10 – Main features of investigated series hybrid-electric vehicle.

### 8.3.2 Co-Optimization Problem

#### Constraints

In comparison with light-duty vehicles, vehicle attributes of heavy-duty vehicles are not explicit, except for the gradeability. Powertrain dimensioning parameters of the reference series hybrid-electric truck is optimized without considering any extra requirements of vehicle attributes. The design objective is to minimize fuel consumption of the reference powertrain over the real-world driving cycles.

The investigated dimensioning parameters include  $\{\mathcal{R}_g, \mathcal{K}_b, \mathcal{I}_m, \mathcal{P}_m\}$ , where battery number  $\mathcal{K}_b$  is an integer parameter. Without taking extra vehicle attributes into account, the dimensioning parameters of  $\mathcal{R}_g$  and  $\mathcal{K}_b$  are restricted to a range based on the reference values. As for the electric motor for the traction purpose, the design space is strictly constrained at the lower boundary derived from the gradeability. Without losing reality, design space of the dimensioning parameters are written as

$$\mathcal{R}_g \in [0.9, 1.1], \quad (8.6)$$

$$\mathcal{K}_b \in [40, 56], \quad (8.7)$$

$$\mathcal{T}_m \in [400, 550], \quad (8.8)$$

$$\mathcal{T}_m \in [103, 140]. \quad (8.9)$$

### Approaches

Instead of the bi-level co-optimization, each dimensioning parameter is separately evaluated through VHOT, GRAB-ECO, and FACE with the discretized design space. The real-world missions are solely applied to the heavy-duty vehicles. Therefore, the investigated missions are based on real-world driving cycles, such as the Inner-City Driving Cycle ICDC and the Sub-Urban Driving Cycle SUDC (see Fig. 8.7 and 8.8).

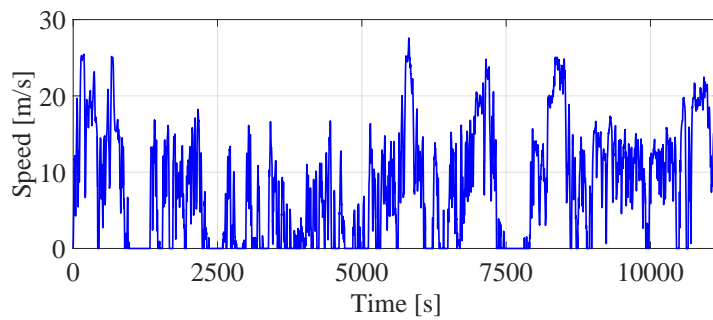


Figure 8.7 – Speed trajectory of ICDC.

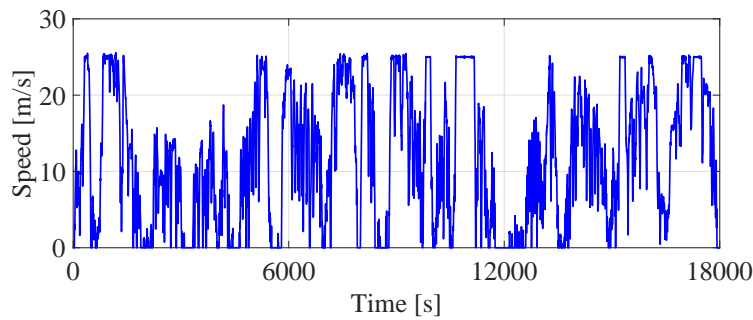


Figure 8.8 – Speed trajectory of SUDC.

### 8.3.3 Result and Discussion

Concerning the dimensioning parameter  $\mathcal{R}_g$ , it only influenced the efficiency of auxiliary power unit, but not on the vehicle performance. Fig. 8.9 summarizes the influence of  $\mathcal{R}_g$

on the minimal fuel consumption over ICDC and SUDC. The fuel consumption slightly decreased as the gear ratio increased due to the efficiency increment of best-efficiency point of the auxiliary power unit.

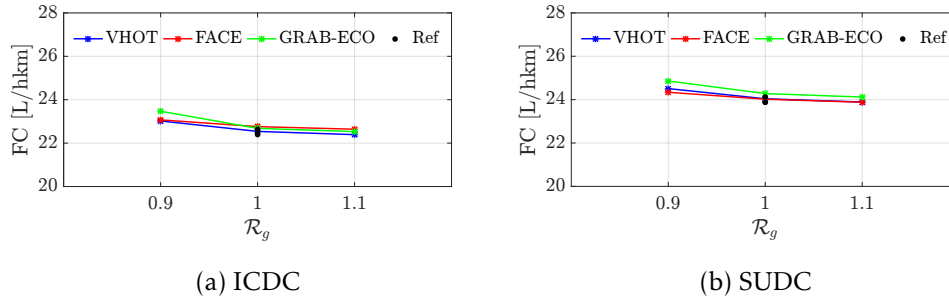


Figure 8.9 – Energy consumption in function of gear ratio between engine and generator.

As shown in Fig. 8.10, battery cell number slightly reduced the minimal fuel consumption over ICDC; whereas, the impact of battery cell number on the minimal fuel consumption was negligible. However, FACE showed different prediction of the minimal fuel consumption over ICDC. Note that, the increment of battery cell number did not change the gross weight of the heavy-duty truck, but reduce the maximum allowable payload. Therefore, a smaller number of battery cells was favored in the condition that the all-electric range could meet the requirement.

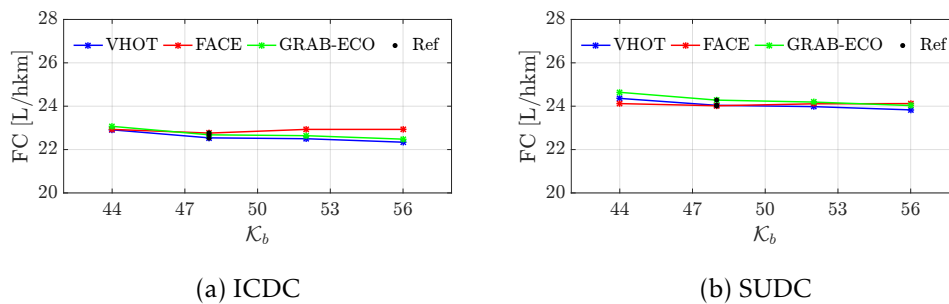


Figure 8.10 – Energy consumption in function of battery cell number.

As for the traction motor, effects of the rated torque is depicted in Fig. 8.11. Over both missions, the minimal fuel consumption was significantly reduced by enlarging the rated torque of the traction motor. With the increase of the rated torque, the base speed of the traction motor decreased, leading to a squeeze of the high efficiency zone at lower motor speed, where the operating points distributed. In addition, the increment of rated torque would further enhanced the gradeability compared with the reference

series hybrid-electric truck.

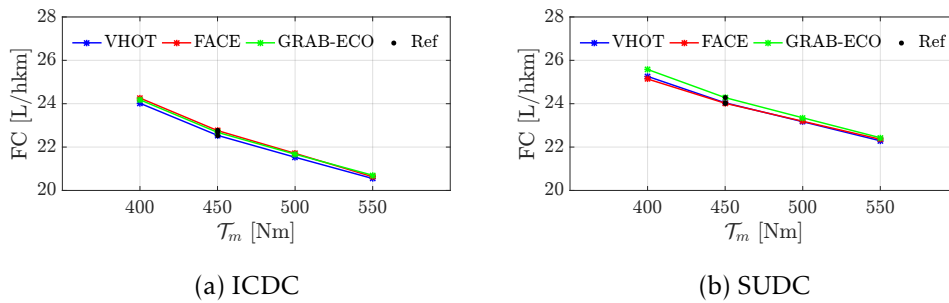


Figure 8.11 – Energy consumption in function of rated torque of traction motor.

Fig. 8.12 presents the influence of the rated power of the traction motor on the minimal fuel consumption. The increment of the rated power led to an opposite effects compared with the rated torque. While maintaining the rated torque, the high efficiency zone was shifted to higher speed as the rated power increased. As a result, the average efficiency of motor operating points was reduced.

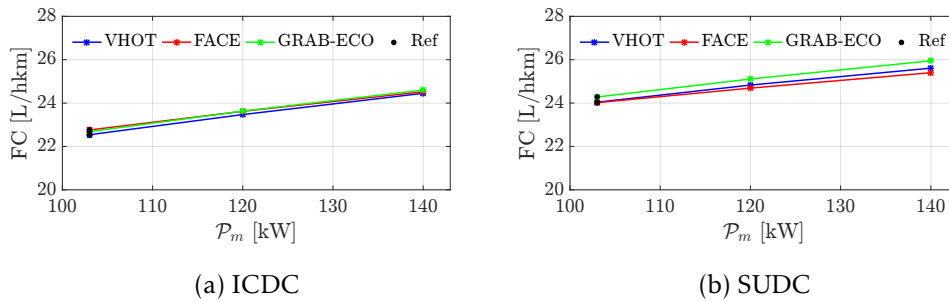


Figure 8.12 – Energy consumption in function of rated power of traction motor.

Table 8.11 reports the computation time of evaluations via VHOT, SHM, and FACE over missions of ICDC and SUDC. Compared with the computation time of VHOT, GRAB-ECO reduced the computation time by orders of magnitude; whereas FACE took the least computation time.

	VHOT	GRAB-ECO	FACE
$t(\text{ICDC})$ [s]	634.4	15	1.05
$t(\text{SUDC})$ [s]	885.2	15.3	1.10

Table 8.11 – Average computation time of each function evaluation.

## 8.4 Co-Optimization of a Parallel Hybrid-Electric Vehicle

A parallel plug-in hybrid-electric vehicle is investigated to reduce energy consumption over given missions. Bi-level co-optimization is applied to optimize the dimensioning parameters of the reference vehicle and to investigate the impact of the different techniques of control optimization and of missions on the minimal energy consumption. In addition, the uni-level co-optimization based on FACE is implemented to optimize dimensioning parameters of powertrain components such that the energy consumption is minimized.

### 8.4.1 Reference Vehicle

The reference parallel hybrid-electric vehicle is a light-duty plug-in vehicle of P2 configuration, whose main features are summarized in Table 8.12.

Vehicle	$m_v$ [kg]	1814
	$R_w$ [m]	0.3173
	$C_{v0}$ [N]	93.5
	$C_{v1}$ [N/(m/s)]	5.29
	$C_{v2}$ [N/(m/s) <sup>2</sup> ]	0.536
Engine	$\mathcal{I}_e$	SI/NA/SB
	$\mathcal{V}_e$ [L]	1.4
	$\mathcal{T}_e$ [Nm]	131
	$\mathcal{P}_e$ [kW]	60
Battery	$\mathcal{I}_b$	HP
	$\mathcal{Q}_b$ [Ah]	31
	$\mathcal{K}_b$	60
Electric Motor	$\mathcal{I}_m$	PMSM
	$\mathcal{T}_m$ [Nm]	36
	$\mathcal{P}_m$ [kW]	38
Drivetrain	$\mathcal{I}_t$	MT5
	$\mathcal{R}_m$	3.31

Table 8.12 – Main features of investigated parallel hybrid-electric vehicle.

### 8.4.2 Co-Optimization Problem

The co-optimization problem of powertrain design and control is briefly formulated including design constraints, the investigated dimensioning parameters, and their

resulting design space. The co-optimization problem is solved through both bi-level and uni-level co-optimization approaches.

### Constraints

The vehicle performance is described in terms of two modes: the conventional and electric vehicle mode. Thus, the main design constraints are summarized as

vehicle top speed in [km/h] :	$\geq 145$ ,
vehicle top speed in [km/h] in electric mode :	$\geq 55$ ,
acceleration time to 100 in [s] :	$\leq 13$ ,
acceleration time to 50 in [s] in electric mode :	$\leq 9$ ,
gradeability in [%] :	$\geq 25$ ,
gradeability in [%] in electric mode:	$\geq 13$ .

The dimensioning parameters to optimize are listed in  $\{\mathcal{I}_e, \mathcal{V}_e, \mathcal{I}_t, \mathcal{P}_m, \mathcal{K}_b\}$ , where engine technology  $\mathcal{I}_e$ , transmission technology  $\mathcal{I}_t$ , and battery cell number  $\mathcal{K}_b$  are integer variables.

According to the desired top vehicle speed and acceleration time in conventional vehicle mode, the lower boundary of engine displacement of each engine technology is individually evaluated through Eq. 7.11 and 7.16. Furthermore, the lower boundary of the design space of the engine displacement is set to the minimum value of the four types of engines. However, effective penalty function will be applied to avoid violation of lower boundaries corresponding to engine types.

Despite two types of transmissions, the gear ratios are defined by the predictive analytic model of transmission in Eq. 2.24 and 2.26. The last gear is evaluated to satisfy the top vehicle speed at the engine speed of rated power; whereas the first gear meets the demanded torque for the desired gradeability.

As for the rated power of electric motor, its lower boundary is calculated to meet the requirement of acceleration time in electric mode. Moreover, the battery cell number allows the battery to provide sufficient power to the electric motor/generator.

Consequently, the resulting design space is summarized as

$$\mathcal{I}_e \in \{SI/NA/SB, SI/NA/LB, SI/TC, CI/TC\}, \quad (8.10)$$

$$\mathcal{V}_e \in [1.17, 2.65], \quad (8.11)$$

$$\mathcal{I}_t \in \{MT-5, MT-6\}, \quad (8.12)$$

$$\mathcal{P}_m \in [21, 57], \quad (8.13)$$

$$\mathcal{K}_b \in [31, 100]. \quad (8.14)$$

### Approaches

Bi-level co-optimization is implemented to optimize the previously mentioned dimensioning parameters. Moreover, two different techniques for powertrain control optimization are applied in the bi-level co-optimization approach, which are VHOT and SHM.

Based on FACE, the uni-level co-optimization approach is applied to optimize a single dimensioning parameter within its design space as well. Due to high nonlinearity of FACE for parallel hybrid-electric vehicles, the exhaustive search method is applied as a design optimization technique.

### 8.4.3 Result and Discussion

Results of several investigations on the optimization of dimensioning parameters, the impact of techniques of powertrain control, and the influences of missions are reported and discussed as follows.

#### Comparison with Reference Vehicle

Compared with the fuel consumption of the reference vehicle, the trajectory of fuel consumption (marked by FC) and function evaluation (denoted by  $K_{fcn}$ ) through the bi-level co-optimization approach is illustrated in Fig. 8.13. As the iteration increased, the minimal fuel consumption became stabilized. The minimized fuel consumption of the optimized vehicle was reduced by 21% compared with the reference vehicle. However, the function evaluation augmented exponentially as iteration increased, thereby leading to significant increment of computation time.

#### Impact of Control Optimizer

Concerning the control optimization through SHM and VHOT, the trajectories of their fuel consumption and function evaluations are comparatively depicted in Fig. 8.14. The minimized fuel consumption of VHOT was slightly higher than that of SHM. Furthermore, the bi-level co-optimization via VHOT required more iterations than that through SHM under the same exit criteria of DIRECT. Yet both of them had similar number of function evaluations.

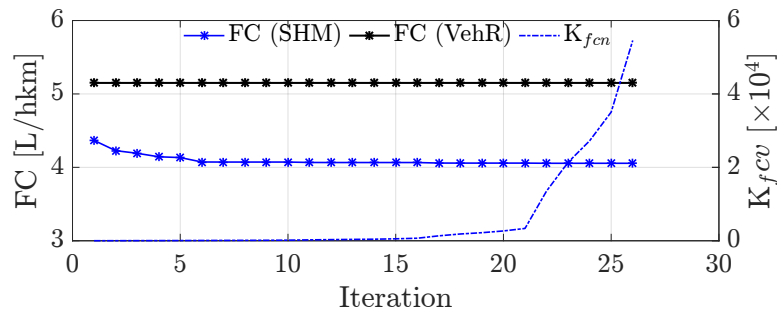


Figure 8.13 – Trajectory of bi-level co-optimization through SHM.

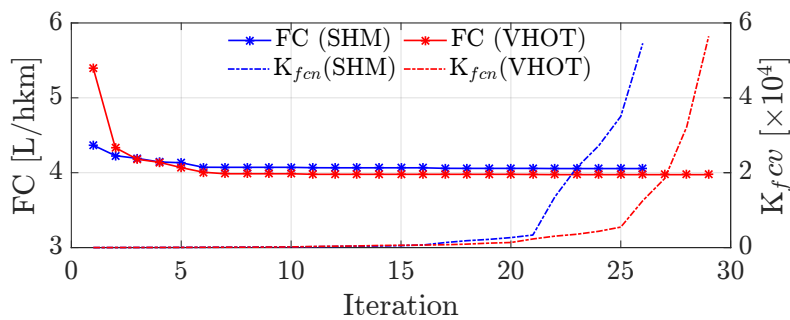


Figure 8.14 – Trajectory comparison of bi-level co-optimization through SHM and VHOT.

The detailed computational characteristics are summarized in Table 8.13. The VHOT took twice as much average time per function evaluation as SHM did. However, the average computation time of SHM was larger than the one in Chapter 4.5.2. The reason is due to extra time required to handling the data in-between two optimization levels.

	Iteration	Evaluation	CPU Time [h]	Average Time [s]
SHM	26	54568	1.77	0.1165
VHOT	29	56451	3.94	0.2511

Table 8.13 – Computational characteristics of bi-level co-optimization via SHM and VHOT.

Table 8.14 reports the dimensioning parameters of the optimized vehicle over NEDC through SHM and VHOT. Except for the type of internal combustion engine, remaining dimensioning parameters were different from each other due to different techniques of powertrain control optimization. The optimal dimensioning parameters of VehN(SHM)

were evaluated via VHOT, resulting a higher fuel consumption (4.00 L/hkm) than VehN(VHOT). The same situation occurred that VehN(SHM) had a lower fuel consumption than VehN(VHOT) evaluated through SHM. Therefore, the different optimal design parameters were caused by the implementation of the powertrain control optimization techniques.

	$\mathcal{I}_e$	$\mathcal{V}_e$ [L]	$\mathcal{I}_t$	$\mathcal{P}_m$ [kW]	$\mathcal{K}_b$
VehN(SHM)	CI/TC	1.24	MT-5	22.0	48
VehN(VHOT)	CI/TC	1.40	MT-5	23.9	54

Table 8.14 – Dimensioning parameters of optimized parallel hybrid-electric vehicles based on SHM and VHOT.

Additionally, a few relevant signals, including speed of engine and motor ( $\omega_e$  and  $\omega_m$ ), demanded power at wheels ( $P_w$ ), engine power ( $P_e$ ), and state of charge of battery (marked as SOC) are comparatively depicted in Fig. 8.15 in terms of SHM and VHOT. Although the final SOC is not the same as the initial one, the difference between those two was handled in the evaluation of minimal fuel consumption by interpolation method.

### Impact of Mission

The vehicle propulsion system of the reference vehicle is further optimized over extra missions, which are FTP-72 and HYWFET. The control optimization in the bi-level co-optimization approach is uniformly done through SHM.

As depicted in Fig. 8.16, fuel consumption of the optimized vehicles were compared with the reference vehicle over each investigated mission. VehN, VehF, and VehH referred to the optimized vehicles based on NEDC, FTP-72, and HYWFET, respectively. To summarize, the minimal fuel consumption was mission-dependent. Because NEDC consists of the urban and extra-urban driving condition, VehN was the good compromise among these three missions.

The percentage of tractive energy and operating time of each mode are illustrated in Fig. 8.17 for the corresponding optimized vehicles. Mode 0 indicated the standstill condition; whereas the other modes corresponded to the sequential elements in Eq. 4.38. In particular, mode 1 was the unconstrained solution; mode 2 was the pure electric mode; and mode 3 was hybrid mode that engine worked at best-efficiency condition.

Table 8.15 summarizes the computational characteristics through the bi-level co-optimization approach. Compared with the computation time of a single function evaluation in Chapter 4.5.2, the average computation time of a single function eval-

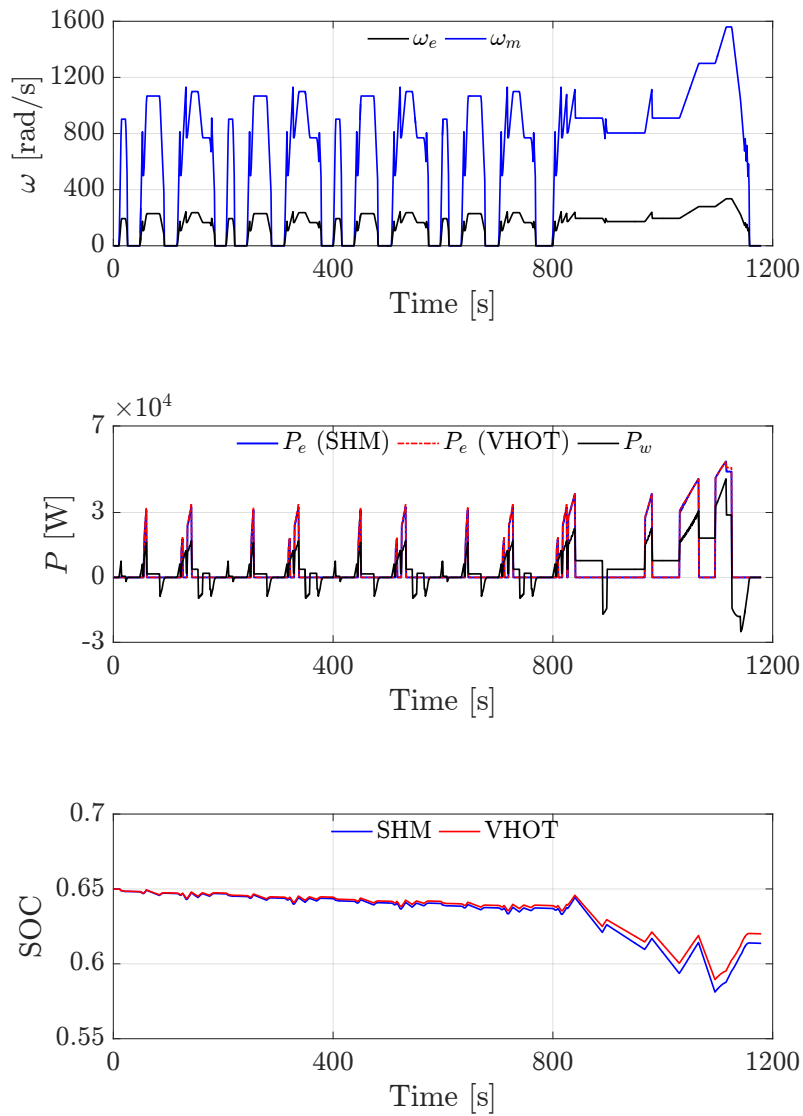


Figure 8.15 – Trajectory of relevant signals over NEDC.

uation increased over tested missions due to the data manipulation in-between two optimization levels. Moreover, the average computation time was affected by the duration of the investigated missions.

As listed in Table 8.16, the dimensioning parameters of optimized vehicles are compared with the ones of the reference vehicle. Optimal dimensioning parameters were mission-dependent. Despite the same type of transmission, the resulting gear

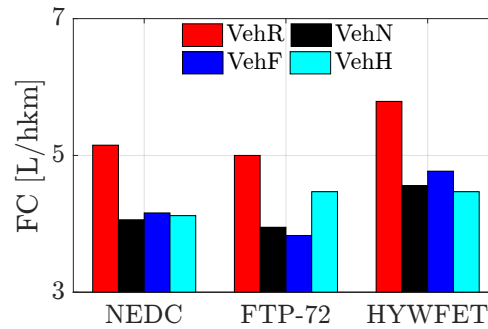


Figure 8.16 – Energy consumption of reference and optimized parallel hybrid-electric vehicles over different missions.

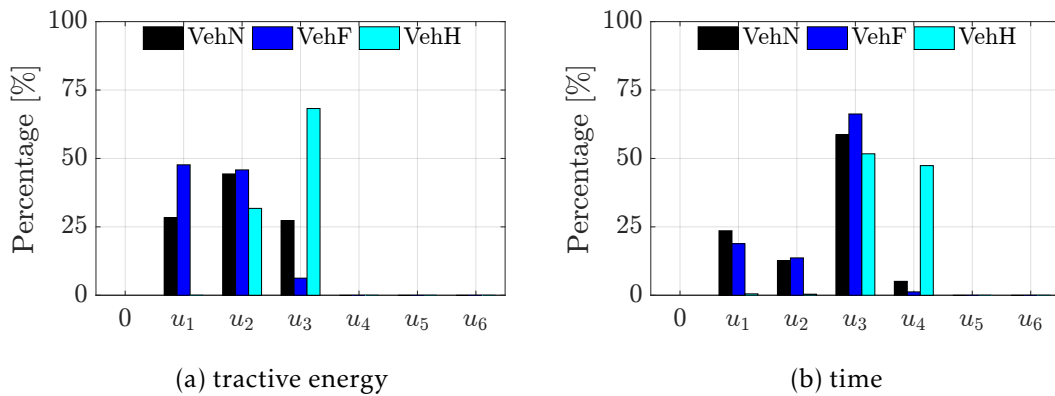


Figure 8.17 – Operating mode percentage in terms of time and demanded energy.

	Iteration	Evaluation	CPU Time [h]	Average Time [s]
VehN	26	54569	1.77	0.1165
VehF	27	58587	3.51	0.2163
VehH	29	112733	2.78	0.0889

Table 8.15 – Computational characteristics of bi-level co-optimization approach based on various missions.

ratios according to different engine displacements are summarized in Table 8.17. Note that, the optimized gear ratios did not take extra constraints into account.

As a consequence of the optimal dimensioning parameters, vehicle performance of each optimized vehicle is summarized in Table 8.18. Due to the restriction of the optimal gear ratio, the maximum vehicle speed in electric vehicle mode did not reach 50 km/h over HYWFET. The acceleration performance in both conventional and electric

	$\mathcal{I}_e$	$\mathcal{V}_e$ [L]	$\mathcal{T}_e$ [Nm]	$\mathcal{P}_e$ [kW]	$\mathcal{I}_t$	$\mathcal{P}_m$ [kW]	$\mathcal{K}_b$
VehR	SI/NA/SB	1.40	130	60	MT-5	38	36
VehN	CI/TC	1.24	184	60	MT-5	22	48
VehF	CI/TC	2.00	297	97	MT-5	22	48
VehH	CI/TC	1.00	149	49	MT-5	22	82

Table 8.16 – Dimensioning parameters of optimized parallel hybrid-electric vehicles based on various missions.

	$\mathcal{R}_{t1}$	$\mathcal{R}_{t2}$	$\mathcal{R}_{t3}$	$\mathcal{R}_{t4}$	$\mathcal{R}_{t5}$	$\mathcal{R}_m$
VehR	15.506	8.213	5.815	4.425	3.483	27.12
VehN	14.757	8.181	5.393	3.943	3.189	38.10
VehF	9.121	5.734	4.298	3.551	3.163	26.92
VehH	18.249	9.697	6.072	4.186	3.205	44.93

Table 8.17 – Gear ratios of optimized parallel hybrid-electric vehicles based on various missions.

vehicle mode is illustrated in Fig. 8.18.

	$v_{top}$ [km/h]	$t_{100}$ [s]	$\alpha$ [%]	$v_{top,ev}$ [km/h]	$t_{50}$ [s]	$\alpha_{ev}$ [%]
VehR	137	19.89	22.92	79	7.72	10.48
VehN	150	14.10	31.59	56	9.16	12.14
VehF	151	9.44	31.59	80	10.06	8.55
VehH	144	18.05	31.59	48	NA	18.15

Table 8.18 – Performance of optimized parallel hybrid-electric vehicles based on various missions.

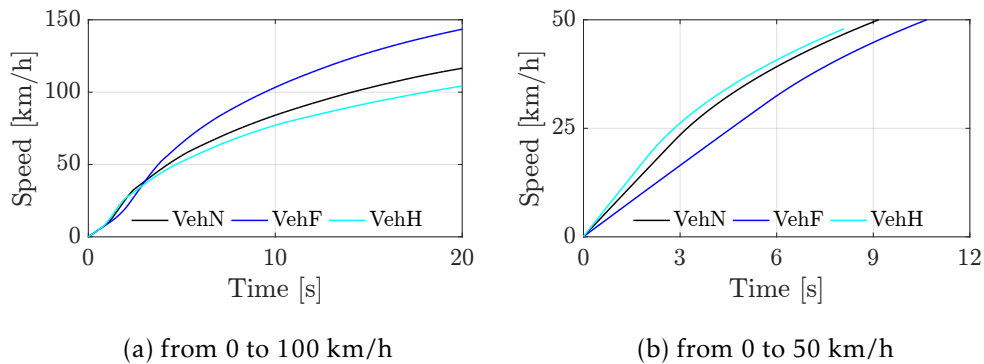


Figure 8.18 – Acceleration performance of optimized and reference parallel hybrid-electric vehicles.

### Uni-Level Co-Optimization Approach

The uni-level co-optimization is applied to optimize the dimensioning parameters of powertrain components in the reference vehicle so that the energy consumption is minimized. Due to the high nonlinearity of FACE, the full-space search method is implemented to separately optimize two dimensioning parameters, including engine displacement and capacity of battery cells.

The engine displacement is optimized within the space in Eq. 8.11. Result of the minimal fuel consumption is illustrated as a function of the engine displacement in Fig. 8.19. The minimal fuel consumption was a linear function of engine displacement, indicating downsizing of internal combustion engines was still helpful to reduce the fuel consumption. Under the same the requirement of vehicle performance, the optimum engine displacement was the smallest value and saved the most fuel.

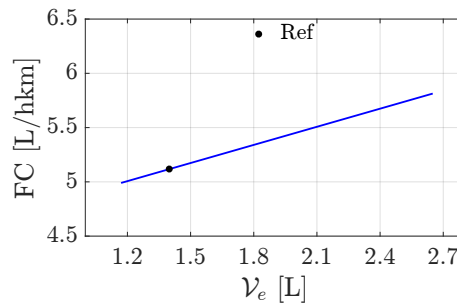


Figure 8.19 – Influence of engine displacement on fuel consumption.

The capacity of battery cells  $Q_b$  is investigated through the uni-level co-optimization approach. The design space of  $Q_b$  is from 31 to 53 Ah. As shown in Fig. 8.20, the minimum fuel consumption was achieved by the largest capacity of battery cell within its design space. The reason is simply due to the least internal resistance of the 53 Ah battery cell.

Considering the total computation time, it was about 0.4 s for the optimization of two dimensioning parameters through the uni-level co-optimization approach.

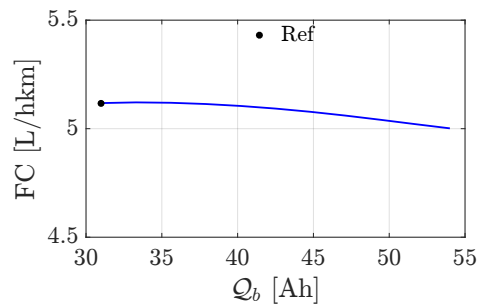


Figure 8.20 – Influence of battery cell capacity on fuel consumption.

## 8.5 Co-Optimization of a Parallel Hybrid-Electric Truck

In this case study, a prototype of hybrid-electric truck is optimized to reduce fuel consumption. Based on the analysis of experimental data, optimizations are performed on two aspects, which are powertrain control optimization and powertrain design optimization.

Concerning the control optimization, the minimal fuel consumption is achieved by optimal control laws with or without the consideration of the optimization of gear shift strategy. In regard with design optimization, fuel consumption is further minimized by optimizing dimensioning parameters of powertrain components.

### 8.5.1 Reference Vehicle

The reference truck is a parallel hybrid-electric truck in terms of P2 configuration. The main features of powertrain components are listed in Table 8.19, whereas the investigated mission is shown in Fig. 8.21.

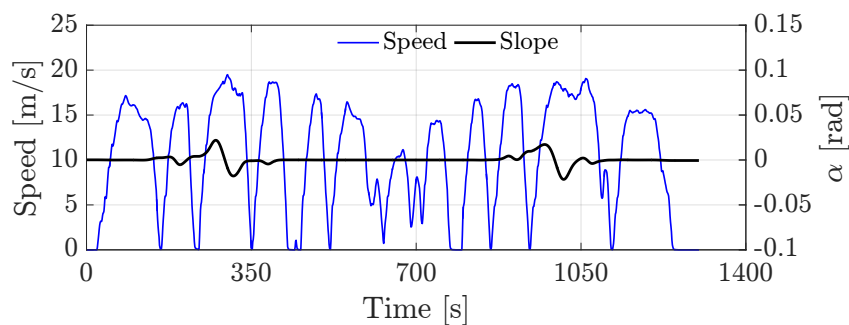


Figure 8.21 – Investigated mission for reference hybrid-electric truck.

Vehicle	$m_v$ [kg]	17000
	$R_w$ [m]	0.5
	$C_{ar}A_{ar}$ [m <sup>2</sup> ]	6
Engine	$\mathcal{I}_e$	CI/TC
	$\mathcal{V}_e$ [L]	9
	$\mathcal{T}_e$ [Nm]	1600
	$\mathcal{P}_e$ [kW]	235
Battery	$\mathcal{I}_b$	LiB
	$\mathcal{E}_b$ [kWh]	18
Electric Motor	$\mathcal{I}_m$	PMSM
	$\mathcal{T}_m$ [Nm]	1050
	$\mathcal{P}_m$ [kW]	150
Drivetrain	$\mathcal{I}_t$	AMT-12
	$\mathcal{R}_{fd}$	3.07

Table 8.19 – Main features of investigated parallel hybrid-electric truck.

A particular model of rolling resistance tailored for heavy-duty vehicles is implemented, which is by

$$C_{rr}(v) = C_{r,iso} + a(v^2 - v_0^2) + b(v - v_0), \quad (8.15)$$

where the speed  $v$  and  $v_0$  are in [km/h], coefficients  $C_{r,iso}$ ,  $a$ , and  $b$  refer to [78].

## 8.5.2 Co-Optimization Problem

As stated, optimization analysis of the reference hybrid-electric truck is performed at two distinct aspects: powertrain control optimization and powertrain design optimization.

### Control Optimization

Control optimization is performed to benchmark the minimal fuel consumption of the reference hybrid-electric truck. The control optimization contains a single optimization of control laws splitting the power between different energy sources, and a combined optimization of control laws and gear shift strategy.

Considering the powertrain control optimization, both VHOT and SHM are implemented based on the grid-point data and predictive analytic models, respectively. Therefore, the accuracy of predictive models are cross-verified. Concerning the combined control optimization, gear shift strategy is optimized only through SHM by

enlarging the full control space in the array operation.

### Design Optimization

As for the powertrain design optimization, no design constraint is applied due to the limited range of the design space compared with dimensioning parameters of real powertrain components. The investigated dimensioning parameters consist of  $\{\mathcal{V}_e, \mathcal{I}_t, \mathcal{R}_{fd}, \mathcal{K}_b\}$ , where transmission technology  $\mathcal{I}_t$  and battery cell number  $\mathcal{K}_b$  are integer variables.

The design space of engine displacement is slightly enlarged with respect to the real powertrain components, due to the high fidelity of the predictive analytic models. Thus, the design space of engine displacement is

$$\mathcal{V}_e \in [8, 18]. \quad (8.16)$$

The design space of the transmission technological parameter is

$$\mathcal{I}_t \in \{\text{AMT-12, AMT-14}\}, \quad (8.17)$$

where AMT-12 stands for automated manual transmission of 12 speeds, and AMT-14 for that of 14 speeds.

As for the ratio of final drive, the design space is

$$\mathcal{R}_{fd} \in [2.5, 4.9], \quad (8.18)$$

where boundary values are collected from public available brochures of Scania's trucks.

The design space of battery cell number is evenly deviated based on the one of reference vehicle.

The bi-level co-optimization approach is used to optimize the dimensioning parameters of powertrain components through the combination of DIRECT and SHM.

### 8.5.3 Result and Discussion

#### Comparison of VHOT and SHM

The minimal fuel consumption of the reference vehicle evaluated by VHOT is based on the original data of powertrain components; whereas SHM evaluates the minimal fuel consumption based on analytic models of powertrain components. Fig. 8.22 shows the minimized fuel consumption evaluated based on VHOT and SHM. The discrepancy of

the minimized fuel consumption was about 0.35 L/hkm (about 1.9%). Therefore, SHM was capable of minimizing fuel consumption.

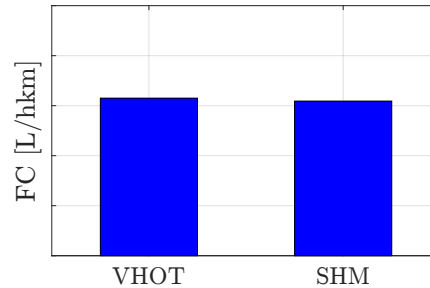


Figure 8.22 – Minimal fuel consumption of the reference hybrid-electric truck.

### Minimization of Fuel Consumption through Control Optimization

Considering different control optimizations, the minimized fuel consumption is comparatively illustrated in Fig. 8.23. The fuel consumption of the reference vehicle was denoted by REF; whereas EMO and GSO indicate the minimal fuel consumption evaluated with optimal energy management strategy, and the combined optimal energy management with the optimal gear shift, respectively. The improvements of EMO and GSO on the fuel consumption corresponded to about 33% and 41% compared with the reference vehicle. A further improvement of 7% on fuel consumption was obtained by adding optimal gear shift strategy.

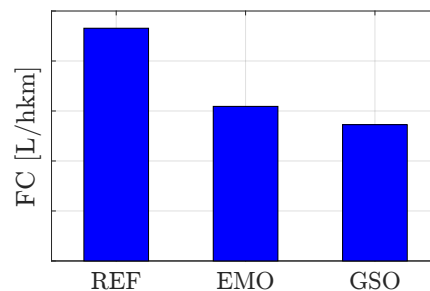


Figure 8.23 – Minimized fuel consumption of different powertrain control optimizations.

Additionally, the cumulative electrochemical power of battery is presented in Fig. 8.24. The final varied electrochemical energy was required to be the same as the reference one. Despite slight differences between the optimized final energy and the

reference one, the minimized fuel consumption had accounted for the difference of varied electrochemical energy of battery.

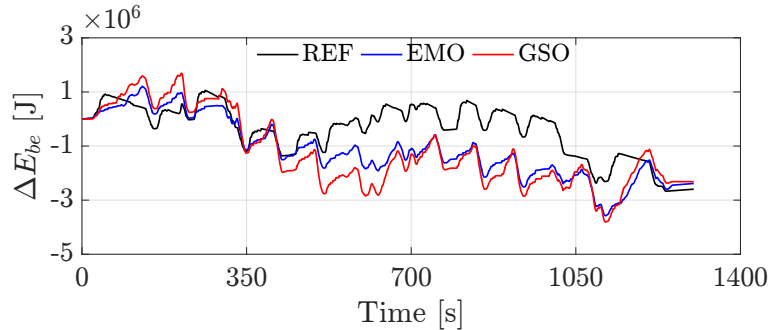


Figure 8.24 – Trajectory of varied electrochemical energy of battery over investigated mission.

The optimized gear shift schedule obtained through the gear shift optimization (GSO) is presented in Fig. 8.25. The highest gear number in the optimized gear shift schedule was less frequently used compared with that in the reference vehicle.

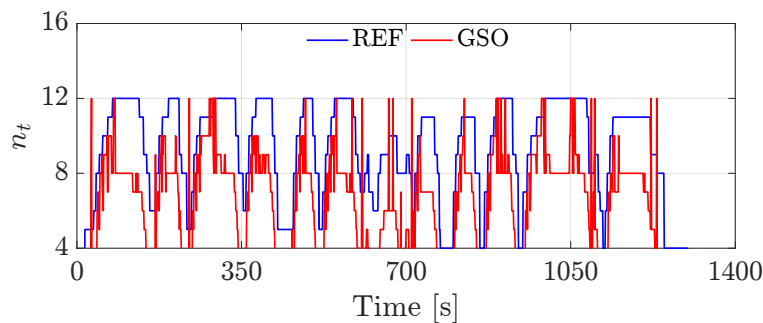


Figure 8.25 – Optimized gear shift schedule over the mission.

Fig. 8.26 shows the comparison of the operating points of the engine based on reference data, single energy management optimization, and combined optimization with optimal gear shift schedule. As optimization level increased, the operating points of the internal combustion engine were shifted to concentrate on the higher efficiency area. Compared with reference data, energy management optimization removed the operating points at boundaries. Moreover, the gear shift optimization centralized operating points at the highest efficiency zone.

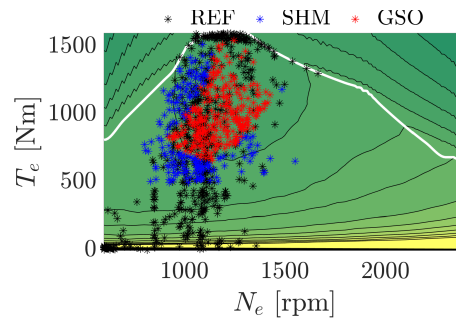


Figure 8.26 – Operating points of internal combustion engine on its fuel consumption map.

### Minimization of Fuel Consumption through Design Optimization

In the bi-level co-optimization approach, the dimensioning parameters of powertrain components are optimized to further reduce fuel consumption. However, the electric motor/generator is always maintained the same in the investigation of powertrain design optimization.

As shown in Fig. 8.27, the fuel consumption of optimized powertrain and the one of gear shift optimization are compared with the reference vehicle. Slight reduction of fuel consumption was achieved by the powertrain optimization, which was about 1.6%.

The optimal dimensioning parameters are summarized in Table 8.20. The optimal battery cell number was the upper boundary of its design space. The improvement on battery was not significant because of its high efficiency and the limited design space. As the engine downsized and the operating points shifted, the fuel consumption was further reduced through powertrain design optimization.

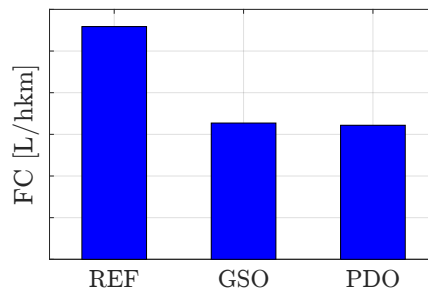


Figure 8.27 – Minimized fuel consumption of powertrain control and design optimizations.

---

	$\mathcal{V}_e$ [L]	$\mathcal{I}_t$	$\mathcal{R}_{fd}$
Reference	9.3	AMT-12	3.07
Optimized	8.0	AMT-14	4.34

Table 8.20 – Dimensioning parameters of optimized hybrid-electric truck.



# Conclusion

## Summary

In this thesis, the subject of co-optimization of control and design for advanced propulsion systems has been investigated. The background and state-of-the-art review in Chapter 1 presents the current situation of control and design optimization for advanced vehicle propulsion systems, particularly for hybrid-electric vehicles. Optimal control of hybrid-electric vehicle tends to be more complex in order to speed up optimization and contain more control variables. Bi-level optimization is a widely applied approach for the optimal design of hybrid-electric vehicles. Reducing computation time of the bi-level optimization approach becomes one important target.

Analytic models of the main powertrain components of a hybrid-electric vehicle are described at descriptive and predictive level. Descriptive analytic models describe individual powertrain components, including internal combustion engine, drivetrain, battery, and electric motor/generator; whereas predictive analytic models are capable of representing an entire class of similar components as a function of their dimensioning parameters. In addition to analytic models of powertrain components, the analytic model of vehicle load is also introduced as a function of coast-down coefficients and speed.

Chapter 3 summarizes quasi-static simulation methods of energy consumption evaluation for various types of vehicles. The typology is composed of conventional vehicle and battery-electric vehicle in the class of single-source vehicles, as well as series and parallel hybrid vehicles in the family of hybrid-electric vehicles. In the last section, single-source vehicles are evaluated through quasi-static simulations in backward approach in order to further validate the accuracy of analytic models of powertrain components.

Two novel methods of control optimization, namely SHM and GRAB-ECO, are introduced in details for series and parallel hybrid-electric vehicles in Chapter 4. SHM is

a PMP-based optimal control technique characterized by semi-analytic nature. Semi-analytic refers to analytic solutions to the minimization of Hamiltonian function; however, numeric evaluation of energy consumption works alongside the dimension of time. Thanks to the analytic solutions, the full control space in SHM is reduced to limited number of cases, thus leading to a short computation time. As for GRAB-ECO, it is developed based on the maximization of average operating efficiency of the primary energy sources that have the worst efficiency of energy conversion. With GRAB-ECO, the control space is further diminished to only two cases. Therefore, GRAB-ECO requires even less computation time than SHM. In the last section, both SHM and GRAB-ECO are benchmarked by the standard approaches of PMP.

Fully-Analytic energy Consumption Estimation (FACE) is developed for single-source vehicles, as introduced in Chapter 5. As an analytic model for energy consumption approximation, FACE is the sum of numerous terms that are in function of dimensioning-related variables and cycle-related parameters. The dimensioning-related variables are expressed as a function of dimensioning parameters of powertrain components, whereas the cycle-related parameters are constant values that are evaluated a priori of a reference vehicle. FACE for conventional and battery-electric vehicles is introduced separately, and then validated by comparing the results with those through quasi-static simulation in the last section.

Chapter 6 also presents the FACE dedicated to series and parallel hybrid-electric vehicles. As for series hybrid-electric vehicles, FACE is developed based on GRAB-ECO with further simplifications; whereas, FACE for parallel hybrid-electric vehicles results from SHM. Nevertheless, development of FACE for hybrid electric vehicles faces same difficulties, which are the development of suitable analytic models of assembled components (such as, auxiliary power unit in series hybrid-electric vehicles and electric drive unit in parallel hybrid-electric vehicles), and the treatment of optimal control for minimal energy consumption. Similarly to the one for single-source vehicles, FACE for hybrid-electric vehicles also depends on reference vehicles and missions. The capability of approximation of the minimal energy consumption is benchmarked by the quasi-static simulation method in the last section.

Based on previously established theories, co-optimization of control and design for advanced vehicle propulsion systems is formulated with generic issues in Chapter 7, and then investigated with specific case in Chapter 8. Particularly, Chapter 7 restates the design objectives, summarizes generic design constraints, and introduces the co-optimization approaches.

A few cases studies of co-optimization of control and design are investigated through

the bi-level optimization and uni-level co-optimization approaches. These cases consist of a conventional vehicle, a battery-electric vehicle, a series hybrid-electric truck, a parallel hybrid-electric vehicle in light-duty application, and a parallel hybrid-electric truck.

## **Contribution and Limitation**

### **Contribution**

In the subject of co-optimization of control and design for advanced vehicle propulsion systems, the energy consumption has been successfully minimized with the improved bi-level co-optimization and newly developed uni-level co-optimization approach. The main contributions of this thesis are summarized in three aspects as follows.

### **Dual-Level Analytic Models**

Dual-level analytic models are developed for the main powertrain components, including internal combustion engines, stepped-ratio transmissions, batteries, and electric motor/generators. The descriptive analytic models describe an individual given component, are directly applied in the evaluation of energy consumption for various types of vehicles, and benefit the development of analytic Hamiltonian function. The predictive analytic models represent an entire class of similar components as a function of the dimensioning parameters, and are applied to the optimization of vehicle propulsion system design.

The average error of the identification set of light-duty engines is about 2.62% and 5.24% at descriptive and predictive level, respectively; whereas the one of heavy-duty engines is about 1.49% and 2.88% at descriptive and predictive level, respectively.

Over NEDC, the average error of fuel consumption is 0.02% and 1.36% due to the analytic models of stepped-ratio transmissions at descriptive and predictive level, respectively. For the same reason, the average error of fuel consumption is 0.20% and 0.61% over HYWFET.

Concerning the average error of quadratic battery model, it is 1.41% and 1.48% at descriptive and predictive level, respectively. As for the piece-wise linear battery model, it is 5.14% and 6.56%. Despite higher average error and less operating range, piece-wise linear model is applied only in the application of FACE for parallel hybrid-electric vehicles so that the dimensioning parameters of battery and electric motor/generator can be optimally sized.

The average error of the identification set of electric motor/generator of PMSM is 3.79% and 4.59% at descriptive and predictive level, respectively. While, the one of AIM is 2.61% and 4.81%, respectively.

### **Fast-Running Control Optimizations**

The fast-running control optimizations are essential in reducing the computation time in the bi-level co-optimization approach. Successful fast-running optimal control methods are developed that are SHM and GRAB-ECO.

SHM is a semi-analytic optimal control technique based on PMP. Minimizing the analytic Hamiltonian function in SHM results in reduced size of full control space with respect to standard approaches of PMP, thus leading to less computation time. Compared with VHOT, the computation time can be reduced from half second to fifty milliseconds.

GRAB-ECO approximates the minimal energy consumption of hybrid-electric vehicles based on the maximization of the average operating efficiency of the primary energy source that has the worst efficiency. The control space of GRAB-ECO is further reduced to two operations: pure electric operation and hybrid operation. With good accuracy of the minimal energy consumption approximation, GRAB-ECO can further reduce the computation time to about ten milliseconds.

### **Fully-Analytic Design Optimization**

Thanks to the analytic models of powertrain components and vehicle load, FACE has been developed for single-source and hybrid-electric vehicles. FACE approximates energy consumption for various vehicle with their dimensioning parameters only. The cycle-related parameters in FACE are evaluated a priori based on reference vehicles.

Considering the optimal design of vehicle propulsion systems, FACE can be minimized by different types of nonlinear solvers or even the exhaustive search method. Regardless of the nonlinear solver, the computation time of FACE only takes a few seconds, which is much less than the bi-level optimization approach.

### **Limitation**

Considering the fast-running control optimizations for hybrid-electric vehicles, both SHM and GRAB-ECO evaluate the minimal energy consumption without considering the instantaneous constraints of state variable, which is the state of charge of battery.

As for FACE except for series hybrid-electric vehicles, it requires reference values of cycle-related parameters and the adjoint state variable. The dependency of reference vehicle would limit the application of FACE.

## **Future Work**

Despite the contributions completed, many opportunities are for extending this thesis. Several aspects are briefly introduced below.

### **State Constraint**

As the instantaneous state constraints were not considering in SHM and GRAB-ECO, their influences on the minimal energy consumption of hybrid-electric vehicle need to be assessed in terms of accuracy and computation time.

### **Power-Split Hybrid-Electric Vehicle**

In this thesis, only series and parallel hybrid-electric vehicles have been investigated due to limited time. Power-split hybrid-electric vehicles should also be included to exhaustively optimize the design of vehicle propulsion system.

### **Vehicle Design Criteria**

The design constraints of the case studies only considers fundamental design criteria, such as the top speed of vehicle, gradeability, acceleration, and all-electric range. However, there are still more design criteria that may affect the optimal dimensioning parameters. Therefore, more realistic optimal design for vehicle propulsion systems will benefit from the consideration of abundance of design criteria.

### **Dedicated Solver for FACE**

Optimal design of a vehicle propulsion system via the uni-level co-optimization is actually a nonlinear programming problem. In this case, a nonlinear solver of MATLAB has been used in the case study of a conventional vehicle. However, this nonlinear solver failed the other case studies for a battery- and hybrid-electric vehicle because of increased nonlinearity of FACE. Therefore, a dedicated solver is highly required for the FACE so that the optimal dimensioning parameters are easily found and the energy consumption is minimized.



# Bibliography

- [1] Fatih Birol. *World energy outlook 2015*. Paris: OECD/IEA, 2015.
- [2] Josh Miller, Li Du, and Drew Kodjak. *Impacts of world-class vehicle efficiency and emissions regulations in select G20 countries*. Report. ICCT: International Council on Clean Transportation, 2017.
- [3] Peter Mock. *2020–2030 CO<sub>2</sub> standards for new cars and light-commercial vehicles in the European Union*. Report. ICCT: International Council on Clean Transportation, 2016.
- [4] Wenzhong Gao and Sachin Kumar Porandla. “Design optimization of a parallel hybrid electric powertrain”. In: *Vehicle Power and Propulsion, 2005 IEEE Conference*. IEEE. 2005, 6–pp.
- [5] Federico Millo, Jianning Zhao, Luciano Rolando, Claudio Cubito, and Rocco Fuso. “Optimizing the design of a plug-in hybrid electric vehicle from the early phase: an advanced sizing methodology”. In: *Computer-Aided Design and Applications* 12.sup1 (2015), pp. 22–32.
- [6] Theo Hofman and Maarten Steinbuch. “Topology optimization of hybrid power trains”. In: *Optimization and Optimal Control in Automotive Systems*. Springer, 2014, pp. 181–198.
- [7] Viktor Larsson, Lars Johannesson, and Bo Egardt. “Analytic solutions to the dynamic programming subproblem in hybrid vehicle energy management”. In: *IEEE Transactions on Vehicular Technology* 64.4 (2015), pp. 1458–1467.
- [8] J.W.G. Turner, A. Popplewell, R. Patel, T.R. Johnson, N.J. Darnton, S. Richardson, S.W. Bredda, R.J. Tudor, C.I. Bithell, R. Jackson, S.M. Remmert, R.F. Cracknell, J.X. Fernandes, A.G.J. Lewis, S. Akehurst, C.J. Brace, C. Copeland, R. Martinez-Botas, A. Romagnoli, and A.A. Burluka. “Ultra Boost for Economy: Extending the Limits of Extreme Engine Downsizing”. In: *SAE Int. J. Engines* 7 (Apr. 2014), pp. 387–417. DOI: 10.4271/2014-01-1185. URL: <http://doi.org/10.4271/2014-01-1185>.
- [9] Xingyu Xue and John Rutledge. “Potentials of Electrical Assist and Variable Geometry Turbocharging System for Heavy-Duty Diesel Engine Downsizing”. In: *SAE Technical Paper*. SAE International, Mar. 2017. DOI: 10.4271/2017-01-1035. URL: <http://doi.org/10.4271/2017-01-1035>.

- [10] Chao Cheng and Akintomide Akinola. "Piston Friction Reduction by Reducing Piston Compression Height for Large Bore Engine Applications". In: *SAE Int. J. Engines* 10 (Mar. 2017). doi: 10.4271/2017-01-1044. URL: <http://doi.org/10.4271/2017-01-1044>.
- [11] Michael H. Shelby, Thomas G. Leone, Kevin D. Byrd, and Frank K. Wong. "Fuel Economy Potential of Variable Compression Ratio for Light Duty Vehicles". In: *SAE Int. J. Engines* 10 (Mar. 2017). doi: 10.4271/2017-01-0639. URL: <http://doi.org/10.4271/2017-01-0639>.
- [12] Young Suk Jo, Leslie Bromberg, and John Heywood. "Optimal Use of Ethanol in Dual Fuel Applications: Effects of Engine Downsizing, Spark Retard, and Compression Ratio on Fuel Economy". In: *SAE Int. J. Engines* 9 (Apr. 2016), pp. 1087–1101. doi: 10.4271/2016-01-0786. URL: <http://doi.org/10.4271/2016-01-0786>.
- [13] Roberto Finesso, Omar Mareello, Daniela Misul, Ezio Spessa, Massimo Violante, Yixin Yang, Gilles Hardy, and Christian Maier. "Development and Assessment of Pressure-Based and Model-Based Techniques for the MFB50 Control of a Euro VI 3.0L Diesel Engine". In: *SAE Int. J. Engines* 10 (Mar. 2017). doi: 10.4271/2017-01-0794. URL: <http://doi.org/10.4271/2017-01-0794>.
- [14] Kevin A. Newman and Paul Dekraker. "Modeling the Effects of Transmission Gear Count, Ratio Progression, and Final Drive Ratio on Fuel Economy and Performance Using ALPHA". In: *SAE Technical Paper*. SAE International, Apr. 2016. doi: 10.4271/2016-01-1143. URL: <http://dx.doi.org/10.4271/2016-01-1143>.
- [15] A Moawad and A Rousseau. "Impact of Transmission Technologies on Fuel Efficiency—Final Report". In: *National Highway Traffic Safety Administration (NHTSA): Washington, DC, USA, Report No. DOT HS 811* (2012), p. 667.
- [16] Kevin Newman, John Kargul, and Daniel Barba. "Development and Testing of an Automatic Transmission Shift Schedule Algorithm for Vehicle Simulation". In: *SAE Int. J. Engines* 8 (Apr. 2015), pp. 1417–1427. doi: 10.4271/2015-01-1142. URL: <http://doi.org/10.4271/2015-01-1142>.
- [17] Namdoo Kim, Aymeric Rousseau, and Henning Lohse-Busch. "Advanced Automatic Transmission Model Validation Using Dynamometer Test Data". In: *SAE Technical Paper*. SAE International, Apr. 2014. doi: 10.4271/2014-01-1778. URL: <http://dx.doi.org/10.4271/2014-01-1778>.
- [18] Andrew Moskalik, Aaron Hula, Daniel Barba, and John Kargul. "Investigating the Effect of Advanced Automatic Transmissions on Fuel Consumption Using Vehicle Testing and Modeling". In: *SAE Int. J. Engines* 9 (Apr. 2016), pp. 1916–1928. doi: 10.4271/2016-01-1142. URL: <http://doi.org/10.4271/2016-01-1142>.

- [19] SoDuk Lee, Jeff Cherry, Michael Safoutin, and Joseph McDonald. "Modeling and Validation of 12V Lead-Acid Battery for Stop-Start Technology". In: *SAE Technical Paper*. SAE International, Mar. 2017. DOI: 10.4271/2017-01-1211. URL: <http://doi.org/10.4271/2017-01-1211>.
- [20] Peter Slowik, Nikita Pavlenko, and Nic Lutsey. *Assessment of next-generation electric vehicle technologies*. Report. ICCT: International Council on Clean Transportation, 2016.
- [21] Hyeokjin Kim, Hua Chen, Dragan Maksimović, and Robert Erickson. "Boost composite converter design based on drive cycle weighted losses in electric vehicle powertrain applications". In: *Energy Conversion Congress and Exposition (ECCE), 2016 IEEE*. IEEE. 2016, pp. 1–7.
- [22] Mohammad Gerami Tehrani, Juuso Kelkka, Jussi Sopanen, Aki Mikkola, and Kimmo Kerkkänen. "Transmission configuration effect on total efficiency of Electric Vehicle powertrain". In: *Power Electronics and Applications (EPE'14-ECCE Europe), 2014 16th European Conference on*. IEEE. 2014, pp. 1–9.
- [23] Bo Zhu, Nong Zhang, Paul Walker, Xingxing Zhou, Wenzhang Zhan, Yueyuan Wei, and Nanji Ke. "Gear shift schedule design for multi-speed pure electric vehicles". In: *Proceedings of the Institution of Mechanical Engineers, Part D: Journal of Automobile Engineering* 229.1 (2015), pp. 70–82.
- [24] Wissam Dib, Alexandre Chasse, Philippe Moulin, Antonio Sciarretta, and Gilles Corde. "Optimal energy management for an electric vehicle in eco-driving applications". In: *Control Engineering Practice* 29 (2014), pp. 299–307.
- [25] Kesavan Ramakrishnan, Massimiliano Gobbi, and Gianpiero Mastinu. "Multi-objective optimization of in-wheel motor powertrain and validation using vehicle simulator". In: *Ecological Vehicles and Renewable Energies (EVER), 2015 Tenth International Conference on*. IEEE. 2015, pp. 1–9.
- [26] Yu Wang, Enli Lü, Huazhong Lu, Nong Zhang, and Xingxing Zhou. "Comprehensive design and optimization of an electric vehicle powertrain equipped with a two-speed dual-clutch transmission". In: *Advances in Mechanical Engineering* 9.1 (2017), p. 1687814016683144.
- [27] Jimmy Kapadia, Daniel Kok, Mark Jennings, Ming Kuang, Brandon Masterson, Richard Isaacs, Alan Dona, Chuck Wagner, and Thomas Gee. "Powersplit or Parallel - Selecting the Right Hybrid Architecture". In: *SAE Int. J. Alt. Power*. 6 (Mar. 2017), pp. 68–76. DOI: 10.4271/2017-01-1154. URL: <http://doi.org/10.4271/2017-01-1154>.
- [28] H Mosbech. "Optimal control of a hybrid vehicle". In: *Proceedings International Symposium on Automotive Technology & Automation (ISATA 80)*. 1980, pp. 303–320.
- [29] Richard Bellman. *The theory of dynamic programming*. Tech. rep. DTIC Document, 1954.

- [30] Stephen P. Boyd and Lieven Vandenberghe. *Convex Optimization*. Berichte über verteilte messysteme. Cambridge University Press, 2004. ISBN: 9780521833783. URL: <https://books.google.fr/books?id=mYm0bLd3fcoC>.
- [31] Viet Ngo, Theo Hofman, Maarten Steinbuch, and Alex Serrarens. “Optimal control of the gearshift command for hybrid electric vehicles”. In: *IEEE Transactions on Vehicular Technology* 61.8 (2012), pp. 3531–3543.
- [32] Tobias Nüesch, Philipp Elbert, Michael Flankl, Christopher Onder, and Lino Guzzella. “Convex optimization for the energy management of hybrid electric vehicles considering engine start and gearshift costs”. In: *Energies* 7.2 (2014), pp. 834–856.
- [33] Mitra Pourabdollah, Emilia Silvas, Nikolce Murgovski, Maarten Steinbuch, and Bo Egardt. “Optimal sizing of a series PHEV: Comparison between convex optimization and particle swarm optimization”. In: *IFAC-PapersOnLine* 48.15 (2015), pp. 16–22.
- [34] Philipp Elbert. “Noncausal and causal optimization strategies for hybrid electric vehicles”. PhD thesis. ETH Zurich, 2014.
- [35] Philipp Elbert, Tobias Nüesch, Andreas Ritter, Nikolce Murgovski, and Lino Guzzella. “Engine on/off control for the energy management of a serial hybrid electric bus via convex optimization”. In: *IEEE Transactions on Vehicular Technology* 63.8 (2014), pp. 3549–3559.
- [36] Iqbal Husain. *Electric and Hybrid Vehicles: Design Fundamentals*. Taylor & Francis, 2003. ISBN: 9780203009390. URL: <https://books.google.fr/books?id=bQFuTCGNYWgC>.
- [37] Mehrdad Ehsani, Khwaja M Rahman, and Hamid A Toliyat. “Propulsion system design of electric and hybrid vehicles”. In: *IEEE Transactions on industrial electronics* 44.1 (1997), pp. 19–27.
- [38] Clement Fauvel, Vikesh Napal, and Aymeric Rousseau. “Medium and Heavy Duty Hybrid Electric Vehicle Sizing to Maximize Fuel Consumption Displacement on Real World Drive Cycles”. In: *Power (W)* 178968.179355 (2012), pp. 0–22.
- [39] GR Mineeshma, Renji V Chacko, S Amal, ML Sreedevi, and V Vishnu. “Component Sizing of Electric Vehicle/Hybrid Electric Vehicle subsystems using Backward modelling approach”. In: *Power Electronics, Drives and Energy Systems (PEDES), 2016 IEEE International Conference on*. IEEE. 2016, pp. 1–5.
- [40] John M. Miller. *Propulsion Systems for Hybrid Vehicles*. Energy Engineering. Institution of Engineering and Technology, 2010. ISBN: 9781849191470. URL: <https://books.google.fr/books?id=soYx4iubw4cC>.
- [41] Mehrdad Ehsani, Yimin Gao, and Ali Emadi. *Modern Electric, Hybrid Electric, and Fuel Cell Vehicles: Fundamentals, Theory, and Design, Second Edition*. Power Electronics and Applications Series. CRC Press, 2009. ISBN: 9781420054002. URL: [https://books.google.fr/books?id=Rue%5C\\_FhZsV40C](https://books.google.fr/books?id=Rue%5C_FhZsV40C).

- [42] Lino Guzzella and Antonio Sciarretta. *Vehicle Propulsion Systems: Introduction to Modeling and Optimization*. SpringerLink : Bücher. Springer Berlin Heidelberg, 2012. ISBN: 9783642359132. URL: <https://books.google.fr/books?id=aVNEAAAAQBAJ>.
- [43] Dennis Assanis, G Delagrammatikas, R Fellini, Z Filipi, J Liedtke, N Michelena, P Papalambros, D Reyes, D Rosenbaum, A Sales, et al. "Optimization Approach to Hybrid Electric Propulsion System Design". In: *Journal of Structural Mechanics* 27.4 (1999), pp. 393–421.
- [44] Joseph Frédéric Bonnans, Thérèse Guilbaud, Ahmed Ketfi-Cherif, Dirk von Wissel, Claudia Sagastizábal, and Housnaa Zidani. "Parametric Optimization of Hybrid Car Engines". In: *Optimization and Engineering* 5.4 (Dec. 2004), pp. 395–415. ISSN: 1573-2924. DOI: 10.1023/B:OPTE.0000042032.47856.e5. URL: <http://dx.doi.org/10.1023/B:OPTE.0000042032.47856.e5>.
- [45] Jinming Liu. "Modeling, configuration and control optimization of power-split hybrid vehicles". PhD thesis. The University of Michigan, 2007.
- [46] Xiaowu Zhang, Huei Peng, and Jing Sun. "Not just for fuel economy: a systematic design and exhaustive search for hybrid multimode light trucks". In: *IFAC-PapersOnLine* 48.15 (2015), pp. 1–7.
- [47] Olle Sundström. "Optimal control and design of hybrid-electric vehicles". PhD thesis. ETH Zurich, 2009.
- [48] Søren Bruhn Ebbesen. "Optimal sizing and control of hybrid electric vehicles". PhD thesis. ETH Zurich, 2012.
- [49] Nicolas Marc, Eric Prada, Antonio Sciarretta, Shadab Anwer, Franck Vangraefscheppe, François Badin, Alain Charlet, and Pascal Higelin. "Sizing and fuel consumption evaluation methodology for hybrid light duty vehicles". In: *World Battery, Hybrid and Fuel Cell Electric Vehicle Symposium & Exhibition*. Vol. 4. 2010, pp. 249–258.
- [50] Delphine Sinoquet, Gregory Rousseau, and Yohan Milhau. "Design optimization and optimal control for hybrid vehicles". In: *Optimization and Engineering* 12.1 (2011), pp. 199–213.
- [51] Xi Zhang and Chris Mi. *Vehicle Power Management: Modeling, Control and Optimization*. Power Systems. Springer London, 2011. ISBN: 9780857297358. URL: <https://books.google.fr/books?id=ZOGekQEACAAJ>.
- [52] Brian Su-Ming Fan. "Multidisciplinary optimization of hybrid electric vehicles: component sizing and power management logic". PhD thesis. University of Waterloo, 2011.
- [53] Dong-ge Li, Yuan Zou, Xiao-song Hu, and Feng-chun Sun. "Optimal sizing and control strategy design for heavy hybrid electric truck". In: *Vehicle Power and Propulsion Conference (VPPC), 2012 IEEE*. IEEE. 2012, pp. 1100–1106.

- [54] Nikolce Murgovski, Lars Johannesson, Jonas Sjöberg, and Bo Egardt. “Component sizing of a plug-in hybrid electric powertrain via convex optimization”. In: *Mechatronics* 22.1 (2012), pp. 106–120.
- [55] Nikolce Murgovski, Lars Mårdh Johannesson, and Jonas Sjöberg. “Engine on/off control for dimensioning hybrid electric powertrains via convex optimization”. In: *IEEE Transactions on Vehicular Technology* 62.7 (2013), pp. 2949–2962.
- [56] Mitra Pourabdollah, Nikolce Murgovski, Anders Grauers, and Bo Egardt. “Optimal sizing of a parallel PHEV powertrain”. In: *IEEE Transactions on Vehicular Technology* 62.6 (2013), pp. 2469–2480.
- [57] Emilia Silvas. “Integrated optimal design for hybrid electric vehicles”. PhD thesis. Technische Universiteit Eindhoven, 2015.
- [58] Moncef Hammadi, Maurizio Iebba, Felipe Camargo Rosa, Ottorino Veneri, Clemente Capasso, Stanislao Patalano, and Giovanni Copertino. “System approach to the pre-design of electric propulsion systems for road vehicles”. In: *Systems Engineering (ISSE), 2015 IEEE International Symposium on*. IEEE. 2015, pp. 229–236.
- [59] Jianning Zhao and Antonio Sciarretta. “Design and Control Co-Optimization for Hybrid Powertrains: Development of Dedicated Optimal Energy Management Strategy”. In: *IFAC-PapersOnLine* 49.11 (2016), pp. 277–284.
- [60] Jianning Zhao, Antonio Sciarretta, and Lars Eriksson. “GRAB-ECO for Minimal Fuel Consumption Estimation of Parallel Hybrid Electric Vehicles”. In: *Oil & Gas Science and Technology* (2017). under rebuttal.
- [61] Daniel E Finkel. “DIRECT optimization algorithm user guide”. In: (2003).
- [62] Bo Egardt, Nikolce Murgovski, Mitra Pourabdollah, and Lars Johannesson Mardh. “Electromobility studies based on convex optimization: Design and control issues regarding vehicle electrification”. In: *IEEE Control Systems* 34.2 (2014), pp. 32–49.
- [63] Giorgio Rizzoni, Lino Guzzella, and Bernd M Baumann. “Unified modeling of hybrid electric vehicle drivetrains”. In: *IEEE/ASME transactions on mechatronics* 4.3 (1999), pp. 246–257.
- [64] Edward K. Nam and Robert Giannelli. *Fuel consumption modeling of conventional and advanced technology vehicles in the physical emission rate estimator (PERE)*. Report. US Environmental Protection Agency (EPA), 2005.
- [65] Alexandre Chasse and Antonio Sciarretta. “Supervisory control of hybrid powertrains: An experimental benchmark of offline optimization and online energy management”. In: *Control engineering practice* 19.11 (2011), pp. 1253–1265.
- [66] Fabrice Le Berr, Abdenour Abdelli, D-M Postariu, and R Benlamine. “Design and Optimization of Future Hybrid and Electric Propulsion Systems: An Advanced Tool Integrated in a Complete Workflow to Study Electric Devices”. In: *Oil & Gas Science and Technology–Revue d’IFP Energies nouvelles* 67.4 (2012), pp. 547–562.

- [67] Wisdom Enang and Chris Bannister. “Modelling and control of hybrid electric vehicles (A comprehensive review)”. In: *Renewable and Sustainable Energy Reviews* 74 (2017), pp. 1210–1239.
- [68] Byungho Lee, SoDuk Lee, Jeff Cherry, Anthony Neam, James Sanchez, and Ed Nam. “Development of Advanced Light-Duty Powertrain and Hybrid Analysis Tool”. In: *SAE Technical Paper*. SAE International, Apr. 2013. DOI: 10.4271/2013-01-0808. URL: <http://dx.doi.org/10.4271/2013-01-0808>.
- [69] Kevin Newman, John Kargul, and Daniel Barba. “Benchmarking and Modeling of a Conventional Mid-Size Car Using ALPHA”. In: *SAE Technical Paper*. SAE International, Apr. 2015. DOI: 10.4271/2015-01-1140. URL: <http://dx.doi.org/10.4271/2015-01-1140>.
- [70] *EPA standard shift schedules*. Accessed in April, 2016. URL: <http://www.epa.gov/otaq/cert/cfeis/stdshift.txt>.
- [71] Antonio Sciarretta. “Control of hybrid vehicles”. In: *Hybrid Vehicles: From Components to System*. Ed. by François Badin. Editions Technip, 2013, pp. 369–413.
- [72] Antonio Sciarretta, Jean-Charles Dabadie, and Gregory Font. “Automatic model-based generation of optimal management strategies for hybrid powertrains”. In: *SIA Powertrain: The low CO<sub>2</sub> spark ignition engine of the future and its hybridization*. SIA Powertrain - Versailles 2015. 2015.
- [73] TSanguinetti. *Step-by-step select and optimize your hybrid powertrain architecture*. Accessed in November, 2017. URL: <http://community.plm.automation.siemens.com/t5/1D-Simulation-Knowledge-Base/Step-by-step-select-and-optimize-your-hybrid-powertrain/ta-p/366583>.
- [74] Marius-Dorin Surcel, Jan Michaelsen, Richard Carme, and Mark Brown. “Performance Evaluation of Heavy-Duty Vehicles Equipped with Automatic Transmissions and Powertrain Adaptive Systems in Forestry Transportation”. In: *SAE Technical Paper*. SAE International, Oct. 2007. DOI: 10.4271/2007-01-4212. URL: <http://dx.doi.org/10.4271/2007-01-4212>.
- [75] Olivier de Weck and Karen Willcox. *ESD.77 Multidisciplinary System Design Optimization*. 2010. URL: <https://ocw.mit.edu>.
- [76] INL. *2013 Volkswagen Jetta TDI: Advanced Vehicle Testing – Baseline Testing Results*. Accessed in April, 2016. URL: <https://energy.gov/sites/prod/files/2014/02/f8/fact2013volkswagenjettatdi.pdf>.
- [77] INL. *2013 Nissan Leaf: Advanced Vehicle Testing – Baseline Testing Results*. Accessed in April, 2017. URL: <https://energy.gov/sites/prod/files/2015/01/f19/fact2013nissanleaf.pdf>.
- [78] Tony Sandberg. *Heavy truck modeling for fuel consumption simulations and measurements*. University of Linköping, 2001.



## Résumé

Des technologies avancées sont très demandées dans l'industrie automobile pour respecter les réglementations de consommation de carburant de plus en plus rigoureuses. La co-optimisation du dimensionnement et du contrôle des groupes motopropulseurs avec une efficacité de calcul améliorée est étudiée dans cette thèse.

Afin d'effectuer la co-optimisation, les composants du groupe motopropulseur du véhicule – y compris les moteurs, les boîtes de vitesses, les batteries et les moteurs électriques – sont modélisés analytiquement. Ces modèles analytiques sont développés au niveau descriptif et prédictif. Les modèles descriptifs décrivent les composants individuels du groupe motopropulseur, tandis que les modèles prédictifs sont capables de représenter une classe entière de composants similaires en fonction des paramètres de dimensionnement.

Ces modèles sont appliqués selon l'approche quasi statique backward pour évaluer la consommation d'énergie des véhicules à moteur, des véhicules électriques et des véhicules électriques hybrides sur des profils de mission donnés. En particulier, la consommation d'énergie des véhicules hybrides-électriques est minimisée avec des techniques de contrôle optimales pour tout ensemble de paramètres de dimensionnement donné.

Les lois de contrôle optimales basées sur le Principe Minimum de Pontryagin (PMP) sont utilisées comme base de référence. Une variante du PMP, la Selective Hamiltonian Minimization (SHM), est appliquée pour évaluer la consommation d'énergie minimale dans un temps de calcul raccourci par rapport au PMP standard. Grâce aux modèles analytiques développés, la fonction Hamiltonienne peut être exprimée sous une forme analytique et, par conséquent, un problème d'optimisation sans contraintes peut être résolu de manière analytique. Les contraintes imposées par les limites physiques des composants peuvent modifier l'espace de contrôle de SHM, dont la taille est cependant considérablement réduite par rapport au PMP standard.

Une méthode supplémentaire, la GRaphical-Analysis-Based energy Consumption Optimization (GRAB-ECO), est développée pour approximer la consommation d'énergie minimale des véhicules hybrides-électriques à travers de la maximisation de l'efficacité

opérationnelle moyenne de la source d'énergie primaire (la source avec la plus mauvaise efficacité de conversion d'énergie). Avec GRAB-ECO, l'espace de contrôle est encore diminué par rapport à la SHM, ce qui entraîne une réduction supplémentaire du temps de calcul.

Une méthode de calcul de la consommation d'énergie entièrement analytique (FACE) est ensuite établie sur la base des modèles analytiques des composants et, pour les véhicules hybrides-électriques, les approximations susmentionnées de la consommation d'énergie minimale. Avec FACE, la consommation d'énergie (minimale) de tous les types de systèmes de propulsion est calculée sous forme analytique en fonction des caractéristiques du cycle et des paramètres de dimensionnement.

En ce qui concerne l'optimisation de la conception des groupes motopropulseurs, l'approche à deux niveaux a été étudiée, dans lequel l'optimiseur du design est un algorithme d'optimisation mathématique, tandis que l'optimiseur du contrôle est soit la SHM soit la GRAB-ECO. Alternativement, FACE est appliqué pour optimiser directement les paramètres de dimensionnement sur la base des fonctions analytiques développées.

Plusieurs cas d'étude sont présentés en détail dans cette thèse, ce qui montre une réduction efficace du temps de calcul requis par le processus global de co-optimisation par rapport aux techniques standard.

# Appendix **B**

## Contour Maps of Chapter 2

Additional graphical results of powertrain components are illustrated in this chapter. The associated components contain the internal combustion engine for light- and heavy-duty applications. Moreover, results of electric motor/generator, including PMSMs and AIMS, are summarized as well.

### B.1 Internal Combustion Engine

Remained results of internal combustion engines are illustrated in terms of grid-point data, description, and prediction. Features of these engines are listed in Table 2.4 and 2.5 for light- and heavy-duty applications, respectively.

The remained light-duty engines are illustrated in Fig. B.1–B.13, whereas the rest heavy-duty engines are depicted in Fig. B.14–B.22.

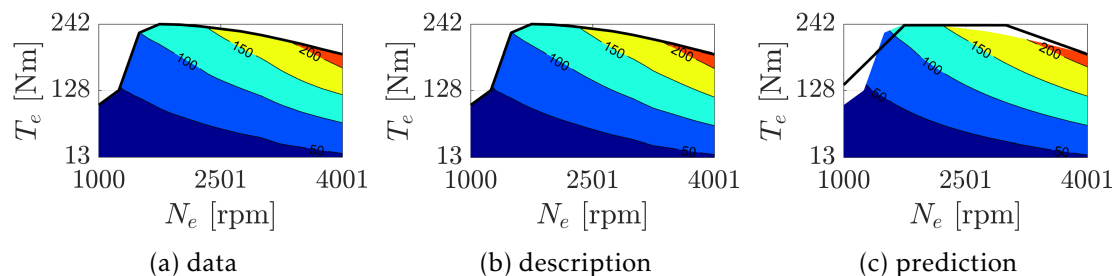


Figure B.1 – Map of burned fuel power of light-duty engine ID2.

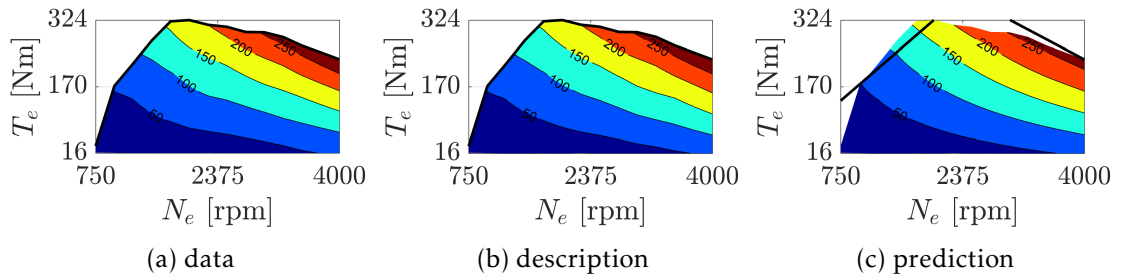


Figure B.2 – Map of burned fuel power of light-duty engine ID3.

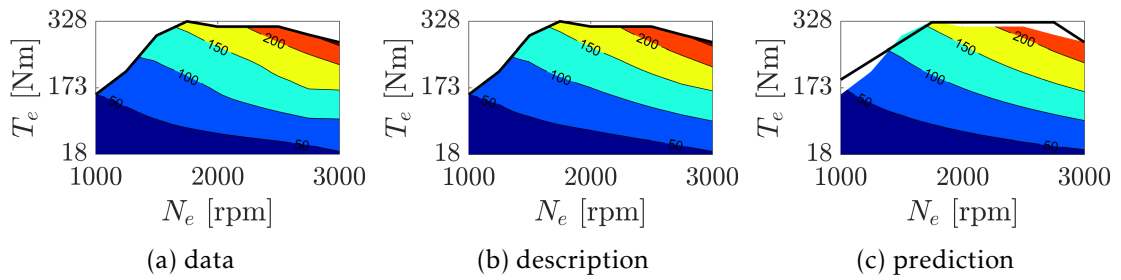


Figure B.3 – Map of burned fuel power of light-duty engine ID4.

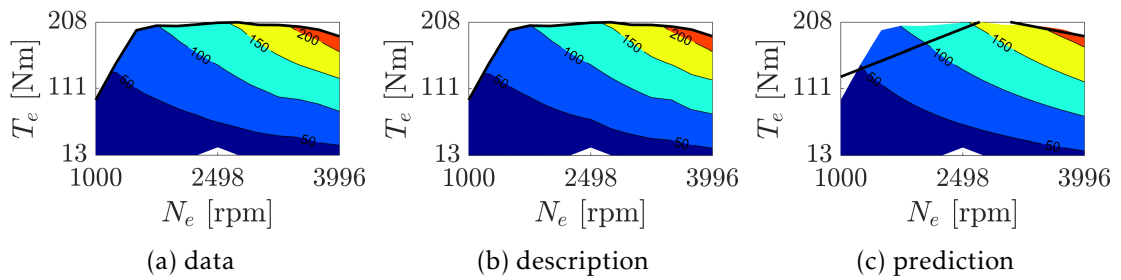


Figure B.4 – Map of burned fuel power of light-duty engine ID5.

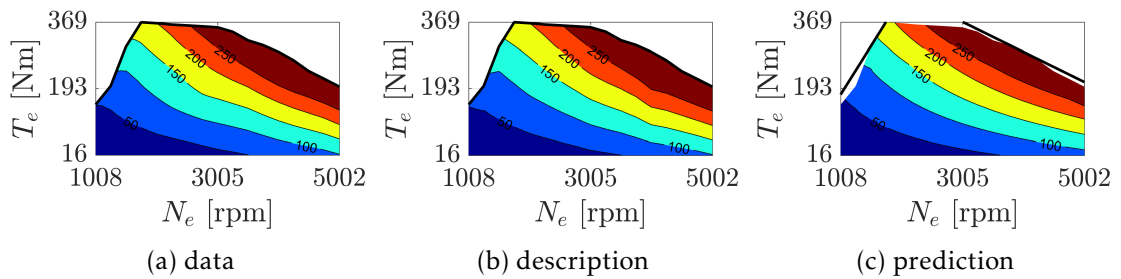


Figure B.5 – Map of burned fuel power of light-duty engine ID6.

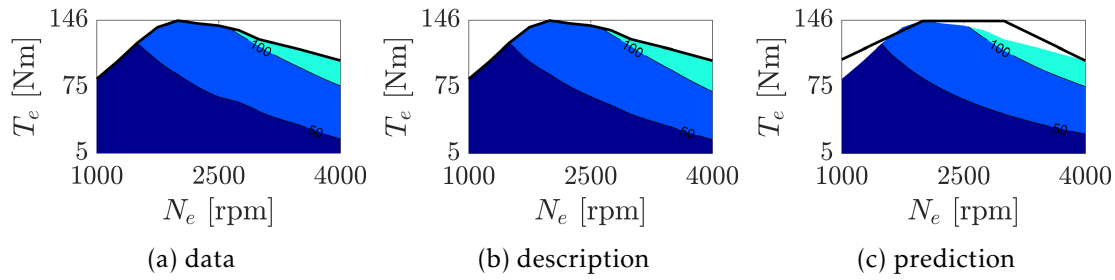


Figure B.6 – Map of burned fuel power of light-duty engine ID7.

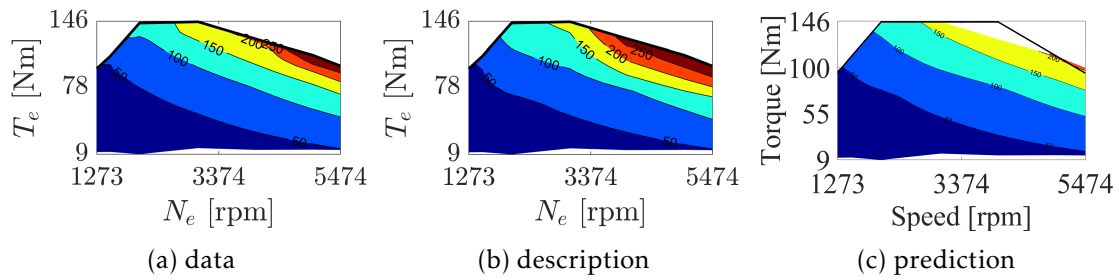


Figure B.7 – Map of burned fuel power of light-duty engine ID8.

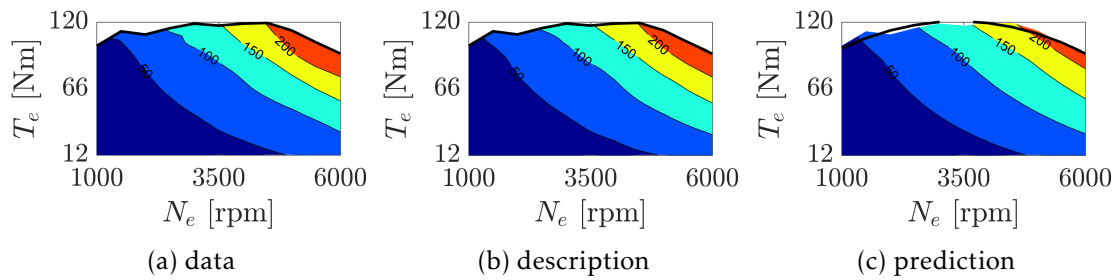


Figure B.8 – Map of burned fuel power of light-duty engine ID9.

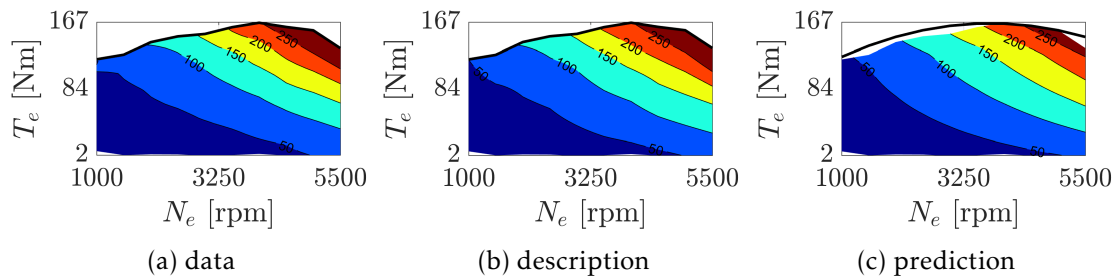


Figure B.9 – Map of burned fuel power of light-duty engine ID10.

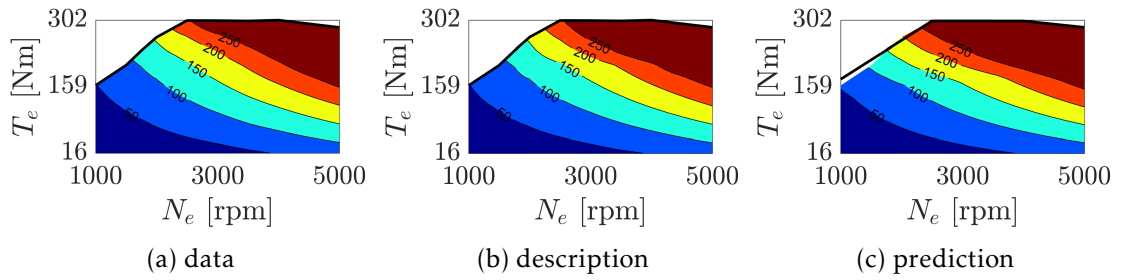


Figure B.10 – Map of burned fuel power of light-duty engine ID11.

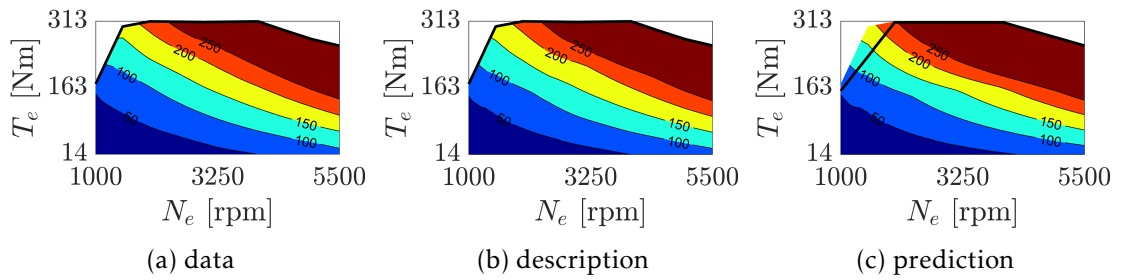


Figure B.11 – Map of burned fuel power of light-duty engine ID12.

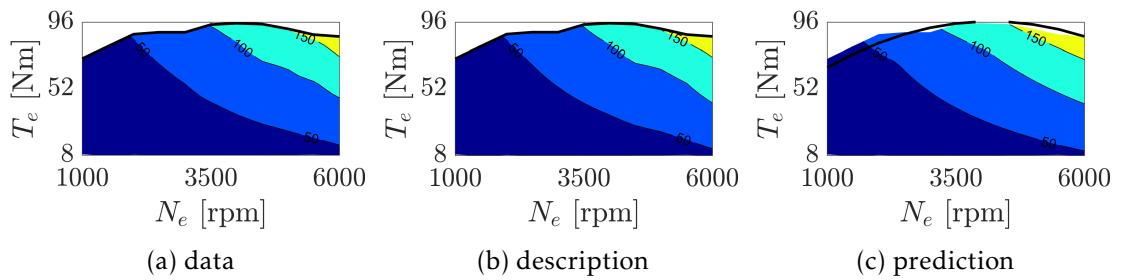


Figure B.12 – Map of burned fuel power of light-duty engine ID13.

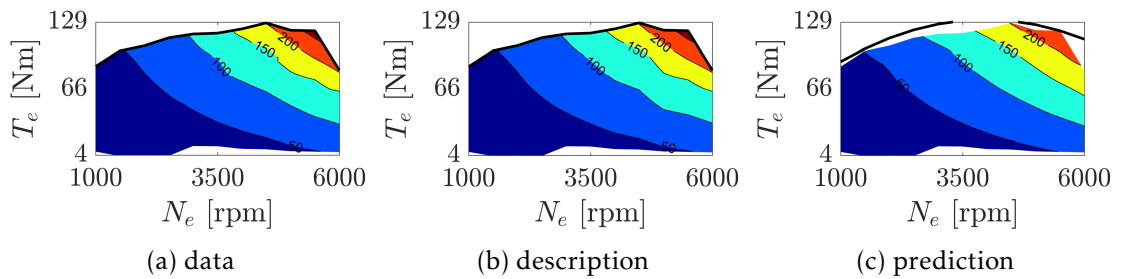


Figure B.13 – Map of burned fuel power of light-duty engine ID14.

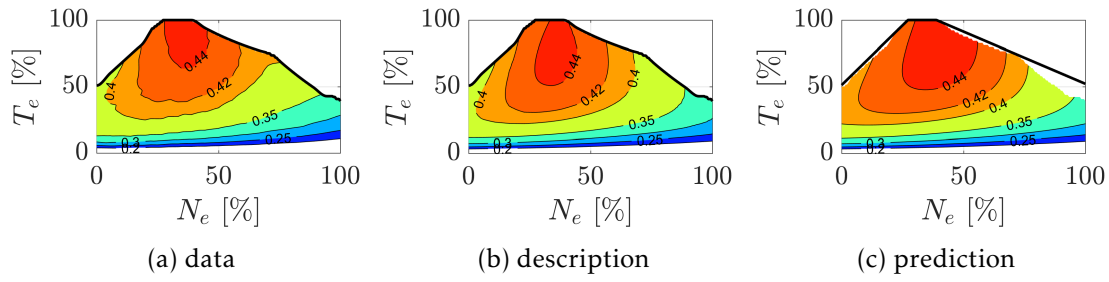


Figure B.14 – Efficiency map of heavy-duty engine ID1.

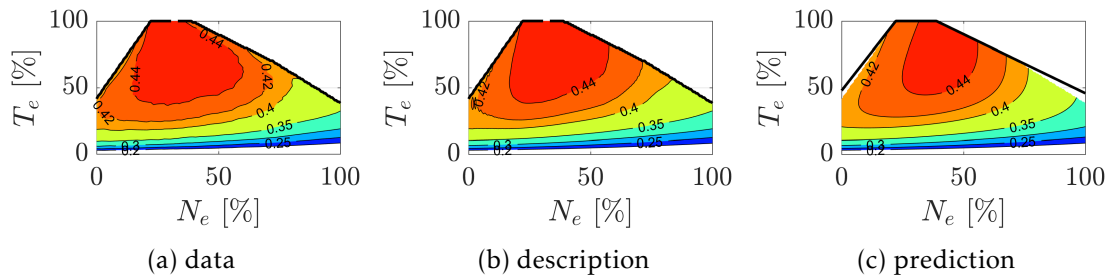


Figure B.15 – Efficiency map of heavy-duty engine ID3.

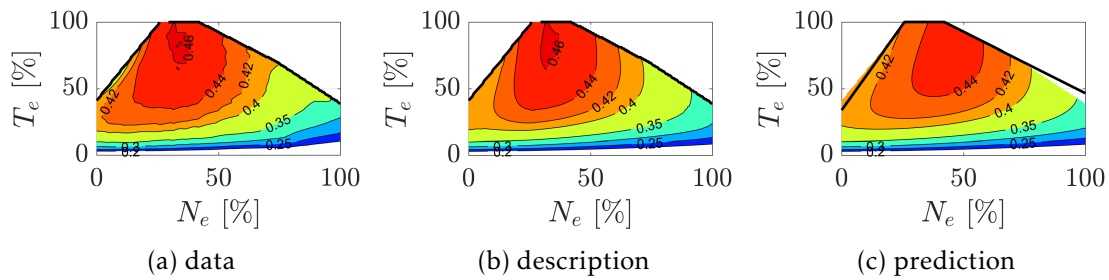


Figure B.16 – Efficiency map of heavy-duty engine ID4.

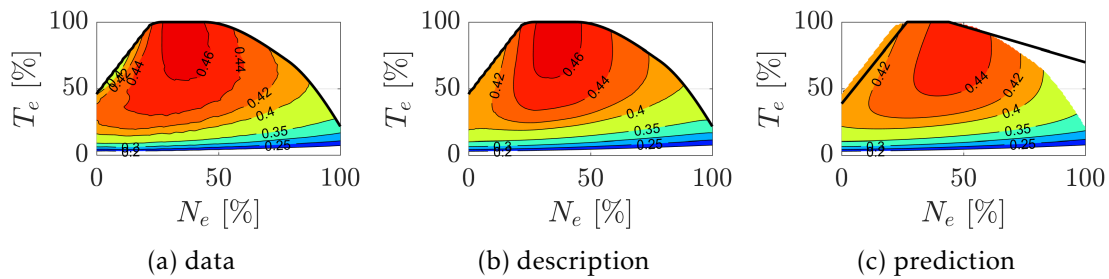


Figure B.17 – Efficiency map of heavy-duty engine ID5.

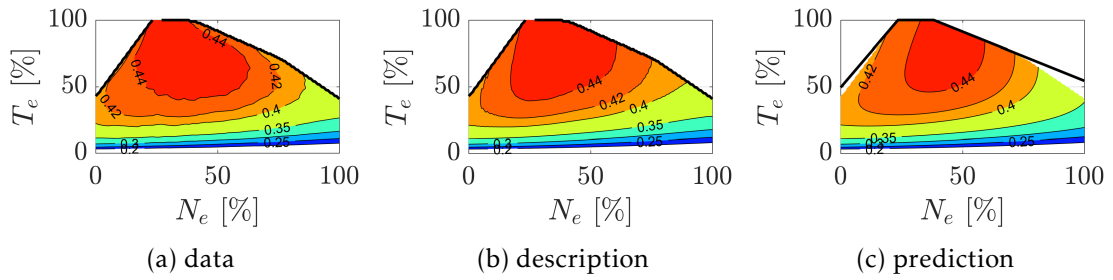


Figure B.18 – Efficiency map of heavy-duty engine ID6.

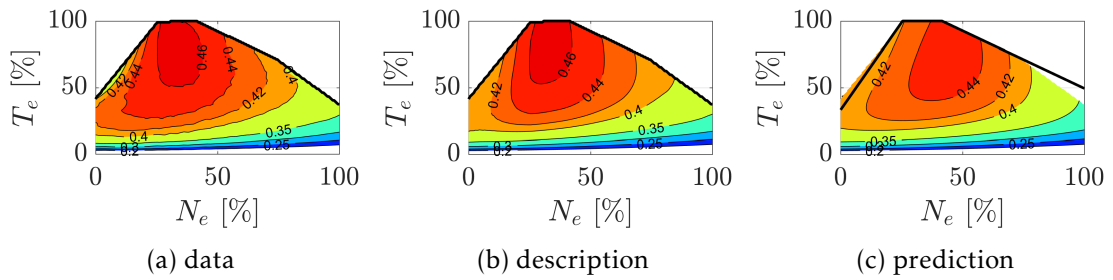


Figure B.19 – Efficiency map of heavy-duty engine ID7.

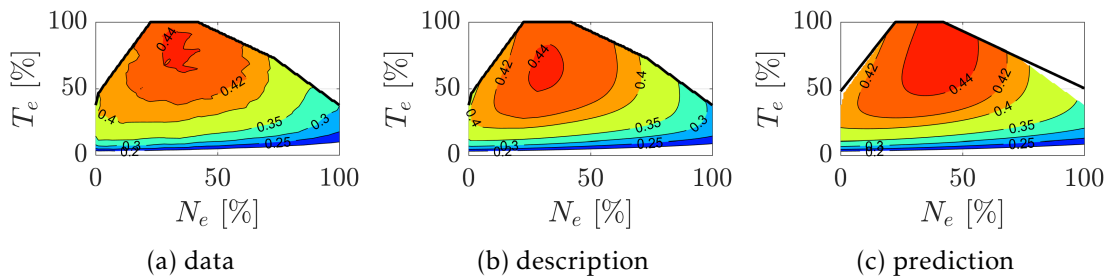


Figure B.20 – Efficiency map of heavy-duty engine ID8.

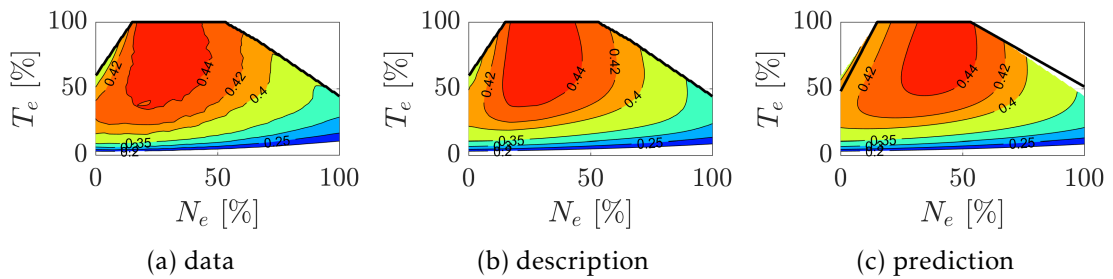


Figure B.21 – Efficiency map of heavy-duty engine ID9.

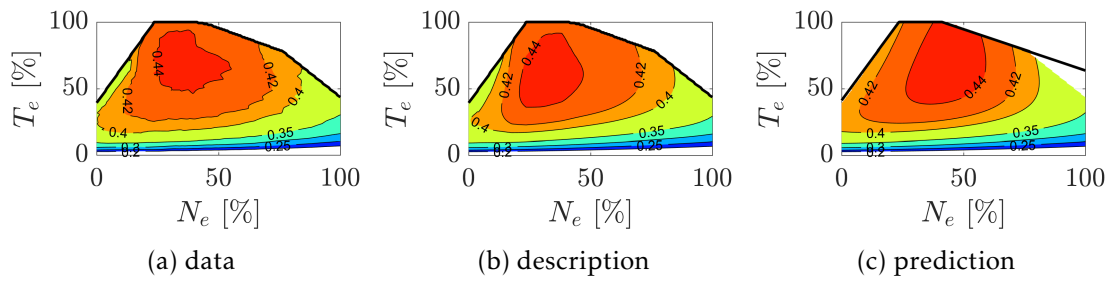


Figure B.22 – Efficiency map of heavy-duty engine ID10.

## B.2 Electric Motor/Generator

Remained results of electric motor/generator are illustrated in terms of grid-point data, description, and prediction. Features of these electric machines are listed in Table 2.14 and 2.15 for PMSM and AIM, respectively.

The remained PMSMs are illustrated in Fig. B.23–B.36, whereas the rest AIMs are depicted in Fig. B.37–B.51.

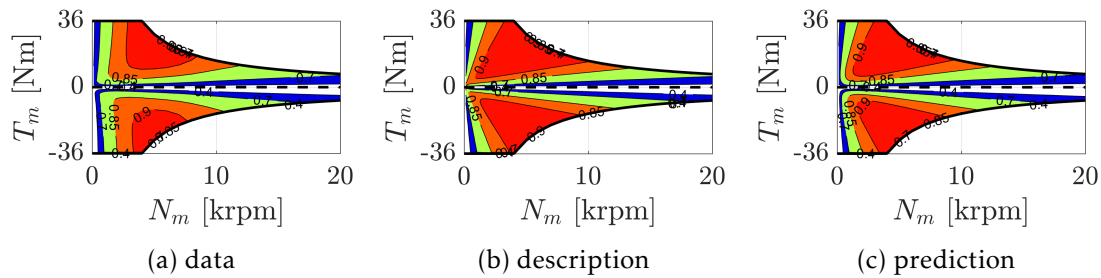


Figure B.23 – Efficiency map of PMSM ID1.

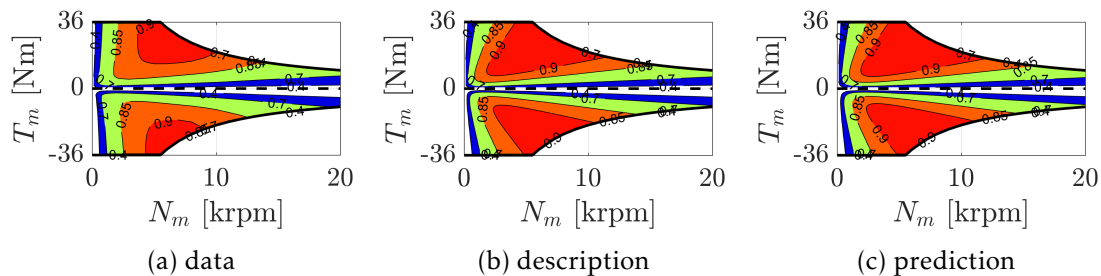


Figure B.24 – Efficiency map of PMSM ID2.

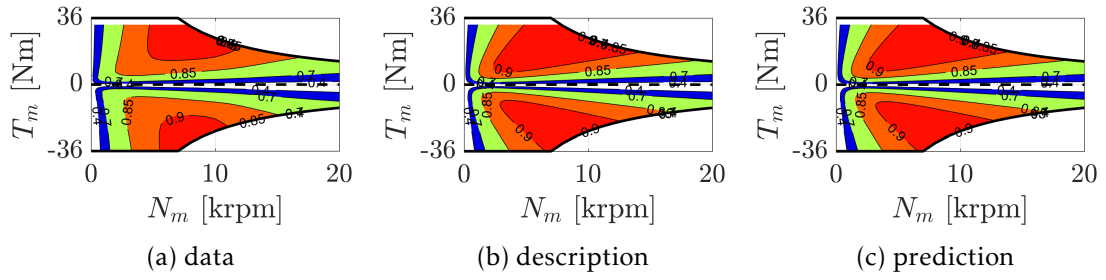


Figure B.25 – Efficiency map of PMSM ID3.

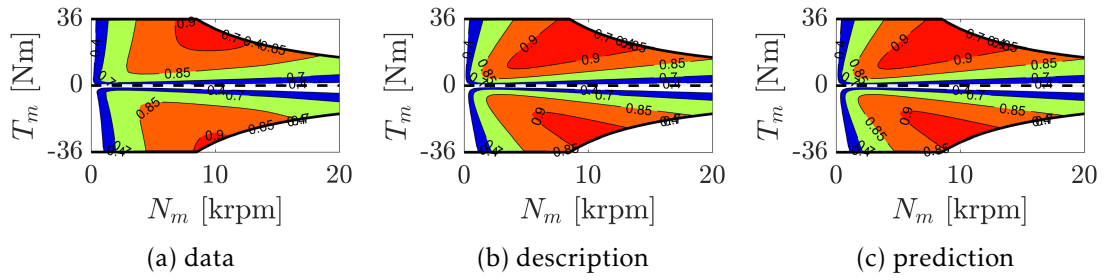


Figure B.26 – Efficiency map of PMSM ID4.

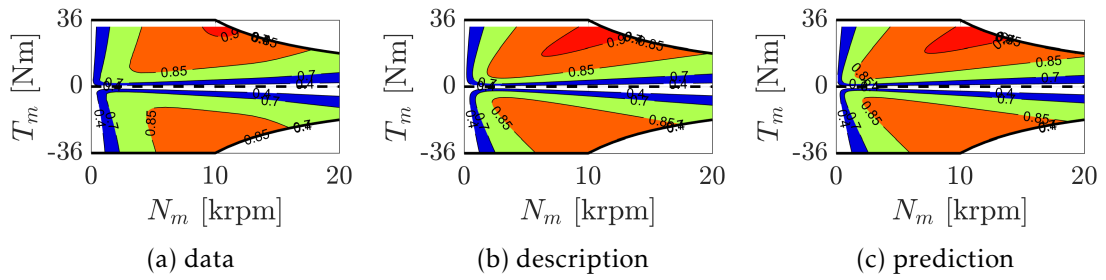


Figure B.27 – Efficiency map of PMSM ID5.

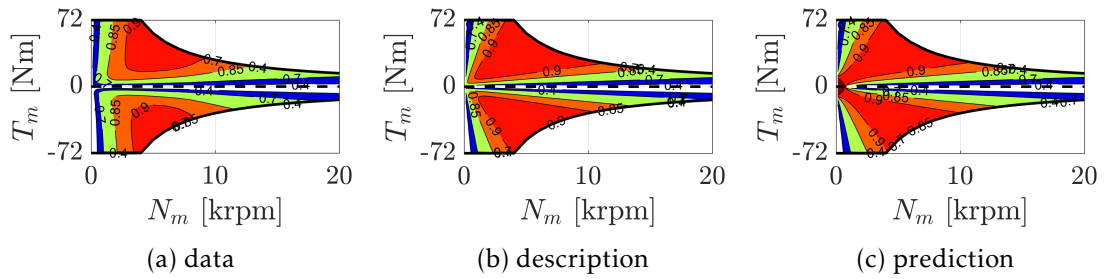


Figure B.28 – Efficiency map of PMSM ID6.

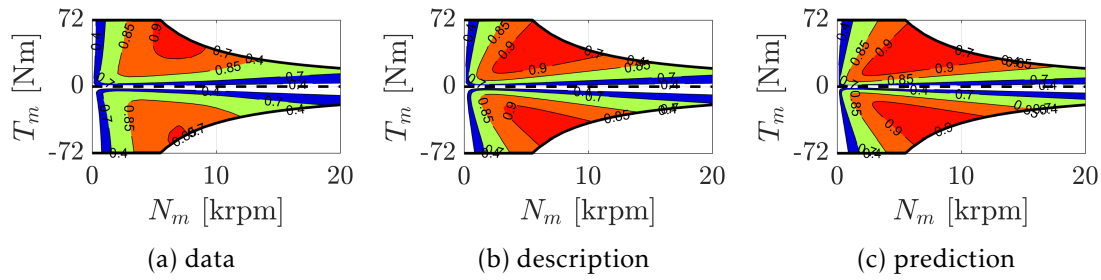


Figure B.29 – Efficiency map of PMSM ID7.

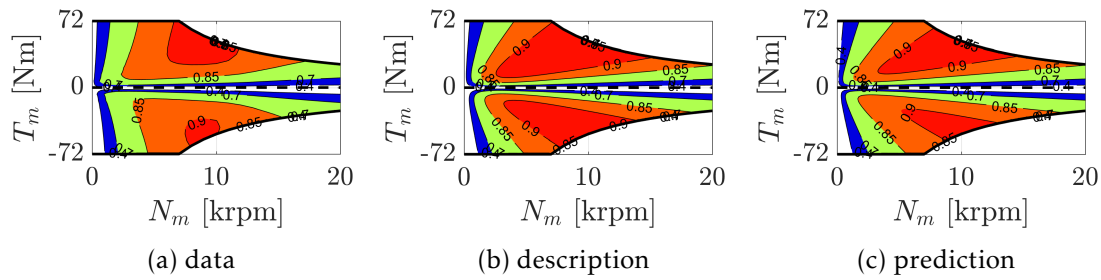


Figure B.30 – Efficiency map of PMSM ID8.

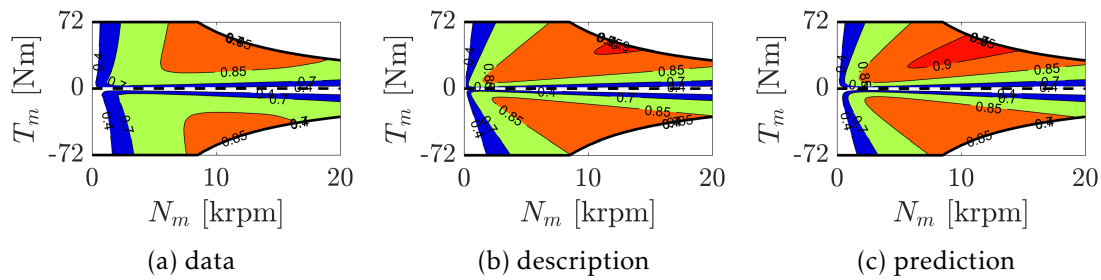


Figure B.31 – Efficiency map of PMSM ID9.

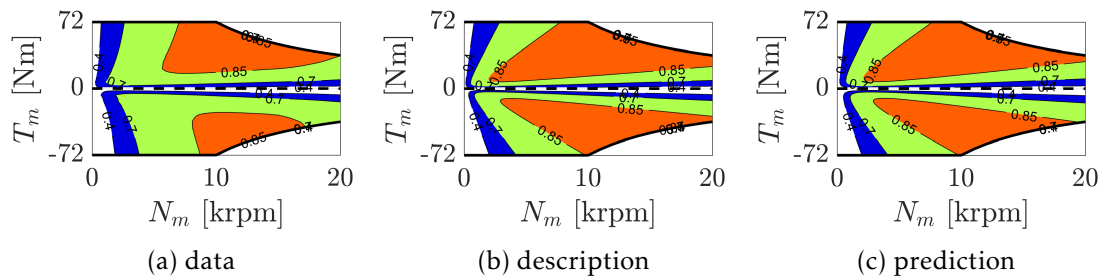


Figure B.32 – Efficiency map of PMSM ID10.

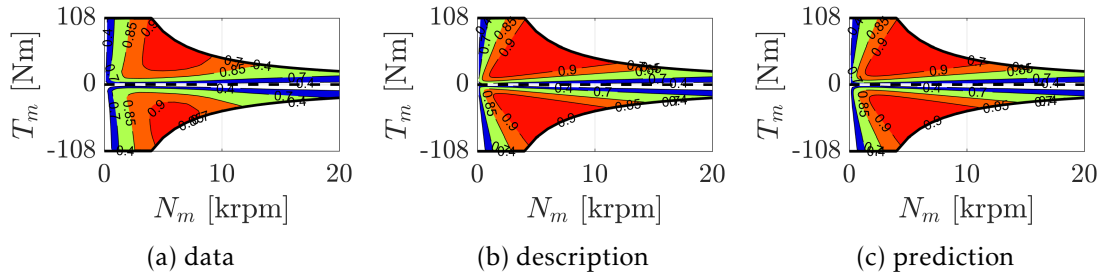


Figure B.33 – Efficiency map of PMSM ID11.

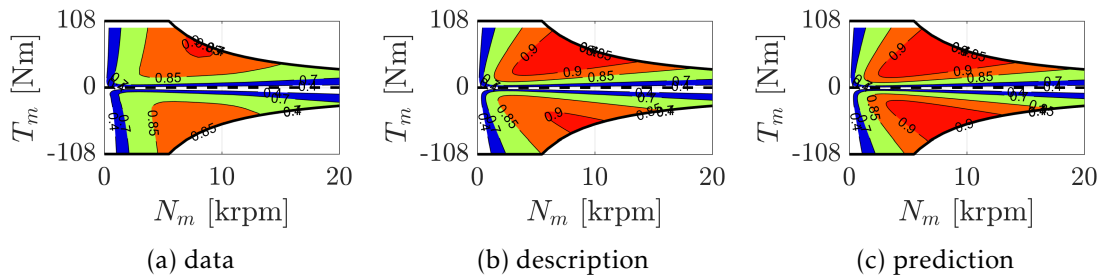


Figure B.34 – Efficiency map of PMSM ID12.

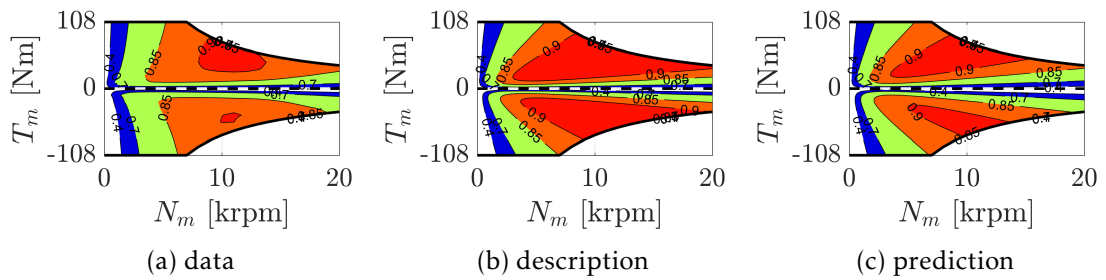


Figure B.35 – Efficiency map of PMSM ID13.

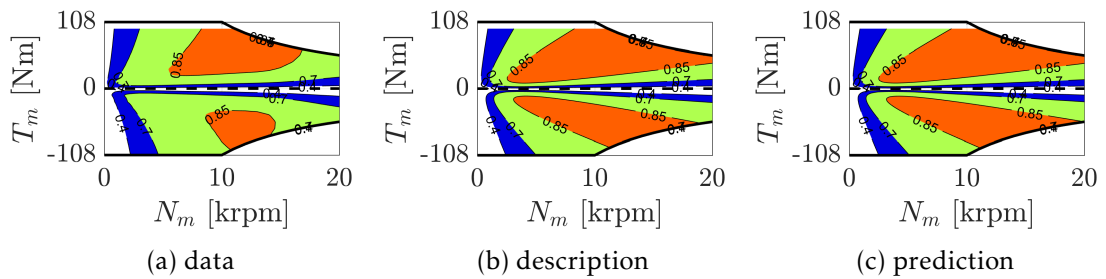


Figure B.36 – Efficiency map of PMSM ID15.

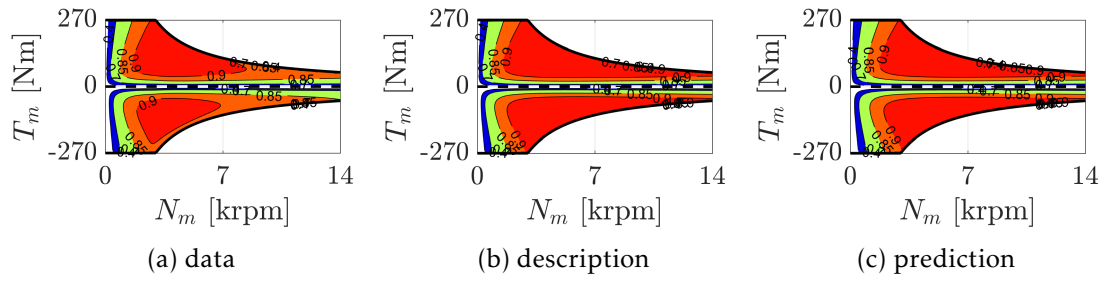


Figure B.37 – Efficiency map of AIM ID1.

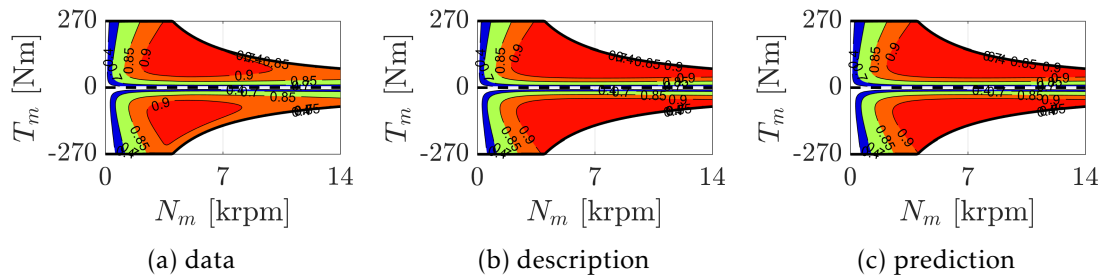


Figure B.38 – Efficiency map of AIM ID2.

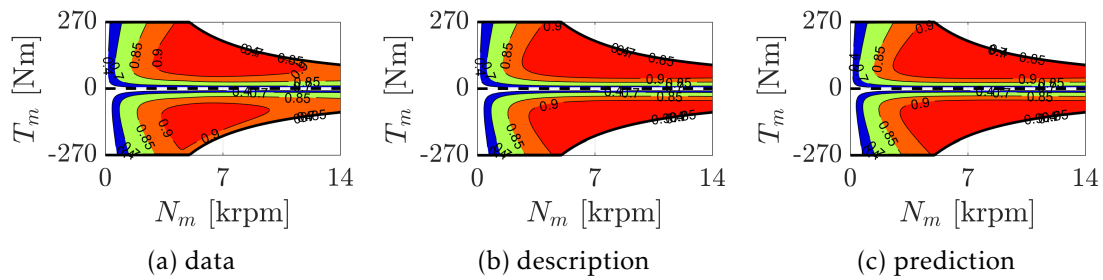


Figure B.39 – Efficiency map of AIM ID3.

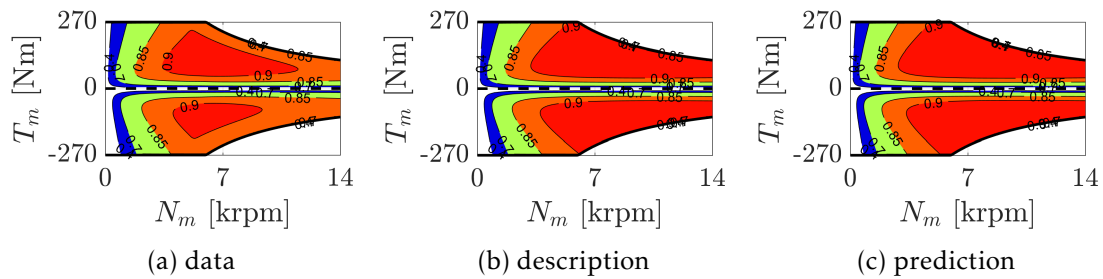


Figure B.40 – Efficiency map of AIM ID4.

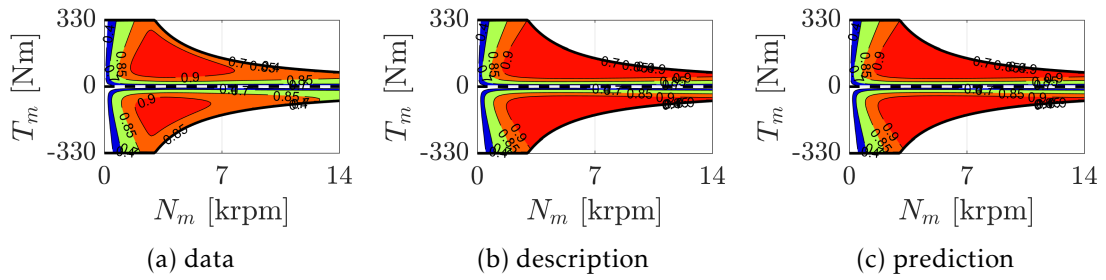


Figure B.41 – Efficiency map of AIM ID5.

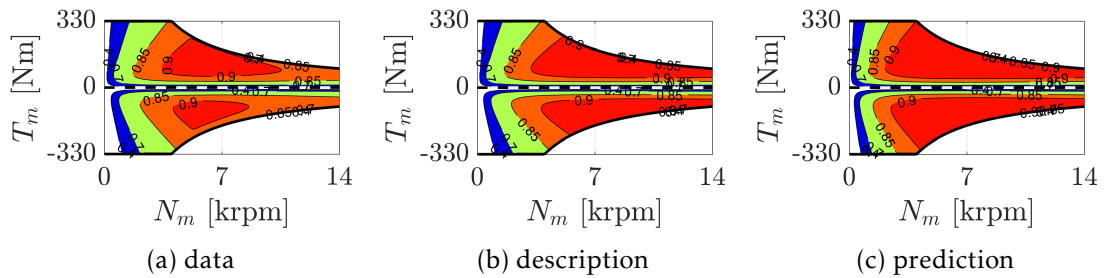


Figure B.42 – Efficiency map of AIM ID6.

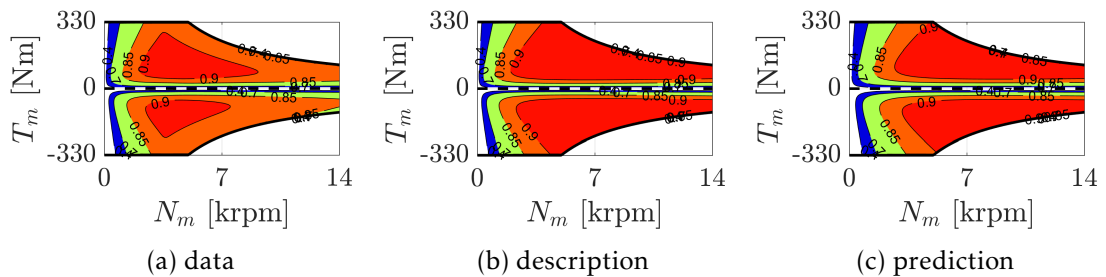


Figure B.43 – Efficiency map of AIM ID7.

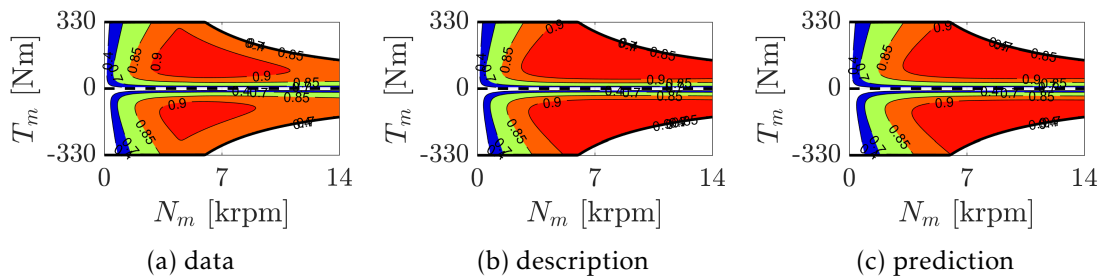


Figure B.44 – Efficiency map of AIM ID8.

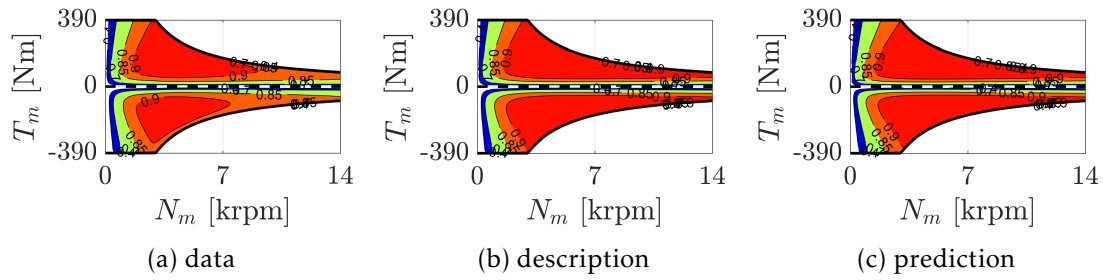


Figure B.45 – Efficiency map of AIM ID9.

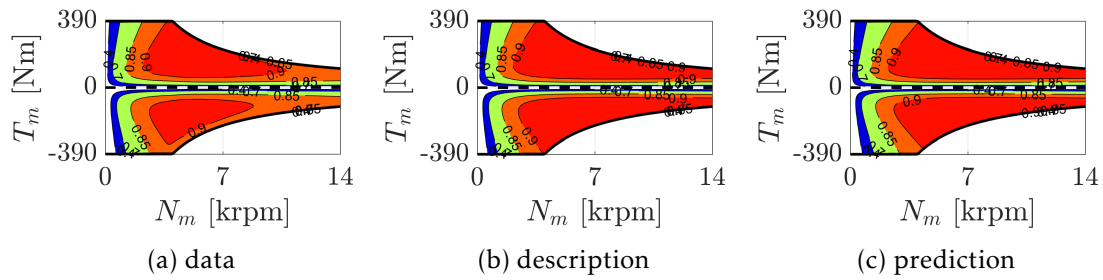


Figure B.46 – Efficiency map of AIM ID10.

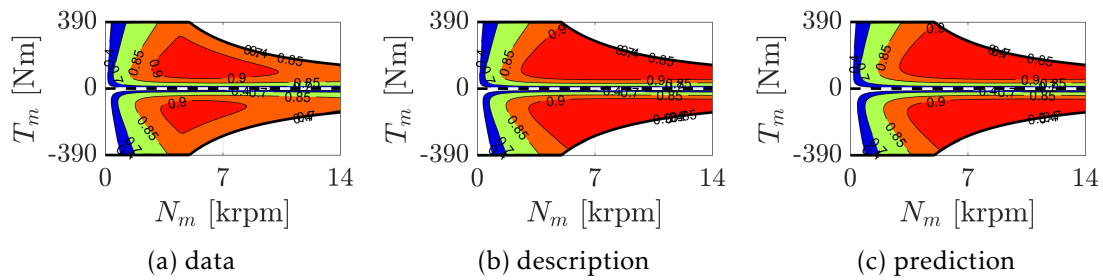


Figure B.47 – Efficiency map of AIM ID11.

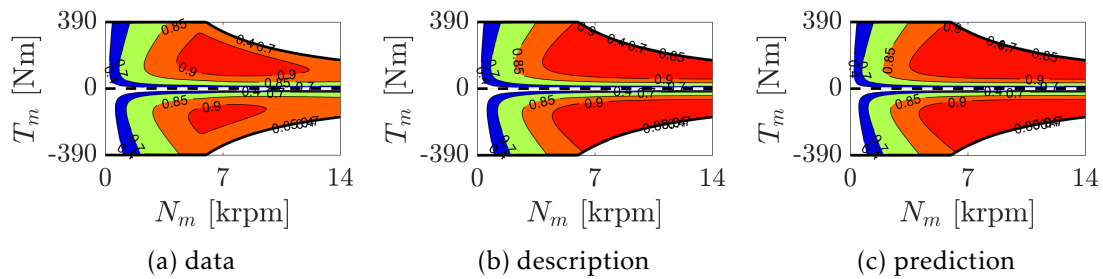


Figure B.48 – Efficiency map of AIM ID12.

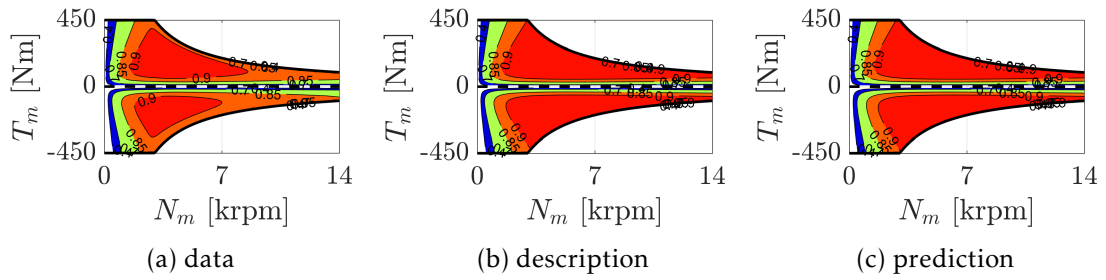


Figure B.49 – Efficiency map of AIM ID13.

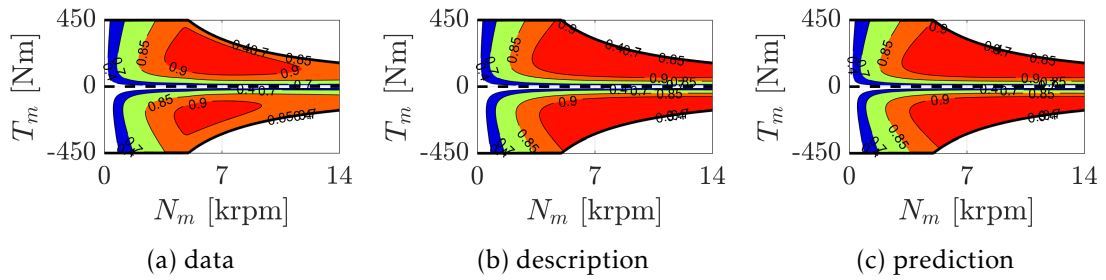


Figure B.50 – Efficiency map of AIM ID15.

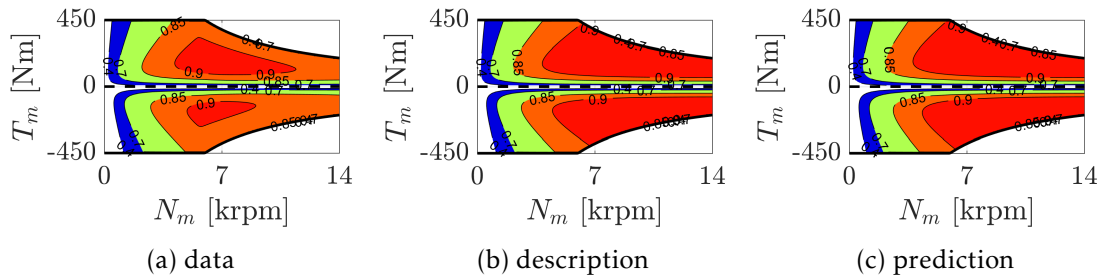


Figure B.51 – Efficiency map of AIM ID16.

## Implemented Missions

In this chapter, additional implemented missions of this thesis are briefly introduced in terms of characteristics and trajectories. The implemented missions are composed of the New European Driving Cycle (NEDC), the Federal Test Procedure (FTP-72) cycle, the Highway Fuel Economy Test (HYWFET) cycle, the Inner City Driving Cycle (ICDC), and the Suburban Driving Cycle (SUDC).

### C.1 Main Characteristics

The main characteristics of the previously mentioned missions are summarized in Table C.1, where distance of trip  $D_{trip}$ , trip duration  $t_{total}$ , idling time  $t_{idle}$ , average speed  $v_{avg}$ , and maximal speed  $v_{max}$  are included.

	NEDC	FTP-72	HYWFET	ICDC	SUDC
$D_{trip}$ [km]	10.9	12.1	16.5	90	211
$t_{total}$ [s]	1180	1370	765	11175	18000
$t_{idle}$ [s]	267	259	0	2850	3274
$v_{avg}$ [km/h]	33.35	31.5	77.7	39.03	49.5
$v_{max}$ [km/h]	120	91.25	96.4	99	92

Table C.1 – Features of various missions applied in this thesis.

### C.2 Graphical Illustration

Apart from the trajectory of NEDC is depicted in Chapter 3, history of remained missions are individually illustrated in Fig. C.1–8.8.

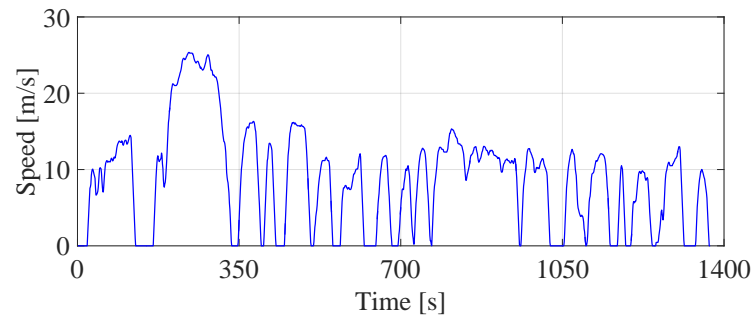


Figure C.1 – Speed trajectory of FTP-72.

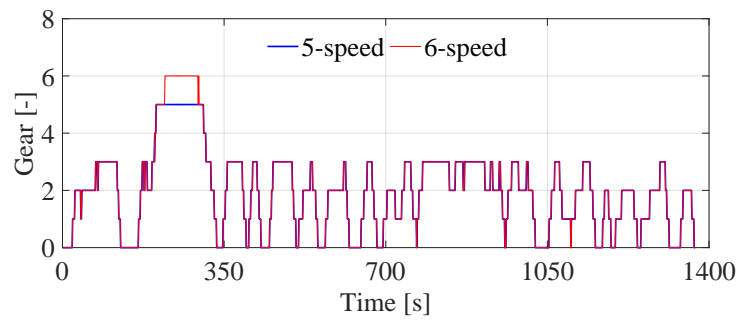


Figure C.2 – Gear shift schedule of FTP-72.

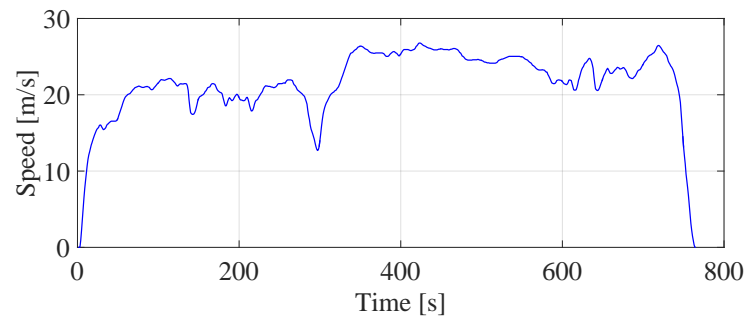


Figure C.3 – Speed trajectory of HYWFET.

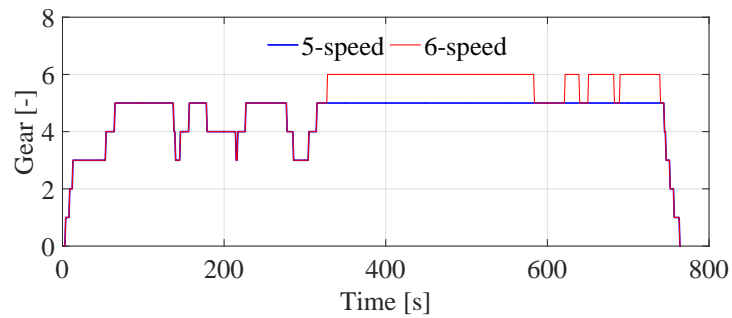


Figure C.4 – Gear shift schedule of HYWFET.

# Appendix D

## Detailed Dimension-Related Parameters of Chapter 5

Due to the huge size and large quantity of the dimension-related parameters in Eq. 5.2 and 5.14, they are composed individually in Section D.1 for conventional vehicles and in Section D.2 for battery-electric vehicles.

In the following dimension-related equations, the descriptive parameters  $k_{(\dots)}$  may exist for the sake of equation size. These descriptive parameters  $k_{(\dots)}$  can be further replaced with the predictive coefficients  $c_{(\dots)}$  through analytic models of powertrain components at predictive level that are described in Chapter 2.

### D.1 Conventional Vehicle

$$\mathcal{D}_{100} = \frac{c_{e3}C_{v0}}{k_{t6}} + \frac{c_{e1}k_{t0}\mathcal{R}_{fd}\mathcal{V}_e}{4\pi R_w}, \quad (\text{D.1})$$

$$\mathcal{D}_{101} = \frac{c_{e1}k_{t1}\mathcal{R}_{fd}\mathcal{V}_e}{4\pi R_w}, \quad (\text{D.2})$$

$$\mathcal{D}_{102} = \frac{c_{e1}k_{t2}\mathcal{R}_{fd}\mathcal{V}_e}{4\pi R_w}, \quad (\text{D.3})$$

$$\mathcal{D}_{103} = \frac{c_{e1}k_{t3}\mathcal{R}_{fd}\mathcal{V}_e}{4\pi R_w}, \quad (\text{D.4})$$

$$\mathcal{D}_{104} = \frac{c_{e1}k_{t4}\mathcal{R}_{fd}\mathcal{V}_e}{4\pi R_w}, \quad (\text{D.5})$$

$$\mathcal{D}_{110} = \frac{c_{e3}m_v}{k_{t6}}, \quad (\text{D.6})$$

$$\mathcal{D}_{200} = \frac{15c_{e2}k_{t0}^2k_{t6}\mathcal{V}_e\mathcal{R}_{fd}^2 + 60c_{e4}C_{v0}k_{t0}\pi R_w\mathcal{R}_{fd} + 2c_{e3}C_{v1}\pi^2 R_w^2}{2k_{t6}\pi^2 R_w^2}, \quad (\text{D.7})$$

$$\mathcal{D}_{201} = \frac{15k_{t1}\mathcal{R}_{fd}(2c_{e4}C_{v0}\pi R_w + c_{e2}k_{t0}k_{t6}\mathcal{R}_{fd}\mathcal{V}_e)}{k_{t6}\pi^2 R_w^2}, \quad (\text{D.8})$$

$$\mathcal{D}_{202} = \frac{15\mathcal{R}_{fd}(4c_{e4}C_{v0}k_{t2}\pi R_w + c_{e2}(k_{t1}^2 + 2k_{t0}k_{t2}))k_{t6}\mathcal{R}_{fd}\mathcal{V}_e}{2k_{t6}\pi^2 R_w^2}, \quad (\text{D.9})$$

$$\mathcal{D}_{203} = \frac{15\mathcal{R}_{fd}(2c_{e4}C_{v0}k_{t3}\pi R_w + c_{e2}(k_{t1}k_{t2} + k_{t0}k_{t3}))k_{t6}\mathcal{R}_{fd}\mathcal{V}_e}{k_{t6}\pi^2 R_w^2}, \quad (\text{D.10})$$

$$\mathcal{D}_{204} = \frac{15\mathcal{R}_{fd}(4c_{e4}C_{v0}k_{t4}\pi R_w + c_{e2}(k_{t1}^2 + 2k_{t1}k_{t3} + 2k_{t0}k_{t4}))k_{t6}\mathcal{R}_{fd}\mathcal{V}_e}{2k_{t6}\pi^2 R_w^2}, \quad (\text{D.11})$$

$$\mathcal{D}_{205} = \frac{15c_{e2}(k_{t2}k_{t3} + k_{t1}k_{t4})\mathcal{R}_{fd}^2\mathcal{V}_e}{\pi^2 R_w^2}, \quad (\text{D.12})$$

$$\mathcal{D}_{206} = \frac{15c_{e2}(k_{t3}^2 + 2k_{t2}k_{t4})\mathcal{R}_{fd}^2\mathcal{V}_e}{2\pi^2 R_w^2}, \quad (\text{D.13})$$

$$\mathcal{D}_{207} = \frac{15c_{e2}k_{t3}k_{t4}\mathcal{R}_{fd}^2\mathcal{V}_e}{\pi^2 R_w^2}, \quad (\text{D.14})$$

$$\mathcal{D}_{208} = \frac{15c_{e2}k_{t4}^2\mathcal{R}_{fd}^2\mathcal{V}_e}{2\pi^2 R_w^2}, \quad (\text{D.15})$$

$$\mathcal{D}_{210} = \frac{30c_{e4}k_{t0}m_v\mathcal{R}_{fd}}{k_{t6}\pi R_w}, \quad (\text{D.16})$$

$$\mathcal{D}_{211} = \frac{30c_{e4}k_{t1}m_v\mathcal{R}_{fd}}{k_{t6}\pi R_w}, \quad (\text{D.17})$$

$$\mathcal{D}_{212} = \frac{30c_{e4}k_{t2}m_v\mathcal{R}_{fd}}{k_{t6}\pi R_w}, \quad (\text{D.18})$$

$$\mathcal{D}_{213} = \frac{30c_{e4}k_{t3}m_v\mathcal{R}_{fd}}{k_{t6}\pi R_w}, \quad (\text{D.19})$$

$$\mathcal{D}_{214} = \frac{30c_{e4}k_{t4}m_v\mathcal{R}_{fd}}{k_{t6}\pi R_w}, \quad (\text{D.20})$$

$$\mathcal{D}_{300} = \frac{900c_{e5}C_{v0}k_{t0}^2\mathcal{R}_{fd}^2 + \pi R_w(30c_{e4}C_{v1}k_{t0}\mathcal{R}_{fd} + c_{e3}C_{v2}\pi R_w)}{k_{t6}\pi^2 R_w^2}, \quad (\text{D.21})$$

$$\mathcal{D}_{301} = \frac{30k_{t1}\mathcal{R}_{fd}(60c_{e5}C_{v0}k_{t0}\mathcal{R}_{fd} + c_{e4}C_{v1}\pi R_w)}{k_{t6}\pi^2 R_w^2}, \quad (\text{D.22})$$

$$\mathcal{D}_{302} = \frac{30\mathcal{R}_{fd}(30c_{e5}C_{v0}(k_{t1}^2 + 2k_{t0}k_{t2})\mathcal{R}_{fd} + c_{e4}C_{v1}k_{t2}\pi R_w)}{k_{t6}\pi^2 R_w^2}, \quad (\text{D.23})$$

$$\mathcal{D}_{303} = \frac{30\mathcal{R}_{fd}(60c_{e5}C_{v0}(k_{t1}k_{t2} + k_{t0}k_{t3})\mathcal{R}_{fd} + c_{e4}C_{v1}k_{t3}\pi R_w)}{k_{t6}\pi^2 R_w^2}, \quad (\text{D.24})$$

$$\mathcal{D}_{304} = \frac{30\mathcal{R}_{fd} \left( 30c_{e5}C_{v0} \left( k_{t2}^2 + 2k_{t1}k_{t3} + 2k_{t0}k_{t4} \right) \mathcal{R}_{fd} + c_{e4}C_{v1}k_{t4}\pi R_w \right)}{k_{t6}\pi^2 R_w^2}, \quad (\text{D.25})$$

$$\mathcal{D}_{305} = \frac{1800c_{e5}C_{v0}(k_{t2}k_{t3} + k_{t1}k_{t4})\mathcal{R}_{fd}^2}{k_{t6}\pi^2 R_w^2}, \quad (\text{D.26})$$

$$\mathcal{D}_{306} = \frac{900c_{e5}C_{v0} \left( k_{t3}^2 + 2k_{t2}k_{t4} \right) \mathcal{R}_{fd}^2}{k_{t6}\pi^2 R_w^2}, \quad (\text{D.27})$$

$$\mathcal{D}_{307} = \frac{1800c_{e5}C_{v0}k_{t3}k_{t4}\mathcal{R}_{fd}^2}{k_{t6}\pi^2 R_w^2}, \quad (\text{D.28})$$

$$\mathcal{D}_{308} = \frac{900c_{e5}C_{v0}k_{t4}^2\mathcal{R}_{fd}^2}{k_{t6}\pi^2 R_w^2}, \quad (\text{D.29})$$

$$\mathcal{D}_{310} = \frac{900c_{e5}k_{t0}^2 m_v \mathcal{R}_{fd}^2}{k_{t6}\pi^2 R_w^2}, \quad (\text{D.30})$$

$$\mathcal{D}_{311} = \frac{1800c_{e5}k_{t0}k_{t1} m_v \mathcal{R}_{fd}^2}{k_{t6}\pi^2 R_w^2}, \quad (\text{D.31})$$

$$\mathcal{D}_{312} = \frac{900c_{e5} \left( k_{t1}^2 + 2k_{t0}k_{t2} \right) m_v \mathcal{R}_{fd}^2}{k_{t6}\pi^2 R_w^2}, \quad (\text{D.32})$$

$$\mathcal{D}_{313} = \frac{1800c_{e5}(k_{t1}k_{t2} + k_{t0}k_{t3})m_v \mathcal{R}_{fd}^2}{k_{t6}\pi^2 R_w^2}, \quad (\text{D.33})$$

$$\mathcal{D}_{314} = \frac{900c_{e5} \left( k_{t2}^2 + 2k_{t1}k_{t3} + 2k_{t0}k_{t4} \right) m_v \mathcal{R}_{fd}^2}{k_{t6}\pi^2 R_w^2}, \quad (\text{D.34})$$

$$\mathcal{D}_{315} = \frac{1800c_{e5}(k_{t2}k_{t3} + k_{t1}k_{t4})m_v \mathcal{R}_{fd}^2}{k_{t6}\pi^2 R_w^2}, \quad (\text{D.35})$$

$$\mathcal{D}_{316} = \frac{900c_{e5} \left( k_{t3}^2 + 2k_{t2}k_{t4} \right) m_v \mathcal{R}_{fd}^2}{k_{t6}\pi^2 R_w^2}, \quad (\text{D.36})$$

$$\mathcal{D}_{317} = \frac{1800c_{e5}k_{t3}k_{t4}m_v \mathcal{R}_{fd}^2}{k_{t6}\pi^2 R_w^2}, \quad (\text{D.37})$$

$$\mathcal{D}_{318} = \frac{900c_{e5}k_{t4}^2 m_v \mathcal{R}_{fd}^2}{k_{t6}\pi^2 R_w^2}, \quad (\text{D.38})$$

$$\mathcal{D}_{400} = \frac{30k_{t0}\mathcal{R}_{fd}(30c_{e5}C_{v1}k_{t0}\mathcal{R}_{fd} + c_{e4}C_{v2}\pi R_w)}{k_{t6}\pi^2 R_w^2}, \quad (\text{D.39})$$

$$\mathcal{D}_{401} = \frac{30k_{t1}\mathcal{R}_{fd}(60c_{e5}C_{v1}k_{t0}\mathcal{R}_{fd} + c_{e4}C_{v2}\pi R_w)}{k_{t6}\pi^2 R_w^2}, \quad (\text{D.40})$$

$$\mathcal{D}_{402} = \frac{30\mathcal{R}_{fd} \left( 30c_{e5}C_{v1} \left( k_{t1}^2 + 2k_{t0}k_{t2} \right) \mathcal{R}_{fd} + c_{e4}C_{v2}k_{t2}\pi R_w \right)}{k_{t6}\pi^2 R_w^2}, \quad (\text{D.41})$$

$$\mathcal{D}_{403} = \frac{30\mathcal{R}_{fd} \left( 60c_{e5}C_{v1} \left( k_{t1}k_{t2} + k_{t0}k_{t3} \right) \mathcal{R}_{fd} + c_{e4}C_{v2}k_{t3}\pi R_w \right)}{k_{t6}\pi^2 R_w^2}, \quad (\text{D.42})$$

$$\mathcal{D}_{404} = \frac{30\mathcal{R}_{fd} \left( 30c_{e5}C_{v1} \left( k_{t2}^2 + 2k_{t1}k_{t3} + 2k_{t0}k_{t4} \right) \mathcal{R}_{fd} + c_{e4}C_{v2}k_{t4}\pi R_w \right)}{k_{t6}\pi^2 R_w^2}, \quad (\text{D.43})$$

$$\mathcal{D}_{405} = \frac{1800c_{e5}C_{v1} \left( k_{t2}k_{t3} + k_{t1}k_{t4} \right) \mathcal{R}_{fd}^2}{k_{t6}\pi^2 R_w^2}, \quad (\text{D.44})$$

$$\mathcal{D}_{406} = \frac{900c_{e5}C_{v1} \left( k_{t3}^2 + 2k_{t2}k_{t4} \right) \mathcal{R}_{fd}^2}{k_{t6}\pi^2 R_w^2}, \quad (\text{D.45})$$

$$\mathcal{D}_{407} = \frac{1800c_{e5}C_{v1}k_{t3}k_{t4}\mathcal{R}_{fd}^2}{k_{t6}\pi^2 R_w^2}, \quad (\text{D.46})$$

$$\mathcal{D}_{408} = \frac{900c_{e5}C_{v1}k_{t4}^2\mathcal{R}_{fd}^2}{k_{t6}\pi^2 R_w^2}, \quad (\text{D.47})$$

$$\mathcal{D}_{500} = \frac{900c_{e5}C_{v2}k_{t0}^2\mathcal{R}_{fd}^2}{k_{t6}\pi^2 R_w^2}, \quad (\text{D.48})$$

$$\mathcal{D}_{501} = \frac{1800c_{e5}C_{v2}k_{t0}k_{t1}\mathcal{R}_{fd}^2}{k_{t6}\pi^2 R_w^2}, \quad (\text{D.49})$$

$$\mathcal{D}_{502} = \frac{900c_{e5}C_{v2} \left( k_{t1}^2 + 2k_{t0}k_{t2} \right) \mathcal{R}_{fd}^2}{k_{t6}\pi^2 R_w^2}, \quad (\text{D.50})$$

$$\mathcal{D}_{503} = \frac{1800c_{e5}C_{v2} \left( k_{t1}k_{t2} + k_{t0}k_{t3} \right) \mathcal{R}_{fd}^2}{k_{t6}\pi^2 R_w^2}, \quad (\text{D.51})$$

$$\mathcal{D}_{504} = \frac{900c_{e5}C_{v2} \left( k_{t2}^2 + 2k_{t1}k_{t3} + 2k_{t0}k_{t4} \right) \mathcal{R}_{fd}^2}{k_{t6}\pi^2 R_w^2}, \quad (\text{D.52})$$

$$\mathcal{D}_{505} = \frac{1800c_{e5}C_{v2} \left( k_{t2}k_{t3} + k_{t1}k_{t4} \right) \mathcal{R}_{fd}^2}{k_{t6}\pi^2 R_w^2}, \quad (\text{D.53})$$

$$\mathcal{D}_{506} = \frac{900c_{e5}C_{v2} \left( k_{t3}^2 + 2k_{t2}k_{t4} \right) \mathcal{R}_{fd}^2}{k_{t6}\pi^2 R_w^2}, \quad (\text{D.54})$$

$$\mathcal{D}_{507} = \frac{1800c_{e5}C_{v2}k_{t3}k_{t4}\mathcal{R}_{fd}^2}{k_{t6}\pi^2 R_w^2}, \quad (\text{D.55})$$

$$\mathcal{D}_{508} = \frac{900c_{e5}C_{v2}k_{t4}^2\mathcal{R}_{fd}^2}{k_{t6}\pi^2 R_w^2}. \quad (\text{D.56})$$

## D.2 Battery-Electric Vehicle

The dimension-related parameters of battery-electric vehicles are clustered into two categories because of depleting or charging condition of battery corresponding to the propulsion or braking operations.

Dimension-related parameters of the depleting condition of battery are

$$\mathcal{D}_{00}^{b1} = \frac{k_{b0}k_d^4\mathcal{R}_d^4 + (k_d^2k_{m1}\mathcal{R}_d^2 + C_{v0}^2k_{m5}R_w^2)(k_{b1}k_d^2\mathcal{R}_d^2 + k_{b2}k_d^2k_{m1}\mathcal{R}_d^2 + C_{v0}^2k_{b2}k_{m5}R_w^2)}{k_d^4\mathcal{R}_d^4}, \quad (\text{D.57})$$

$$\mathcal{D}_{01}^{b1} = \frac{2C_{v0}k_{m5}m_vR_w^2(k_{b1}k_d^2\mathcal{R}_d^2 + 2k_{b2}(k_d^2k_{m1}\mathcal{R}_d^2 + C_{v0}^2k_{m5}R_w^2))}{k_d^4\mathcal{R}_d^4}, \quad (\text{D.58})$$

$$\mathcal{D}_{02}^{b1} = \frac{k_{m5}m_v^2R_w^2(k_{b1}k_d^2\mathcal{R}_d^2 + 2k_{b2}k_d^2k_{m1}\mathcal{R}_d^2 + 6C_{v0}^2k_{b2}k_{m5}R_w^2)}{k_d^4\mathcal{R}_d^4}, \quad (\text{D.59})$$

$$\mathcal{D}_{03}^{b1} = \frac{4C_{v0}k_{b2}k_{m5}m_v^3R_w^4}{k_d^4\mathcal{R}_d^4}, \quad (\text{D.60})$$

$$\mathcal{D}_{04}^{b1} = \frac{k_{b2}k_{m5}m_v^4R_w^4}{k_d^4\mathcal{R}_d^4}, \quad (\text{D.61})$$

$$\begin{aligned} \mathcal{D}_{10}^{b1} = & \frac{4C_{v0}^3C_{v1}k_{b2}k_{m5}^2R_w^4}{k_d^4\mathcal{R}_d^4} + \frac{4C_{v0}C_{v1}k_{b2}k_{m1}k_{m5}R_w^2}{k_d^2\mathcal{R}_d^2} + \frac{2C_{v0}^3k_{b2}k_{m4}k_{m5}R_w^2}{k_d^3\mathcal{R}_d^2} \\ & + \frac{2C_{v0}C_{v1}k_{b1}k_{m5}R_w^2}{k_d^2\mathcal{R}_d^2} + \frac{2C_{v0}^2k_{b2}k_{m2}k_{m5}R_w}{k_d^2\mathcal{R}_d} + \frac{2C_{v0}k_{b2}k_{m1}k_{m4}}{k_d} + \frac{C_{v0}k_{b1}k_{m4}}{k_d} \\ & + \frac{k_{b1}k_{m2}\mathcal{R}_d}{R_w} + \frac{2k_{b2}k_{m1}k_{m2}\mathcal{R}_d}{R_w}, \end{aligned} \quad (\text{D.62})$$

$$\begin{aligned} \mathcal{D}_{11}^{b1} = & \frac{12C_{v0}^2C_{v1}k_{b2}k_{m5}^2m_vR_w^4}{k_d^4\mathcal{R}_d^4} + \frac{4C_{v1}k_{b2}k_{m1}k_{m5}m_vR_w^2}{k_d^2\mathcal{R}_d^2} + \frac{6C_{v0}^2k_{b2}k_{m4}k_{m5}m_vR_w^2}{k_d^3\mathcal{R}_d^2} \\ & + \frac{2C_{v1}k_{b1}k_{m5}m_vR_w^2}{k_d^2\mathcal{R}_d^2} + \frac{4C_{v0}k_{b2}k_{m2}k_{m5}m_vR_w}{k_d^2\mathcal{R}_d} + \frac{2k_{b2}k_{m1}k_{m4}m_v}{k_d} + \frac{k_{b1}k_{m4}m_v}{k_d}, \end{aligned} \quad (\text{D.63})$$

$$\mathcal{D}_{12}^{b1} = \frac{2k_{b2}k_{m5}m_v^2R_w(k_d^2k_{m2}\mathcal{R}_d^3 + 3C_{v0}k_dk_{m4}R_w\mathcal{R}_d^2 + 6C_{v0}C_{v1}k_{m5}R_w^3)}{k_d^4\mathcal{R}_d^4}, \quad (\text{D.64})$$

$$\mathcal{D}_{13}^{b1} = \frac{2k_{b2}k_{m5}m_v^3R_w^2(k_dk_{m4}\mathcal{R}_d^2 + 2C_{v1}k_{m5}R_w^2)}{k_d^4\mathcal{R}_d^4}, \quad (\text{D.65})$$

$$\mathcal{D}_{20}^{b1} = \frac{6C_{v0}^2C_{v1}^2k_{b2}k_{m5}^2R_w^4}{k_d^4\mathcal{R}_d^4} + \frac{4C_{v0}^3C_{v2}k_{b2}k_{m5}^2R_w^4}{k_d^4\mathcal{R}_d^4} + \frac{2C_{v1}^2k_{b2}k_{m1}k_{m5}R_w^2}{k_d^2\mathcal{R}_d^2}$$

$$\begin{aligned}
& + \frac{4C_{v0}C_{v2}k_{b2}k_{m1}k_{m5}R_w^2}{k_d^2\mathcal{R}_d^2} + \frac{6C_{v0}^2C_{v1}k_{b2}k_{m4}k_{m5}R_w^2}{k_d^3\mathcal{R}_d^2} + \frac{C_{v1}^2k_{b1}k_{m5}R_w^2}{k_d^2\mathcal{R}_d^2} \\
& + \frac{2C_{v0}C_{v2}k_{b1}k_{m5}R_w^2}{k_d^2\mathcal{R}_d^2} + \frac{4C_{v0}C_{v1}k_{b2}k_{m2}k_{m5}R_w}{k_d^2\mathcal{R}_d} + \frac{C_{v0}^2k_{b2}k_{m4}^2}{k_d^2} \\
& + \frac{2C_{v1}k_{b2}k_{m1}k_{m4}}{k_d} + \frac{C_{v1}k_{b1}k_{m4}}{k_d} + \frac{2C_{v0}^2k_{b2}k_{m3}k_{m5}}{k_d^2} + \frac{2C_{v0}k_{b2}k_{m2}k_{m4}R_d}{k_dR_w} \\
& + \frac{k_{b2}k_{m2}^2\mathcal{R}_d^2}{R_w^2} + \frac{k_{b1}k_{m3}\mathcal{R}_d^2}{R_w^2} + \frac{2k_{b2}k_{m1}k_{m3}\mathcal{R}_d^2}{R_w^2}, \tag{D.66}
\end{aligned}$$

$$\begin{aligned}
\mathcal{D}_{21}^{b1} &= \frac{12C_{v0}C_{v1}^2k_{b2}k_{m5}^2m_vR_w^4}{k_d^4\mathcal{R}_d^4} + \frac{12C_{v0}^2C_{v2}k_{b2}k_{m5}^2m_vR_w^4}{k_d^4\mathcal{R}_d^4} + \frac{4C_{v2}k_{b2}k_{m1}k_{m5}m_vR_w^2}{k_d^2\mathcal{R}_d^2} \\
& + \frac{12C_{v0}C_{v1}k_{b2}k_{m4}k_{m5}m_vR_w^2}{k_d^3\mathcal{R}_d^2} + \frac{2C_{v2}k_{b1}k_{m5}m_vR_w^2}{k_d^2\mathcal{R}_d^2} + \frac{4C_{v1}k_{b2}k_{m2}k_{m5}m_vR_w}{k_d^2\mathcal{R}_d} \\
& + \frac{2C_{v0}k_{b2}k_{m4}^2m_v}{k_d^2} + \frac{4C_{v0}k_{b2}k_{m3}k_{m5}m_v}{k_d^2} + \frac{2k_{b2}k_{m2}k_{m4}m_vR_d}{k_dR_w}, \tag{D.67}
\end{aligned}$$

$$\mathcal{D}_{22}^{b1} = \frac{k_{b2}m_v^2(k_d^2(k_{m4}^2 + 2k_{m3}k_{m5})\mathcal{R}_d^4 + 6C_{v1}k_dk_{m4}k_{m5}R_w^2\mathcal{R}_d^2 + 6(C_{v1}^2 + 2C_{v0}C_{v2})k_{m5}^2R_w^4)}{k_d^4\mathcal{R}_d^4}, \tag{D.68}$$

$$\mathcal{D}_{23}^{b1} = \frac{4C_{v2}k_{b2}k_{m5}^2m_v^3R_w^4}{k_d^4\mathcal{R}_d^4}, \tag{D.69}$$

$$\begin{aligned}
\mathcal{D}_{30}^{b1} &= \frac{4C_{v0}C_{v1}^3k_{b2}k_{m5}^2R_w^4}{k_d^4\mathcal{R}_d^4} + \frac{12C_{v0}^2C_{v1}C_{v2}k_{b2}k_{m5}^2R_w^4}{k_d^4\mathcal{R}_d^4} + \frac{4C_{v1}C_{v2}k_{b2}k_{m1}k_{m5}R_w^2}{k_d^2\mathcal{R}_d^2} \\
& + \frac{6C_{v0}C_{v1}^2k_{b2}k_{m4}k_{m5}R_w^2}{k_d^3\mathcal{R}_d^2} + \frac{6C_{v0}^2C_{v2}k_{b2}k_{m4}k_{m5}R_w^2}{k_d^3\mathcal{R}_d^2} + \frac{2C_{v1}C_{v2}k_{b1}k_{m5}R_w^2}{k_d^2\mathcal{R}_d^2} \\
& + \frac{2C_{v1}^2k_{b2}k_{m2}k_{m5}R_w}{k_d^2\mathcal{R}_d} + \frac{4C_{v0}C_{v2}k_{b2}k_{m2}k_{m5}R_w}{k_d^2\mathcal{R}_d} + \frac{2C_{v0}C_{v1}k_{b2}k_{m4}^2}{k_d^2} \\
& + \frac{2C_{v2}k_{b2}k_{m1}k_{m4}}{k_d} + \frac{C_{v2}k_{b1}k_{m4}}{k_d} + \frac{4C_{v0}C_{v1}k_{b2}k_{m3}k_{m5}}{k_d^2} + \frac{2C_{v1}k_{b2}k_{m2}k_{m4}R_d}{k_dR_w} \\
& + \frac{2C_{v0}k_{b2}k_{m3}k_{m4}\mathcal{R}_d^2}{k_dR_w^2} + \frac{2k_{b2}k_{m2}k_{m3}\mathcal{R}_d^3}{R_w^3}, \tag{D.70}
\end{aligned}$$

$$\begin{aligned}
\mathcal{D}_{31}^{b1} &= \frac{4C_{v1}^3k_{b2}k_{m5}^2m_vR_w^4}{k_d^4\mathcal{R}_d^4} + \frac{24C_{v0}C_{v1}C_{v2}k_{b2}k_{m5}^2m_vR_w^4}{k_d^4\mathcal{R}_d^4} + \frac{6C_{v1}^2k_{b2}k_{m4}k_{m5}m_vR_w^2}{k_d^3\mathcal{R}_d^2} \\
& + \frac{12C_{v0}C_{v2}k_{b2}k_{m4}k_{m5}m_vR_w^2}{k_d^3\mathcal{R}_d^2} + \frac{4C_{v2}k_{b2}k_{m2}k_{m5}m_vR_w}{k_d^2\mathcal{R}_d} + \frac{2C_{v1}k_{b2}k_{m4}^2m_v}{k_d^2}
\end{aligned}$$

$$+ \frac{4C_{v1}k_{b2}k_{m3}k_{m5}m_v}{k_d^2} + \frac{2k_{b2}k_{m3}k_{m4}m_v\mathcal{R}_d^2}{k_d R_w^2}, \quad (\text{D.71})$$

$$\mathcal{D}_{32}^{b1} = \frac{6C_{v2}k_{b2}k_{m5}m_v^2 R_w^2 (k_d k_{m4} \mathcal{R}_d^2 + 2C_{v1} k_{m5} R_w^2)}{k_d^4 \mathcal{R}_d^4}, \quad (\text{D.72})$$

$$\begin{aligned} \mathcal{D}_{40}^{b1} = & \frac{k_{b2}k_{m3}^2\mathcal{R}_d^4}{R_w^4} + \frac{2C_{v1}k_{b2}k_{m3}k_{m4}\mathcal{R}_d^2}{k_d R_w^2} + \frac{2C_{v2}k_{b2}k_{m2}k_{m4}\mathcal{R}_d}{k_d R_w} + \frac{C_{v1}^2 k_{b2}k_{m4}^2}{k_d^2} \\ & + \frac{2C_{v0}C_{v2}k_{b2}k_{m4}^2}{k_d^2} + \frac{2C_{v1}^2 k_{b2}k_{m3}k_{m5}}{k_d^2} + \frac{4C_{v0}C_{v2}k_{b2}k_{m3}k_{m5}}{k_d^2} + \frac{4C_{v1}C_{v2}k_{b2}k_{m2}k_{m5}R_w}{k_d^2 \mathcal{R}_d} \\ & + \frac{2C_{v2}^2 k_{b2}k_{m1}k_{m5}R_w^2}{k_d^2 \mathcal{R}_d^2} + \frac{2C_{v1}^3 k_{b2}k_{m4}k_{m5}R_w^2}{k_d^3 \mathcal{R}_d^2} + \frac{12C_{v0}C_{v1}C_{v2}k_{b2}k_{m4}k_{m5}R_w^2}{k_d^3 \mathcal{R}_d^2} \\ & + \frac{C_{v2}^2 k_{b1}k_{m5}R_w^2}{k_d^2 \mathcal{R}_d^2} + \frac{C_{v1}^4 k_{b2}k_{m5}^2 R_w^4}{k_d^4 \mathcal{R}_d^4} + \frac{6C_{v0}^2 C_{v2}^2 k_{b2}k_{m5}^2 R_w^4}{k_d^4 \mathcal{R}_d^4} + \frac{12C_{v0}C_{v1}^2 C_{v2}k_{b2}k_{m5}^2 R_w^4}{k_d^4 \mathcal{R}_d^4}, \end{aligned} \quad (\text{D.73})$$

$$\begin{aligned} \mathcal{D}_{41}^{b1} = & \frac{12C_{v0}C_{v2}^2 k_{b2}k_{m5}^2 m_v R_w^4}{k_d^4 \mathcal{R}_d^4} + \frac{12C_{v1}^2 C_{v2}k_{b2}k_{m5}^2 m_v R_w^4}{k_d^4 \mathcal{R}_d^4} + \frac{12C_{v1}C_{v2}k_{b2}k_{m4}k_{m5}m_v R_w^2}{k_d^3 \mathcal{R}_d^2} \\ & + \frac{2C_{v2}k_{b2}k_{m4}^2 m_v}{k_d^2} + \frac{4C_{v2}k_{b2}k_{m3}k_{m5}m_v}{k_d^2}, \end{aligned} \quad (\text{D.74})$$

$$\mathcal{D}_{42}^{b1} = \frac{6C_{v2}^2 k_{b2}k_{m5}^2 m_v^2 R_w^4}{k_d^4 \mathcal{R}_d^4}, \quad (\text{D.75})$$

$$\begin{aligned} \mathcal{D}_{50}^{b1} = & \frac{12C_{v0}C_{v1}C_{v2}^2 k_{b2}k_{m5}^2 R_w^4}{k_d^4 \mathcal{R}_d^4} + \frac{4C_{v1}^3 C_{v2}k_{b2}k_{m5}^2 R_w^4}{k_d^4 \mathcal{R}_d^4} + \frac{6C_{v0}C_{v2}^2 k_{b2}k_{m4}k_{m5}R_w^2}{k_d^3 \mathcal{R}_d^2} \\ & + \frac{6C_{v1}^2 C_{v2}k_{b2}k_{m4}k_{m5}R_w^2}{k_d^3 \mathcal{R}_d^2} + \frac{2C_{v2}^2 k_{b2}k_{m2}k_{m5}R_w}{k_d^2} + \frac{2C_{v1}C_{v2}k_{b2}k_{m4}^2}{k_d^2} \\ & + \frac{4C_{v1}C_{v2}k_{b2}k_{m3}k_{m5}}{k_d^2} + \frac{2C_{v2}k_{b2}k_{m3}k_{m4}\mathcal{R}_d^2}{k_d R_w^2}, \end{aligned} \quad (\text{D.76})$$

$$\mathcal{D}_{51}^{b1} = \frac{6C_{v2}^2 k_{b2}k_{m5}m_v R_w^2 (k_d k_{m4} \mathcal{R}_d^2 + 2C_{v1} k_{m5} R_w^2)}{k_d^4 \mathcal{R}_d^4}, \quad (\text{D.77})$$

$$\begin{aligned} \mathcal{D}_{60}^{b1} = & \frac{4C_{v0}C_{v2}^3 k_{b2}k_{m5}^2 R_w^4}{k_d^4 \mathcal{R}_d^4} + \frac{6C_{v1}^2 C_{v2}^2 k_{b2}k_{m5}^2 R_w^4}{k_d^4 \mathcal{R}_d^4} + \frac{6C_{v1}C_{v2}^2 k_{b2}k_{m4}k_{m5}R_w^2}{k_d^3 \mathcal{R}_d^2} + \frac{C_{v2}^2 k_{b2}k_{m4}^2}{k_d^2} \\ & + \frac{2C_{v2}^2 k_{b2}k_{m3}k_{m5}}{k_d^2}, \end{aligned} \quad (\text{D.78})$$

$$\mathcal{D}_{61}^{b1} = \frac{4C_{v2}^3 k_{b2}k_{m5}^2 m_v R_w^4}{k_d^4 \mathcal{R}_d^4}, \quad (\text{D.79})$$

$$D_{70}^{b1} = \frac{2C_{v2}^3 k_{b2} k_{m5} R_w^2 (k_d k_{m4} \mathcal{R}_d^2 + 2C_{v1} k_{m5} R_w^2)}{k_d^4 \mathcal{R}_d^4}, \quad (\text{D.80})$$

$$D_{80}^{b1} = \frac{C_{v2}^4 k_{b2} k_{m5}^2 R_w^4}{k_d^4 \mathcal{R}_d^4}, \quad (\text{D.81})$$

where  $\mathcal{R}_d$  is defined as

$$\mathcal{R}_d = \mathcal{R}_m \mathcal{R}_{fd}; \quad (\text{D.82})$$

and the parameter  $k_d$  is equal to the coefficient  $c_{t7}$ .

Dimension-related parameters of the charging condition of battery are expressed as

$$D_{00}^{b2} = \frac{k_{b0} \mathcal{R}_d^4 + (k_{m1} \mathcal{R}_d^2 + C_{v0}^2 k_d^2 k_{m5} R_w^2) (k_{b1} \mathcal{R}_d^2 + k_{b2} k_{m1} \mathcal{R}_d^2 + C_{v0}^2 k_{b2} k_d^2 k_{m5} R_w^2)}{\mathcal{R}_d^4}, \quad (\text{D.83})$$

$$D_{01}^{b2} = \frac{2C_{v0} k_d^2 k_{m5} m_v R_w^2 (k_{b1} \mathcal{R}_d^2 + 2k_{b2} (k_{m1} \mathcal{R}_d^2 + C_{v0}^2 k_d^2 k_{m5} R_w^2))}{\mathcal{R}_d^4}, \quad (\text{D.84})$$

$$D_{02}^{b2} = \frac{k_d^2 k_{m5} m_v^2 R_w^2 (k_{b1} \mathcal{R}_d^2 + 2k_{b2} k_{m1} \mathcal{R}_d^2 + 6C_{v0}^2 k_{b2} k_d^2 k_{m5} R_w^2)}{\mathcal{R}_d^4}, \quad (\text{D.85})$$

$$D_{03}^{b2} = \frac{4C_{v0} k_{b2} k_d^4 k_{m5}^2 m_v^3 R_w^4}{\mathcal{R}_d^4}, \quad (\text{D.86})$$

$$D_{04}^{b2} = \frac{k_{b2} k_d^4 k_{m5}^2 m_v^4 R_w^4}{\mathcal{R}_d^4}, \quad (\text{D.87})$$

$$\begin{aligned} D_{10}^{b2} = & \frac{4C_{v0}^3 C_{v1} k_{b2} k_{d6}^4 k_{m5}^2 R_w^4}{\mathcal{R}_d^4} + \frac{2C_{v0} C_{v1} k_{b1} k_{d6}^2 k_{m5} R_w^2}{\mathcal{R}_d^2} + \frac{4C_{v0} C_{v1} k_{b2} k_{d6}^2 k_{m1} k_{m5} R_w^2}{\mathcal{R}_d^2} \\ & + \frac{2C_{v0}^3 k_{b2} k_{d6}^3 k_{m4} k_{m5} R_w^2}{\mathcal{R}_d^2} + \frac{2C_{v0}^2 k_{b2} k_{d6}^2 k_{m2} k_{m5} R_w}{\mathcal{R}_d} + \frac{k_{b1} k_{m2} \mathcal{R}_d}{R_w} + \frac{2k_{b2} k_{m1} k_{m2} \mathcal{R}_d}{R_w} \\ & + C_{v0} k_{b1} k_{d6} k_{m4} + 2C_{v0} k_{b2} k_{d6} k_{m1} k_{m4}, \end{aligned} \quad (\text{D.88})$$

$$\begin{aligned} D_{11}^{b2} = & \frac{12C_{v0}^2 C_{v1} k_{b2} k_{d6}^4 k_{m5}^2 m_v R_w^4}{\mathcal{R}_d^4} + \frac{2C_{v1} k_{b1} k_{d6}^2 k_{m5} m_v R_w^2}{\mathcal{R}_d^2} + \frac{4C_{v1} k_{b2} k_{d6}^2 k_{m1} k_{m5} m_v R_w^2}{\mathcal{R}_d^2} \\ & + \frac{6C_{v0}^2 k_{b2} k_{d6}^3 k_{m4} k_{m5} m_v R_w^2}{\mathcal{R}_d^2} + \frac{4C_{v0} k_{b2} k_{d6}^2 k_{m2} k_{m5} m_v R_w}{\mathcal{R}_d} + k_{b1} k_{d6} k_{m4} m_v \\ & + 2k_{b2} k_{d6} k_{m1} k_{m4} m_v, \end{aligned} \quad (\text{D.89})$$

$$D_{12}^{b2} = \frac{2k_{b2} k_d^2 k_{m5} m_v^2 R_w (k_{m2} \mathcal{R}_d^3 + 3C_{v0} k_d R_w (k_{m4} \mathcal{R}_d^2 + 2C_{v1} k_d k_{m5} R_w^2))}{\mathcal{R}_d^4}, \quad (\text{D.90})$$

$$D_{13}^{b2} = \frac{2k_{b2}k_d^3k_{m5}m_v^3R_w^2(k_{m4}\mathcal{R}_d^2 + 2C_{v1}k_dk_{m5}R_w^2)}{\mathcal{R}_d^4}, \quad (D.91)$$

$$\begin{aligned} D_{20}^{b2} = & \frac{6C_{v0}^2C_{v1}k_{b2}k_{d6}^4k_{m5}^2R_w^4}{\mathcal{R}_d^4} + \frac{4C_{v0}^3C_{v2}k_{b2}k_{d6}^4k_{m5}^2R_w^4}{\mathcal{R}_d^4} + \frac{C_{v1}^2k_{b1}k_{d6}^2k_{m5}R_w^2}{\mathcal{R}_d^2} \\ & + \frac{2C_{v0}C_{v2}k_{b1}k_{d6}^3k_{m5}R_w^2}{\mathcal{R}_d^2} + \frac{2C_{v1}^2k_{b2}k_{d6}^2k_{m1}k_{m5}R_w^2}{\mathcal{R}_d^2} + \frac{4C_{v0}C_{v2}k_{b2}k_{d6}^2k_{m1}k_{m5}R_w^2}{\mathcal{R}_d^2} \\ & + \frac{6C_{v0}^2C_{v1}k_{b2}k_{d6}^3k_{m4}k_{m5}R_w^2}{\mathcal{R}_d^2} + \frac{4C_{v0}C_{v1}k_{b2}k_{d6}^2k_{m2}k_{m5}R_w}{\mathcal{R}_d} + \frac{2C_{v0}k_{b2}k_{d6}k_{m2}k_{m4}R_d}{R_w} \\ & + \frac{k_{b2}k_{m2}^2\mathcal{R}_d^2}{R_w^2} + \frac{k_{b1}k_{m3}\mathcal{R}_d^2}{R_w^2} + \frac{2k_{b2}k_{m1}k_{m3}\mathcal{R}_d^2}{R_w^2} + C_{v0}^2k_{b2}k_{d6}^2k_{m4}^2 + C_{v1}k_{b1}k_{d6}k_{m4} \\ & + 2C_{v1}k_{b2}k_{d6}k_{m1}k_{m4} + 2C_{v0}^2k_{b2}k_{d6}^2k_{m3}k_{m5}, \end{aligned} \quad (D.92)$$

$$\begin{aligned} D_{21}^{b2} = & \frac{12C_{v0}C_{v1}^2k_{b2}k_{d6}^4k_{m5}^2m_vR_w^4}{\mathcal{R}_d^4} + \frac{12C_{v0}^2C_{v2}k_{b2}k_{d6}^4k_{m5}^2m_vR_w^4}{\mathcal{R}_d^4} + \frac{2C_{v2}k_{b1}k_{d6}^2k_{m5}m_vR_w^2}{\mathcal{R}_d^2} \\ & + \frac{4C_{v2}k_{b2}k_{d6}^2k_{m1}k_{m5}m_vR_w^2}{\mathcal{R}_d^2} + \frac{12C_{v0}C_{v1}k_{b2}k_{d6}^3k_{m4}k_{m5}m_vR_w^2}{\mathcal{R}_d^2} + \frac{4C_{v1}k_{b2}k_{d6}^2k_{m2}k_{m5}m_vR_w}{\mathcal{R}_d} \\ & + \frac{2k_{b2}k_{d6}k_{m2}k_{m4}m_vR_d}{R_w} + 2C_{v0}k_{b2}k_{d6}^2k_{m4}^2m_v + 4C_{v0}k_{b2}k_{d6}^2k_{m3}k_{m5}m_v, \end{aligned} \quad (D.93)$$

$$\begin{aligned} D_{22}^{b2} = & \frac{6C_{v1}^2k_{b2}k_{d6}^4k_{m5}^2m_v^2R_w^4}{\mathcal{R}_d^4} + \frac{12C_{v0}C_{v2}k_{b2}k_{d6}^4k_{m5}^2m_v^2R_w^4}{\mathcal{R}_d^4} + \frac{6C_{v1}k_{b2}k_{d6}^3k_{m4}k_{m5}m_v^2R_w^2}{\mathcal{R}_d^2} \\ & + k_{b2}k_{d6}^2k_{m4}^2m_v^2 + 2k_{b2}k_{d6}^2k_{m3}k_{m5}m_v^2, \end{aligned} \quad (D.94)$$

$$D_{23}^{b2} = \frac{4C_{v2}k_{b2}k_{d6}^4k_{m5}^2m_v^3R_w^4}{\mathcal{R}_d^4}, \quad (D.95)$$

$$\begin{aligned} D_{30}^{b2} = & \frac{4C_{v0}C_{v1}^3k_{b2}k_{d6}^4k_{m5}^2R_w^4}{\mathcal{R}_d^4} + \frac{12C_{v0}^2C_{v1}C_{v2}k_{b2}k_{d6}^4k_{m5}^2R_w^4}{\mathcal{R}_d^4} + \frac{2C_{v1}C_{v2}k_{b1}k_{d6}^2k_{m5}R_w^2}{\mathcal{R}_d^2} \\ & + \frac{4C_{v1}C_{v2}k_{b2}k_{d6}^2k_{m1}k_{m5}R_w^2}{\mathcal{R}_d^2} + \frac{6C_{v0}C_{v1}^2k_{b2}k_{d6}^3k_{m4}k_{m5}R_w^2}{\mathcal{R}_d^2} + \frac{6C_{v0}^2C_{v2}k_{b2}k_{d6}^3k_{m4}k_{m5}R_w^2}{\mathcal{R}_d^2} \\ & + \frac{2C_{v1}^2k_{b2}k_{d6}^2k_{m2}k_{m5}R_w}{\mathcal{R}_d} + \frac{4C_{v0}C_{v2}k_{b2}k_{d6}^2k_{m2}k_{m5}R_w}{\mathcal{R}_d} + \frac{2C_{v1}k_{b2}k_{d6}k_{m2}k_{m4}R_d}{R_w} \\ & + \frac{2C_{v0}k_{b2}k_{d6}k_{m3}k_{m4}R_d^2}{R_w^2} + \frac{2k_{b2}k_{m2}k_{m3}\mathcal{R}_d^3}{R_w^3} + 2C_{v0}C_{v1}k_{b2}k_{d6}^2k_{m4}^2 + C_{v2}k_{b1}k_{d6}k_{m4} \\ & + 2C_{v2}k_{b2}k_{d6}k_{m1}k_{m4} + 4C_{v0}C_{v1}k_{b2}k_{d6}^2k_{m3}k_{m5}, \end{aligned} \quad (D.96)$$

$$D_{31}^{b2} = \frac{4C_{v1}^3k_{b2}k_{d6}^4k_{m5}^2m_vR_w^4}{\mathcal{R}_d^4} + \frac{24C_{v0}C_{v1}C_{v2}k_{b2}k_{d6}^4k_{m5}^2m_vR_w^4}{\mathcal{R}_d^4} + \frac{6C_{v1}^2k_{b2}k_{d6}^3k_{m4}k_{m5}m_vR_w^2}{\mathcal{R}_d^2}$$

$$\begin{aligned}
& + \frac{12C_{v0}C_{v2}k_{b2}k_{d6}^3k_{m4}k_{m5}m_vR_w^2}{\mathcal{R}_d^2} + \frac{4C_{v2}k_{b2}k_{d6}^2k_{m2}k_{m5}m_vR_w}{\mathcal{R}_d} + \frac{2k_{b2}k_{d6}k_{m3}k_{m4}m_v\mathcal{R}_d^2}{R_w^2} \\
& + 2C_{v1}k_{b2}k_{d6}^2k_{m4}^2m_v + 4C_{v1}k_{b2}k_{d6}^2k_{m3}k_{m5}m_v, \tag{D.97}
\end{aligned}$$

$$D_{32}^{b2} = \frac{6C_{v2}k_{b2}k_{d6}^3k_{m5}m_v^2R_w^2(k_{m4}\mathcal{R}_d^2 + 2C_{v1}k_dk_{m5}R_w^2)}{\mathcal{R}_d^4}, \tag{D.98}$$

$$\begin{aligned}
D_{40}^{b2} &= \frac{k_{b2}k_{m3}^2\mathcal{R}_d^4}{R_w^4} + \frac{2C_{v1}k_{b2}k_{d6}k_{m3}k_{m4}\mathcal{R}_d^2}{R_w^2} + \frac{2C_{v2}k_{b2}k_{d6}k_{m2}k_{m4}\mathcal{R}_d}{R_w} \\
& + \frac{4C_{v1}C_{v2}k_{b2}k_{d6}^2k_{m2}k_{m5}R_w}{\mathcal{R}_d} + \frac{C_{v2}^2k_{b1}k_{d6}^2k_{m5}R_w^2}{\mathcal{R}_d^2} + \frac{2C_{v2}^2k_{b2}k_{d6}^2k_{m1}k_{m5}R_w^2}{\mathcal{R}_d^2} \\
& + \frac{2C_{v1}^3k_{b2}k_{d6}^3k_{m4}k_{m5}R_w^2}{\mathcal{R}_d^2} + \frac{12C_{v0}C_{v1}C_{v2}k_{b2}k_{d6}^3k_{m4}k_{m5}R_w^2}{\mathcal{R}_d^2} + \frac{C_{v1}^4k_{b2}k_{d6}^4k_{m5}^2R_w^4}{\mathcal{R}_d^4} \\
& + \frac{6C_{v0}^2C_{v2}^2k_{b2}k_{d6}^4k_{m5}^2R_w^4}{\mathcal{R}_d^4} + \frac{12C_{v0}C_{v1}^2C_{v2}k_{b2}k_{d6}^4k_{m5}^2R_w^4}{\mathcal{R}_d^4} + C_{v1}^2k_{b2}k_{d6}^2k_{m4}^2 \\
& + 2C_{v0}C_{v2}k_{b2}k_{d6}^2k_{m4}^2 + 2C_{v1}^2k_{b2}k_{d6}^2k_{m3}k_{m5} + 4C_{v0}C_{v2}k_{b2}k_{d6}^2k_{m3}k_{m5}, \tag{D.99}
\end{aligned}$$

$$\begin{aligned}
D_{41}^{b2} &= \frac{12C_{v0}C_{v2}^2k_{b2}k_{d6}^4k_{m5}^2m_vR_w^4}{\mathcal{R}_d^4} + \frac{12C_{v1}^2C_{v2}k_{b2}k_{d6}^4k_{m5}^2m_vR_w^4}{\mathcal{R}_d^4} \\
& + \frac{12C_{v1}C_{v2}k_{b2}k_{d6}^3k_{m4}k_{m5}m_vR_w^2}{\mathcal{R}_d^2} + 2C_{v2}k_{b2}k_{d6}^2k_{m4}^2m_v + 4C_{v2}k_{b2}k_{d6}^2k_{m3}k_{m5}m_v, \tag{D.100}
\end{aligned}$$

$$D_{42}^{b2} = \frac{6C_{v2}^2k_{b2}k_{d6}^4k_{m5}^2m_v^2R_w^4}{\mathcal{R}_d^4}, \tag{D.101}$$

$$\begin{aligned}
D_{50}^{b2} &= \frac{12C_{v0}C_{v1}C_{v2}^2k_{b2}k_{d6}^4k_{m5}^2R_w^4}{\mathcal{R}_d^4} + \frac{4C_{v1}^3C_{v2}k_{b2}k_{d6}^4k_{m5}^2R_w^4}{\mathcal{R}_d^4} + \frac{6C_{v0}C_{v2}^2k_{b2}k_{d6}^3k_{m4}k_{m5}R_w^2}{\mathcal{R}_d^2} \\
& + \frac{6C_{v1}^2C_{v2}k_{b2}k_{d6}^3k_{m4}k_{m5}R_w^2}{\mathcal{R}_d^2} + \frac{2C_{v2}^2k_{b2}k_{d6}^2k_{m2}k_{m5}R_w}{\mathcal{R}_d} + \frac{2C_{v2}k_{b2}k_{d6}k_{m3}k_{m4}\mathcal{R}_d^2}{R_w^2} \\
& + 2C_{v1}C_{v2}k_{b2}k_{d6}^2k_{m4}^2 + 4C_{v1}C_{v2}k_{b2}k_{d6}^2k_{m3}k_{m5}, \tag{D.102}
\end{aligned}$$

$$D_{51}^{b2} = \frac{6C_{v2}^2k_{b2}k_{d6}^3k_{m5}m_vR_w^2(k_{m4}\mathcal{R}_d^2 + 2C_{v1}k_dk_{m5}R_w^2)}{\mathcal{R}_d^4}, \tag{D.103}$$

$$\begin{aligned}
D_{60}^{b2} &= \frac{4C_{v0}C_{v2}^3k_{b2}k_{d6}^4k_{m5}^2R_w^4}{\mathcal{R}_d^4} + \frac{6C_{v1}^2C_{v2}k_{b2}k_{d6}^4k_{m5}^2R_w^4}{\mathcal{R}_d^4} + \frac{6C_{v1}C_{v2}^2k_{b2}k_{d6}^3k_{m4}k_{m5}R_w^2}{\mathcal{R}_d^2} \\
& + C_{v2}^2k_{b2}k_{d6}^2k_{m4}^2 + 2C_{v2}^2k_{b2}k_{d6}^2k_{m3}k_{m5}, \tag{D.104}
\end{aligned}$$

$$D_{61}^{b2} = \frac{4C_{v2}^3k_{b2}k_{d6}^4k_{m5}^2m_vR_w^4}{\mathcal{R}_d^4}, \tag{D.105}$$

$$\mathcal{D}_{70}^{b2} = \frac{2C_{v2}^3 k_{b2} k_d^3 k_{m5} R_w^2 (k_{m4} \mathcal{R}_d^2 + 2C_{v1} k_d k_{m5} R_w^2)}{\mathcal{R}_d^4}, \quad (\text{D.106})$$

$$\mathcal{D}_{80}^{b2} = \frac{C_{v2}^4 k_{b2} k_d^4 k_{m5}^2 R_w^4}{\mathcal{R}_d^4}. \quad (\text{D.107})$$



## Detailed Dimension-Related Parameters of Chapter 6

Dimension-related parameters of FACE for series and parallel hybrid electric vehicles are summarized in this chapter.

### E.1 Series Hybrid Electric Vehicle

$$\begin{aligned} \mathbf{n}_1 = & \mathbf{p}_8^3 \mathcal{V}_e \left( 16384 k_{g0} \pi^{18} \mathcal{R}_g^2 \mathbf{p}_6 - 8192 k_{g1} \pi^{18} \mathcal{R}_g^3 \mathbf{p}_3 \omega_{ei} + 16384 k_{g1} \pi^{18} \mathcal{R}_g^3 \mathbf{p}_6 \omega_{ei} \right. \\ & - 16384 k_{g2} \pi^{18} \mathcal{R}_g^4 \mathbf{p}_3 \omega_{ei}^2 + 16384 k_{g2} \pi^{18} \mathcal{R}_g^4 \mathbf{p}_6 \omega_{ei}^2 - 16000 k_{g3} \pi^9 \mathcal{R}_g^2 \mathcal{V}_e (\mathbf{p}_2 \mathbf{p}_6 - \mathbf{p}_3 \mathbf{p}_5 \omega_{ei}) \\ & \left. + 15625 k_{g4} \mathbf{p}_1^2 \mathbf{p}_6 \mathcal{V}_e^2 - 15625 k_{g4} \mathbf{p}_1 \mathbf{p}_3 \mathbf{p}_4 \mathcal{V}_e^2 \omega_{ei} \right)^2, \end{aligned} \quad (\text{E.1})$$

$$\begin{aligned} \mathbf{d}_1 = & -64 \pi^9 \mathcal{R}_g^2 \mathbf{p}_3^2 \omega_{ei}^2 \left( -65536 k_{g0} \pi^{18} \mathcal{R}_g^2 \mathbf{p}_3^2 \mathbf{p}_7^2 \omega_{ei}^2 + 163840 k_{g0} \pi^{18} \mathcal{R}_g^2 \mathbf{p}_3^2 \mathbf{p}_8 \mathbf{p}_9 \mathcal{V}_e^2 \omega_{ei}^2 \right. \\ & + 32768 k_{g1} \pi^{18} \mathcal{R}_g^3 (\mathbf{p}_3^2 \omega_{ei}^3 (5 \mathbf{p}_8 \mathbf{p}_9 \mathcal{V}_e^2 - 2 \mathbf{p}_7^2) + \mathbf{p}_6 \mathbf{p}_8^3 \mathcal{V}_e^2) - 65536 k_{g2} \pi^{18} \mathcal{R}_g^4 \mathbf{p}_3^2 \mathbf{p}_7^2 \omega_{ei}^4 \\ & + 163840 k_{g2} \pi^{18} \mathcal{R}_g^4 \mathbf{p}_3^2 \mathbf{p}_8 \mathbf{p}_9 \mathcal{V}_e^2 \omega_{ei}^4 - 16384 k_{g2} \pi^{18} \mathcal{R}_g^4 \mathbf{p}_3 \mathbf{p}_8^3 \mathcal{V}_e^2 \omega_{ei} \\ & + 65536 k_{g2} \pi^{18} \mathcal{R}_g^4 \mathbf{p}_6 \mathbf{p}_8^3 \mathcal{V}_e^2 \omega_{ei} - 32000 k_{g3} \pi^9 \mathcal{R}_g^2 \mathcal{V}_e (\mathbf{p}_3 \omega_{ei} (\mathbf{p}_2 \mathbf{p}_3 \omega_{ei} (5 \mathbf{p}_8 \mathbf{p}_9 \mathcal{V}_e^2 \\ & - 2 \mathbf{p}_7^2) - \mathbf{p}_{10} \mathbf{p}_8^3 \mathcal{V}_e^2) + 2 \mathbf{p}_5 \mathbf{p}_6 \mathbf{p}_8^3 \mathcal{V}_e^2) - 62500 k_{g4} \mathbf{p}_1^2 \mathbf{p}_3^2 \mathbf{p}_7^2 \mathcal{V}_e^2 \omega_{ei}^2 \\ & \left. + 156250 k_{g4} \mathbf{p}_1^2 \mathbf{p}_3^2 \mathbf{p}_8 \mathbf{p}_9 \mathcal{V}_e^4 \omega_{ei}^2 + 62500 k_{g4} \mathbf{p}_1 \mathbf{p}_4 \mathbf{p}_6 \mathbf{p}_8^3 \mathcal{V}_e^4 - 15625 k_{g4} \mathbf{p}_{11} \mathbf{p}_3 \mathbf{p}_8^3 \mathcal{V}_e^4 \omega_{ei} \right), \end{aligned} \quad (\text{E.2})$$

$$\begin{aligned} \mathbf{n}_2 = & \frac{1}{2097152 \pi^{27} \mathcal{R}_g^4} \left( 8192 \pi^{18} \mathcal{R}_g^2 \left( -2 k_{g0} \mathbf{p}_6 + k_{g1} \mathcal{R}_g \mathbf{p}_3 \omega_{ei} - 2 k_{g1} \mathcal{R}_g \mathbf{p}_6 \omega_{ei} + 2 k_{g2} \mathcal{R}_g^2 \mathbf{p}_3 \omega_{ei}^2 \right. \right. \\ & - 2 k_{g2} \mathcal{R}_g^2 \mathbf{p}_6 \omega_{ei}^2) + 125 \mathcal{V}_e (128 k_{g3} \pi^9 \mathcal{R}_g^2 (\mathbf{p}_2 \mathbf{p}_6 - \mathbf{p}_3 \mathbf{p}_5 \omega_{ei}) \\ & \left. \left. + 125 k_{g4} \mathbf{p}_1 \mathcal{V}_e (\mathbf{p}_3 \mathbf{p}_4 \omega_{ei} - \mathbf{p}_1 \mathbf{p}_6) \right) \right)^2, \end{aligned} \quad (\text{E.3})$$

$$\begin{aligned}
\mathbf{d}_2 = & -\frac{4k_{g0}\mathbf{p}_3^4\mathbf{p}_7^2\omega_{ei}^4}{\mathbf{p}_8^3\mathcal{V}_e} + \frac{10k_{g0}\mathbf{p}_3^4\mathbf{p}_9\mathcal{V}_e\omega_{ei}^4}{\mathbf{p}_8^2} - \frac{4k_{g1}\mathcal{R}_g\mathbf{p}_3^4\mathbf{p}_7^2\omega_{ei}^5}{\mathbf{p}_8^3\mathcal{V}_e} + \frac{10k_{g1}\mathcal{R}_g\mathbf{p}_3^4\mathbf{p}_9\mathcal{V}_e\omega_{ei}^5}{\mathbf{p}_8^2} \\
& + \frac{10k_{g2}\mathcal{R}_g^2\mathbf{p}_3^4\mathbf{p}_9\mathcal{V}_e\omega_{ei}^6}{\mathbf{p}_8^2} + \frac{125k_{g3}\mathbf{p}_{10}\mathbf{p}_3^3\mathcal{V}_e^2\omega_{ei}^3}{64\pi^9} + \frac{125k_{g3}\mathbf{p}_2\mathbf{p}_3^4\mathbf{p}_7^2\omega_{ei}^4}{32\pi^9\mathbf{p}_8^3} \\
& - \frac{625k_{g3}\mathbf{p}_2\mathbf{p}_3^4\mathbf{p}_9\mathcal{V}_e^2\omega_{ei}^4}{64\pi^9\mathbf{p}_8^2} - \frac{125k_{g3}\mathbf{p}_3^2\mathbf{p}_5\mathbf{p}_6\mathcal{V}_e^2\omega_{ei}^2}{32\pi^9} - \frac{15625k_{g4}\mathbf{p}_1^2\mathbf{p}_3^4\mathbf{p}_7^2\mathcal{V}_e\omega_{ei}^4}{4096\pi^{18}\mathcal{R}_g^2\mathbf{p}_8^3} \\
& + \frac{78125k_{g4}\mathbf{p}_1^2\mathbf{p}_3^4\mathbf{p}_9\mathcal{V}_e^3\omega_{ei}^4}{8192\pi^{18}\mathcal{R}_g^2\mathbf{p}_8^2} + \frac{15625k_{g4}\mathbf{p}_1\mathbf{p}_3^2\mathbf{p}_4\mathbf{p}_6\mathcal{V}_e^3\omega_{ei}^2}{4096\pi^{18}\mathcal{R}_g^2} - \frac{15625k_{g4}\mathbf{p}_{11}\mathbf{p}_3^3\mathcal{V}_e^3\omega_{ei}^3}{16384\pi^{18}\mathcal{R}_g^2} \\
& + 2k_{g1}\mathcal{R}_g\mathbf{p}_3^2\mathbf{p}_6\mathcal{V}_e\omega_{ei}^2 - \frac{4k_{g2}\mathcal{R}_g^2\mathbf{p}_3^4\mathbf{p}_7^2\omega_{ei}^6}{\mathbf{p}_8^3\mathcal{V}_e} - k_{g2}\mathcal{R}_g^2\mathbf{p}_3^3\mathcal{V}_e\omega_{ei}^3 + 4k_{g2}\mathcal{R}_g^2\mathbf{p}_3^2\mathbf{p}_6\mathcal{V}_e\omega_{ei}^3, \quad (\text{E.4})
\end{aligned}$$

$$\begin{aligned}
\mathbf{p}_1 = & 16c_{e10}\pi^4\omega_{ei}^3 + 8c_{e11}\pi^3\omega_{ei}^4 + 4c_{e12}\pi^2\omega_{ei}^5 + 2c_{e13}\pi\omega_{ei}^6 + c_{e14}\omega_{ei}^7 + 128c_{e7}\pi^7 \\
& + 64c_{e8}\pi^6\omega_{ei} + 32c_{e9}\pi^5\omega_{ei}^2, \quad (\text{E.5})
\end{aligned}$$

$$\begin{aligned}
\mathbf{p}_2 = & 16c_{e10}\pi^4\omega_{ei}^4 + 8c_{e11}\pi^3\omega_{ei}^5 + 4c_{e12}\pi^2\omega_{ei}^6 + 2c_{e13}\pi\omega_{ei}^7 + c_{e14}\omega_{ei}^8 + 128c_{e7}\pi^7\omega_{ei} \\
& + 64c_{e8}\pi^6\omega_{ei}^2 + 32c_{e9}\pi^5\omega_{ei}^3, \quad (\text{E.6})
\end{aligned}$$

$$\begin{aligned}
\mathbf{p}_3 = & 32c_{e1}\pi^8 + 2000c_{e10}c_{e3}\pi^4\omega_{ei}^3 + 1000c_{e11}c_{e3}\pi^3\omega_{ei}^4 + 500c_{e12}c_{e3}\pi^2\omega_{ei}^5 \\
& + 250c_{e13}c_{e3}\pi\omega_{ei}^6 + 125c_{e14}c_{e3}\omega_{ei}^7 + 960c_{e2}\pi^7\omega_{ei} + 16000c_{e3}c_{e7}\pi^7 \\
& + 8000c_{e3}c_{e8}\pi^6\omega_{ei} + 4000c_{e3}c_{e9}\pi^5\omega_{ei}^2, \quad (\text{E.7})
\end{aligned}$$

$$\begin{aligned}
\mathbf{p}_4 = & 48c_{e10}\pi^4\omega_{ei}^2 + 32c_{e11}\pi^3\omega_{ei}^3 + 20c_{e12}\pi^2\omega_{ei}^4 + 12c_{e13}\pi\omega_{ei}^5 + 7c_{e14}\omega_{ei}^6 + 64c_{e8}\pi^6 \\
& + 64c_{e9}\pi^5\omega_{ei}, \quad (\text{E.8})
\end{aligned}$$

$$\begin{aligned}
\mathbf{p}_5 = & 32c_{e10}\pi^4\omega_{ei}^3 + 20c_{e11}\pi^3\omega_{ei}^4 + 12c_{e12}\pi^2\omega_{ei}^5 + 7c_{e13}\pi\omega_{ei}^6 + 4c_{e14}\omega_{ei}^7 + 64c_{e7}\pi^7 \\
& + 64c_{e8}\pi^6\omega_{ei} + 48c_{e9}\pi^5\omega_{ei}^2, \quad (\text{E.9})
\end{aligned}$$

$$\begin{aligned}
\mathbf{p}_6 = & 16c_{e1}\pi^8 + 4000c_{e10}c_{e3}\pi^4\omega_{ei}^3 + 2500c_{e11}c_{e3}\pi^3\omega_{ei}^4 + 1500c_{e12}c_{e3}\pi^2\omega_{ei}^5 \\
& + 875c_{e13}c_{e3}\pi\omega_{ei}^6 + 500c_{e14}c_{e3}\omega_{ei}^7 + 960c_{e2}\pi^7\omega_{ei} + 8000c_{e3}c_{e7}\pi^7 \\
& + 8000c_{e3}c_{e8}\pi^6\omega_{ei} + 6000c_{e3}c_{e9}\pi^5\omega_{ei}^2, \quad (\text{E.10})
\end{aligned}$$

$$\begin{aligned}
\mathbf{p}_7 = & 16c_{e1}\pi^8\mathcal{V}_e + 4000c_{e10}c_{e3}\pi^4\mathcal{V}_e\omega_{ei}^3 + 2500c_{e11}c_{e3}\pi^3\mathcal{V}_e\omega_{ei}^4 + 1500c_{e12}c_{e3}\pi^2\mathcal{V}_e\omega_{ei}^5 \\
& + 875c_{e13}c_{e3}\pi\mathcal{V}_e\omega_{ei}^6 + 500c_{e14}c_{e3}\mathcal{V}_e\omega_{ei}^7 + 960c_{e2}\pi^7\mathcal{V}_e\omega_{ei} + 8000c_{e3}c_{e7}\pi^7\mathcal{V}_e \\
& + 8000c_{e3}c_{e8}\pi^6\mathcal{V}_e\omega_{ei} + 6000c_{e3}c_{e9}\pi^5\mathcal{V}_e\omega_{ei}^2, \quad (\text{E.11})
\end{aligned}$$

$$\begin{aligned}
\mathbf{p}_8 = & 32c_{e1}\pi^8\omega_{ei} + 2000c_{e10}c_{e3}\pi^4\omega_{ei}^4 + 1000c_{e11}c_{e3}\pi^3\omega_{ei}^5 + 500c_{e12}c_{e3}\pi^2\omega_{ei}^6 \\
& + 250c_{e13}c_{e3}\pi\omega_{ei}^7 + 125c_{e14}c_{e3}\omega_{ei}^8 + 960c_{e2}\pi^7\omega_{ei}^2 + 16000c_{e3}c_{e7}\pi^7\omega_{ei} \\
& + 8000c_{e3}c_{e8}\pi^6\omega_{ei}^2 + 4000c_{e3}c_{e9}\pi^5\omega_{ei}^3, \quad (\text{E.12})
\end{aligned}$$

$$\begin{aligned}
\mathbf{p}_9 = & 1200c_{e10}c_{e3}\pi^4\omega_{ei}^2 + 1000c_{e11}c_{e3}\pi^3\omega_{ei}^3 + 750c_{e12}c_{e3}\pi^2\omega_{ei}^4 + 525c_{e13}c_{e3}\pi\omega_{ei}^5 \\
& + 350c_{e14}c_{e3}\omega_{ei}^6 + 96c_{e2}\pi^7 + 800c_{e3}c_{e8}\pi^6 + 1200c_{e3}c_{e9}\pi^5\omega_{ei}, \quad (\text{E.13})
\end{aligned}$$

$$\mathbf{p}_{10} = 48c_{e10}\pi^4\omega_{ei}^2 + 40c_{e11}\pi^3\omega_{ei}^3 + 30c_{e12}\pi^2\omega_{ei}^4 + 21c_{e13}\pi\omega_{ei}^5 + 14c_{e14}\omega_{ei}^6 + 32c_{e8}\pi^6$$

$$+ 48c_{e9}\pi^5\omega_{ei}, \quad (\text{E.14})$$

$$\begin{aligned} \mathbf{p}_{11} = & 3840c_{e10}^2\pi^8\omega_{ei}^4 + 5376c_{e10}c_{e11}\pi^7\omega_{ei}^5 + 3584c_{e10}c_{e12}\pi^6\omega_{ei}^6 + 2304c_{e10}c_{e13}\pi^5\omega_{ei}^7 \\ & + 1440c_{e10}c_{e14}\pi^4\omega_{ei}^8 + 12288c_{e10}c_{e7}\pi^{11}\omega_{ei} + 12288c_{e10}c_{e8}\pi^{10}\omega_{ei}^2 \\ & + 10240c_{e10}c_{e9}\pi^9\omega_{ei}^3 + 1792c_{e11}^2\pi^6\omega_{ei}^6 + 2304c_{e11}c_{e12}\pi^5\omega_{ei}^7 + 1440c_{e11}c_{e13}\pi^4\omega_{ei}^8 \\ & + 880c_{e11}c_{e14}\pi^3\omega_{ei}^9 + 12288c_{e11}c_{e7}\pi^{10}\omega_{ei}^2 + 10240c_{e11}c_{e8}\pi^9\omega_{ei}^3 \\ & + 7680c_{e11}c_{e9}\pi^8\omega_{ei}^4 + 720c_{e12}^2\pi^4\omega_{ei}^8 + 880c_{e12}c_{e13}\pi^3\omega_{ei}^9 + 528c_{e12}c_{e14}\pi^2\omega_{ei}^{10} \\ & + 10240c_{e12}c_{e7}\pi^9\omega_{ei}^3 + 7680c_{e12}c_{e8}\pi^8\omega_{ei}^4 + 5376c_{e12}c_{e9}\pi^7\omega_{ei}^5 + 264c_{e13}^2\pi^2\omega_{ei}^{10} \\ & + 312c_{e13}c_{e14}\pi\omega_{ei}^{11} + 7680c_{e13}c_{e7}\pi^8\omega_{ei}^4 + 5376c_{e13}c_{e8}\pi^7\omega_{ei}^5 + 3584c_{e13}c_{e9}\pi^6\omega_{ei}^6 \\ & + 91c_{e14}^2\omega_{ei}^{12} + 5376c_{e14}c_{e7}\pi^7\omega_{ei}^5 + 3584c_{e14}c_{e8}\pi^6\omega_{ei}^6 + 2304c_{e14}c_{e9}\pi^5\omega_{ei}^7 \\ & + 8192c_{e7}c_{e9}\pi^{12} + 4096c_{e8}^2\pi^{12} + 12288c_{e8}c_{e9}\pi^{11}\omega_{ei} + 6144c_{e9}^2\pi^{10}\omega_{ei}^2. \end{aligned} \quad (\text{E.15})$$

## E.2 Parallel Hybrid Electric Vehicle

To reduce the dimension of dimension-related parameters of FACE for parallel hybrid-electric vehicles, the piece-wise linear model of light-duty engines in Chapter 2.2.2 has been rewritten as

$$P_{ef}(\omega_e, P_e) = \begin{cases} k_{f0}\omega_e + k_{f1}\omega_e^2 + (k_{f2} + k_{f3}\omega_e + k_{f4}\omega_e^2)P_e, & P_e \leq P_{ec}(\omega_e), \\ k_{f0}\omega_e + k_{f1}\omega_e^2 + (k_{f2} - k_{f5} + k_{f3}\omega_e + k_{f4}\omega_e^2)P_{ec} + k_{f5}P_e, & P_e \geq P_{ec}(\omega_e), \end{cases} \quad (\text{E.16})$$

where parameters  $k_{fi}$  ( $i = 0, \dots, 5$ ) are derived from Chapter 2.2.2.

The dimension-related parameters are given as follows.

$$D_{10}^{e1v} = \frac{C_{v0}k_{f2}}{k_{t6}} + \frac{k_{f0}\mathcal{R}_{dn}}{R_w}, \quad (\text{E.17})$$

$$D_{11}^{e1v} = \frac{k_{f2}m_v}{k_{t6}} \quad (\text{E.18})$$

$$D_{20}^{e1v} = \frac{C_{v0}k_{f3}\mathcal{R}_{dn}}{k_{t6}R_w} + \frac{C_{v1}k_{f2}}{k_{t6}} + \frac{k_{f1}\mathcal{R}_{dn}^2}{R_w^2} - \frac{k_{f2}^2\mathcal{R}_{dn}^2R_m^2}{2k_{b4}k_{m4}R_w^2s} + \frac{k_{f2}k_{m3}\mathcal{R}_{dn}^2R_m^2}{2k_{m4}R_w^2}, \quad (\text{E.19})$$

$$D_{21}^{e1v} = \frac{k_{f3}m_v\mathcal{R}_{dn}}{k_{t6}R_w}, \quad (\text{E.20})$$

$$D_{30}^{e1v} = \frac{C_{v0}k_{f4}\mathcal{R}_{dn}^2}{k_{t6}R_w^2} + \frac{C_{v1}k_{f3}\mathcal{R}_{dn}}{k_{t6}R_w} + \frac{C_{v2}k_{f2}}{k_{t6}} - \frac{k_{f2}k_{f3}\mathcal{R}_{dn}^3R_m^2}{k_{b4}k_{m4}R_w^3s} + \frac{k_{f3}k_{m3}\mathcal{R}_{dn}^3R_m^2}{2k_{m4}R_w^3}, \quad (\text{E.21})$$

$$D_{31}^{e1v} = \frac{k_{f4}m_v\mathcal{R}_{dn}^2}{k_{t6}R_w^2}, \quad (\text{E.22})$$

$$D_{40}^{e1v} = \frac{C_{v1}k_{f4}\mathcal{R}_{dn}^2}{k_{t6}R_w^2} + \frac{C_{v2}k_{f3}\mathcal{R}_{dn}}{k_{t6}R_w} - \frac{k_{f2}k_{f4}\mathcal{R}_{dn}^4R_m^2}{k_{b4}k_{m4}R_w^4s} - \frac{k_{f3}^2\mathcal{R}_{dn}^4R_m^2}{2k_{b4}k_{m4}R_w^4s} + \frac{k_{f4}k_{m3}\mathcal{R}_{dn}^4R_m^2}{2k_{m4}R_w^4}, \quad (\text{E.23})$$

$$D_{50}^{e1v} = \frac{C_{v2}k_{f4}\mathcal{R}_{dn}^2}{k_{t6}R_w^2} - \frac{k_{f3}k_{f4}\mathcal{R}_{dn}^5R_m^2}{k_{b4}k_{m4}R_w^5s}, \quad (\text{E.24})$$

$$D_{60}^{e1v} = -\frac{k_{f4}^2\mathcal{R}_{dn}^6R_m^2}{2k_{b4}k_{m4}R_w^6s}, \quad (\text{E.25})$$

$$D_{10}^{e2v} = \frac{C_{v0}k_{f2}}{k_{t6}} + \frac{k_{f0}\mathcal{R}_{dn}}{R_w}, \quad (\text{E.26})$$

$$D_{11}^{e2v} = \frac{k_{f2}m_v}{k_{t6}}, \quad (\text{E.27})$$

$$D_{20}^{e2v} = \frac{C_{v0}k_{f3}\mathcal{R}_{dn}}{k_{t6}R_w} + \frac{C_{v1}k_{f2}}{k_{t6}} + \frac{k_{f1}\mathcal{R}_{dn}^2}{R_w^2} - \frac{k_{f2}^2\mathcal{R}_{dn}^2R_m^2}{2k_{b6}k_{m4}R_w^2s} + \frac{k_{f2}k_{m3}\mathcal{R}_{dn}^2R_m^2}{2k_{m4}R_w^2}, \quad (\text{E.28})$$

$$D_{21}^{e2v} = \frac{k_{f3}m_v\mathcal{R}_{dn}}{k_{t6}R_w}, \quad (\text{E.29})$$

$$D_{30}^{e2v} = \frac{C_{v0}k_{f4}\mathcal{R}_{dn}^2}{k_{t6}R_w^2} + \frac{C_{v1}k_{f3}\mathcal{R}_{dn}}{k_{t6}R_w} + \frac{C_{v2}k_{f2}}{k_{t6}} - \frac{k_{f2}k_{f3}\mathcal{R}_{dn}^3R_m^2}{k_{b6}k_{m4}R_w^3s} + \frac{k_{f3}k_{m3}\mathcal{R}_{dn}^3R_m^2}{2k_{m4}R_w^3}, \quad (\text{E.30})$$

$$D_{31}^{e2v} = \frac{k_{f4}m_v\mathcal{R}_{dn}^2}{k_{t6}R_w^2}, \quad (\text{E.31})$$

$$D_{40}^{e2v} = \frac{C_{v1}k_{f4}\mathcal{R}_{dn}^2}{k_{t6}R_w^2} + \frac{C_{v2}k_{f3}\mathcal{R}_{dn}}{k_{t6}R_w} - \frac{k_{f2}k_{f4}\mathcal{R}_{dn}^4R_m^2}{k_{b6}k_{m4}R_w^4s} - \frac{k_{f3}^2\mathcal{R}_{dn}^4R_m^2}{2k_{b6}k_{m4}R_w^4s} + \frac{k_{f4}k_{m3}\mathcal{R}_{dn}^4R_m^2}{2k_{m4}R_w^4}, \quad (\text{E.32})$$

$$D_{50}^{e2v} = \frac{C_{v2}k_{f4}\mathcal{R}_{dn}^2}{k_{t6}R_w^2} - \frac{k_{f3}k_{f4}\mathcal{R}_{dn}^5R_m^2}{k_{b6}k_{m4}R_w^5s}, \quad (\text{E.33})$$

$$D_{60}^{e2v} = -\frac{k_{f4}^2\mathcal{R}_{dn}^6R_m^2}{2k_{b6}k_{m4}R_w^6s}, \quad (\text{E.34})$$

$$D_{ij}^{e3v} = 0, \quad (\text{E.35})$$

$$D_{ij}^{e4v} = 0, \quad (\text{E.36})$$

$$D_{10}^{e5v} = \frac{k_{f0}\mathcal{R}_{dn}}{R_w} + \frac{k_{f2}k_{f6}k_{fc}\mathcal{R}_{dn}}{R_w}, \quad (\text{E.37})$$

$$D_{20}^{e5v} = \frac{k_{f1}\mathcal{R}_{dn}^2}{R_w^2} + \frac{k_{f2}k_{f7}k_{fc}\mathcal{R}_{dn}^2}{R_w^2} + \frac{k_{f3}k_{f6}k_{fc}\mathcal{R}_{dn}^2}{R_w^2}, \quad (\text{E.38})$$

$$D_{30}^{e5v} = \frac{k_{f2}k_{f8}k_{fc}\mathcal{R}_{dn}^3}{R_w^3} + \frac{k_{f3}k_{f7}k_{fc}\mathcal{R}_{dn}^3}{R_w^3} + \frac{k_{f4}k_{f6}k_{fc}\mathcal{R}_{dn}^3}{R_w^3}, \quad (\text{E.39})$$

$$D_{40}^{e5v} = \frac{k_{f3}k_{f8}k_{fc}\mathcal{R}_{dn}^4}{R_w^4} + \frac{k_{f4}k_{f7}k_{fc}\mathcal{R}_{dn}^4}{R_w^4}, \quad (\text{E.40})$$

$$D_{50}^{e5v} = \frac{k_{f4}k_{f8}k_{fc}\mathcal{R}_{dn}^5}{R_w^5}, \quad (\text{E.41})$$

$$D_{10}^{e6v} = \frac{k_{f0}\mathcal{R}_{dn}}{R_w} + \frac{k_{f2}k_{f6}k_{fc}\mathcal{R}_{dn}}{R_w}, \quad (\text{E.42})$$

$$D_{20}^{e6v} = \frac{k_{f1}\mathcal{R}_{dn}^2}{R_w^2} + \frac{k_{f2}k_{f7}k_{fc}\mathcal{R}_{dn}^2}{R_w^2} + \frac{k_{f3}k_{f6}k_{fc}\mathcal{R}_{dn}^2}{R_w^2}, \quad (\text{E.43})$$

$$D_{30}^{e6v} = \frac{k_{f2}k_{f8}k_{fc}\mathcal{R}_{dn}^3}{R_w^3} + \frac{k_{f3}k_{f7}k_{fc}\mathcal{R}_{dn}^3}{R_w^3} + \frac{k_{f4}k_{f6}k_{fc}\mathcal{R}_{dn}^3}{R_w^3}, \quad (\text{E.44})$$

$$D_{40}^{e6v} = \frac{k_{f3}k_{f8}k_{fc}\mathcal{R}_{dn}^4}{R_w^4} + \frac{k_{f4}k_{f7}k_{fc}\mathcal{R}_{dn}^4}{R_w^4}, \quad (\text{E.45})$$

$$D_{50}^{e6v} = \frac{k_{f4}k_{f8}k_{fc}\mathcal{R}_{dn}^5}{R_w^5}, \quad (\text{E.46})$$

$$D_{10}^{e7v} = \frac{C_{v0}k_{f2}}{k_{t6}} + \frac{k_{f0}\mathcal{R}_{dn}}{R_w} - \frac{k_{f2}\mathcal{R}_{dn}R_m\bar{T}_m}{R_w}, \quad (\text{E.47})$$

$$D_{11}^{e7v} = \frac{k_{f2}m_v}{k_{t6}}, \quad (\text{E.48})$$

$$D_{20}^{e7v} = \frac{C_{v0}k_{f3}\mathcal{R}_{dn}}{k_{t6}R_w} + \frac{C_{v1}k_{f2}}{k_{t6}} + \frac{k_{f1}\mathcal{R}_{dn}^2}{R_w^2} - \frac{k_{f3}\mathcal{R}_{dn}^2R_m\bar{T}_m}{R_w^2}, \quad (\text{E.49})$$

$$D_{21}^{e7v} = \frac{k_{f3}m_v\mathcal{R}_{dn}}{k_{t6}R_w}, \quad (\text{E.50})$$

$$D_{30}^{e7v} = \frac{C_{v0}k_{f4}\mathcal{R}_{dn}^2}{k_{t6}R_w^2} + \frac{C_{v1}k_{f3}\mathcal{R}_{dn}}{k_{t6}R_w} + \frac{C_{v2}k_{f2}}{k_{t6}} - \frac{k_{f4}\mathcal{R}_{dn}^3R_m\bar{T}_m}{R_w^3}, \quad (\text{E.51})$$

$$D_{31}^{e7v} = \frac{k_{f4}m_v\mathcal{R}_{dn}^2}{k_{t6}R_w^2}, \quad (\text{E.52})$$

$$D_{40}^{e7v} = \frac{C_{v1}k_{f4}\mathcal{R}_{dn}^2}{k_{t6}R_w^2} + \frac{C_{v2}k_{f3}\mathcal{R}_{dn}}{k_{t6}R_w}, \quad (\text{E.53})$$

$$D_{50}^{e7v} = \frac{C_{v2}k_{f4}\mathcal{R}_{dn}^2}{k_{t6}R_w^2}, \quad (\text{E.54})$$

$$D_{10}^{e8v} = \frac{C_{v0}k_{f2}}{k_{t6}} + \frac{k_{f0}\mathcal{R}_{dn}}{R_w} - \frac{k_{f2}\mathcal{R}_{dn}R_m\bar{T}_m}{R_w}, \quad (\text{E.55})$$

$$D_{11}^{e8v} = \frac{k_{f2}m_v}{k_{t6}}, \quad (\text{E.56})$$

$$D_{20}^{e8v} = \frac{C_{v0}k_{f3}\mathcal{R}_{dn}}{k_{t6}R_w} + \frac{C_{v1}k_{f2}}{k_{t6}} + \frac{k_{f1}\mathcal{R}_{dn}^2}{R_w^2} - \frac{k_{f3}\mathcal{R}_{dn}^2R_m\bar{T}_m}{R_w^2}, \quad (\text{E.57})$$

$$D_{21}^{e8v} = \frac{k_{f3}m_v\mathcal{R}_{dn}}{k_{t6}R_w}, \quad (\text{E.58})$$

$$D_{30}^{e8v} = \frac{C_{v0}k_{f4}\mathcal{R}_{dn}^2}{k_{t6}R_w^2} + \frac{C_{v1}k_{f3}\mathcal{R}_{dn}}{k_{t6}R_w} + \frac{C_{v2}k_{f2}}{k_{t6}} - \frac{k_{f4}\mathcal{R}_{dn}^3 R_m T_m}{R_w^3}, \quad (\text{E.59})$$

$$D_{31}^{e8v} = \frac{k_{f4}m_v\mathcal{R}_{dn}^2}{k_{t6}R_w^2}, \quad (\text{E.60})$$

$$D_{40}^{e8v} = \frac{C_{v1}k_{f4}\mathcal{R}_{dn}^2}{k_{t6}R_w^2} + \frac{C_{v2}k_{f3}\mathcal{R}_{dn}}{k_{t6}R_w}, \quad (\text{E.61})$$

$$D_{50}^{e8v} = \frac{C_{v2}k_{f4}\mathcal{R}_{dn}^2}{k_{t6}R_w^2}, \quad (\text{E.62})$$

$$D_{10}^{e9v} = \frac{k_{f0}\mathcal{R}_{dn}}{R_w} + \frac{0.8k_{f2}k_{f6}\mathcal{R}_{dn}}{R_w} + \frac{0.2k_{f6}k_{f6}\mathcal{R}_{dn}}{R_w}, \quad (\text{E.63})$$

$$D_{20}^{e9v} = \frac{1.k_{f1}\mathcal{R}_{dn}^2}{R_w^2} + \frac{0.8k_{f2}k_{f7}\mathcal{R}_{dn}^2}{R_w^2} + \frac{0.8k_{f3}k_{f6}\mathcal{R}_{dn}^2}{R_w^2} + \frac{0.2k_{f6}k_{f7}\mathcal{R}_{dn}^2}{R_w^2}, \quad (\text{E.64})$$

$$D_{30}^{e9v} = \frac{0.8k_{f2}k_{f8}\mathcal{R}_{dn}^3}{R_w^3} + \frac{0.8k_{f3}k_{f7}\mathcal{R}_{dn}^3}{R_w^3} + \frac{0.8k_{f4}k_{f6}\mathcal{R}_{dn}^3}{R_w^3} + \frac{0.2k_{f6}k_{f8}\mathcal{R}_{dn}^3}{R_w^3}, \quad (\text{E.65})$$

$$D_{40}^{e9v} = \frac{0.8k_{f3}k_{f8}\mathcal{R}_{dn}^4}{R_w^4} + \frac{0.8k_{f4}k_{f7}\mathcal{R}_{dn}^4}{R_w^4}, \quad (\text{E.66})$$

$$D_{50}^{e9v} = \frac{0.8k_{f4}k_{f8}\mathcal{R}_{dn}^5}{R_w^5}, \quad (\text{E.67})$$

$$D_{10}^{e10v} = \frac{k_{f0}\mathcal{R}_{dn}}{R_w} + \frac{0.8k_{f2}k_{f6}\mathcal{R}_{dn}}{R_w} + \frac{0.2k_{f6}k_{f6}\mathcal{R}_{dn}}{R_w}, \quad (\text{E.68})$$

$$D_{20}^{e10v} = \frac{1.k_{f1}\mathcal{R}_{dn}^2}{R_w^2} + \frac{0.8k_{f2}k_{f7}\mathcal{R}_{dn}^2}{R_w^2} + \frac{0.8k_{f3}k_{f6}\mathcal{R}_{dn}^2}{R_w^2} + \frac{0.2k_{f6}k_{f7}\mathcal{R}_{dn}^2}{R_w^2}, \quad (\text{E.69})$$

$$D_{30}^{e10v} = \frac{0.8k_{f2}k_{f8}\mathcal{R}_{dn}^3}{R_w^3} + \frac{0.8k_{f3}k_{f7}\mathcal{R}_{dn}^3}{R_w^3} + \frac{0.8k_{f4}k_{f6}\mathcal{R}_{dn}^3}{R_w^3} + \frac{0.2k_{f6}k_{f8}\mathcal{R}_{dn}^3}{R_w^3}, \quad (\text{E.70})$$

$$D_{40}^{e10v} = \frac{0.8k_{f3}k_{f8}\mathcal{R}_{dn}^4}{R_w^4} + \frac{0.8k_{f4}k_{f7}\mathcal{R}_{dn}^4}{R_w^4}, \quad (\text{E.71})$$

$$D_{50}^{e10v} = \frac{0.8k_{f4}k_{f8}\mathcal{R}_{dn}^5}{R_w^5}, \quad (\text{E.72})$$

$$D_{00}^{b1v} = k_{b3} + k_{b4}k_{m0}, \quad (\text{E.73})$$

$$D_{10}^{b1v} = \frac{k_{b4}k_{m1}\mathcal{R}_{dn}R_m}{R_w}, \quad (\text{E.74})$$

$$D_{20}^{b1v} = \frac{k_{f2}^2\mathcal{R}_{dn}^2R_m^2}{4k_{b4}k_{m4}R_w^2s^2} + \frac{k_{b4}k_{m2}\mathcal{R}_{dn}^2R_m^2}{R_w^2} - \frac{k_{b4}k_{m3}^2\mathcal{R}_{dn}^2R_m^2}{4k_{m4}R_w^2}, \quad (\text{E.75})$$

$$\mathcal{D}_{30}^{b1v} = \frac{k_{f2}k_{f3}\mathcal{R}_{dn}^3 R_m^2}{2k_{b4}k_{m4}R_w^3 s^2}, \quad (\text{E.76})$$

$$\mathcal{D}_{40}^{b1v} = \frac{k_{f2}k_{f4}\mathcal{R}_{dn}^4 R_m^2}{2k_{b4}k_{m4}R_w^4 s^2} + \frac{k_{f3}^2\mathcal{R}_{dn}^4 R_m^2}{4k_{b4}k_{m4}R_w^4 s^2}, \quad (\text{E.77})$$

$$\mathcal{D}_{50}^{b1v} = \frac{k_{f3}k_{f4}\mathcal{R}_{dn}^5 R_m^2}{2k_{b4}k_{m4}R_w^5 s^2}, \quad (\text{E.78})$$

$$\mathcal{D}_{60}^{b1v} = \frac{k_{f4}^2\mathcal{R}_{dn}^6 R_m^2}{4k_{b4}k_{m4}R_w^6 s^2}, \quad (\text{E.79})$$

$$\mathcal{D}_{00}^{b2v} = k_{b5} + k_{b6}k_{m0}, \quad (\text{E.80})$$

$$\mathcal{D}_{10}^{b2v} = \frac{k_{b6}k_{m1}\mathcal{R}_{dn}R_m}{R_w}, \quad (\text{E.81})$$

$$\mathcal{D}_{20}^{b2v} = \frac{k_{f2}^2\mathcal{R}_{dn}^2 R_m^2}{4k_{b6}k_{m4}R_w^2 s^2} + \frac{k_{b6}k_{m2}\mathcal{R}_{dn}^2 R_m^2}{R_w^2} - \frac{k_{b6}k_{m3}^2\mathcal{R}_{dn}^2 R_m^2}{4k_{m4}R_w^2}, \quad (\text{E.82})$$

$$\mathcal{D}_{30}^{b2v} = \frac{k_{f2}k_{f3}\mathcal{R}_{dn}^3 R_m^2}{2k_{b6}k_{m4}R_w^3 s^2}, \quad (\text{E.83})$$

$$\mathcal{D}_{40}^{b2v} = \frac{k_{f2}k_{f4}\mathcal{R}_{dn}^4 R_m^2}{2k_{b6}k_{m4}R_w^4 s^2} + \frac{k_{f3}^2\mathcal{R}_{dn}^4 R_m^2}{4k_{b6}k_{m4}R_w^4 s^2}, \quad (\text{E.84})$$

$$\mathcal{D}_{50}^{b2v} = \frac{k_{f3}k_{f4}\mathcal{R}_{dn}^5 R_m^2}{2k_{b6}k_{m4}R_w^5 s^2}, \quad (\text{E.85})$$

$$\mathcal{D}_{60}^{b2v} = \frac{k_{f4}^2\mathcal{R}_{dn}^6 R_m^2}{4k_{b6}k_{m4}R_w^6 s^2}, \quad (\text{E.86})$$

$$\mathcal{D}_{00}^{b3v} = \frac{C_{v0}k_{b4}k_{m4}R_w^2}{k_{t6}^2\mathcal{R}_{dn}^2 R_m^2} + k_{b3} + k_{b4}k_{m0}, \quad (\text{E.87})$$

$$\mathcal{D}_{01}^{b3v} = \frac{2C_{v0}k_{b4}k_{m4}m_v R_w^2}{k_{t6}^2\mathcal{R}_{dn}^2 R_m^2}, \quad (\text{E.88})$$

$$\mathcal{D}_{02}^{b3v} = \frac{k_{b4}k_{m4}m_v^2 R_w^2}{k_{t6}^2\mathcal{R}_{dn}^2 R_m^2}, \quad (\text{E.89})$$

$$\mathcal{D}_{10}^{b3v} = \frac{2C_{v0}C_{v1}k_{b4}k_{m4}R_w^2}{k_{t6}^2\mathcal{R}_{dn}^2 R_m^2} + \frac{C_{v0}k_{b4}k_{m3}}{k_{t6}} + \frac{k_{b4}k_{m1}\mathcal{R}_{dn}R_m}{R_w}, \quad (\text{E.90})$$

$$\mathcal{D}_{11}^{b3v} = \frac{2C_{v1}k_{b4}k_{m4}m_v R_w^2}{k_{t6}^2\mathcal{R}_{dn}^2 R_m^2} + \frac{k_{b4}k_{m3}m_v}{k_{t6}}, \quad (\text{E.91})$$

$$\mathcal{D}_{20}^{b3v} = \frac{2C_{v0}C_{v2}k_{b4}k_{m4}R_w^2}{k_{t6}^2\mathcal{R}_{dn}^2 R_m^2} + \frac{C_{v1}^2k_{b4}k_{m4}R_w^2}{k_{t6}^2\mathcal{R}_{dn}^2 R_m^2} + \frac{C_{v1}k_{b4}k_{m3}}{k_{t6}} + \frac{k_{b4}k_{m2}\mathcal{R}_{dn}^2 R_m^2}{R_w^2}, \quad (\text{E.92})$$

$$\mathcal{D}_{21}^{b3v} = \frac{2C_{v2}k_{b4}k_{m4}m_v R_w^2}{k_{t6}^2 \mathcal{R}_{dn}^2 R_m^2}, \quad (\text{E.93})$$

$$\mathcal{D}_{30}^{b3v} = \frac{2C_{v1}C_{v2}k_{b4}k_{m4}R_w^2}{k_{t6}^2 \mathcal{R}_{dn}^2 R_m^2} + \frac{C_{v2}k_{b4}k_{m3}}{k_{t6}}, \quad (\text{E.94})$$

$$\mathcal{D}_{40}^{b3v} = \frac{C_{v2}^2 k_{b4} k_{m4} R_w^2}{k_{t6}^2 \mathcal{R}_{dn}^2 R_m^2}, \quad (\text{E.95})$$

$$\mathcal{D}_{00}^{b4v} = \frac{C_{v0}^2 k_{b6} k_{m4} k_{t6}^2 R_w^2}{\mathcal{R}_{dn}^2 R_m^2} + k_{b5} + k_{b6} k_{m0}, \quad (\text{E.96})$$

$$\mathcal{D}_{01}^{b4v} = \frac{2C_{v0}k_{b6}k_{m4}k_{t6}^2 m_v R_w^2}{\mathcal{R}_{dn}^2 R_m^2}, \quad (\text{E.97})$$

$$\mathcal{D}_{02}^{b4v} = \frac{k_{b6}k_{m4}k_{t6}^2 m_v^2 R_w^2}{\mathcal{R}_{dn}^2 R_m^2}, \quad (\text{E.98})$$

$$\mathcal{D}_{10}^{b4v} = \frac{2C_{v0}C_{v1}k_{b6}k_{m4}k_{t6}^2 R_w^2}{\mathcal{R}_{dn}^2 R_m^2} + C_{v0}k_{b6}k_{m3}k_{t6} + \frac{k_{b6}k_{m1}\mathcal{R}_{dn}R_m}{R_w}, \quad (\text{E.99})$$

$$\mathcal{D}_{11}^{b4v} = \frac{2C_{v1}k_{b6}k_{m4}k_{t6}^2 m_v R_w^2}{\mathcal{R}_{dn}^2 R_m^2} + k_{b6}k_{m3}k_{t6}m_v, \quad (\text{E.100})$$

$$\mathcal{D}_{20}^{b4v} = \frac{2C_{v0}C_{v2}k_{b6}k_{m4}k_{t6}^2 R_w^2}{\mathcal{R}_{dn}^2 R_m^2} + \frac{C_{v1}^2 k_{b6} k_{m4} k_{t6}^2 R_w^2}{\mathcal{R}_{dn}^2 R_m^2} + \frac{k_{b6}k_{m2}\mathcal{R}_{dn}^2 R_m^2}{R_w^2} + C_{v1}k_{b6}k_{m3}k_{t6}, \quad (\text{E.101})$$

$$\mathcal{D}_{21}^{b4v} = \frac{2C_{v2}k_{b6}k_{m4}k_{t6}^2 m_v R_w^2}{\mathcal{R}_{dn}^2 R_m^2}, \quad (\text{E.102})$$

$$\mathcal{D}_{30}^{b4v} = \frac{2C_{v1}C_{v2}k_{b6}k_{m4}k_{t6}^2 R_w^2}{\mathcal{R}_{dn}^2 R_m^2} + C_{v2}k_{b6}k_{m3}k_{t6}, \quad (\text{E.103})$$

$$\mathcal{D}_{40}^{b4v} = \frac{C_{v2}^2 k_{b6} k_{m4} k_{t6}^2 R_w^2}{\mathcal{R}_{dn}^2 R_m^2}, \quad (\text{E.104})$$

$$\mathcal{D}_{00}^{b5v} = \frac{C_{v0}^2 k_{b4} k_{m4} R_w^2}{k_{t6}^2 \mathcal{R}_{dn}^2 R_m^2} - \frac{2C_{v0}k_{b4}k_{f6}k_{fc}k_{m4}R_w}{k_{t6}\mathcal{R}_{dn}R_m^2} + k_{b3} + \frac{k_{b4}k_{f6}^2 k_{fc}^2 k_{m4}}{R_m^2} + k_{b4}k_{m0}, \quad (\text{E.105})$$

$$\mathcal{D}_{01}^{b5v} = \frac{2C_{v0}k_{b4}k_{m4}m_v R_w^2}{k_{t6}^2 \mathcal{R}_{dn}^2 R_m^2} - \frac{2k_{b4}k_{f6}k_{fc}k_{m4}m_v R_w}{k_{t6}\mathcal{R}_{dn}R_m^2}, \quad (\text{E.106})$$

$$\mathcal{D}_{02}^{b5v} = \frac{k_{b4}k_{m4}m_v^2 R_w^2}{k_{t6}^2 \mathcal{R}_{dn}^2 R_m^2}, \quad (\text{E.107})$$

$$\mathcal{D}_{10}^{b5v} = \frac{2C_{v0}C_{v1}k_{b4}k_{m4}R_w^2}{k_{t6}^2 \mathcal{R}_{dn}^2 R_m^2} - \frac{2C_{v0}k_{b4}k_{f7}k_{fc}k_{m4}}{k_{t6}R_m^2} + \frac{C_{v0}k_{b4}k_{m3}}{k_{t6}} - \frac{2C_{v1}k_{b4}k_{f6}k_{fc}k_{m4}R_w}{k_{t6}\mathcal{R}_{dn}R_m^2}$$

$$+ \frac{2k_{b4}k_{f6}k_{f7}k_{fc}^2k_{m4}\mathcal{R}_{dn}}{R_m^2R_w} - \frac{k_{b4}k_{f6}k_{fc}k_{m3}\mathcal{R}_{dn}}{R_w} + \frac{k_{b4}k_{m1}\mathcal{R}_{dn}R_m}{R_w}, \quad (\text{E.108})$$

$$\mathcal{D}_{11}^{b5v} = \frac{2C_{v1}k_{b4}k_{m4}m_vR_w^2}{k_{t6}^2\mathcal{R}_{dn}^2R_m^2} - \frac{2k_{b4}k_{f7}k_{fc}k_{m4}m_v}{k_{t6}R_m^2} + \frac{k_{b4}k_{m3}m_v}{k_{t6}}, \quad (\text{E.109})$$

$$\begin{aligned} \mathcal{D}_{20}^{b5v} &= \frac{2C_{v0}C_{v2}k_{b4}k_{m4}R_w^2}{k_{t6}^2\mathcal{R}_{dn}^2R_m^2} - \frac{2C_{v0}k_{b4}k_{f8}k_{fc}k_{m4}\mathcal{R}_{dn}}{k_{t6}R_m^2R_w} + \frac{C_{v1}^2k_{b4}k_{m4}R_w^2}{k_{t6}^2\mathcal{R}_{dn}^2R_m^2} - \frac{2C_{v1}k_{b4}k_{f7}k_{fc}k_{m4}}{k_{t6}R_m^2} \\ &+ \frac{C_{v1}k_{b4}k_{m3}}{k_{t6}} - \frac{2C_{v2}k_{b4}k_{f6}k_{fc}k_{m4}R_w}{k_{t6}\mathcal{R}_{dn}R_m^2} + \frac{2k_{b4}k_{f6}k_{f8}k_{fc}^2k_{m4}\mathcal{R}_{dn}^2}{R_m^2R_w^2} + \frac{k_{b4}k_{f7}^2k_{fc}^2k_{m4}\mathcal{R}_{dn}^2}{R_m^2R_w^2} \\ &- \frac{k_{b4}k_{f7}k_{fc}k_{m3}\mathcal{R}_{dn}^2}{R_w^2} + \frac{k_{b4}k_{m2}\mathcal{R}_{dn}^2R_m^2}{R_w^2}, \end{aligned} \quad (\text{E.110})$$

$$\mathcal{D}_{21}^{b5v} = \frac{2C_{v2}k_{b4}k_{m4}m_vR_w^2}{k_{t6}^2\mathcal{R}_{dn}^2R_m^2} - \frac{2k_{b4}k_{f8}k_{fc}k_{m4}m_v\mathcal{R}_{dn}}{k_{t6}R_m^2R_w}, \quad (\text{E.111})$$

$$\begin{aligned} \mathcal{D}_{30}^{b5v} &= \frac{2C_{v1}C_{v2}k_{b4}k_{m4}R_w^2}{k_{t6}^2\mathcal{R}_{dn}^2R_m^2} - \frac{2C_{v1}k_{b4}k_{f8}k_{fc}k_{m4}\mathcal{R}_{dn}}{k_{t6}R_m^2R_w} - \frac{2C_{v2}k_{b4}k_{f7}k_{fc}k_{m4}}{k_{t6}R_m^2} \\ &+ \frac{C_{v2}k_{b4}k_{m3}}{k_{t6}} + \frac{2k_{b4}k_{f7}k_{f8}k_{fc}^2k_{m4}\mathcal{R}_{dn}^3}{R_m^2R_w^3} - \frac{k_{b4}k_{f8}k_{fc}k_{m3}\mathcal{R}_{dn}^3}{R_w^3}, \end{aligned} \quad (\text{E.112})$$

$$\mathcal{D}_{40}^{b5v} = \frac{C_{v2}^2k_{b4}k_{m4}R_w^2}{k_{t6}^2\mathcal{R}_{dn}^2R_m^2} - \frac{2C_{v2}k_{b4}k_{f8}k_{fc}k_{m4}\mathcal{R}_{dn}}{k_{t6}R_m^2R_w} + \frac{k_{b4}k_{f8}^2k_{fc}^2k_{m4}\mathcal{R}_{dn}^4}{R_m^2R_w^4}, \quad (\text{E.113})$$

$$\mathcal{D}_{00}^{b6v} = \frac{C_{v0}k_{b6}k_{m4}R_w^2}{k_{t6}^2\mathcal{R}_{dn}^2R_m^2} - \frac{2C_{v0}k_{b6}k_{f6}k_{fc}k_{m4}R_w}{k_{t6}\mathcal{R}_{dn}R_m^2} + k_{b5} + \frac{k_{b6}k_{f6}^2k_{fc}^2k_{m4}}{R_m^2} + k_{b6}k_{m0}, \quad (\text{E.114})$$

$$\mathcal{D}_{01}^{b6v} = \frac{2C_{v0}k_{b6}k_{m4}m_vR_w^2}{k_{t6}^2\mathcal{R}_{dn}^2R_m^2} - \frac{2k_{b6}k_{f6}k_{fc}k_{m4}m_vR_w}{k_{t6}\mathcal{R}_{dn}R_m^2}, \quad (\text{E.115})$$

$$\mathcal{D}_{02}^{b6v} = \frac{k_{b6}k_{m4}m_v^2R_w^2}{k_{t6}^2\mathcal{R}_{dn}^2R_m^2}, \quad (\text{E.116})$$

$$\begin{aligned} \mathcal{D}_{10}^{b6v} &= \frac{2C_{v0}C_{v1}k_{b6}k_{m4}R_w^2}{k_{t6}^2\mathcal{R}_{dn}^2R_m^2} - \frac{2C_{v0}k_{b6}k_{f7}k_{fc}k_{m4}}{k_{t6}R_m^2} + \frac{C_{v0}k_{b6}k_{m3}}{k_{t6}} - \frac{2C_{v1}k_{b6}k_{f6}k_{fc}k_{m4}R_w}{k_{t6}\mathcal{R}_{dn}R_m^2} \\ &+ \frac{2k_{b6}k_{f6}k_{f7}k_{fc}^2k_{m4}\mathcal{R}_{dn}}{R_m^2R_w} - \frac{k_{b6}k_{f6}k_{fc}k_{m3}\mathcal{R}_{dn}}{R_w} + \frac{k_{b6}k_{m1}\mathcal{R}_{dn}R_m}{R_w}, \end{aligned} \quad (\text{E.117})$$

$$\mathcal{D}_{11}^{b6v} = \frac{2C_{v1}k_{b6}k_{m4}m_vR_w^2}{k_{t6}^2\mathcal{R}_{dn}^2R_m^2} - \frac{2k_{b6}k_{f7}k_{fc}k_{m4}m_v}{k_{t6}R_m^2} + \frac{k_{b6}k_{m3}m_v}{k_{t6}}, \quad (\text{E.118})$$

$$\begin{aligned} \mathcal{D}_{20}^{b6v} &= \frac{2C_{v0}C_{v2}k_{b6}k_{m4}R_w^2}{k_{t6}^2\mathcal{R}_{dn}^2R_m^2} - \frac{2C_{v0}k_{b6}k_{f8}k_{fc}k_{m4}\mathcal{R}_{dn}}{k_{t6}R_m^2R_w} + \frac{C_{v1}^2k_{b6}k_{m4}R_w^2}{k_{t6}^2\mathcal{R}_{dn}^2R_m^2} - \frac{2C_{v1}k_{b6}k_{f7}k_{fc}k_{m4}}{k_{t6}R_m^2} \\ &+ \frac{C_{v1}k_{b6}k_{m3}}{k_{t6}} - \frac{2C_{v2}k_{b6}k_{f6}k_{fc}k_{m4}R_w}{k_{t6}\mathcal{R}_{dn}R_m^2} + \frac{2k_{b6}k_{f6}k_{f8}k_{fc}^2k_{m4}\mathcal{R}_{dn}^2}{R_m^2R_w^2} + \frac{k_{b6}k_{f7}^2k_{fc}^2k_{m4}\mathcal{R}_{dn}^2}{R_m^2R_w^2} \end{aligned}$$

$$- \frac{k_{b6}k_{f7}k_{fc}k_{m3}\mathcal{R}_{dn}^2}{R_w^2} + \frac{k_{b6}k_{m2}\mathcal{R}_{dn}^2 R_m^2}{R_w^2}, \quad (\text{E.119})$$

$$\mathcal{D}_{21}^{b6v} = \frac{2C_{v2}k_{b6}k_{m4}m_v R_w^2}{k_{t6}^2 \mathcal{R}_{dn}^2 R_m^2} - \frac{2k_{b6}k_{f8}k_{fc}k_{m4}m_v \mathcal{R}_{dn}}{k_{t6} R_m^2 R_w}, \quad (\text{E.120})$$

$$\begin{aligned} \mathcal{D}_{30}^{b6v} &= \frac{2C_{v1}C_{v2}k_{b6}k_{m4}R_w^2}{k_{t6}^2 \mathcal{R}_{dn}^2 R_m^2} - \frac{2C_{v1}k_{b6}k_{f8}k_{fc}k_{m4}\mathcal{R}_{dn}}{k_{t6} R_m^2 R_w} - \frac{2C_{v2}k_{b6}k_{f7}k_{fc}k_{m4}}{k_{t6} R_m^2} \\ &+ \frac{C_{v2}k_{b6}k_{m3}}{k_{t6}} + \frac{2k_{b6}k_{f7}k_{f8}k_{fc}^2 k_{m4}\mathcal{R}_{dn}^3}{R_m^2 R_w^3} - \frac{k_{b6}k_{f8}k_{fc}k_{m3}\mathcal{R}_{dn}^3}{R_w^3}, \end{aligned} \quad (\text{E.121})$$

$$\mathcal{D}_{40}^{b6v} = \frac{C_{v2}^2 k_{b6}k_{m4}R_w^2}{k_{t6}^2 \mathcal{R}_{dn}^2 R_m^2} - \frac{2C_{v2}k_{b6}k_{f8}k_{fc}k_{m4}\mathcal{R}_{dn}}{k_{t6} R_m^2 R_w} + \frac{k_{b6}k_{f8}^2 k_{fc}^2 k_{m4}\mathcal{R}_{dn}^4}{R_m^2 R_w^4}, \quad (\text{E.122})$$

$$\mathcal{D}_{00}^{b7v} = k_{b3} + k_{b4}k_{m0} + k_{b4}k_{m4}\overline{T}_m^2, \quad (\text{E.123})$$

$$\mathcal{D}_{10}^{b7v} = \frac{k_{b4}k_{m1}\mathcal{R}_{dn}R_m}{R_w} + \frac{k_{b4}k_{m3}\mathcal{R}_{dn}R_m\overline{T}_m}{R_w}, \quad (\text{E.124})$$

$$\mathcal{D}_{20}^{b7v} = \frac{k_{b4}k_{m2}\mathcal{R}_{dn}^2 R_m^2}{R_w^2}, \quad (\text{E.125})$$

$$\mathcal{D}_{00}^{b8v} = k_{b5} + k_{b6}k_{m0} + k_{b6}k_{m4}\underline{T}_m^2, \quad (\text{E.126})$$

$$\mathcal{D}_{10}^{b8v} = \frac{k_{b6}k_{m1}\mathcal{R}_{dn}R_m}{R_w} + \frac{k_{b6}k_{m3}\mathcal{R}_{dn}R_m\underline{T}_m}{R_w}, \quad (\text{E.127})$$

$$\mathcal{D}_{20}^{b8v} = \frac{k_{b6}k_{m2}\mathcal{R}_{dn}^2 R_m^2}{R_w^2}, \quad (\text{E.128})$$

$$\mathcal{D}_{00}^{b9v} = \frac{C_{v0}^2 k_{b4}k_{m4}R_w^2}{k_{t6}^2 \mathcal{R}_{dn}^2 R_m^2} - \frac{2C_{v0}k_{b4}k_{f6}k_{m4}R_w}{k_{t6}\mathcal{R}_{dn}R_m^2} + k_{b3} + \frac{k_{b4}k_{f6}^2 k_{m4}}{R_m^2} + k_{b4}k_{m0}, \quad (\text{E.129})$$

$$\mathcal{D}_{01}^{b9v} = \frac{2C_{v0}k_{b4}k_{m4}m_v R_w^2}{k_{t6}^2 \mathcal{R}_{dn}^2 R_m^2} - \frac{2k_{b4}k_{f6}k_{m4}m_v R_w}{k_{t6}\mathcal{R}_{dn}R_m^2}, \quad (\text{E.130})$$

$$\mathcal{D}_{02}^{b9v} = \frac{k_{b4}k_{m4}m_v^2 R_w^2}{k_{t6}^2 \mathcal{R}_{dn}^2 R_m^2}, \quad (\text{E.131})$$

$$\begin{aligned} \mathcal{D}_{10}^{b9v} &= \frac{2C_{v0}C_{v1}k_{b4}k_{m4}R_w^2}{k_{t6}^2 \mathcal{R}_{dn}^2 R_m^2} - \frac{2C_{v0}k_{b4}k_{f7}k_{m4}}{k_{t6}R_m^2} + \frac{C_{v0}k_{b4}k_{m3}}{k_{t6}} - \frac{2C_{v1}k_{b4}k_{f6}k_{m4}R_w}{k_{t6}\mathcal{R}_{dn}R_m^2} \\ &+ \frac{2k_{b4}k_{f6}k_{f7}k_{m4}\mathcal{R}_{dn}}{R_m^2 R_w} - \frac{k_{b4}k_{f6}k_{m3}\mathcal{R}_{dn}}{R_w} + \frac{k_{b4}k_{m1}\mathcal{R}_{dn}R_m}{R_w}, \end{aligned} \quad (\text{E.132})$$

$$\mathcal{D}_{11}^{b9v} = \frac{2C_{v1}k_{b4}k_{m4}m_v R_w^2}{k_{t6}^2 \mathcal{R}_{dn}^2 R_m^2} - \frac{2k_{b4}k_{f7}k_{m4}m_v}{k_{t6}R_m^2} + \frac{k_{b4}k_{m3}m_v}{k_{t6}}, \quad (\text{E.133})$$

$$\mathcal{D}_{20}^{b9v} = \frac{2C_{v0}C_{v2}k_{b4}k_{m4}R_w^2}{k_{t6}^2 \mathcal{R}_{dn}^2 R_m^2} - \frac{2C_{v0}k_{b4}k_{f8}k_{m4}\mathcal{R}_{dn}}{k_{t6}R_m^2 R_w} + \frac{C_{v1}^2 k_{b4}k_{m4}R_w^2}{k_{t6}^2 \mathcal{R}_{dn}^2 R_m^2} - \frac{2C_{v1}k_{b4}k_{f7}k_{m4}}{k_{t6}R_m^2}$$

$$\begin{aligned}
& + \frac{C_{v1}k_{b4}k_{m3}}{k_{t6}} - \frac{2C_{v2}k_{b4}k_{f6}k_{m4}R_w}{k_{t6}\mathcal{R}_{dn}R_m^2} + \frac{2k_{b4}k_{f6}k_{f8}k_{m4}\mathcal{R}_{dn}^2}{R_m^2R_w^2} + \frac{k_{b4}k_{f7}^2k_{m4}\mathcal{R}_{dn}^2}{R_m^2R_w^2} \\
& - \frac{k_{b4}k_{f7}k_{m3}\mathcal{R}_{dn}^2}{R_w^2} + \frac{k_{b4}k_{m2}\mathcal{R}_{dn}^2R_m^2}{R_w^2}, \tag{E.134}
\end{aligned}$$

$$D_{21}^{b9v} = \frac{2C_{v2}k_{b4}k_{m4}m_vR_w^2}{k_{t6}^2\mathcal{R}_{dn}^2R_m^2} - \frac{2k_{b4}k_{f8}k_{m4}m_v\mathcal{R}_{dn}}{k_{t6}R_m^2R_w}, \tag{E.135}$$

$$\begin{aligned}
D_{30}^{b9v} &= \frac{2C_{v1}C_{v2}k_{b4}k_{m4}R_w^2}{k_{t6}^2\mathcal{R}_{dn}^2R_m^2} - \frac{2C_{v1}k_{b4}k_{f8}k_{m4}\mathcal{R}_{dn}}{k_{t6}R_m^2R_w} - \frac{2C_{v2}k_{b4}k_{f7}k_{m4}}{k_{t6}R_m^2} + \frac{C_{v2}k_{b4}k_{m3}}{k_{t6}} \\
& + \frac{2k_{b4}k_{f7}k_{f8}k_{m4}\mathcal{R}_{dn}^3}{R_m^2R_w^3} - \frac{k_{b4}k_{f8}k_{m3}\mathcal{R}_{dn}^3}{R_w^3}, \tag{E.136}
\end{aligned}$$

$$D_{40}^{b9v} = \frac{C_{v2}^2k_{b4}k_{m4}R_w^2}{k_{t6}^2\mathcal{R}_{dn}^2R_m^2} - \frac{2C_{v2}k_{b4}k_{f8}k_{m4}\mathcal{R}_{dn}}{k_{t6}R_m^2R_w} + \frac{k_{b4}k_{f8}^2k_{m4}\mathcal{R}_{dn}^4}{R_m^4R_w^4}, \tag{E.137}$$

$$D_{00}^{b10v} = \frac{C_{v0}^2k_{b6}k_{m4}R_w^2}{k_{t6}^2\mathcal{R}_{dn}^2R_m^2} - \frac{2C_{v0}k_{b6}k_{f6}k_{m4}R_w}{k_{t6}\mathcal{R}_{dn}R_m^2} + k_{b5} + \frac{k_{b6}k_{f6}^2k_{m4}}{R_m^2} + k_{b6}k_{m0}, \tag{E.138}$$

$$D_{01}^{b10v} = \frac{2C_{v0}k_{b6}k_{m4}m_vR_w^2}{k_{t6}^2\mathcal{R}_{dn}^2R_m^2} - \frac{2k_{b6}k_{f6}k_{m4}m_vR_w}{k_{t6}\mathcal{R}_{dn}R_m^2}, \tag{E.139}$$

$$D_{02}^{b10v} = \frac{k_{b6}k_{m4}m_v^2R_w^2}{k_{t6}^2\mathcal{R}_{dn}^2R_m^2}, \tag{E.140}$$

$$\begin{aligned}
D_{10}^{b10v} &= \frac{2C_{v0}C_{v1}k_{b6}k_{m4}R_w^2}{k_{t6}^2\mathcal{R}_{dn}^2R_m^2} - \frac{2C_{v0}k_{b6}k_{f7}k_{m4}}{k_{t6}R_m^2} + \frac{C_{v0}k_{b6}k_{m3}}{k_{t6}} - \frac{2C_{v1}k_{b6}k_{f6}k_{m4}R_w}{k_{t6}\mathcal{R}_{dn}R_m^2} \\
& + \frac{2k_{b6}k_{f6}k_{f7}k_{m4}\mathcal{R}_{dn}}{R_m^2R_w} - \frac{k_{b6}k_{f6}k_{m3}\mathcal{R}_{dn}}{R_w} + \frac{k_{b6}k_{m1}\mathcal{R}_{dn}R_m}{R_w}, \tag{E.141}
\end{aligned}$$

$$D_{11}^{b10v} = \frac{2C_{v1}k_{b6}k_{m4}m_vR_w^2}{k_{t6}^2\mathcal{R}_{dn}^2R_m^2} - \frac{2k_{b6}k_{f7}k_{m4}m_v}{k_{t6}R_m^2} + \frac{k_{b6}k_{m3}m_v}{k_{t6}}, \tag{E.142}$$

$$\begin{aligned}
D_{20}^{b10v} &= \frac{2C_{v0}C_{v2}k_{b6}k_{m4}R_w^2}{k_{t6}^2\mathcal{R}_{dn}^2R_m^2} - \frac{2C_{v0}k_{b6}k_{f8}k_{m4}\mathcal{R}_{dn}}{k_{t6}R_m^2R_w} + \frac{C_{v1}^2k_{b6}k_{m4}R_w^2}{k_{t6}^2\mathcal{R}_{dn}^2R_m^2} - \frac{2C_{v1}k_{b6}k_{f7}k_{m4}}{k_{t6}R_m^2} \\
& + \frac{C_{v1}k_{b6}k_{m3}}{k_{t6}} - \frac{2C_{v2}k_{b6}k_{f6}k_{m4}R_w}{k_{t6}\mathcal{R}_{dn}R_m^2} + \frac{2k_{b6}k_{f6}k_{f8}k_{m4}\mathcal{R}_{dn}^2}{R_m^2R_w^2} + \frac{k_{b6}k_{f7}^2k_{m4}\mathcal{R}_{dn}^2}{R_m^2R_w^2} \\
& - \frac{k_{b6}k_{f7}k_{m3}\mathcal{R}_{dn}^2}{R_w^2} + \frac{k_{b6}k_{m2}\mathcal{R}_{dn}^2R_m^2}{R_w^2}, \tag{E.143}
\end{aligned}$$

$$D_{21}^{b10v} = \frac{2C_{v2}k_{b6}k_{m4}m_vR_w^2}{k_{t6}^2\mathcal{R}_{dn}^2R_m^2} - \frac{2k_{b6}k_{f8}k_{m4}m_v\mathcal{R}_{dn}}{k_{t6}R_m^2R_w}, \tag{E.144}$$

$$D_{30}^{b10v} = \frac{2C_{v1}C_{v2}k_{b6}k_{m4}R_w^2}{k_{t6}^2\mathcal{R}_{dn}^2R_m^2} - \frac{2C_{v1}k_{b6}k_{f8}k_{m4}\mathcal{R}_{dn}}{k_{t6}R_m^2R_w} - \frac{2C_{v2}k_{b6}k_{f7}k_{m4}}{k_{t6}R_m^2} + \frac{C_{v2}k_{b6}k_{m3}}{k_{t6}}$$

$$+ \frac{2k_{b6}k_{f7}k_{f8}k_{m4}\mathcal{R}_{dn}^3}{R_m^2R_w^3} - \frac{k_{b6}k_{f8}k_{m3}\mathcal{R}_{dn}^3}{R_w^3}, \quad (\text{E.145})$$

$$D_{40}^{b10v} = \frac{C_{v2}^2k_{b6}k_{m4}R_w^2}{k_{t6}^2\mathcal{R}_{dn}^2R_m^2} - \frac{2C_{v2}k_{b6}k_{f8}k_{m4}\mathcal{R}_{dn}}{k_{t6}R_m^2R_w} + \frac{k_{b6}k_{f8}^2k_{m4}\mathcal{R}_{dn}^4}{R_m^2R_w^4}, \quad (\text{E.146})$$

where the variable  $\mathcal{R}_{dn}$  is further split into each gear ratio.





# Contents

<b>Abstract</b>	<b>xv</b>
<b>Acknowledgements</b>	<b>xvii</b>
<b>Acronyms</b>	<b>xix</b>
<b>List of Symbols</b>	<b>xxiii</b>
<b>Table of Contents</b>	<b>xxix</b>
<b>List of Tables</b>	<b>xxxv</b>
<b>List of Figures</b>	<b>xxxix</b>
<b>Introduction</b>	<b>1</b>
Background . . . . .	1
Motivation . . . . .	2
Objective . . . . .	3
Contribution . . . . .	4
<b>I Modeling of Advanced Vehicle Propulsion Systems</b>	<b>7</b>
<b>1 State-of-the-Art Review</b>	<b>9</b>
1.1 Need for Better Energy Efficiency . . . . .	9
1.2 Single-Source Vehicle . . . . .	10
1.3 Hybrid-Electric Vehicle: Architecture and Control . . . . .	12
1.4 Hybrid-Electric Vehicle: Powertrain Design . . . . .	20
<b>2 Modeling for Energy Consumption Evaluation</b>	<b>27</b>
2.1 Modeling of Vehicle Propulsion System . . . . .	27
2.2 Internal Combustion Engine . . . . .	29
2.3 Drivetrain . . . . .	38
2.4 Battery . . . . .	45

2.5	Electric Motor/Generator . . . . .	50
2.6	Vehicle Load Estimation . . . . .	57
<b>II Numeric Evaluation of Energy Consumption for Advanced Vehicle Propulsion Systems</b>		<b>59</b>
<b>3</b>	<b>Energy Consumption Evaluation for Single-Source Vehicles</b>	<b>61</b>
3.1	Simulation Method . . . . .	61
3.2	Simulation Set-Up . . . . .	63
3.3	Numeric Evaluation of Energy Consumption . . . . .	67
<b>4</b>	<b>Minimal Energy Consumption of Hybrid-Electric Vehicles</b>	<b>71</b>
4.1	Optimal Control Problem Formulation . . . . .	71
4.2	Fully Numeric Solution . . . . .	73
4.3	Semi-Analytic Solution . . . . .	74
4.4	Approximate Solution . . . . .	79
4.5	Evaluation of Minimal Energy Consumption . . . . .	86
<b>III Fully-Analytic Energy Consumption Estimation for Advanced Vehicle Propulsion Systems</b>		<b>95</b>
<b>5</b>	<b>Analytic Energy Consumption of Single-Source Vehicles</b>	<b>97</b>
5.1	Conventional Vehicle . . . . .	97
5.2	Battery-Electric Vehicle . . . . .	100
5.3	Analytic Evaluation of Energy Consumption . . . . .	103
<b>6</b>	<b>Analytic Minimal Energy Consumption of Hybrid-Electric Vehicles</b>	<b>107</b>
6.1	Series Hybrid-Electric Vehicle . . . . .	107
6.2	Parallel Hybrid-Electric Vehicle . . . . .	109
6.3	Analytic Evaluation of Minimal Energy Consumption . . . . .	114
<b>IV Design and Control Co-Optimization for Advanced Vehicle Propulsion Systems</b>		<b>117</b>
<b>7</b>	<b>Optimal Design Problem Formulation</b>	<b>119</b>
7.1	Design Objective . . . . .	119
7.2	Design Constraint . . . . .	120
7.3	Design Method . . . . .	126
<b>8</b>	<b>Optimal Design of Vehicle Propulsion Systems</b>	<b>129</b>
8.1	Design Optimization of a Conventional Vehicle . . . . .	129
8.2	Design Optimization of a Battery-Electric Vehicle . . . . .	134

Contents	221
<hr/>	
8.3 Co-Optimization of a Series Hybrid-Electric Truck . . . . .	139
8.4 Co-Optimization of a Parallel Hybrid-Electric Vehicle . . . . .	144
8.5 Co-Optimization of a Parallel Hybrid-Electric Truck . . . . .	153
<b>Conclusion</b>	<b>161</b>
Summary . . . . .	161
Contribution and Limitation . . . . .	163
Future Work . . . . .	165
<b>Bibliography</b>	<b>167</b>
<b>A Résumé</b>	<b>175</b>
<b>B Contour Maps of Chapter 2</b>	<b>177</b>
B.1 Internal Combustion Engine . . . . .	177
B.2 Electric Motor/Generator . . . . .	183
<b>C Implemented Missions</b>	<b>191</b>
C.1 Main Characteristics . . . . .	191
C.2 Graphical Illustration . . . . .	191
<b>D Detailed Dimension-Related Parameters of Chapter 5</b>	<b>193</b>
D.1 Conventional Vehicle . . . . .	193
D.2 Battery-Electric Vehicle . . . . .	197
<b>E Detailed Dimension-Related Parameters of Chapter 6</b>	<b>205</b>
E.1 Series Hybrid Electric Vehicle . . . . .	205
E.2 Parallel Hybrid Electric Vehicle . . . . .	207
<b>Contents</b>	<b>219</b>





**Titre :** Co-Optimisation du Dimensionnement et du Contrôle des Groupe Motopropulseurs Innovants

**Mots clés :** optimisation du dimensionnement, optimisation du contrôle, groupes motopropulseurs, véhicule électrique hybride, véhicule électrique, véhicule conventionnel

**Résumé :**

Des technologies avancées sont très demandées dans l'industrie automobile pour respecter les réglementations de consommation de carburant de plus en plus rigoureuses. La co-optimisation du dimensionnement et du contrôle des groupes motopropulseurs avec une efficacité de calcul améliorée est étudiée dans cette thèse.

Les composants des groupes motopropulseurs, tels que le moteur, la batterie et le moteur électrique, sont modélisés analytiquement au niveau descriptif et prédictif afin de permettre une optimisation du contrôle rapide et une optimisation du dimensionnement scalable. La consommation d'énergie minimale des véhicules hybrides-électriques est évaluée par des nouvelles méthodes optimales. Ces méthodes –

y compris Selective Hamiltonian Minimization et GRaphical-Analysis-Based energy Consumption Optimization – permettent d'évaluer une consommation minimale d'énergie avec une efficacité de calcul améliorée. De plus, la méthode de Fully-Analytic energy Consumption Evaluation (FACE) approxime la consommation d'énergie minimale sous forme analytique en fonction des caractéristiques de la mission et des paramètres de conception des composants du groupe motopropulseur.

Plusieurs cas d'études sont présentées en détail par rapport aux approches de co-optimisation à bi-niveaux et à uni-niveau, ce qui montre une réduction efficace du temps de calcul requis par le processus global de co-optimisation.

**Title :** Design and Control Co-Optimization for Advanced Vehicle Propulsion Systems

**Keywords :** design optimization, control optimization, vehicle propulsion system, hybrid-electric vehicle, battery-electric vehicle, conventional vehicle

**Abstract :**

Advanced technologies are highly demanded in automotive industry to meet the more and more stringent regulations of fuel consumption. Co-optimization of design and control for vehicle propulsion systems with an enhanced computational efficiency is investigated in this thesis.

Powertrain components, such as internal combustion engines, batteries, and electric motor/generators, are analytically modeled at descriptive and predictive level correspondingly for the development of fast-running control optimization and for the scalability of design optimization. The minimal fuel consumption of a hybrid-electric vehicle is evaluated through novel optimization methods.

These methods – including the Selective Hamiltonian Minimization, and the GRaphical-Analysis-Based energy Consumption Optimization – are able to evaluate the minimal energy consumption with the enhanced computational efficiency. In addition, the Fully-Analytic energy Consumption Evaluation method approximates the minimal energy consumption in closed form as a function of the mission characteristics and the design parameters of powertrain components.

A few case studies are presented in details via the bi-level and uni-level co-optimization approaches, showing an effective improvement in the computational efficiency for the overall co-optimization process.

